Centrifuge modelling of drained lateral pile - soil response

Application for offshore wind turbine support structures

Klinkvort, Rasmus Tofte

Publication date:
2013

Document Version
Publisher's PDF, also known as Version of record

Citation (APA):
Klinkvort, R. T. (2013). *Centrifuge modelling of drained lateral pile - soil response: Application for offshore wind turbine support structures*. Technical University of Denmark.

Centrifuge modelling of drained lateral pile - soil response

- Application for offshore wind turbine support structures

Rasmus Tofte Klinkvort

Ph.D. Thesis

Department of Civil Engineering
Technical University of Denmark

2012

Supervisors:

Associate Professor Ole Hededal, Technical University of Denmark - DTU, Denmark
Professor Sarah Springman, Swiss Federal Institute of Technology - ETH Zurich, Switzerland

Assessment Committee:

Professor Jürgen Grabe, Technical University Hamburg-Harburg - TUHH, Germany
University Lecturer Byron Byrne, University of Oxford, England
Associate Professor Anette Krogsbøll, Technical University of Denmark - DTU, Denmark

Centrifuge modelling of drained lateral pile - soil response
-Application for offshore wind turbine support structures

Printed by DTU-Tryk
Department of Civil Engineering
Technical University of Denmark
ISBN: 9788778773579
ISSN: -

Preface

This thesis is submitted as a partial fulfilment of the requirements for the Danish Ph.D. degree. The work title of the project has been "Cyclic laterally response of wind turbine monopile foundation in saturated sand". The thesis is divided into two parts. The first part introduces the research field, discusses the methodology, highlights the major findings and provides an overview of the work carried out within this project along with a discussion. The second part is a collection of papers which constitute the basis of the work and describe the work in greater detail and serves as scientific documentation.

Lyngby, the 29th of June 2012

Rasmus Tofte Klinkvort

Acknowledgements

I acknowledge the supervision and inspiration given to me by my supervisor Associate Professor Ole Hededal. As a part of the Ph.D. studies I went to ETH Zurich working with their Geotechnical group. The time at ETH was inspiring and I would like to thank Professor Sarah Springman for sharing her knowledge of centrifuge modelling with me. Furthermore, I thank Caspar Thrane Leth for the introduction to centrifuge modelling and discussions concerning laterally loaded piles.

To maintain focus on the scientific content of the thesis, a well written thesis is important. For helping me with proofreading the manuscript I would like to give a big thanks to Einar Thór Ingólfsson and Morten Møller van Gils Hansen.

Abstract

The installation and foundation cost of offshore wind turbines is substantial, and today energy from offshore wind is not competitive with energy from more classical energy production methods. The goal of this research project has been to develop simple engineering tools, which can be used in the design of a technical optimal and cost beneficial solution for an offshore wind turbine foundation and thereby reduce the price of energy from offshore wind turbines. The methodologies developed in this thesis hopefully contribute to a better understanding within this field.

Monopiles are one of the most popular foundation methods today for offshore wind turbines. These piles are often installed in dense sand at water depths ranging from 10-30 meters. A monopile is a single, large diameter tubular steel pile. The current design methodology originates from tests on long slender piles but is also used for monopiles today. Therefore it appears that the methodology for monopiles lacks scientific justification and a better understanding of rigid piles is needed.

More than 70 centrifuge tests on laterally loaded rigid model piles have been carried out in connection with this thesis to get a better understanding of rigid piles. The tests have been performed in homogeneously dense dry or saturated Fontainebleau sand in order to mimic simplified drained offshore soil conditions.

Approximately half of the tests have been carried out to investigate the centrifuge procedure in order to create a methodology of testing that enables the transformation of result from tests in model scale to prototype scale. The grain size to pile diameter ratio, the non-linear stress distribution and the pile installation was identified from this investigation as important parameters in reliable scaling of centrifuge results.

The remaining tests were used to investigate the pile - soil interaction to gain a better in-sight into the complex problem. A monotonic test series was carried out initially and then pile - soil interaction curves were deduced from these tests and compared with methodologies used today. The results indicate that the current methodologies can be improved and a modification

to the methodology has been proposed. Secondly, a cyclic test series was carried out. The accumulation of displacement and the change in secant stiffness of the total response of these tests were evaluated. A simple mathematical model was proposed to predict the accumulation of displacement and change in secant stiffness using the observations seen in the centrifuge.

With the centrifuge test observation as basis, an cyclic pile - soil interaction element was developed. The element can be used in Winkler type analysis where the soil is modelled as spring elements and the rest of the structure as beam elements. The model was calibrated against monotonic and cyclic centrifuge tests. The element predicts the hysteresis seen on element level in an acceptable way, but does not predict the accumulation of displacements and change in secant stiffness as seen in the experiments. The element used in a dynamic analysis gives an estimate of the frictional soil damping. The capabilities of the element were demonstrated by a series of free decay simulations where the logarithmic decrement could be calculated afterwards.

Altogether, the methodologies developed in this thesis can be directly used in the design of offshore monopiles, with a scientific justification based on centrifuge model scale tests.

Resumé

Omkostningerne for havvindmølle fundamenter er store og i dag er energi fra havvindmøller, ikke konkurrencedygtig med energi fra mere klassiske energi produktionsmetoder. Målet med dette forskningsprojekt er at udvikle simple tekniske værktøjer, der kan bruges i udformningen af en teknisk optimal og omkostningseffektiv løsning for et havvindmølle fundament og derved være med til at gøre prisen på energi fra havvindmøller lavere. De udviklede metoder i denne afhandling bidrager til en bedre forståelse inden for dette område.

Monopæle er i dag en af de mest populære fundaments metoder til havvindmøller. Disse pæle er ofte installeret i tætpakket sand på vanddybder, der spænder fra 10-30 meter. En monopæl er en cylindrisk stålpæl med stor diameter. De nuværende design metoder stammer fra test på lange, slanke pæle, men bruges i dag også til design af monopæle. Det videnskabelige grundlag for design af monopæle er mangelfuldt og en bedre forståelse af opførelsen af stive monopæle er derfor nødvendig.

I forbindelse med denne afhandling er der udført mere end 70 centrifuge test for at få en bedre forståelse af opførelsen af tværbelastede stive pæle. Alle tests er blevet udført i homogent tætpakket tørt eller vandmættet Fontainebleau sand for at efterligne drænede jordbundsforhold.

Omkring halvdelen af forsøgene er udført for at undersøge centrifuge udførelses teknikken med henblik på at skabe en metode til at transformere resultater fra forsøg i model skala til resultater i prototype skala. Fra denne undersøgelse blev forholdet mellem kornstørrelse og pæle diameter, den ikke-lineære spændingsfordeling og pæleinstallationen identificeret som vigtige parametre i en pålidelig skalering af centrifuge resultaterne.

Resten af testene blev anvendt til at undersøge pæl-jord interaktionen og derved få et større indblik i det komplekse problem. Først blev en statisk test serie gennemført hvorfra pæl - jord interaktions kurver blev udledt og sammenlignet med eksisterende metoder. Resultaterne viste, at de nuværende metoder kan forbedres, og en modifikation af metoden blev foreslået. Dernæst blev en cyklisk test serie udført, hvorfra akkumulering af flytning og ændring i sekant stivhed af den samlede reaktion blev målt. En simpel matematisk

model til at forudsige akkumulering af flytning og ændring i sekant stivhed blev foreslået baseret på observationer set i centrifugen.

Med resultaterne fra centrifugen som grundlag blev et cyklisk pæl - jord interaktions element udviklet. Elementet kan bruges i en Winkler-type analyse, hvor jorden er modelleret som fjedre elementer og resten af strukturen, som bjælker elementer. Modellen blev kalibreret til de statiske og cykliske centrifuge forsøg, og elementet forudsiger hysterese set på element niveau i en acceptabel form. Modellen kan dog ikke forudsige akkumuleringen af flytninger og ændringer i sekant stivhed, som det var observeret i centrifuge forsøgene. Elementet kan anvendes i en dynamisk analyse, hvor det kan bruges til at giver et skøn over jorddæmpningen fra friktion. Opførelsen af elementet blev demonstreret ved en række frie svingnings simuleringer, hvor det logaritmiske dekrement bagefter kunne beregnes.

Metoderne udviklet i denne afhandling kan anvendes direkte i designet af offshore monopæle, med en videnskabelig belæg baseret på centrifuge forsøg udført i model skala.

Contents

I Extended summary **1**

1 Introduction **3**
1.1 Offshore wind farms . . . 3
1.2 Loads on offshore wind turbines . . . 4
1.3 Monopile support for offshore wind turbines . . . 6
1.4 Work hypothesis . . . 7

2 Background review **11**
2.1 Ultimate bearing capacity . . . 11
2.2 Pile - soil interaction . . . 14
2.2.1 Comments on recent design methodology . . . 16
2.3 Recent research . . . 18
2.3.1 Monotonic response . . . 19
2.3.2 Cyclic response . . . 20
2.3.3 Comments to recent research . . . 21

3 Methodology **23**
3.1 Physical modelling . . . 24
3.1.1 Dimensional analysis . . . 25
3.2 Centrifuge modelling . . . 28
3.3 Soil testing . . . 33
3.4 Methodology validation . . . 35
3.4.1 Scale effects . . . 38
3.4.2 Scaling approach . . . 47
3.4.3 Measurement uncertainties . . . 48
3.5 Summary of methodology validation . . . 49

4 Pile - soil interaction results **51**
4.1 Monotonic loading . . . 53
4.1.1 Stress distribution effect . . . 54
4.1.2 Load eccentricity effect . . . 56

4.1.3 Comparison with FEM 57
4.1.4 New monotonic pile - soil interaction model 59
4.2 Cyclic loading - total response 61
4.2.1 Model framework 62
4.2.2 Evolution of displacements 64
4.2.3 Evolution of secant stiffness 66
4.2.4 Concluding remarks 68
4.3 Cyclic pile - soil interaction response 69
4.3.1 Deformation controlled cyclic loading 69
4.3.2 Force controlled cyclic loading 70
4.3.3 General observations 72
4.4 Summary of pile - soil interaction results 73

5 Pile - soil interaction model **75**
5.1 Cyclic pile - soil interaction spring 75
5.1.1 Calibration and demonstration of response 80
5.2 Dynamic model 84
5.2.1 Validation of dynamic model 85
5.2.2 Estimation of soil damping 87
5.3 Summary of pile - soil interaction model 89

6 Discussion **91**
6.1 Monotonic loading 91
6.1.1 Initial stiffness 92
6.1.2 Maximum bearing capacity 93
6.2 Cyclic loading 93
6.3 Cyclic spring model 94

7 Conclusions **97**

Bibliography **108**

II Papers **109**

Paper I
"Centrifuge modelling of offshore monopile foundation",
R.T. Klinkvort & O. Hededal.
Published in: *Frontiers in Offshore Geotechnics II, 2010* 111

Paper II
"Scale effects in centrifuge modelling of monopiles",
R. T. Klinkvort, O. Hededal & S. Springman.
To be submitted for publication -, *2012* 119

Paper III
"Monotonic soil-structure interaction of monopile support for offshore wind turbines",
R. T. Klinkvort & O. Hededal.
Submitted for publication -, *2012* 147

Paper IV
"Centrifuge modelling of a laterally cyclic loaded pile",
R.T. Klinkvort, C.T. Leth & O. Hededal.
Published in: *Physical Modelling in Geotechnics, 2010* 159

Paper V
"Laterally cyclic loading of monopile in dense sand",
R.T. Klinkvort, O. Hededal & M. Svensson.
Published in: *Proceedings of the 15th European Conference on Soil Mechanics and Geotechnical Engineering, 2011* 167

Paper VI
"Lateral response of monopile supporting an offshore wind turbine",
R. T. Klinkvort & O. Hededal.
Submitted for publication -, *2012* 175

Paper VII
"An elasto-plastic spring element for cyclic loading of piles using the p-y-curve concept",
O. Hededal & R. T. Klinkvort.
Published in: *Numerical Methods in Geotechnical Engineering, 2010* . . 199

Additional work (not included in the thesis)

- R. T. Klinkvort. Single piles under lateral loading, Lecture notes in: Advanced Geotechnical Engineering, DTU - Civil engineering 2008
- R. T. Klinkvort. Monopile foundations for offshore wind turbines, Department of Civil Engineering, Annual Report 2010
- R. T. Klinkvort. Centrifuge modeling of monopiles, 20th European Young Geotechnical Engineers Conference 2010
- R. T. Klinkvort. Hvordan funderes næste generation af havvindmøller, Danskernes Akademi, Invited lecture in DR2. Broadcasted in televison january 2010.
  Homepage:
  `http://www.dr.dk/DR2/Danskernes+akademi/Natur_Matematik/Hvordan_funderes_den_naeste_generation_af_havvindmoeller.htm`
- R. T. Klinkvort, C. T. Leth & O. Hededal. Centrifuge modelling of monopiles in dense sand at The Technical University of Denmark, Eurofuge 2012
- C T Leth S. P. H. Sørensen, R. T. Klinkvort, A. H. Augustesen, L. B. Ibsen and O. Hededal. A snapshot of present research at AAU and DTU on large-diameter piles in coarse-grained materials, Nordic Geotechnical Meeting, NGM2012 2012

Nomenclature

α	Hardening paramter
α	Non-dimensional accumulation of displacement constant
δ	Logarithmic decrement
η	Increase in gravity
γ'	Effective density
κ	Non-dimensional change in secant stiffness constant
ω	Rotational frequency
ϕ'	Effective angle of friction
ϕ_{cr}	Critical state angle
ρ	Sand density
σ'_1	Vertical stress in triaxial test
σ'_3	Radial stress in triaxial test
σ'_v	Effective vertical stress
$\tilde{H}$	Normalised horisontal shear force
$\tilde{K}_s$	Secant stiffness from monotonic test
$\tilde{P}$	Normalised horisontal shear with K_p
$\tilde{p}$	Normalised soil resistance, K
$\tilde{y}$	Normailised pile displacement
ζ_b	Non-dimensional magnitude of the cyclic loading

ζ_c	Non-dimensional characteristic of the cyclic loading
A	Empirical depth factor
C_u	Coefficient of uniformity
CO_2	Carbon dioxide
d	Diameter of pile
d_{50}	Average grain size
E_p	Elasticity modulus pile
E_s	Elasticity modulus sand
e_{max}	Maximum void ratio
e_{min}	Minimum void ratio
E_{py}	Initial stiffness of pile - soil interaction curve
g	Natural gravity acceleration
G_s	Specific gravity of particles
H	Horisontal shear force
H	Step function
H_{wave}	Lateral wave load
H_{wind}	Lateral wind load
I	Pile installation
I_p	Moment of inertia pile
K	Earth pressure coefficient
k	Initial subgrade modulus
K_0	Earth pressure coefficient at rest
K_N	Secant stiffness to a given load cycle
K_p	Passive earth pressure coefficient by Rankine
K_q^0	Earth pressure coefficient at shallow depth by Brinch Hansen

K_q^{∞} Earth pressure coefficient at greater depth by Brinch Hansen

$K_{ult,API}$ Ultimate earth pressure coefficient by API

$K_{ult,BH}$ Ultimate earth pressure coefficient by Brinch Hansen

$K_{ult,B}$ Ultimate earth pressure coefficient by Broms

l_e Load eccentricity

l_L Pile penetration

M Bending moment

m Bending moment in pile

N Number of cycles

N_s Scaling factor

p Soil resistance

p' Effective mean pressure

p_u Current soil yield strength

p_u^{drag} Soil drag capacity

p_u^{face} Soil resistance build up

p_u^{Virgen} Soil resistance virgin curve

P_{max} Maximum cyclic load

P_{min} Minimum cyclic load

P_{mon} Bearing capacity from monotonic test

R Centrifuge radius

R_t Centrifuge radius to sand surface

t Pile thickness

T_b Non-dimensional cyclic load function

T_c Non-dimensional cyclic load function

Y Overall displacements

y	Pile displacement
$y*$	Corrected displacement
y_{bt}	Artificial starting point of virgin curve
z	Depth in soil profile

Part I

Extended summary

Chapter 1

Introduction

As a consequence of recent climatic changes, the focus on alternative sustainable energy has increased in the past decade. It is widely accepted that the emission of carbon dioxide (CO_2) is one of the key reasons for global warming. Renewable energy sources generally have a low CO_2 impact and are therefore a good and sustainable tool in the fight against global warming.

1.1 Offshore wind farms

Several energy producing alternatives are available, and one of these alternative sources is energy from wind turbines, Figure 1.1. Wind turbines generate a small amount of CO_2 emission only from the construction and installation of the turbine, and are today the second largest contributor to sustainable energy production, (Agency, 2009). Onshore wind turbines are easy to install and are today combatable with fossil energy production. There are though some environmental concerns, including visual impact, noise and the risk of bird collision. In particular, the low visual impact but also larger production rates are drivers for offshore wind turbines. The wind conditions at sea level are smooth, and the low wind shear and steeper gradient of wind speed, subjects the offshore wind turbine to smaller turbulence. Low wind turbulence will increase the life time of a wind turbine and the production is about 50% larger compared to onshore turbines due to larger wind turbines,(Agency, 2008).

The installation and foundation costs of offshore wind turbines are greater than those of onshore wind turbines, and today energy from offshore wind is not competitive with energy from more classical energy production methods. Despite the extra cost, several offshore wind turbine farms have been estab-

Figure 1.1: *Offshore wind turbine park, under construction, Picture from: http://apps1.eere.energy.gov/news/news_detail.cfm/news_id=15982*

lished, but if the development in offshore wind farms shall succeed, the price on energy has to become competitive. As seen in Figure 1.2, the price of the support structure for an offshore installed wind turbine is about 20% of the total cost. If this ratio can be cut down by improvement of technical solutions, the total price of an offshore wind turbine and the price of electricity from wind turbines can be reduced.

The goal of this research project is to develop simple engineering tools, which can be used in the design of a technical optimal and cost beneficial solution for offshore wind turbine foundation.

1.2 Loads on offshore wind turbines

Offshore wind turbines are placed in a harsh environment with loads from wind and waves acting on the structure. The wind turbine is a tall and slender construction and is therefore dynamically sensitive. A sketch of the primary forces acting on a wind turbine can be seen in Figure 1.3. The primary forces on an offshore wind turbine are lateral loads from wind and

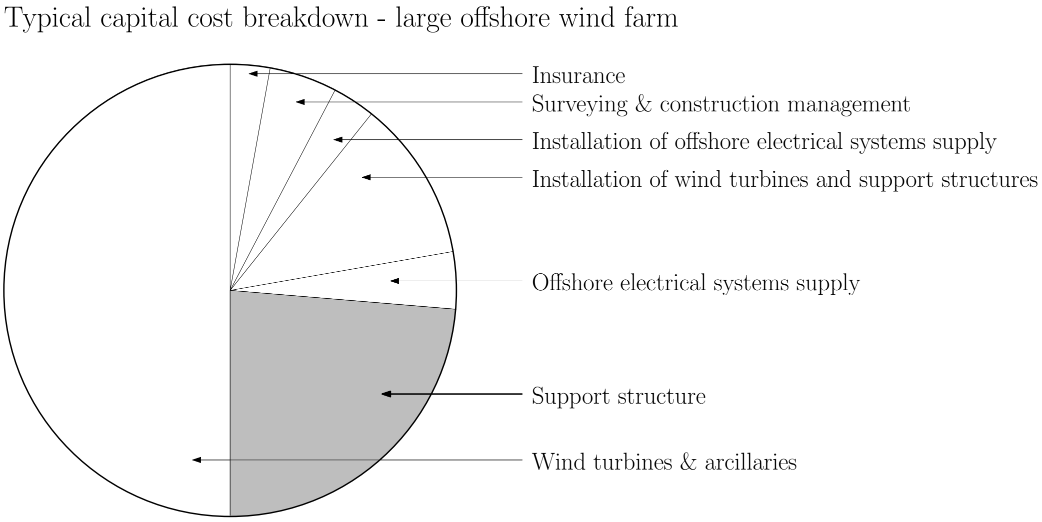

Figure 1.2: *Schematic view of the cost of a offshore wind turbine, reproduced from: http://www.wind-energy-the-facts.org/en/part-i-technology/chapter-5-offshore/wind-farm-design-offshore/*

waves, shown in Figure 1.3 as H_{wind} and H_{wave}. The two forces will both result in random cyclic lateral reactions in the foundation. A typical power spectra of the forces acting on an offshore wind turbine is given in Figure 1.4. The loading frequencies from wind and waves are given here, with a peak wave frequency of about 0.1 Hz and a peak wind frequency of about 0.01Hz. The rotor frequency range, often called 1P, and the blade passing frequency range from a three blade wind turbine, called 3P, are also shown in Figure 1.4. It is important in the design to achieve a first natural frequency of the structure which lies outside these frequencies. This is normally achieved through a design where the entire wind turbine structure has a eigenfrequency in between 1P and 3P, normally called a soft-stiff structure. Considering typical turbines this range is rather narrow, and can be difficult to obtain, special for wind turbines installed at large water depths.

The design of a foundation supporting an offshore wind turbine is carried out in four design limit states, e.g. DNV (2011):

a Ultimate limit state, ULS - Total collapse of the foundation

b Serviceability limit state, SLS - Permanent rotation of turbine tower is exceeded

c Fatigue limit state, FLS - Material collapse due to large number of cycles

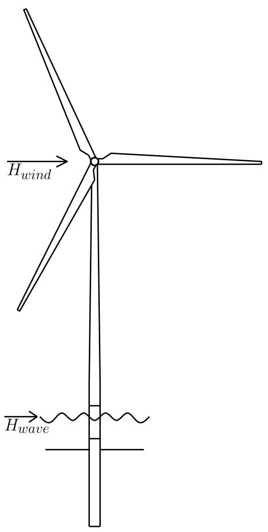

Figure 1.3: Force resultants on offshore wind turbine

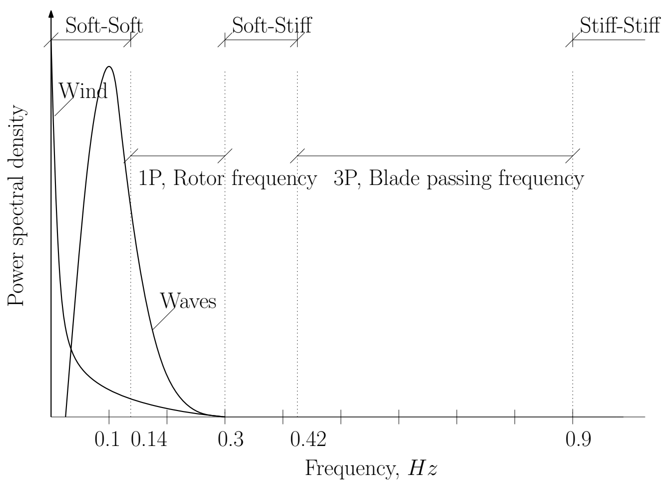

Figure 1.4: Typical range of forcing frequencies for an offshore wind turbine, (DNV, 2011)

d Accident limit state, ALS - Total collapse of foundation from e.g. ship impact

A robust design tool should be capable of handling these design limit states. This includes a description of the ultimate bearing capacity of the foundation in the ULS/ALS situation, which should consider the effects of cyclic loading from different directions and the corresponding accumulation of rotation in SLS situation. In the FLS situation it should give a good prediction of the stiffness of the foundation and thereby also the eigenfrequency of the total wind turbine structure. Furthermore an accurate description of the soil damping is beneficial for all design states due to the load reduction in the resonance regimes.

1.3 Monopile support for offshore wind turbines

Different foundation concepts can be chosen in order to support the offshore wind turbine. This thesis will concentrate on the monopile concept as, installed in dense sand. Dense sand is a typical offshore site condition in the North Sea; here waves have compacted sand to a relative density of around 90% and more.

Monopiles are the most widely used foundation method for offshore wind turbines. These piles are often installed in dense sand at water depths ranging from 5-30 meters. A monopile is a single large diameter tubular steel pile driven 4 to 6 times its diameter into the seabed. The diameter of the piles ranges from 4-6 meters. A picture of a monopile before installation is

***Figure 1.5**: Picture of one of the monopiles used at Walney Wind Farm, Credit: Dong Energy*

shown in Figure 1.5. These piles are driven vertically into the seabed and a transition piece is placed on the top of the monopile, which can correct small rotations during installation. The transition piece is connected to the monopile by a grouted connection and the wind turbine is mounted on top of the transition piece. It is assumed in the stability design of the monopile foundation that these connections are rigid, neglecting any deformation in the connection. As a simplification, the monopile can therefore be treated as a short rigid pile with a relatively large lateral load eccentricity.

1.4 Work hypothesis

A laterally loaded rigid circular pile, with a relative high ratio of shear force to bending moment is investigated in this thesis, neglecting the vertical load.

The investigation is carried out for both monotonic and uni-directional cyclic load scenarios in dense sand. The monotonic and cyclic loading are applied quasi static and it is assumed that no pore pressure develops. The effect of pore pressure accumulations and bi-directional cyclic loading are therefore outside the scope of this thesis.

To establish a work hypothesis, it is important to recognize how soil resistance is acting on the rigid monopile. When a pile is laterally loaded, it will start to move and the soil will resist this movement. The bearing capacity of a laterally loaded pile is an interaction between the pile displacement and the resistance of the soil also known as soil-pile interaction. A sketch of a monopile is shown in Figure 1.6. The monopile is loaded at seabed with a combination of horizontal shear force (H) and bending moment ($M = l_e \cdot H$).

The applied load is carried by the monopile as a combination of of soil

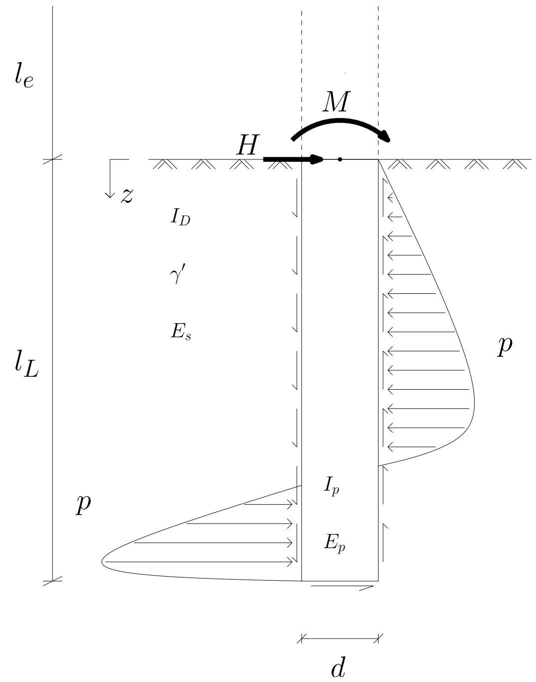

Figure 1.6: *Sketch of forces acting on a laterally loaded pile*

pressures and friction acting on the pile. The soil response from these forces need to be seen from a 3 dimensional perspective. A sketch of the pressures acting on a pile cross section is shown in Figure 1.7. The pile is subjected to soil pressure and friction on the side of the pile. To simplify the 3 dimensional friction and pressure distributions all these factors are merged into one single soil resistance, sometimes called the modulus approach. The soil resistance, (p) can then be calculated as the effective stress at a given depth ($\gamma' \cdot z$) times

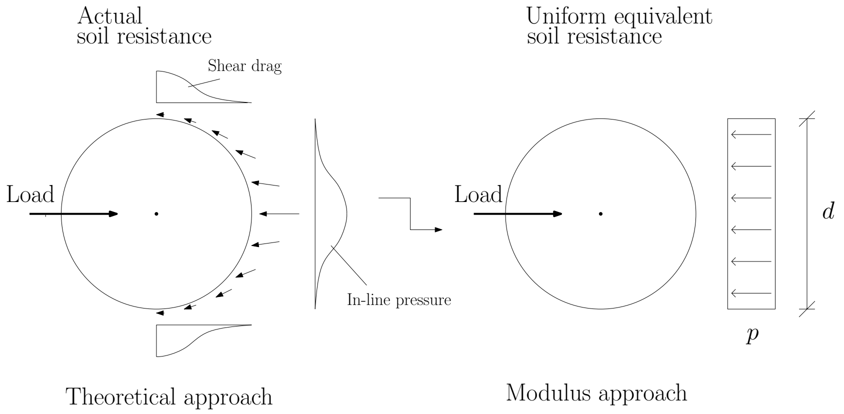

Figure 1.7: *Sketch of soil pressure approximation in a cross section of the pile, after (Smith, 1987)*

an earth pressure coefficient (K) integrated over the width of the pile (d),(Briaud et al. (1983) and Smith (1987)). This can be written as:

$$p = K \cdot d \cdot \sigma'_v \tag{1.1}$$

It is important to recognize that the earth pressure coefficient also incorporates the friction acting on the pile from both horizontal and vertical directions. The parameter can be seen as the difference in the active and passive soil pressure including the friction acting on the pile. This is illustrated in Figure 1.7 where the actual stress distribution is shown to the left, whereas the simplification which is used in the general approximation in (1.1) is shown to the right.

It is the behavior of the simplified non-dimensional soil resistance K which is important for the total performance of the monopile foundation and is therefore the focus of this study. This can done by looking either directly at K, or by looking at the overall response of the pile, knowing that the capacity of the pile is a function of the soil resistance.

$$H = \int_0^{l_L} K \cdot d \cdot \sigma_v \, dz \tag{1.2}$$

The hypothesis of this thesis is that the modulus approach shown in (1.1) is independent of the pile diameter. The non-dimensional soil resistance K is therefore a function of a set of independent parameters as shown in equation (1.3) if full similarity in the geometry is kept constant (const.=$\frac{e_L}{d}$ & const.=$\frac{E_p I_p}{E_s e_L^4}$). Scaled models can therefore be used in the investigation of K.

$$K = f(\phi', z/d, I, N, \zeta_b, \zeta_c) \tag{1.3}$$

Here ϕ' is the effective angle of friction of the sand, z/d is the normalized depth in the soil, I is installation of the pile, N is the number of load cycles, ζ_b is the magnitude of the cyclic loading and ζ_c is the characteristic of the cyclic loading.

By planning a test program that investigates the influence of different parameters independently can be determined. When the influence is known, a model is set up which can handle the four design limit states and can be used to provide a better technical solution for a monopile supporting an offshore wind turbine.

Chapter 2

Background review

With the increase in offshore oil and gas structures in the fifties, focused research began to derive the response of laterally loaded piles. The methods developed at that time are still the basis for offshore monopile design today. This chapter will present the methodology and will be divided into three sections. The first section presents methodologies for calculation of the ultimate bearing capacity. The following section presents examples on formulations of the pile-soil interaction. Finally the state of the art research on monopiles for offshore wind turbines is presented.

2.1 Ultimate bearing capacity

The bearing capacity of a laterally loaded pile can be found knowing the distribution and magnitude of the soil resistance acting on the pile. The soil resistance is determined using the simplification shown in equation (1.1). Broms (1964) presented a very simple method to calculate the bearing capacity of a rigid laterally loaded pile in sand. He assumed an increasing soil resistance acting only on the opposite side of the applied load of the pile. To ensure moment equilibrium a single force is needed at the pile tip. The earth pressure coefficient has to be calculated to determine the soil resistance and is defined as 3 times the passive Rankine pressure as shown (2.1).

$$K_{ult,B} = 3 \cdot K_p = 3 \cdot tan^2(45 + \phi'/2) \tag{2.1}$$

When the ultimate soil resistance distribution is known, the maximum capacity of the pile can be found by a moment equilibrium around the pile toe, for details see Broms (1964).

In reality the soil resistance profile is not as simple as that assumed by Broms (1964). A method with a soil resistance acting on both sides of a rigid pile was presented by Hansen (1961). This approach is slightly more sophisticated and thereby also more complex to use. Based on plasticity theory, Hansen (1961) operates with two different kinds of failure mechanisms when defining the soil pressure coefficient. A failure at shallow depth where the pile pushes the soil up (K_q^0) and a failure at greater depth where the pile pushes the soil around the pile (K_q^∞). The failure at shallow depth can be described as:

$$K_q^0 = e^{\pi/2-\phi'} \cos\phi' \tan(45^o + \phi'/2) - e^{\pi/2-\phi'} \cos\phi' \tan(45^o - \phi'/2) \tag{2.2}$$

and the failure at greater depth is given by

$$K_q^\infty = N_c \cdot d_c^\infty \cdot K_0 \cdot \tan\phi' \tag{2.3}$$

where:

$$N_c = (e^{\pi \tan\phi'} \tan^2(45^o - \phi'/2) - 1) \cot\phi' \tag{2.4}$$

$$d_c^\infty = 1.58 + 4.09 \tan^4\phi' \tag{2.5}$$

$$K_0 = 1 - \sin\phi' \tag{2.6}$$

This is combined in a function which ensures a smooth transition from shallow to failure at greater depth.

$$K_{ult,BH} = \frac{K_q^0 + K_q^\infty \alpha_q \frac{z}{d}}{1 + \alpha_q \frac{z}{d}} \tag{2.7}$$

The value α_q is a parameter which controls the transition from shallow failure to failure at greater depth and is defined by:

$$\alpha_q = \frac{K_q^0}{K_q^\infty - K_q^0} \cdot \frac{K_0 \sin\phi'}{\sin(45^o + \phi'/2)} \tag{2.8}$$

In this approach the soil is divided into a set of layers and a rotation point can then be calculated using moment equilibrium. The maximum capacity of the pile can be calculated by a horizontal equilibrium when the rotation point of the pile is known, for details see Hansen (1961).

The method recommended by design codes, (API, 2007; DNV, 2011) was developed for slender piles. In contrast to the original formulation, the method shown here has been slightly rearrange, in order to fit into the more general framework used in this thesis. Similar to the method by Hansen (1961). This method is a full plastic solution assuming two different failure mechanisms, one at shallow depth and one at greater depth. However, the ultimate earth pressure is found in this approach as the minimum of two expressions given as:

$$K_{ult,API} = A \cdot \min \begin{cases} (C_1 \cdot \frac{z}{d} + C_2) & \text{failure at shallow depth} \\ C_3 & \text{failure at greater depth} \end{cases} \tag{2.9}$$

The lateral bearing capacity coefficients are calculated from the solution by Reese et al. (1974).

$$C_1 = \frac{(1-\sin(\phi')) \cdot \tan(\phi') \cdot \sin(45^o + \frac{\phi'}{2})}{\tan(45^o - \frac{\phi'}{2}) \cdot \cos(\frac{\phi'}{2})} + \frac{\tan^2(45^o + \frac{\phi'}{2}) \cdot \tan(\frac{\phi'}{2})}{\tan(45^o - \frac{\phi'}{2})} \tag{2.10}$$

$$+ ((1 - \sin(\phi') \cdot \tan(45^o + \frac{\phi'}{2}) \cdot (\tan(\phi') \cdot \sin(45^o + \frac{\phi'}{2}) - \tan(\frac{\phi'}{2}))$$

$$C_2 = \frac{\tan(45^o + \frac{\phi'}{2})}{\tan(45^o - \frac{\phi'}{2})} - \tan^2(45^o - \frac{\phi'}{2}) \tag{2.11}$$

$$C_3 = (1 - sin(\phi')) \cdot \tan(\phi') \cdot \tan^4(45^o + \frac{\phi'}{2}) \tag{2.12}$$

$$+ \tan^2(45^o - \frac{\phi'}{2}) \cdot (\tan^8(45^o + \frac{\phi'}{2}) - 1)$$

A is an empirical parameter which was used to fit full scale results on slender piles and was found to be $A = \left(3.0 - \frac{0.8z}{d}\right) \geq 0.9$ for monotonic loading and $A = 0.9$ for cyclic loading.

In Figure 2.1 the soil resistance profile together with the normalized profile for the three different methodologies are shown. The soil resistance profile are generate for a pile with a diameter of $d = 3m$, penetration depth of $l_L = 6d$, load eccentricity of $l_e = 15d$ installed in dense sand with a effective density of $\gamma' = 10kN/m^3$ and a maximum angle of friction of $\phi' = 38^o$ The three different methodologies can then easily be compared and basic observation is here described. The method by Broms (1964) only have a constant soil resistance profile on one of the sides. The method by Hansen (1961) has the same starting value as Broms (1964), but increases with depth. The method used by API (2007) starts with a smaller initial resistance compared to the two other methods, then increases with depth to a point where the resistance is approximately the same as in the method by Hansen (1961), here it start to decrease to point approximately identical with Broms (1964) and then it start to increase again. This behavior is due to the empirical factor A which decreases to a normalized depth of $z = 2.625d$, after this point it has a constant value of 0.9. From a situation like this it is seen that the methodology by Hansen (1961) gives the highest bearing capacity followed

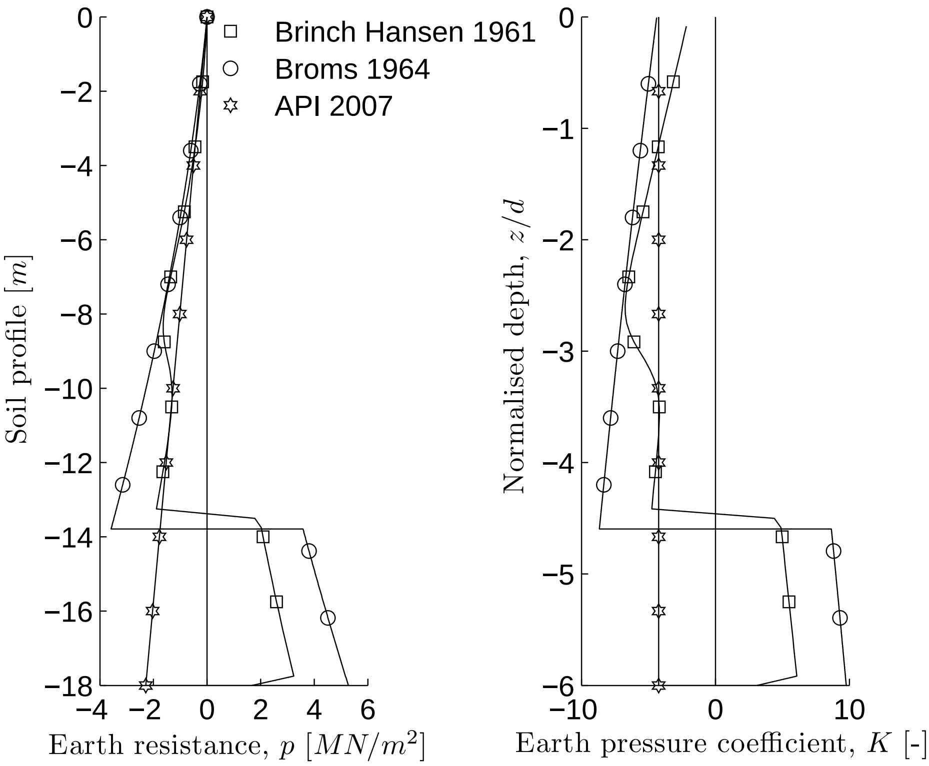

Figure 2.1: *Comparison of soil resistance profiles at failure*

by the method by API (2007) and the simplest method by Broms (1964) also gives the smallest capacity.

Three famous methodologies to calculated the ultimate soil resistance have here been presented, thus there exist several other methodologies e.g. Meyerhofs et al. (1981) and Norris and Abdollaholiaee (1990).

2.2 Pile - soil interaction

Today, the design of monopiles for offshore wind turbines are carried out by modelling the pile as a beam and the soil as a system of uncoupled non-linear springs, API (2007). A sketch of the approach is shown in figure 2.2. The soil is modeled as a set of independent soil layers represented by springs. The characteristics of these springs which describes the soil resistance, p as a function of the displacement, y are defined as pile-soil interaction springs. This method has been used successfully in pile design for offshore oil and gas platforms in many years. The design methodology originates from field tests on long slender piles with a small load eccentricity, (Reese and Matlock, 1956;

McClelland and Focht, 1956). Although this methodology was originally

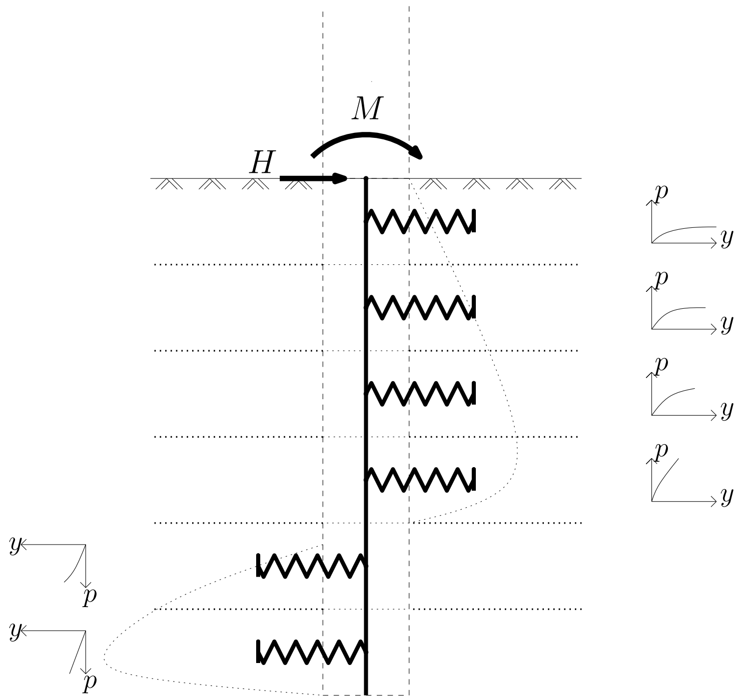

Figure 2.2: *Sketch of the modelling approach used today*

calibrated to slender piles, it is used today for design of large diameter stiff monopiles.

Murchison and O'Neill (1984) investigated four different ways of computing the pile-soil interaction curves for sand. The best of these four was a method invented by Parker and Reese (1970) and reformulated by Murchison and O'Neill (1984). The method was superior to the other methods in finding the pile deflection and the maximum moment on ten different full scale tests. A method invented by Scott (1980) performed better in the determination of the depth to the maximum moment Murchison and O'Neill (1984). The approximation made to simulate the p-y relationship for sand is given in equation (2.13), which is rearranged in order to fit into the general modulus approach.

$$K = K_{ult} \cdot \tanh \left[\frac{k \cdot z}{\sigma'_v} \cdot \frac{1}{K_{ult}} \cdot \frac{y}{d} \right] \tag{2.13}$$

A different shape of the curves was used by Kim et al. (2004). They compared 6 different methodologies to compute the curves with a set of 1g tests, and found that hyperbolic function proposed by Kondner (1963), and shown in (2.14), gave the best predictions of the test results.

$$K = \frac{y/d}{\dfrac{\sigma'_v}{k \cdot z} + \dfrac{1}{K_{ult}} \cdot \dfrac{y}{d}} \tag{2.14}$$

The two methods are similar in the way that both of them only require two parameters, the non-dimensional stiffness, and the ultimate earth pressure coefficient to generate the curves. The value of the soil resistance is then found using (2.13) or (2.14), together with (1.1).

The non-dimensional earth pressure coefficient K is described by three factors; The ultimate earth pressure coefficient K_{ult}, the non-dimensional stiffness, $\frac{k \cdot z}{\sigma_v}$ and the non-dimensional displacement, $\frac{y}{d}$. The design codes (API, 2007; DNV, 2011) recommend using an ultimate earth pressure coefficient (K_{ult}), as presented by Reese et al. (1974), but in principle the methods by (Broms, 1964; Hansen, 1961) can also be used in both methods.

The initial modulus of subgrade reaction, k can be found using a curve, as shown in API (2007). From Figure 2.3, it can be seen that there are two different curves, one for dry and one for saturated sand. It should also be noticed that there is a direct link between relative density and angle of friction, whereas it is not dependent on stress level. This is in contrast to the general accepted observation of Bolton (1986).

Non-linear springs are used in a numerical model for the design of monopiles for offshore wind turbines and enable the designer to calculate a static load response curve for a given pile. The effect of cyclic loading is taken into account through the factor A. Thereby, the maximum bearing capacity used in a ULS/ALS calculation can be found. This results in one overall stiffness and one maximum deformation/rotation due to cyclic loading, which is used in the SLS & FLS analysis.

2.2.1 Comments on recent design methodology

The main limitation of the current design methodology for monopiles is that it uses a semi-empirical approach, based on testing on slender piles. The monopile foundation for offshore wind turbines tends to behave in a more rigid way. This is illustrated in Figure 3.19, showing a comparison between a rigid pile and a slender pile. It can be seen that a rigid pile tends to rotate around a rotation point and thereby generates soil pressure over the total length of the pile. A slender pile will not have a single rotation point, rather the pile deflects around multiple rotation points. The load is mainly taken by

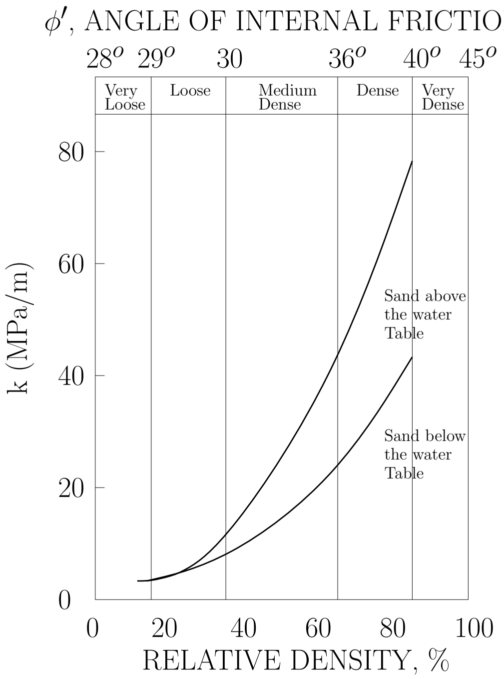

***Figure 2.3**: Initial subgrade modulus as a function of angle of friction, after DNV and RISØ (2001)*

the upper layers and no deflection will develop at the pile toe. The effect of moving from a slender pile behavior to a more rigid pile behavior can change the response of the pile (Poulos and Hull, 1989). Using a semi-empirical approach that is not calibrated to the given pile behavior should be avoided. The main differences between the original test piles and the piles used today for wind turbines are; a) the diameter of the piles is 5-10 times larger, b) they behave in a rigid way and c) the ratio between moment and shear force is much larger. Five main effects have to be investigated in order to verify that the current practice is valid also for rigid large diameter monopiles for offshore wind turbines. 1) The diameter effect, does the non-dimensional soil resistance change if the diameter of the pile is changed? 2) How does the vertical effective soil stress influence the response of the pile? 3) The failure mechanism of the sand changes down through the soil but is it also affected of by how the load is applied? 4) The influence from cyclic loading. In short:

- Diameter, $K = f(d)$?
- Stress, $K = f(\sigma'_v)$?
- Failure mechanism, $K = f(z/d)$ or $K = f(l_e/d)$?

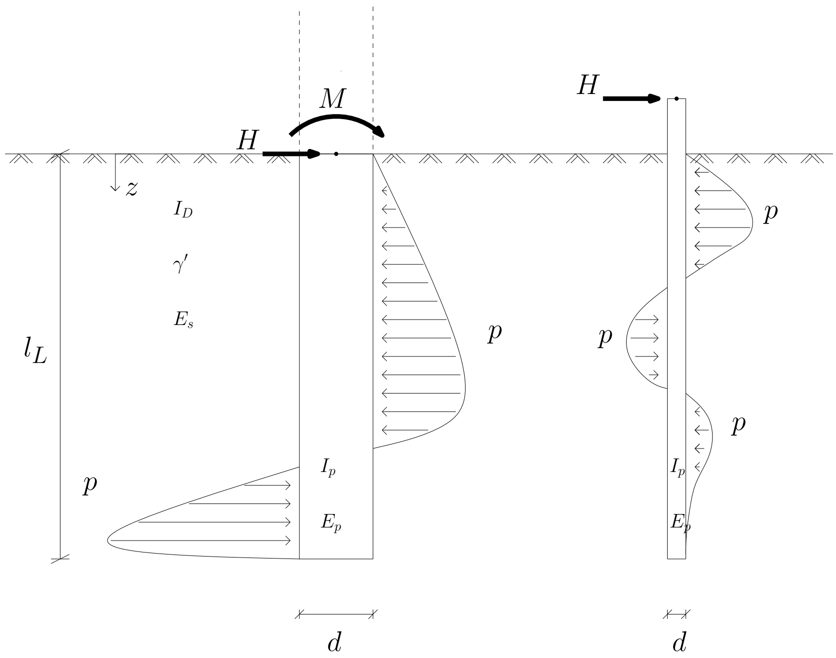

Figure 2.4: *Monopile vs. offshore pile*

- Cyclic loading, $K = f(N, \zeta_b, \zeta_c)$?

The three first items can be investigated by monotonic tests and the cyclic loading from waves and wind is normally investigated by quasi-static cyclic load tests. The influence on the ultimate capacity is crucial for all of the four points, but the stiffness is even more important for monopiles supporting wind turbines.

To investigate these effects, it is important to secure that only the factor which is under investigation is changed. As an example; if the diameter effect is investigated, only the diameter of the pile should be changed, full similarity in the geometry should be kept,($const. = \frac{l_L}{d}$, $const. = \frac{l_e}{d}$ & $const. = \frac{E_p I_p}{E_s e_L^4}$) and also identical soil conditions should be retained.

2.3 Recent research

Significant research has been carried out in the past to improve the understanding of monopile behavior. A table with pile dimensions and load conditions is given in table 2.1 to a give an quick overview of some of this research. The different types of experimental models are here defined; 1g for a scaled experiment performed at 1g, ηg is a scaled experiment performed in a centrifuge, fs denotes full scale measurements and num denotes numerical simulations. The investigations are divide into two sections: One concerning the monotonic response, and one for the cyclic response. Only a short presentation of the research is provided here and common findings are highlighted.

***Table 2.1**: Schematic representation of the review*

Author	Model	Proto. Dia. d [m]	Load ecc. l_e/d	Pene. depth l_L/d	Num. of cycle N [-]
Lesny and Wiemann (2006)	num	1-6	?	6.5-10.6	1
Sørensen et al. (2009)	num	1-7	?	2.9-20	1
Augustesen et al. (2009)	num	4	5.2	6	1
A.-R. and Achmus (2005)	num	7.5	0.2-1	2.7-4	1
Fan and Long (2005)	num	0.3-1.2	0.5	34.4	1
Zhang et al. (2005)	fs-ηg	?	0-27	4.4-16	1
Ashford and Juirna.. (2003)	fs	0.4-1.2	0.4-1.2	10-20	1
Hald et al. (2009)	fs	5	?	6	1
Achmus et al. (2009)	num	1.9	8.8-13.7	7.7-9.5	10000
LeBlanc et al. (2010a)	1g	4	4	5.4	65000
Leblanc et al. (2010b)	1g	4	4	5.4	1000
Peralta and Achmus (2010)	1g	-	4	3.3-8.3	10000
Cuéllar et al. (2009)	1g	7.5	4	4	5000000
Li et al. (2010)	ηg	5	14.4	5	1000
Rosquöet et al. (2007)	ηg	0.72	16.7	3.4	44

2.3.1 Monotonic response

The monotonic response has been investigated by different authors and the conclusions of the findings are contradictory. The ultimate capacity was studied by Zhang et al. (2005), who collected data from 17 different tests both centrifuge and full scale. They presented a method to determine the ultimate capacity of a pile. The model consists of a contribution from the side friction and the resultant soil pressure. The best result was obtained by using Rankine's passive soil pressure coefficient squared for the ultimate soil pressure.

The initial stiffness was investigated by Ashford and Juirnarongrit (2003) and Fan and Long (2005) and they agreed with the original assumption by Terzaghi (1955) that there is no effect from the diameter on the initial stiffness of the pile-soil interaction curves. This is also the conclusion reached by Pender et al. (2007), who compared a series of full scale tests stating that the apparent diameter size effect is a consequence of the distribution of the soil modulus. On the other hand, numerical modelling by Lesny and Wiemann (2006) and Sørensen et al. (2009) suggests an effect of changing the diameter on the initial stiffness of the pile-soil interaction curves.

The general tendency for the different research performed on monopiles is that the current design values of the subgrade modulus, k as shown in figure 2.3, are too large, e.g. Rosquöet et al. (2007), Lesny and Wiemann (2006), Abdel-Rahman and Achmus (2005) and Augustesen et al. (2009). The problem with these findings is that they contradict the findings from full scale monitoring on monopiles, which states that the recommenced value is too small, Hald et al. (2009).

2.3.2 Cyclic response

Cyclic loading is a complex load situation and as a first attempt many researchers have investigated the over all response of piles to understand the problem. LeBlanc et al. (2010a) performed a 1g experiment on a scaled monopile subjected to cyclic lateral loading. Accumulation of rotation and change in secant stiffness was observed. The accumulation model is assumed to follow a power law, this was proposed earlier by Long and Vanneste (1994) for slender piles and also seen by the test by Peralta and Achmus (2010). As a contrast to this, accumulation of displacements observed in centrifuge tests by Rosquöet et al. (2007) and Li et al. (2010), were seen to follow a logarithmic trend.

As an extension of previous studies, Leblanc et al. (2010b) further developed the model to handle random cyclic loading. The model is based on Miner's rule and was validated by a set of experiments with the same setup as used in LeBlanc et al. (2010a). The total framework from (LeBlanc et al., 2010a; Leblanc et al., 2010b) enables the designer to calculate accumulation of rotation and increase in stiffness if the monotonic load-response curve and the load-history is known.

Another scale experiment was performed by Cuéllar et al. (2009). They performed one cyclic load test on a monopile installed in saturated dense sand loaded with 5.000.000 one-way cycles. The magnitude of the cyclic loading was selected to correspond to offshore conditions for a monopile supporting a wind turbine. The main result of this investigation was that the accumulation of rotation changed after around 100.000 cycles. By using colored sand and by performing a vertical cut in the sand next to the pile after the test, an indication of the sand movement in front of the pile was obtained. They concluded that a convective domain was created and sand was traveling from sand surface and down to a given point in the sand layer and then up again.

During the background review, no pile-soil interaction curves from cyclic loading on monopiles was found in the investigated literature. For application in seismic engineering attention has been paid to cyclic interaction curves on long slender piles. Cyclic curves were derived from centrifuge tests by Rosquöet et al. (2007) and a change in stiffness was found and these curves showed hysteretic behavior. They concluded that the ultimate soil resistance decreases due to the cyclic loading of the sand.

Achmus et al. (2009) developed a 3D finite element model of a monopile to predict the response from cyclic loading. Cyclic triaxial tests were used to calibrate the elasto-plastic Mohr–Coulomb constitutive model. This was achieved by degradation of the soil stiffness which allows the pile to accumulate displacements. Design charts were developed from different calculations using this finite element model . These charts can be used to predict the accumulation of displacement for a monopile supporting an offshore wind turbine.

2.3.3 Comments to recent research

Different research activities have been presented and there is not clear agreement on how to deal with possible diameter effects, failure mechanisms etc. The increase in subgrade modules was seen to increase proportionally with the depth by Ashford and Juirnarongrit (2003) and Fan and Long (2005). However, the investigation were based on slender piles. Lesny and Wiemann (2006) and Sørensen et al. (2009) report a diameter effect, in their research the geometrical similarity was not kept constant, which could influence the failure mechanisms. Full scale measurements report a completely different behavior to that observed in model tests. The different observations reported show that there is still a need to improve the knowledge of rigid laterally loaded monopiles, not only for cyclic loading but also for monotonic loading. A more general model describing the soil pile interaction is needed. The model by Achmus et al. (2009) uses a degradation model of the stiffness, which means that the cyclic response becomes softer with the number of cycles. This is not the behavior seen from physical tests and the model can therefore only be used to predict the accumulation of displacement and not the stiffness of the pile - soil interaction.

The response of a monopile supporting an offshore wind turbine is still not well described and more research is therefore needed. In order to investigate the response of a monopile, it is important to investigate the different effects, one at a time. Only in this way, is it possible to determine the effect of each parameter. In the establishment of a more general model that can handle both monotonic and cyclic loading, it could be relevant to use methodologies from seismic design. This could be a Winkler model with a cyclic spring element. Such an element is capable of handling cyclic loading and introduce frictional damping into the system. In this respect, inspiration from the models by Boulanger et al. (1999) and Taciroglu et al. (2006) seems to be appropriate.

Chapter 3

Methodology

Using different methodologies to investigate a given problem will often lead to more reliably results. A triangulation where the problem is investigated using different methods is preferable. This is illustrated in Figure 3.1.

Full scale testing or monitoring is one method which can be used. The big advantage of a method like this is that the testing is performed on a real size structure. This secures that what you measure is a real physical event in the scale that you want to investigate. The disadvantage is that it can be difficult to estimate the soil profile and the load conditions. Furthermore, it is also a expensive way of testing or monitoring. This will often lead to only one or very few tests still the results from these tests are, if uncertainties can be controlled, of high credibility.

On the other hand, testing on a scaled model enables the researcher to create artificial scaled soil profiles; the loading is easier to control and due to the smaller scale it is cheaper to perform, which makes it possible to perform more tests. Testing on a scaled model is also a real physical event, but the results from these tests have to be translated to a larger scale, which can be challenging. The price is smaller and the number of tests can be increased. The results from these test are, if scaling issues are controlled, of a reasonable credibility.

A third method is to create a numerical model which can be used in similar investigations. This is a relatively cheap method which makes it possible to investigate a large number of possible scenarios. Another advantage in numerical modelling is that it gives the researcher the possibility to look in details into the soil-pile response, e.g. stress - strain curves at a given point. The disadvantage is that this is not a real physical event; this means that you need constitutive models that reflect the real physical event. If the numerical model is calibrated to real physical events the method has a good credibility.

Evidently different research methods can be used and the advantages from

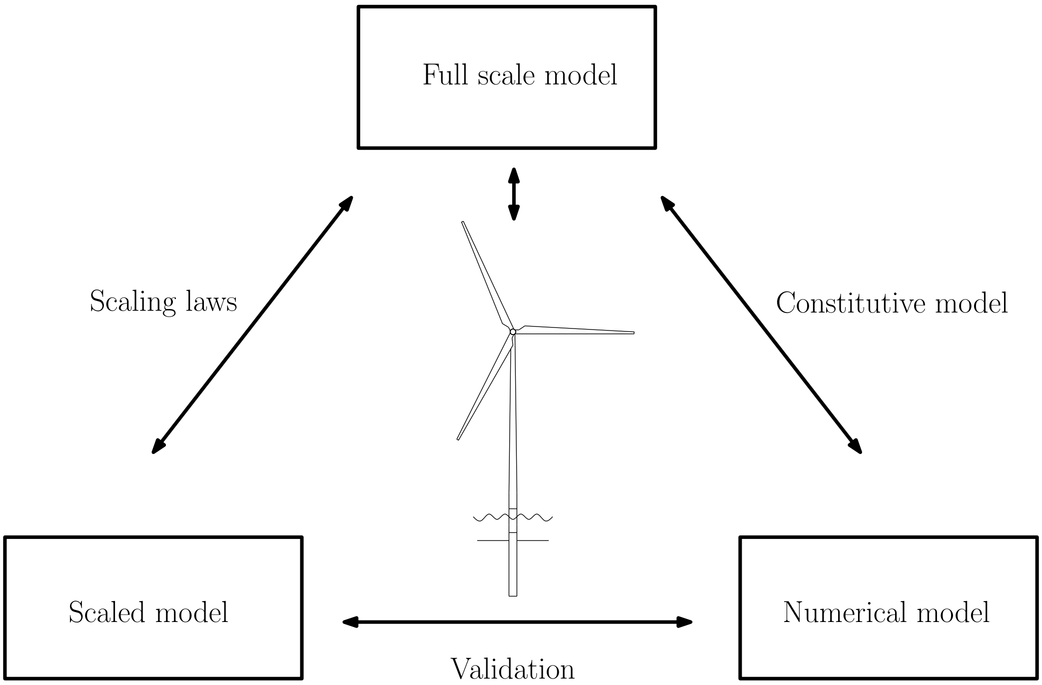

Figure 3.1: *Schematic view of research strategy*

the different methods can be combined. The preferable methodology is to combine all three methods, but money and time may be a challenge. In this thesis numerical and physical modelling is used to investigate the pile-soil interaction for laterally loaded monopiles. This enables a calibration and verification between the physical event and the numerical model and thereby gives a good robust tool in the investigation of the problem. The establishment of a numerical model have not been a part of this thesis, therefore only results presented in (Svensson, 2010; Zania and Hededal, 2011, 2012) will be used.

The findings in this thesis is therefore based on physical modelling and the results from the numerical model is used as a verification on the reliability of the results.

3.1 Physical modelling

The intention of physical modelling is to study the behavior of a given prototype. Physical modelling can be performed as full scale testing but is often used in a reduced scale. The physical modelling presented in this thesis will be based on a set of centrifuge model tests. Dimensional analysis is here used to deduce dimensional products which are used to transform model observation to prototype. The idea is that these non-dimensional products are identical and scale independent. For piles this implies that a possible diameter effect is neglected.

3.1.1 Dimensional analysis

The basic idea in dimensional analysis is that the governing parameter is a function of a set of known independent variables. The goal of the analysis is to reduce the number of parameters and to form dimensionless groups which can be used in the extrapolation to prototype, Fuglsang and Ovesen (1988).

The basis for the dimensional analysis is the Buckingham Theorem which states that if an equation is dimensionally homogenous, it can be transformed to a set of dimensionless products. Langhaar (1951)

The first thing to do in a dimensional analysis is to identify the governing parameters. This requires some initial knowledge to the problem which can be found in e.g. Reese and Impe (2001), Randolph (2003) or Bhattacharya et al. (2011). For a laterally loaded stiff monopile the response is assumed to depend on a set of parameters as shown in (3.1). In this thesis only quasi static monotonic and cyclic loading will be investigated. This implies that no inertia forces are affecting the response and also that only the fully drained case is considered.

$$0 = f(H, p, y, l_e, l_L, d, E_s, E_p, I_p, \gamma', \phi, d_{50}) \Leftrightarrow f(\pi_1, \pi_2, \pi_3, ...) = 0 \tag{3.1}$$

The governing parameters are; lateral load H, soil resistance p, the corresponding displacement y, the load eccentricity l_e, the pile penetration depth l_L, the diameter of the pile d, the elasticity modulus of soil and pile E_s and E_p, the moment of inertia of the pile I_p, the effective density of the soil γ', the angle of friction of the soil ϕ' and the average size of the sand grains d_{50}.

The effective angle of friction is here considered in radians and therefore dimensionless in nature. Using a fundamental system which reduces everything to a combination of length (L), mass (M) and time (t) makes it possible to exchange parameters and the problem can be reduced to a set of non-dimensional products shown in equation (3.2)

$$\frac{H}{\gamma' d^3} = f(\frac{p}{\sigma'_v d}, \frac{y}{d}, \frac{l_e}{d}, \frac{l_L}{d}, \phi, \frac{E_s l_L^4}{E_p I_p}, \frac{d_{50}}{d}) \tag{3.2}$$

Here it be can seen that the original problem which was described by 12 different parameters is now reduced to 8 non-dimensional ratios. From this

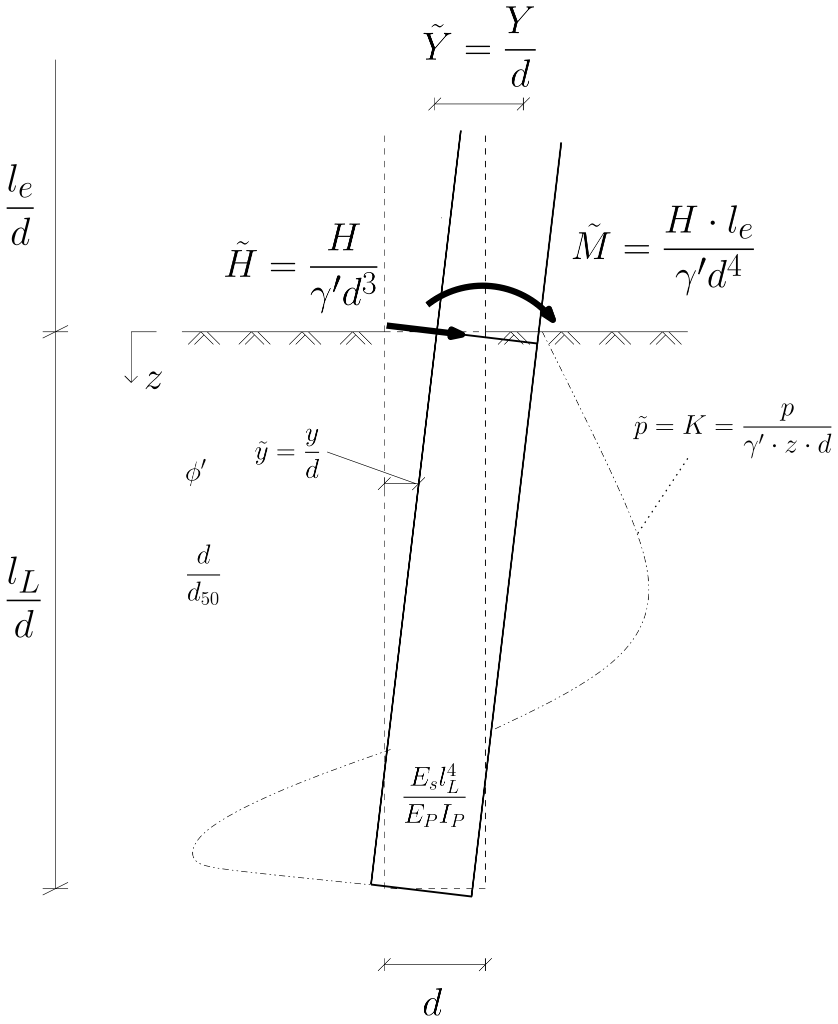

Figure 3.2: *Sketch of pile and governing parameters*

equation we define the non-dimensional parameters, first the non-dimensional horizontal shear force:

$$\tilde{H} = \frac{H}{\gamma' d^3} \tag{3.3}$$

Remembering the definition of the soil resistance shown in equation (1.1), the non-dimensional soil resistance turns out to be identical to the earth pressure coefficient K:

$$\tilde{p} = K = \frac{p}{\gamma' \cdot z \cdot d} = \frac{p}{\sigma'_v \cdot d} \tag{3.4}$$

The geometrical dimensions are all divided with the diameter, leading to the non-dimensional displacement given as:

$$\tilde{y} = \frac{y}{d} \tag{3.5}$$

All of these non-dimensional ratios are shown in Figure 3.2. The hypothesis is that if all these quantities are identical the normalized response is also identical. For a more in-depth review of dimensional analysis see e.g. Wood (2004).

To demonstrate the scaling methodology two Abaqus models were created by Svensson (2010) and Zania and Hededal (2011) and the total response of the piles are presented here. The first model was identical to a centrifuge experiment made on a pile with a diameter of $d = 28mm$, Svensson (2010). The second model was made as the equivalent prototype with a diameter of $d = 2m$, Zania and Hededal (2011). The results from the two calculations

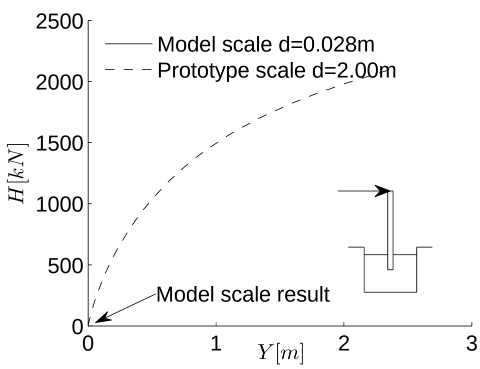

***Figure 3.3**: Abaqus calculation in model and prototype scale*

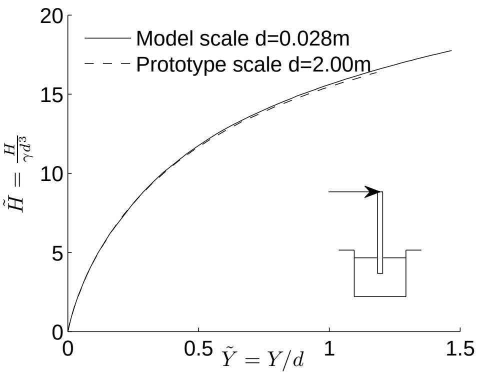

***Figure 3.4**: Normalized response of Abaqus calculations*

shown in the respective scales can be seen in Figure 3.3. Here it can be seen that the magnitude of the response is very different. In Figure 3.4 the normalized responses are shown. It can be seen that if full similarity between the models is achieved the normalized results from tests at different scales are identical.

Similarity

From the dimensional analysis a function of independent dimensionless parameters was identified. The principle is that if all these dimensionless parameters are kept constant, identical normalized results are achieved independent of scale. The geometrical size of the model is easy to scale down still maintaining full similarity. The properties of the sand (ϕ' & E_s) on the other hand are stress dependent which implies that identical stresses in model and prototype are needed in order to maintain similarity. Gravitational acceleration can be increased to achieve this by increasing the effective density corresponding to the geometrical scaling factor (N_s). This can be achieved in a centrifuge. The last parameter in (3.2), the ratio between the grain size and pile diameter, is very difficult to maintain constant between model and prototype. If the grain-size is reduced according to the linear length scale the mechanical properties of the soil are likely to be changed. Here is chosen to use sand with the same grain-size as in a prototype case. The influence from the lack of similarity therefore has to be investigated.

3.2 Centrifuge modelling

To secure stress similarity the soil sample is placed in a centrifuge. The rotation of the centrifuge will introduce an increased gravitational force. The geotechnical centrifuge at DTU is a beam centrifuge, shown in figure 3.5. The

Figure 3.5*: Picture of the geotechnical centrifuge at DTU under testing*

centrifuge facility at DTU was constructed in 1976 and has been upgraded over the years. The capacity of the beam centrifuge is approximately 100 g ton and is capable of providing an artificial gravitation of around 90g, Fuglsang and Nielsen (1988). The maximum arm or radius of the centrifuge is 2.63 m. The increase in gravity (η) can be calculated from Newton's second law of motion as:

$$\eta = R\omega^2/g \tag{3.6}$$

In (3.6) R is the radius to the point of interest, ω is the rotational frequency and g the natural gravity acceleration. The model monopile is placed in the soil container and a loading actuator is mounted on top of the soil barrel. The load setup allows for in-flight installation and lateral loading with high eccentricity. The changes was made to simulate full scale conditions better and because initial observation reported by (Klinkvort et al., 2010; Klinkvort and Hededal, 2010) indicated that it was important to the modelling.

The monopile is installed in-flight by a jack with a deformation controlled rate of 2 mm/s. The pile ready for installation is shown in Figure 3.6. The jack is electrically powered and has a capacity of 20 kN. After monopile installation, the jack is removed and a beam for lateral loading is mounted. The fully equipped monopile ready for a lateral load testing is shown in Figure 3.7. A sketch of the setup is shown in Figure 3.8. The radius to the

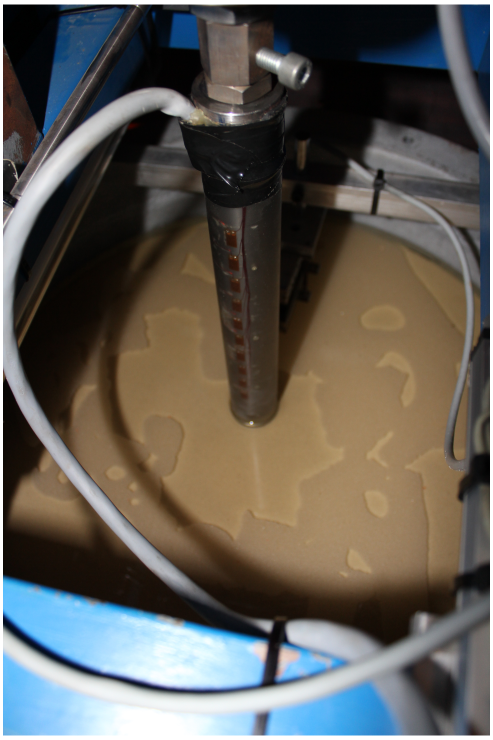

Figure 3.6: *Photo of the setup before installation*

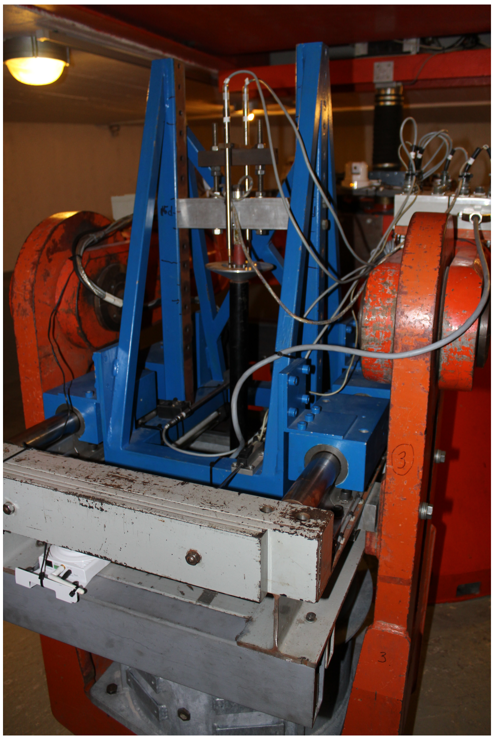

Figure 3.7: *Photo of the setup before laterally loading*

sand surface with this setup is $R_t = 2.221m$. This is the basis load setup as used today, and the main results presented in this thesis are all from this setup.

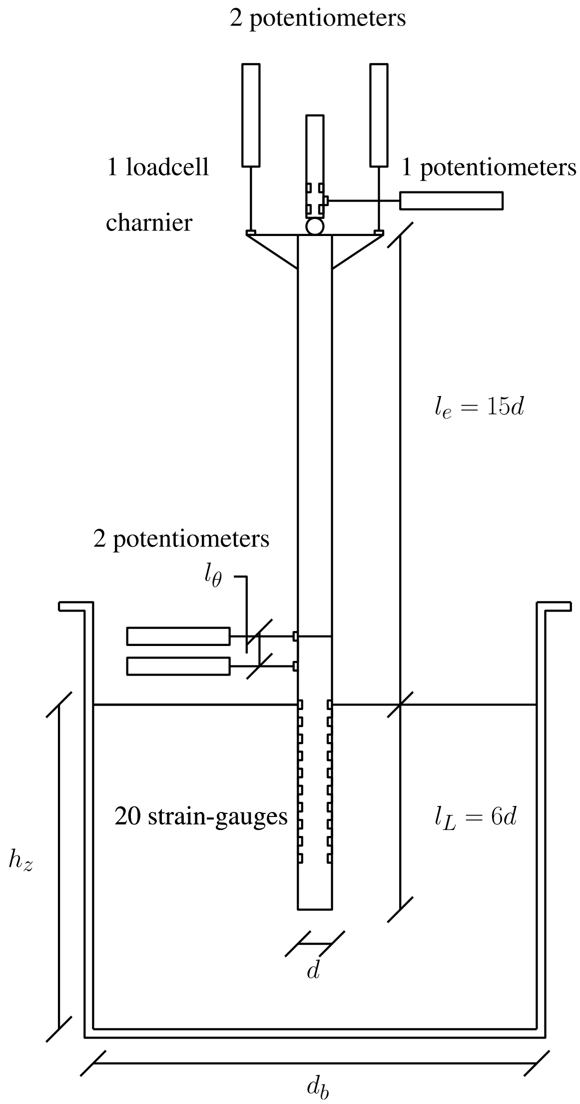

***Figure 3.8**: Sketch of centrifuge test setup*

The loading configuration provides a flexible setup which enables the use of different piles. In Figure 3.7 the pile mounted with strain-gauges is shown. To investigate the monopile-soil interaction two strain-gauge mounted monopiles have been developed. These two piles are shown in Figures 3.9 and 3.10.

Figure 3.9: *Photo of the model monopile mounted with five strain-gauge half bridges*

Figure 3.10: *Photo of the model monopile mounted with ten strain-gauge half bridges*

The first pile shown in Figure 3.9 has a 24 mm solid steel core. On this steel core five Wheatstone half-bridges are glued on and afterwards a 2 mm epoxy layer is applied resulting in a total diameter of 28mm. The five Wheatstone strain-gauge bridges are placed with a spacing of one diameter starting one diameter under sand surface. The construction of the second pile shown in Figure 3.10 is similar. Here the steel core is 36mm and with the epoxy coating the total diameter reaches 40 mm. 10 strain-gauge Wheatstone bridges are mounted with a spacing of a diameter starting with the first level at sand surface. From the strain-gauge Wheatstone bridges the moment in the pile can be measured and from these measurements the pile-soil interaction can be calculated.

The formulation of the beam-column on a flexible foundation was derived by Hetenyi (1946) and is here shown for a pile without any axial load component.

The governing differential equation neglecting the axial force is written as:

$$0 = E_p I_p \frac{d^4 y}{dz^4} - E_{py} y \tag{3.7}$$

In this equation: $E_p I_p$=bending stiffness, y=lateral deflection of the pile at a point z along the length of the pile. The bending moment in the pile is found from integration of (3.7) twice.

$$m = E_p I_p \frac{d^2 y}{dz^2} \tag{3.8}$$

From (3.8) it can be seen that the moment integrated twice with respect to the stiffness is the deflection. This is written as:

$$y = \int\int \frac{m}{E_p I_p} dz dz \tag{3.9}$$

and from (3.7) it can be seen that the soil resistance can be found by differentiating the moment twice.

$$p = \frac{d^2 m}{dz^2} \tag{3.10}$$

It is here important to remember that the soil resistance p is not only the soil pressure, but the total resistance from vertical/horizontal frictions, active/passive soil pressures. The soil resistance p is therefore easily used in the modulus approach showed in (1.1).

The procedure is to fit the moment distribution with a sixth order polynomial and afterwards calculate the pile displacement and soil resistance from this. Different methodologies in the fitting of the moment distribution was carried out e.g. Yang and Liang (2006). The sixth order polynomial was chosen because it could be fitted to the measured moment distribution with a high degree of precision and that afterwards it is easy to integrate and differentiate.

The sixth order polynomial is written as:

$$m(z) = c_6 z^6 + c_5 z^5 + c_4 z^4 + c_3 z^3 + c_2 z^2 + c_1 z + c_0 \tag{3.11}$$

From this moment fit the displacement of the pile can be found by a double integration of the moment curve. The two integration constants turns out to be the rotation and the displacement at soil surface,

$$y = y_0 - \theta_0 z - (\frac{c_6 z^8}{56} + \frac{c_5 z^7}{42} + \frac{c_4 z^6}{30} + \frac{c_5 z^5}{20} + \frac{c_2 z^4}{12} + \frac{c_1 z^3}{6} + \frac{c_0 z^2}{2})/EI \tag{3.12}$$

The soil resistance is found to be a double differentiation of the moment fit, this is written as:

$$p = 30 c_6 z^4 + 20 c_5 z^3 + 12 c_4 z^2 + 6 c_3 z + 2 c_2 \tag{3.13}$$

The pile-soil interaction can then be found knowing the boundary conditions at sand surface. As shown in Figure 3.8 the displacement and rotation is measured above the sand surface. These measurements therefore have to be scaled down to the sand surface. This is easily done due to the linear moment distribution in the monopile above sand surface.

The loading setup of the monopile is based on a feedback controlled LabView code developed under this thesis which controls and collects the data under testing. This setup can perform deformation controlled monotonic testing, deformation and force controlled cyclic testing, and mounted with the loading jack it can perform CPT testing and pile installation. The sample rate of the data is $10Hz$ which is needed in the feedback control algorithm. It consist of 16 channels for strain-gauge measurements, 16 channels for potentiometer measurements, and two output channels used to control the loading equipment under testing.

3.3 Soil testing

The centrifuge tests are all performed in dense homogenous Fontainebleau sand with a relative density of approximately 90% in order to model the North Sea offshore conditions. Leth et al. (2008) has collected classification parameters for the Fontainebleau sand, which can be seen in Table 3.1.

***Table 3.1**: Classification parameters for the Fontainebleau sand*

Specific gravity of particles	G_s	2.646
Minimum void ratio	e_{min}	0.548
Maximum void ratio	e_{max}	0.859
Average grain size	d_{50}	0.18
Coefficient of uniformity	C_u	1.6

A series of triaxial tests have been performed together with the classification parameters. 9 tests have been carried out on samples all with a relative density of $I_D = 0.9$. Four of the tests were performed on dry samples and five of the tests were performed on fully saturated samples. The triaxial apparatus uses a sample height equal to diameter and is constructed according to Jacobsen (1970).

Volume response from the four tests performed on dry samples was difficult to measured. For this reason only maximal mobilized angle of friction was found from these tests. From the five tests performed on fully saturated samples maximum angle of friction, angle of dilation and the stiffness of the sample was determined. The maximum angle of friction was found assuming no cohesion in the sand as:

$$\sin \phi'_{max} = \frac{(\sigma'_1/\sigma'_3)_{max} - 1}{(\sigma'_1/\sigma'_3)_{max} + 1} \tag{3.14}$$

In Figure 3.11 the results from the triaxial testing are shown. The maximum angle of friction is shown in the upper left corner and from this it can be seen that the results from the tests on saturated and dry sand are almost identical. This concludes that the drained behaviour is identical for saturated and dry sand. It can also be seen that the angle of friction is decreases for increasing pressure. The relation proposed by Bolton (1986) to calculated the maximum triaxial angle of friction, is written as:

$$\phi_{max} = \phi_{cr} + 3 \cdot (I_D(10 - ln(p')) - 1) \tag{3.15}$$

Assuming a critical state angle of $\phi_{cr} = 30^o$ seems to capture the behaviour of the tested sand well. This equation is therefore used in the analysis of the physical modelling. Gaudin et al. (2005) performed triaxial tests on Fontainebleau sand also for the application into centrifuge modelling. Here a critical state angle of frictions was measured to be around 30^o which fits with the observations found in this study. From equation (3.15) it can be seen

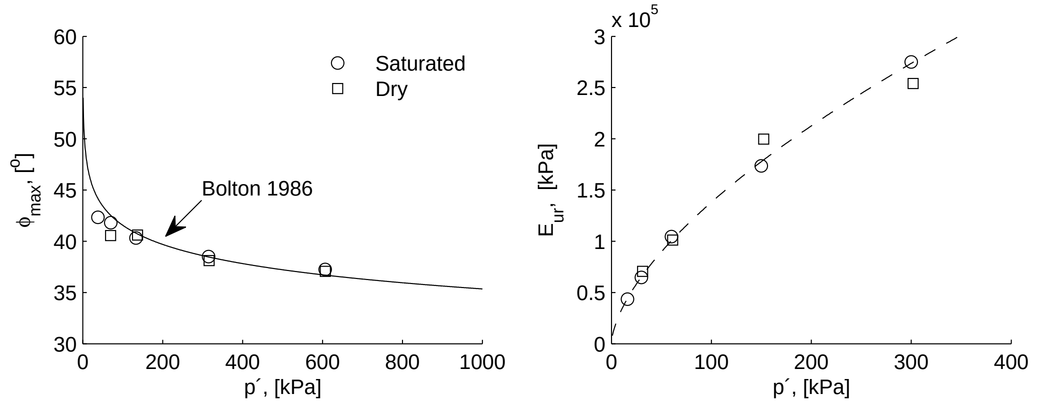

Figure 3.11: *Results from triaxial tests on Fontainebleu sand*

that the maximum angle of friction is a function of the relative density I_D and the mean pressure p'. The unloading - reloading stiffness is also shown in Figure 3.11, like the maximum angle of friction the stiffness of the sand is also depending of the soil pressure. The stiffness as a function of the mean soil pressure can be written as:

$$E_{ur} = E_0 \cdot \left(\frac{p'}{100\text{Kpa}}\right)^{0.6226} \tag{3.16}$$

Here $E_{0,ur} = 138070$Kpa for the unloading reloading stiffness.

3.4 Methodology validation

At the start of this chapter a research strategy was presented in order to investigate the soil-monopile response of a offshore wind turbine foundation. Scale experiments in a centrifuge constitute the main part of this research. The transformation of the data from one scale to another is crucial for the research and this section tries to validate or render the given methodology probable. The results from these tests are presented in the papers Klinkvort et al. (2012) and Klinkvort and Hededal (2012b). The drawing in Figure 3.12 can be used to illustrate how the different centrifuge tests are used in this process. The diameter size of the model monopiles ranges from $d = 16 - 40$mm and the prototype monopiles that is investigated is ranges from $d = 1 - 5$m. Therefore, there is a difference in scale of up to 125 times.

In order to validate the transformation of results from model scale to prototype scale, a methodology called "modelling of models" was used. The principle is to model the same prototype monopile with different sized model

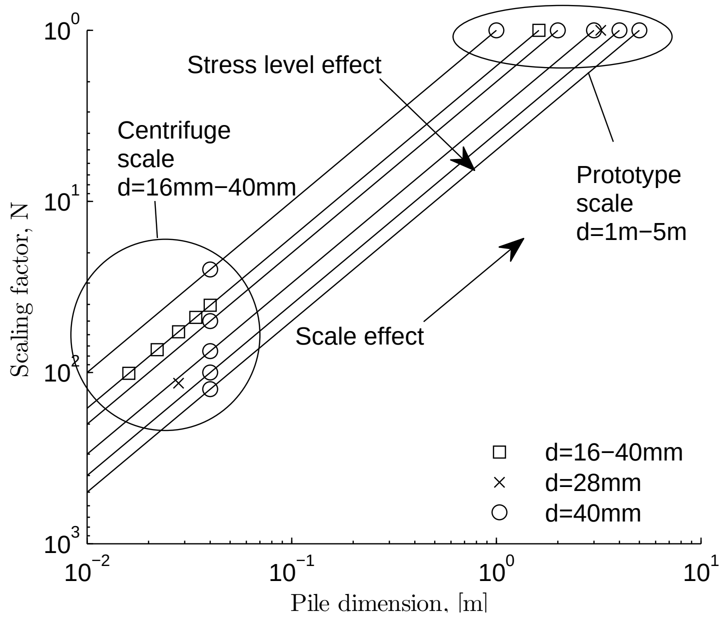

Figure 3.12: *Schematic view of model scale and prototype scale*

monopiles. By changing the acceleration level in the centrifuge nearly full similarity in the models is achieved and identical non-dimensional response should be observed. Only the ratio between grain size and pile diameter is changed. These tests are shown in Figure 3.12 as squares.

After the "modelling of models" the effect from changing the stress field was investigated. Here different stress fields corresponding to different prototype diameter were applied the laterally loaded monopile, shown in Figure 3.12 as circles. In tests likes this, the stress dependent soil behavior can be investigated and the influence from this can be determined.

As a last part of the validation test program, different tests were carried out to investigate the influence of stiffness, roughness and scaling approach.

In total 37 tests were performed and the total test program can be seen in table 3.2. Most of the tests were monotonic tests performed on smooth solid steel piles. Five cyclic tests were also performed indicated by a "c" notation in the table. Two tests were performed on a hollow steel pile indicated by an "h" and one test was performed on a sandblasted pile in order to introduce a rough surface, this is indicated by an "r". Test performed in water saturated sand is indicated by an s. In the table characteristic of the sand is given by I_D and γ', the geometry of the model monopile is given by d, l_e, and l_L, the scaling factor N_s and acceleration at which the pile was installed at.

Table 3.2: *Test program. c=cyclic, h=hollow, r=rough, s=saturated*

Test nr	I_D	Effective density, $[kN/m^3]$	Model. dia. d [mm]	Load ecc. l_e/d	Pen. depth l_L/d	Scaling factor N_s	Install. accel. $[g]$
1	0.86	16.4	16	2.5	6	62.5	1
2	0.86	16.4	22	2.5	6	45.5	1
3	0.90	16.6	28	2.5	6	35.7	1
4	0.83	16.4	34	2.5	6	29.4	1
5	0.92	16.6	40	2.5	6	25	1
6 c	0.80	16.5	16	2.5	6	62.5	1
7 c	0.90	16.6	22	2.5	6	45.5	1
8 c	0.90	16.6	28	2.5	6	35.7	1
9 c	0.86	16.4	34	2.5	6	29.4	1
10 c	0.94	16.7	40	2.5	6	25	1
11	0.92	16.7	16	15	6	62.5	1
12	0.92	16.7	16	15	6	62.5	1
13	0.84	16.4	22	15	6	45.5	1
14	0.86	16.5	28	15	6	35.7	1
15	0.90	16.6	34	15	6	29.4	1
16	0.89	16.6	40	15	6	25	1
17	0.90	16.6	16	15	6	62.5	η
18	0.84	16.4	22	15	6	45.5	η
19	0.96	16.8	28	15	6	35.7	η
20	0.89	16.5	34	15	6	29.4	η
21	0.89	16.4	40	15	6	25	η
22	0.85	16.4	22.4-21.8	15	6	45.5	η
23	0.90	16.6	28.7-27.7	15	6	35.7	η
24	0.91	16.6	35.0-33.5	15	6	29.4	η
25	0.84	16.4	41.4-39.3	15	6	25	η
26	0.93	16.7	40	15	6	25	$\eta/3$
27	0.93	16.7	40	15	6	50	$\eta/3$
28	0.89	16.5	40	15	6	75	$\eta/3$
29	0.86	16.4	40	15	6	100	$\eta/3$
30	0.95	16.8	40	15	6	125	$\eta/3$
31 h	0.93	16.7	40	15	6	75	$\eta/3$
32 h	0.88	16.5	40	15	6	75	$\eta/3$
33 r	0.89	16.5	40	15	6	75	$\eta/3$
34	0.83	16.3	40	15	6	75	$\eta/3$
35 s	0.83	10.1	40	15	6	75	$\eta/3$
36	0.89	16.6	40	15	6	75	$\eta/3$
37 s	0.99	10.5	40	15	6	75	$\eta/3$

3.4.1 Scale effects

Three factors are of particular interest in the "modelling of models" analysis. First of all, the minimum ratio between in this case monopile diameter and average grain-size diameter. This investigate the influence of using the same sand in model and prototype and thereby not having similarity in the modelling of the sand grain-sizes Ovesen (1975).

Secondly; the effect of not having completely identical stress distributions. The height of the centrifuge soil model introduces a parabolic non-linear increase in soil stresses. In comparison with the linear increase that occurs in prototypes, this implies small stress errors between model and prototype. The error is often not larger than 2-3 % and is therefore usually neglected, Schofield (1980).

Finally, the effect of installation is investigated. In-flight installation is important for the vertical response of axially loaded piles. Several studies have shown that the installation method is important for the lateral response as well, Craig (1985) and Dyson and Randolph (2001). The majority of centrifuge tests on laterally loaded monopiles are still performed on piles installed at 1g, e.g. Remaud (1999), Ubilla et al. (2006) and Li et al. (2010).

The "modelling of models" technique has been used before for laterally loaded piles e.g. Remaud (1999) and Nunez et al. (1988) but not for stiff monopiles for wind turbines and normally only the grain-size effect is investigated. Monopiles for wind turbines are different from normal laterally loaded piles because they are short stiff piles subjected to a large degree of bending moment. According to the scaling catalogue from "TC2 -Physical Modelling in Geotechnics" Garnier et al. (2007) no grain size effect was detected in "modelling of models" if the ratio between pile diameter and average grain size was larger than 45, Remaud (1999) or 60, Nunez et al. (1988) for laterally loaded piles. Both of these test series were performed on long slender piles and the results from these tests should be used with caution for short stiff piles.

As an initial study Klinkvort and Hededal (2010) performed "modelling of models" on five stiff monopiles. The test data from these tests are shown in table 3.2 as tests no. 1-10. All piles were installed at 1g and here a relationship between stiffness/strength and applied gravity was reported indicating scale effects. The indication of scale effects was investigated in more detail and the results from this investigation are shown in the following.

Grain size effects

Five tests were performed on piles ranging from $d = 16 - 40mm$, installed at 1g, (Test no. 11-16). The results can be seen in 3.13. It is noticeable that the $d = 16mm$ pile the response is different from all of the others. The test

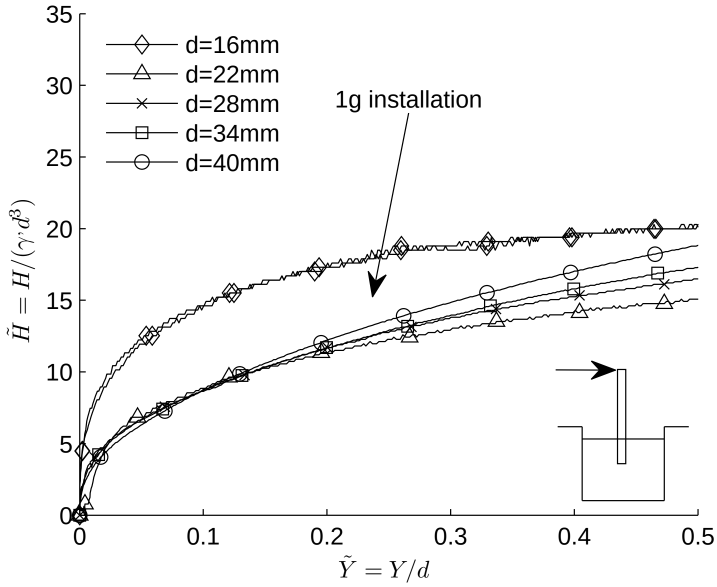

Figure 3.13: *Grain-size effect on 1g installed piles*

with a $d = 16mm$ pile was repeated with identical results. The tendency for the $d = 16mm$ pile is that it shows a large initial stiffness and that it seems to reach a failure plateau. This is clearly an outlier and it is concluded that the ratio between diameter of monopile and diameter of average grain size $d/d_{50} = 88$ is too small which leads to a grain size effect. This ratio is 30% higher than reported by Remaud (1999).

For the four other piles it can be seen that the response is more or less identical until a point of $0.1d$ deflection. At this point the piles behavior start to deviate. The capacity of the piles with large diameter increases more rapidly than the piles with smaller diameter. At a deflection of $0.5d$ the difference between $d = 22mm$ and $d = 40mm$ is about 25%. It was not possible to model identical responses with different sized monopiles with 1g installation of the monopiles .

Installation effects

The same five piles were therefore tested with an in-flight installation procedure, (Test no. 17-21). The $d = 16mm$ pile showed the same behavior as for the 1g installed pile. This confirms the observation that the ratio between diameter of pile and diameter of average grain size is too small. The $d = 16mm$ pile is therefore not shown on the further plots. In Figure 3.14 the lateral response of the 1g - and in-flight installed piles can be seen. It is clearly seen that the piles installed in-flight shows a larger initial stiffness and higher bearing capacity. This is in agreement with the observations made by Craig (1985) and Dyson and Randolph (2001). For the in-flight installed piles the response seems more identical than the piles installed at 1g, but a scale effect is seen with larger initial stiffness' for the smallest piles. This is most evident for the pile with $d = 22mm$. Also here it was not possible to

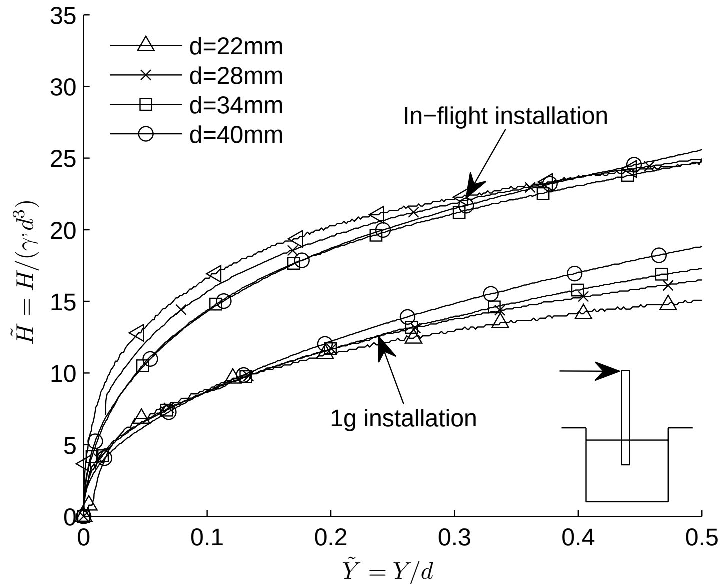

***Figure 3.14**: Effect of installation at different stress levels*

model identical responses.

Non-linear stress distribution effect

The increase in gravity depends on the radius of the rotation and is therefore not constant through a soil sample due to the increase in radius. This introduces a nonlinear stress distribution in the centrifuge soil sample. The stress distribution in the centrifuge soil sample can be written as:

$$\sigma = \int_0^z \rho\omega^2(R_t + z)dz = \rho\omega^2 z(R_t + z/2) \tag{3.17}$$

Where R_t is the radius to the sand surface and z is the distance from sand surface to the point of interest in the sand sample. The stress distribution for a laterally loaded pile should be modelled so exact stresses is achieved in the depth z=2/3L, to minimize the stress error, Taylor (1995). This implies that soil stresses are a bit too small above this point and a bit too large below as illustrated in Figure 3.15.

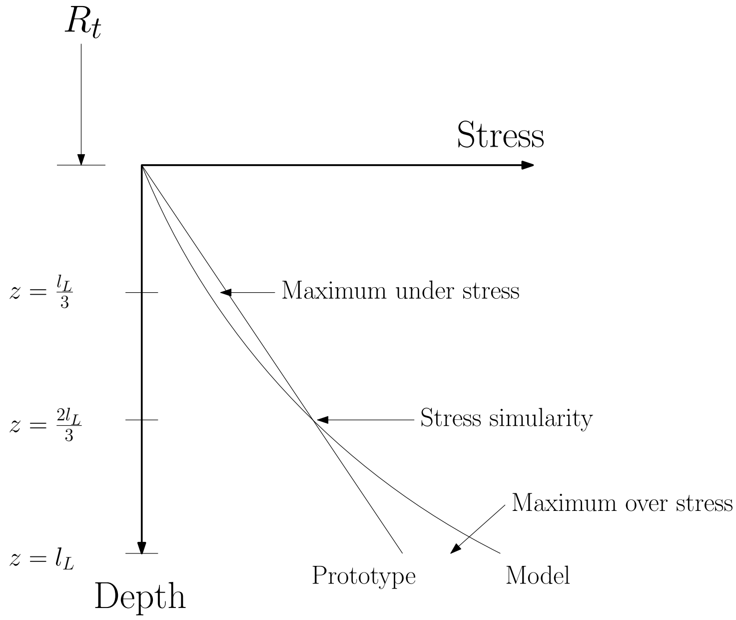

Figure 3.15: *Stress distribution difference between prototype and centrifuge model*

To see if the small difference in stress distribution is the reason for failure in the "modelling of models" approach, conical shaped piles were designed to counteract the change in g-field. Recalling (1.1) for the soil resistance,

$$p = K \cdot d \cdot \sigma'_v \tag{3.18}$$

It can be seen that if the soil stress σ_v is to small compared to prototype the diameter d can be increased in order to have a constant soil resistance p. With this in mind, five conical shaped monopiles were made so the soil resistance was identical with prototype. (Test no.s. 22-25).

The load deflection curves for the conical shaped piles are plotted in Figure 3.16 showing that a very good agreement between the results was achieved.

This demonstrates that if the diameter is larger than $22mm$, the pile is in-flight installed and the non-linear stress distribution is taken into account, one prototype monopile can be modelled using different sized pile. This is fundamental and shows that the scaling approach seems valid, and that no diameter effect is present in this range.

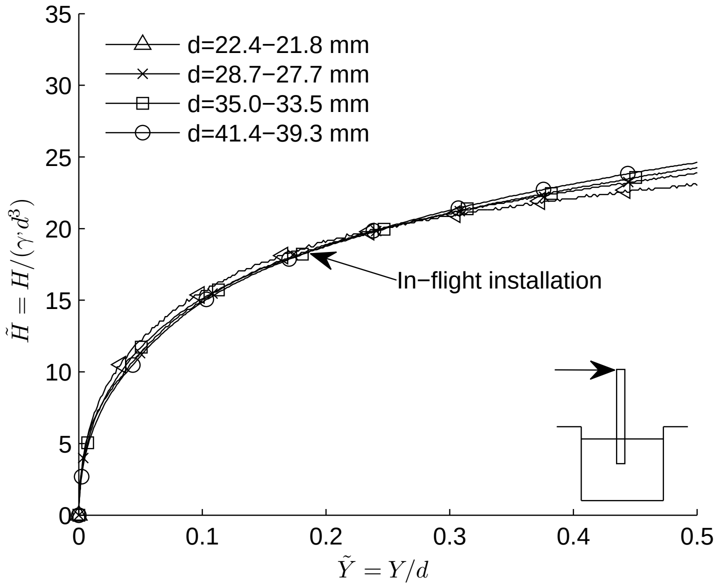

Figure 3.16: *Effect of installation at different stress levels*

Stress level effect

To investigate the stress level effect five different tests on piles with a diameter of $d = 40mm$ with stress levels corresponding to offshore monopiles ranging from 1 to 5 meters in diameter were performed (Test no. 26-30). The overall load - displacement response can be seen in 3.17. Here it is seen, that the pile subjected to the smallest stress level has the highest non-dimensional bearing capacity. The pile with the second lowest stress level has the second highest bearing capacity whereas it seems that the last three piles have identical non-dimensional responses. From the triaxial tests it was seen that the angle of friction is dependent on pressure. A representative angle of friction was calculated for the entire test series. This was carried out using the average relative density and the pressure calculated at a pile depth at 2/3 of the total length. Here it can be seen that the tests performed at low stress levels have a higher mobilized angle of friction. To take this non-linearity into account Rankine's passive earth pressure coefficient is introduced in the normalisation process shown in equation (3.19).

$$K_p = tan^2(45 + \phi'/2) \tag{3.19}$$

The non-dimensional load can then be redefined to be:

$$\tilde{P} = \frac{\tilde{H}}{K_p} = \frac{H}{K_p \cdot \gamma' \cdot d^3} \tag{3.20}$$

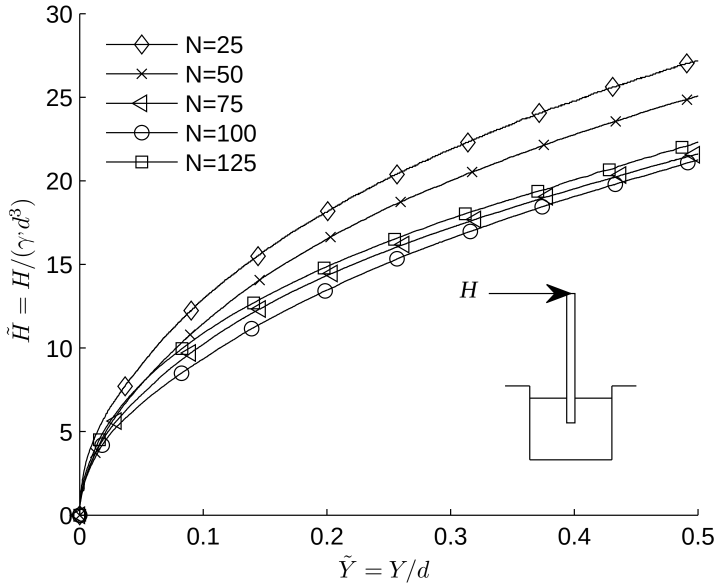

Figure 3.17: *Effect of stress levels*

In Figure 3.18 the overall response with the new normalization is shown.

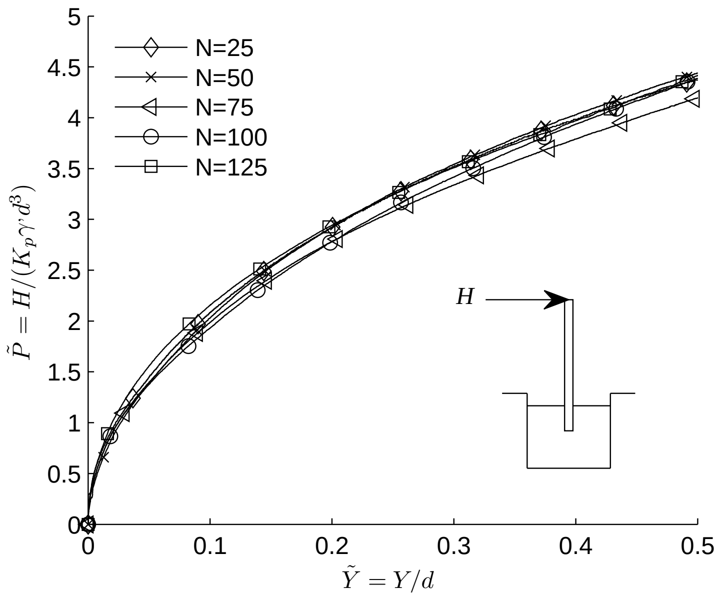

Figure 3.18: *Effect of new normalisation*

Here the response from the five different tests merge into one single characteristic curve. This shows that in these tests the nonlinear soil behavior can be taken into account only using the strength parameter. With this normalization one test can be used for any given prototype diameters. Here it is demonstrated that this is valid in the range of $d = 1 - 5$ meters, but it is assumed that this is also valid for larger diameters.

Stiffness effect

Two tests were performed with a hollow monopile in order to investigate the influence from using a solid steel monopile instead of a hollow monopile,. The hollow monopile was made of steel and the diameter was $d = 40mm$ and the thickness was $t = 2mm$. A comparison between the response from the solid monopile and the hollow monopiles was made and can be seen in Figure 3.19. Two tests were made and the results shows that the overall

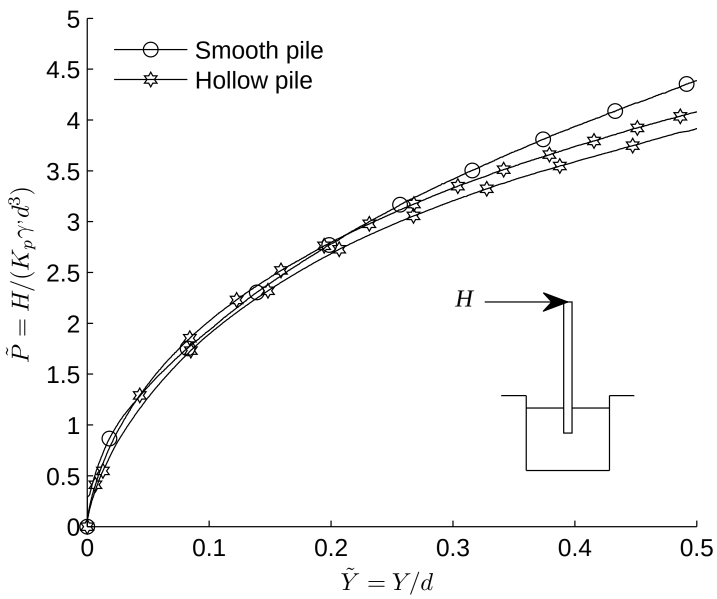

***Figure 3.19**: Effect of stiffness compared to strain-gauge mounted pile*

response is identical with the one from the solid pile (Test no. 28 & 31-32). Two conclusions can be drawn from this; first the stiffness of the piles tested is so stiff that they behave in a rigid manner with identical response as a consequence. This was also the conclusion from the numerical study done by Zania and Hededal (2011). Secondly the influence from installation of a hollow pile where soil will be trapped inside the pile seems negligible.

The non-dimensional stiffness ratio of a pile, neglecting the stiffness of the sand inside the pile, can be calculated by the criteria by Poulos and Hull (1989):

$$\frac{E_p I_p}{E_s l_L^4} = \begin{cases} > 0.208 & \text{Rigid pile behavior} \\ < 0.0025 & \text{Slender pile behavior} \end{cases} \tag{3.21}$$

The non-dimensional stiffness ratio has been calculated from the solid and hollow monopiles and is compared with fictive prototype conditions in table 3.3. From table 3.3 it can be seen that model and prototype piles all have a

Table 3.3: *Test program for validation of methodology*

Scale	Pile diameter d [m]	Pile thickness, t [m]	Pile penetration l_L [m]	Pile stiffness E_p [MPa]	Soil stiffness E_s [MPa]	$\frac{E_p I_p}{E_s l_L^4}$
Model	0.04	0.02	0.24	210000	100	0.079
Model	0.04	0.002	0.24	210000	100	0.047
Proto	4	0.05	24	210000	100	0.007
Proto	6	0.1	24	210000	100	0.052

non-dimensional stiffness ratio which is bigger than the slenderness criteria. Also it can be seen that they are all smaller than the rigid criteria meaning all piles behave in between a pure rigid and a pure slender pile. However, identical response for the piles with different stiffness ratios indicates that these piles behave in a rigid fashion. Two prototype stiffness ratios have been calculated first for a $d = 4m$ in diameter monopile compatible with the piles at e.g. Horns Rev 2 in Denmark and for a monopile with a diameter of $d = 6m$, compared with some of the newest installed monopiles in e.g. the British sector. From Table 3.3 it can be seen that the monopiles installed today is getting closer to the rigid pile criteria and that the stiffness ratio for the hollow pile corresponds well with the stiffness for the newest installed monopiles. With the identical response for the solid and hollow monopiles in mind it therefore seems valid to assume that the solid model monopiles represents a prototype monopile supporting a wind turbine in terms of stiffness.

Roughness effect

The model pile used in the later investigation of the soil-pile interaction is a strain-gauge mounted solid piles with a $2mm$ epoxy coating. This makes the pile very smooth and to give an estimate of the influence from this one test with a sand blasted surface was performed and compared with the smooth monopile (Test no. 28 & 33). The sand blasted sand surface was created in order to mimic the surface of a prototype monopile. The results can be seen

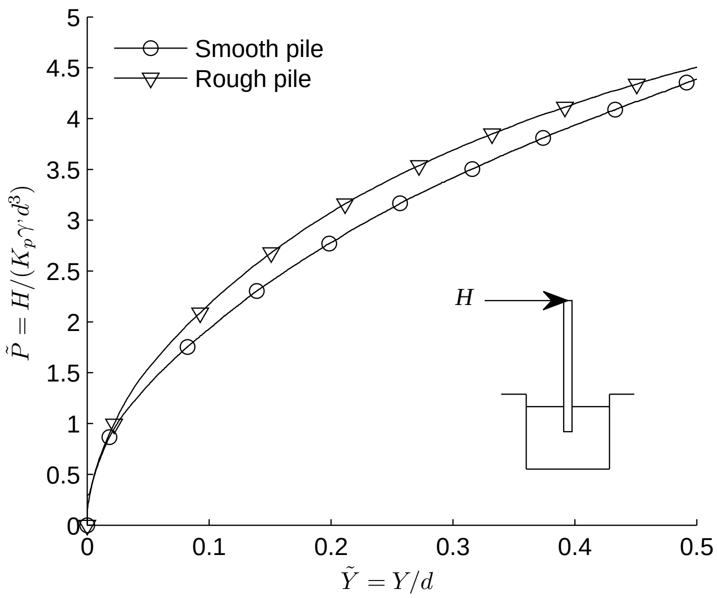

Figure 3.20: *Effect of roughness compared to strain-gauge mounted pile*

in Figure 3.20 where is the normalized response is shown. It can be seen that the response from the sand blasted pile is stiffer compare to the smooth pile. It is therefore expected that the stiffness results from the tests in this thesis is smaller compared to prototype.

Effect of in-flight installation at low elevated stress level

From the "modelling of models" test series it was seen that in-flight installation of the monopile is necessary in order to avoid scale effects. The jack, driving the piles in-flight has a 20 kN limit, corresponding to the force needed for pile with a stress distribution for a prototype diameter $d = 2m$. It was therefore chosen to install these monopiles at an elevated stress level corresponding to one third of the stress level in which the laterally loading was performed. The effect from this in-flight installation but at a lower stress level is shown in Figure 3.21. Here the response from three pile tests are shown. The three piles are installed respectively at 1g, full in-flight and at a lower stress level. As seen before the in-flight installed monopile has a stiffer response and a larger capacity than the 1g installed monopile. The

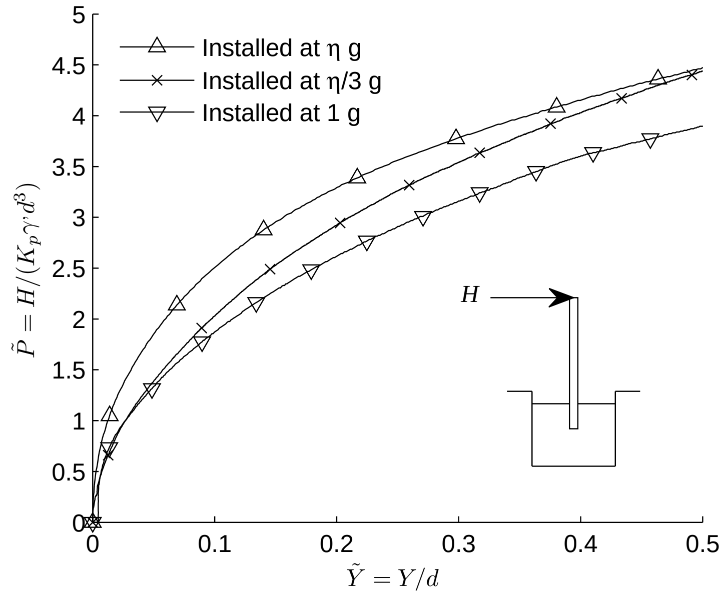

Figure 3.21: *Effect of installation at different stress levels*

monopile installed at lower stress level shows a stiffer response than the 1g installed monopile, but have a smaller stiffness than the monopile installed at full stress level. After deformation of around half a diameter the response converges with the pile installed at full stress level. It is concluded that the piles installed at a third of the full stress level has a smaller initial stiffness but the capacity is almost identical with the monopile installed at full stress level.

3.4.2 Scaling approach

The scaling approach in this thesis is designed so tests in dry conditions can be interpreted as if they were performed in saturated conditions. The basic assumption is that for a quasi static test no excess pore pressure will develop. With no excess pore pressure identical effective stress distribution in the model and prototype can be achieved. This can be written as:

$$\sigma'_{v,p} = \gamma'_{sat} \cdot z_p = \eta \cdot \gamma'_{dry} \cdot z_m \;\Rightarrow\; \eta = \frac{\gamma'_{sat} \cdot z_p}{\gamma'_{dry} \cdot z_m} = \frac{\gamma'_{sat}}{\gamma'_{dry}} \cdot N_s \qquad (3.22)$$

The increase in gravity η and the geometrical scaling factor $N_s = \frac{z_p}{z_m}$ are not identical due to the difference in effective densities. This modelling technique was used by Li et al. (2010). Four monotonic tests were performed, two in saturated sand and two in dry sand with stress levels corresponding to

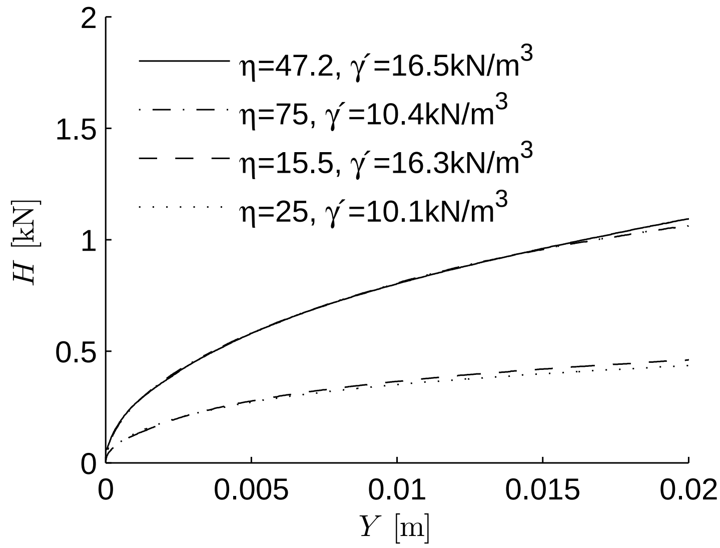

Figure 3.22: *Verification of scaling approach*

respectively 1 and 3 meter in diameter piles. The response of the two tests with a stress distribution corresponding to a one meter diameter pile and the two tests with stress distributions identical to a three meter diameter monopile, can be seen in Figure 3.22 in model scale which shows identical responses. Even though the relative density for the different tests is not 100% identical the difference is so small that it does not affect the results. This confirms the scaling approach as long as fully drained conditions are achieved.

3.4.3 Measurement uncertainties

Testing is always affected by uncertainties; this section tries to quantify the different uncertainties and the effect of these. Two types of measuring devices are used, potentiometers or strain-gauge based load devices. All potentiometers and strain-gauge devices have been calibrated several times during the thesis each time shoving a linear response with only small deviations in the calibration constants. The scatter on the data from the potentiometers are around $1/100mm$ and the error in the calibration constant is estimated to be around 0.5%. The scatter of the strain-gauge based devises is around 1N for the load cell used for laterally loading and around 1Nm for the strain gauge mounted piles. The error of these measurements is a bit larger and estimated to be 2% The validation process shows that using the presented instrumentation and using the given test methodology identical responses can be modelled. This shows that tests can be repeated with identical results as a consequence. This is off course what is sought after and shows that the uncertainties involved in testing are neglectable.

The tests presented previously have all looked at the total response. The pile-soil response in this thesis is found from the moment distribution in the pile. While the deflection of these pile - soil interaction curves are well described it is important to remember that the soil resistance due to the double differentiation can be affected by uncertainties of up to 35%, Rosquoët et al. (2010).

3.5 Summary of methodology validation

37 tests have been performed in order to validate the centrifuge modelling approach. Different factors have been identified and have to be taken into account when the centrifuge tests is used in the investigation of piles in prototype scale. The conclusions are here listed:

1. Identical responses can be modelled using the "modelling of models" approach if, the diameter is larger than $22mm$, the pile is in-flight installed and the non-linear stress distribution is taken into account.

2. Using Rankines passive earth pressure coefficient as a normalisation parameter, one centrifuge test can be interpret as a pile with diameters in the range of $d = 1 - 5$ meters.

3. The solid and hollow model piles shows identical responses.

4. Rough pile shows a stiffer response compared to a smooth pile

5. Piles installed at a third of the full stress level has a smaller initial stiffness but the capacity is almost identical with the monopile installed at full stress level.

6. Using an effective stress scaling approach test in dry sand can represent saturated drained conditions.

Chapter 4

Pile - soil interaction results

In the previous chapter, the centrifuge modelling approach was validated by a series of simple monotonic load tests. The tests were performed on solid steel piles with no instrumentation and only the total response was of interest. To investigate the pile - soil interaction in more details monotonic and cyclic tests have been performed on instrumented model piles. 37 tests have been performed in this investigation , see table 4.1.

An initial study of 9 monotonic and 6 cyclic test were performed on a $d = 16mm$ monopile (Test no. 38-52), these tests are presented in Klinkvort et al. (2010). With the conclusion drawn from this study the load setup was changed and the new load control algorithm was written in order to have a better control of the cyclic loading.

A test series consisting of one monotonic and seven cyclic test were performed on a $d = 28mm$ pile, the initial analysis of these test were presented in Klinkvort et al. (2011),(Test no. 53-60). Afterwards four test were performed on the same pile with a few number of deformation controlled (dc) load cycles, (Test no. 54-60). The few number of strain-gauge bridges on the $d = 28mm$ pile makes the interpretation of the interaction difficult and only pile - soil interaction curves from one depth can be deduced.

The pile with ten strain-gauge bridges ($d = 40mm$) makes it possible to interpreted interaction curves from different levels. In order to investigate the influence of load eccentricity on the pile - soil interaction five test with different load eccentricities were carried out, (Test nr 65-69), Klinkvort and Hededal (2012b).

Finally five supplementary cyclic tests were carried out two in dry sand and three in saturated sand (Test no. 70-74), presented in Klinkvort and Hededal (2012a) together with the results in Test no. 53-60.

Table 4.1: *Test program. c=cyclic, h=hollow, r=rough, s=saturated*

Test nr	I_D	Effective density, $[kN/m^3]$	Model. Dia. d [mm]	Load ecc. l_e/d	Pene. depth l_L/d	Scaling factor N_s	Install.. accel.. $[g]$
38	0.94	16.6	16	2.5	10	62.5	1
39	0.91	16.5	16	2.5	8	62.5	1
40	0.90	16.6	16	2.5	6	62.5	1
41	0.89	16.4	16	4.5	10	62.5	1
42	0.94	16.6	16	4.5	8	62.5	1
43	0.91	16.4	16	4.5	6	62.5	1
44	0.94	16.6	16	6.5	10	62.5	1
45	0.94	16.6	16	6.5	8	62.5	1
46	0.93	16.5	16	6.5	6	62.5	1
47 c	0.92	16.6	16	2.5	10	62.5	1
48 c	0.91	16.5	16	2.5	8	62.5	1
49 c	0.93	16.6	16	2.5	6	62.5	1
50 c	0.94	16.6	16	4.5	8	62.5	1
51 c	0.92	16.5	16	4.5	6	62.5	1
52 c	0.96	16.6	16	6.5	6	62.5	1
53	0.96	16.8	28	15	6	115	1
54 c	0.84	16.4	28	15	6	115	1
55 c	0.86	16.4	28	15	6	115	1
56 c	0.93	16.7	28	15	6	115	1
57 c	0.86	16.4	28	15	6	115	1
58 c	0.84	16.4	28	15	6	115	1
59 c	0.86	16.4	28	15	6	115	1
60 c	0.80	16.2	28	15	6	115	1
61 dc	0.81	16.3	28	15	6	115	1
62 dc	0.95	16.4	28	15	6	115	1
63 dc	0.82	16.3	28	15	6	115	1
64 dc	0.85	16.4	28	15	6	115	1
65 s	0.87	10.2	40	17.25	6	75	$\eta/3$
66 s	0.87	10.2	40	15	6	75	$\eta/3$
67 s	0.87	10.2	40	12.75	6	75	$\eta/3$
68 s	0.94	10.4	40	10.5	6	75	$\eta/3$
69 s	0.90	10.6	40	8.25	6	75	$\eta/3$
70 c	0.93	16.7	40	15	6	75	$\eta/3$
71 c	0.94	16.7	40	15	6	75	$\eta/3$
72 c s	0.97	10.4	40	15	6	75	$\eta/3$
73 c s	0.87	10.2	40	15	6	75	$\eta/3$
74 c s	0.94	10.4	40	15	6	75	$\eta/3$

4.1 Monotonic loading

The monotonic loading is used to determine the monotonic pile-soil interaction curves but also as a reference to the cyclic tests. From the total response it was seen that it was possible to take the stress dependent soil behavior into account by introducing the passive Rankine coefficient. This is also introduced in the normalization of the soil resistance p but here is $K_p(z)$ a function of the given depth. The new normalized soil resistance is written as:

$$\tilde{p} = \frac{K}{K_p} = \frac{p}{K_p \cdot \gamma' \cdot z \cdot d} = \frac{p}{K_p \cdot \sigma'_v \cdot d} \tag{4.1}$$

With this simple normalization it is possible to compare results performed at different stress levels. This is first demonstrated in Figure 4.1 for the overall response. Here the overall response of the $d = 40mm$ pile compared with the response from the $d = 28mm$ pile is shown. On the figure the normalized displacement of the pile is plotted against the normalized force. The monotonic tests in dry and saturated sand performed on different sized models show approximately identical results. Looking at the pile - soil response shown in Figure 4.2, the pile with a diameter of $d = 28mm$ shows initially the same response as the two other piles, but the response starts to deviate from a pile displacement above 0.05 d. A reason for the deviation could be that the $d = 28mm$ pile is installed at $1g$, whereas the $d = 40mm$ piles are installed at an elevated stress field. As demonstrated by Dyson and Randolph (2001) and in Figure 3.21 in the previous chapter $1g$ installation leads to a softer response.

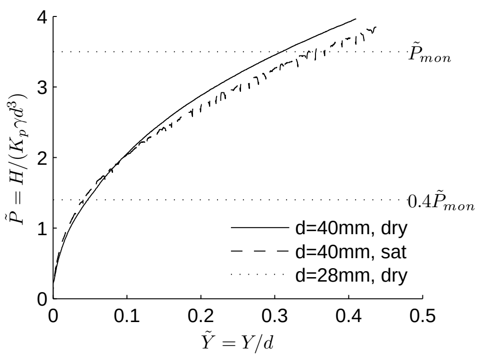

***Figure 4.1**: Overall monotonic response*

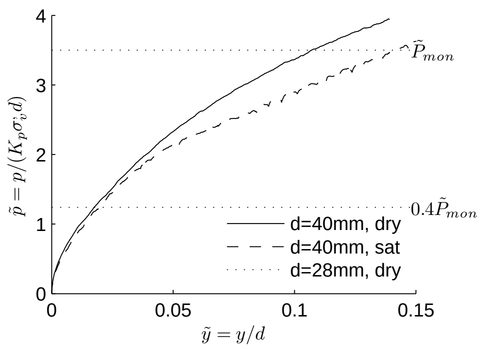

***Figure 4.2**: Pile - soil interaction monotonic response, $z = 2d$*

It can be seen from Figure 4.1 that the ultimate capacity was not reached for any of the tests. Therefore a rotation criterion was used to define the reference bearing capacity. Failure was defined at a rotation of 4 degrees for the piles with a diameter of $d = 40mm$. The maximum normalized force is shown Figure 4.1 as a dotted line. At load level less than 40 % of maximum the monotonic response from the three tests is identical. Since all cyclic tests were performed below this level it is chosen to use the results from the different piles in the investigation. The same tendency is seen if the pile - soil interaction is compared, this is shown Figure 4.2. This confirms that also the interaction curves can be compared.

4.1.1 Stress distribution effect

The normalized interaction curves from five tests with different stress distributions, identical with prototype piles with diameters ranging from 1-5 meters, are shown in Figure 4.3, Klinkvort and Hededal (2012b). Here nor-

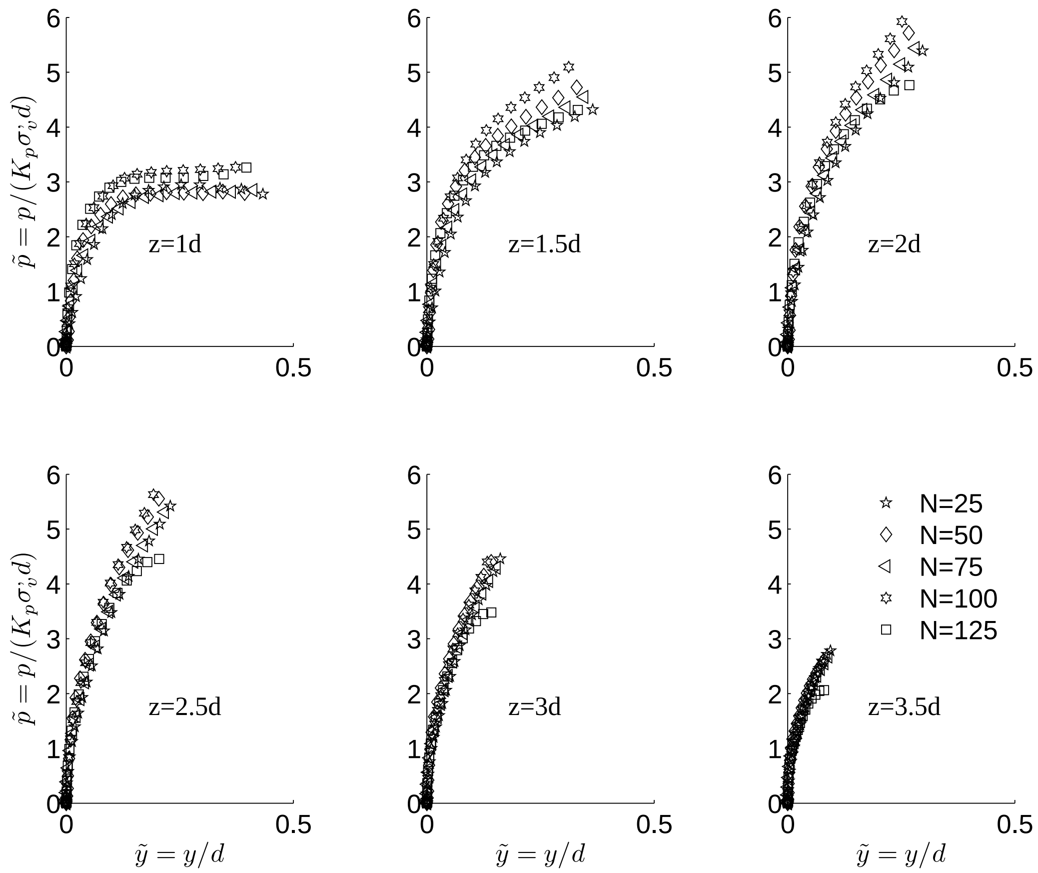

***Figure 4.3**: Monotonic test results on d=40mm pile with five different stress distributions, Test no. 26-30*

malized interaction curves from the six different depths are shown separately. It is seen that the normalized pile - soil interaction curves from the six different levels show a high degree of similarity like the overall response. From this it is concluded that the normalized pile - soil interaction responses have similar normalized behaviour no matter of the stress level. By normalizing the results only through the angle of friction it is demonstrated that the stress level can be taken into account. These curves can then be used for any given prototype stress level when the stress level effect is taken into account.

Depth effect

From the test shown in Figure 4.3 a comparison of the effect of depth can be made. This is shown in Figure 4.4, here the soil pile interaction from three different tests in three different depths but with same vertical stress can be seen.

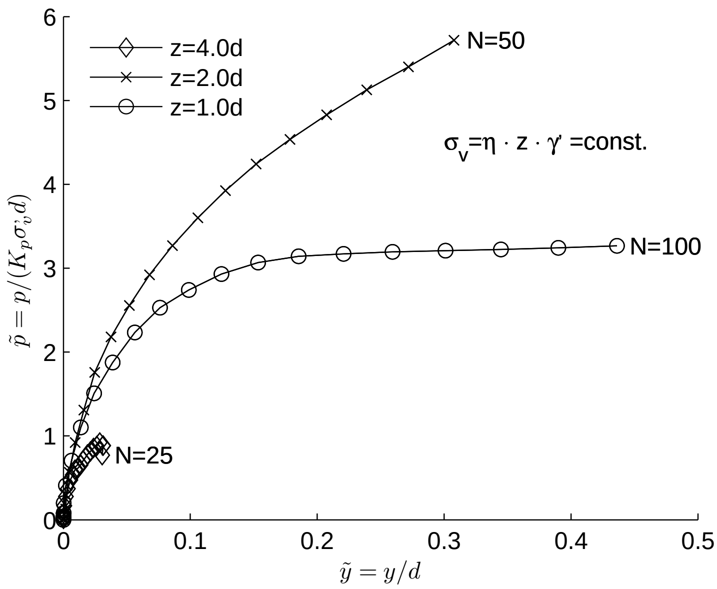

***Figure 4.4**: Effect of depth*

Looking at Figure 4.4 it is clear that the assumption of a constant ultimate earth pressure coefficient as assumed by Broms (1964) and Zhang et al. (2005) is too simple. The curves in $z = 1d$ and $z = 4d$ both seems to have reached the ultimate capacity whereas the curve located $z = 2d$ has not reached the ultimate capacity. The ultimate capacity from $z = 1d$ and $z = 4d$ curves are also very different with a very small normalized capacity for the lover one, but the initial normalized stiffness is for all three curves identical. This clearly shows that the pile - soil interaction is not only dependent of the vertical stress but also of the depth. The very small capacity in $z = 4d$ also indicates that the distance to the rotation point is important.

From this it is also clear that it is important to have full similarity when comparing results in order to document one effect. For example comparing a pile-soil interaction curve $4m$ down in the soil from a $1m$ in diameter pile with a pile-soil interaction curve $4m$ down in the soil from a 6m in diameter pile dos not makes sense, because full similarity is not archived and identical response cannot be expected.

4.1.2 Load eccentricity effect

The load eccentricity of the resultant force component will change due to the nature of the lateral loads. This was investigated by comparing five tests performed on piles with a stress distribution identical with a 3 meter in diameter prototype but with different load eccentricities, Klinkvort and Hededal (2012b). The five tests were all performed in water saturated sand and on a pile with load eccentricities ranging from $l_e = 8.25d - 17.25d = 330 - 690mm$. Using the normalization strategy described in (4.1) the results from the five tests is shown in Figure 4.5. As for the five tests with different stress distributions the results from changing the load eccentricity is shown for the six strain-gauge levels. Again it seems like the responses are similar no matter of the load eccentricity. Scatter is seen in the results but no systematic trend is observed and with the increasing soil stress with depth, the curves seems to merge. It is therefore concluded from these tests that the soil-pile interaction dos not change due to load eccentricity. This is identical with the assumption recommended by API (2007).

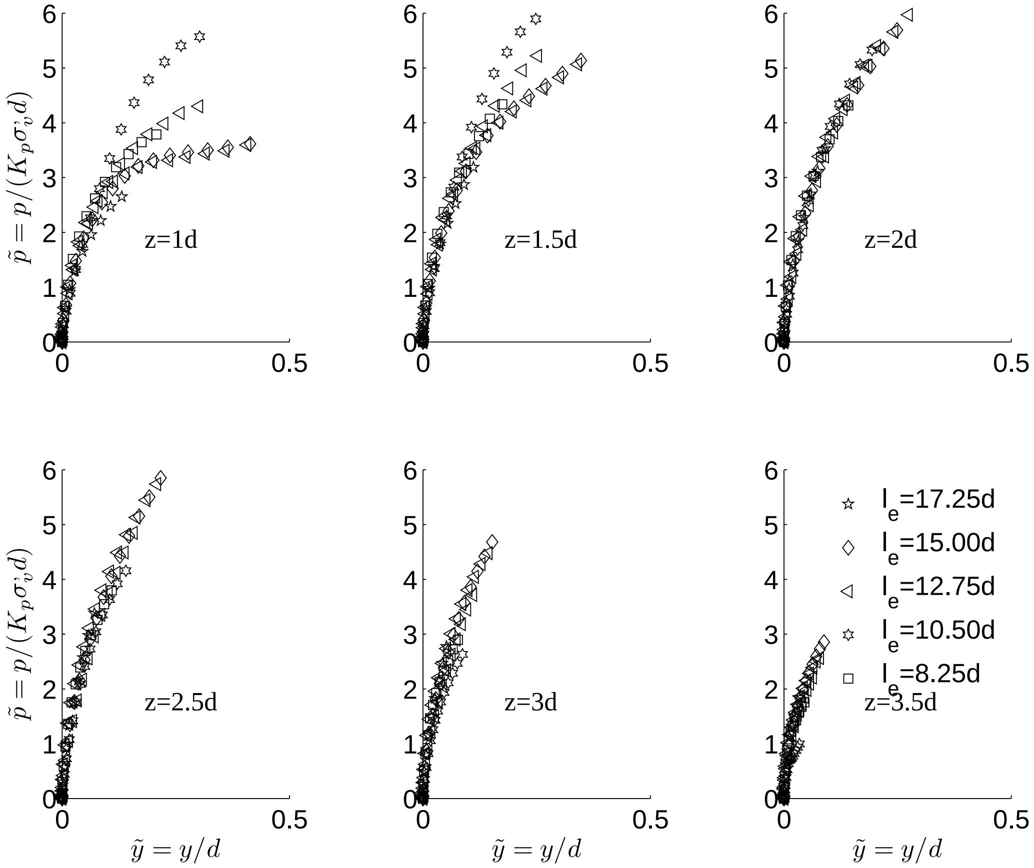

Figure 4.5: *Monotonic test results from d=40mm pile with five different load eccentricities, Test no. 65-69*

4.1.3 Comparison with FEM

Ten different monotonic tests performed with different stress distributions and with different load eccentricities were carried out. The normalized responses from these test should be identical, this was demonstrated in Figure 4.3 and 4.5. These results are compared with a numerical 3D finite element calculation Zania and Hededal (2012) and a winkler calculation using the recommendations from API (2007). The 3D finite element (FE) calculation was carried out on a 2 meter in diameter solid steel pile with a load eccentricity of $l_e = 15d$ and a penetration of $l_L = 6d$. The sand was modelled as Mohr-Coloumb material and the material parameter was deduced from the same triaxial test as shown in Figure 3.11. The interface between pile and soil was carried out using a Coulomb friction law with a angle of friction of $\delta = 21^o$. The FE model and the centrifuge tests with a stress distribution identical to a 2 meter in diameter pile have full similarity and the results can therefore be compared. For more details of the numerical model see Zania and Hededal (2012). Also a calculation using the API (2007) methodology has been performed. Here an initial subgrade modulus of $k = 40MPa/m$ found using Figure 2.3 have been used. The results of the two calculations can be seen together with the centrifuge results in Figure 4.6. The pile-soil interaction

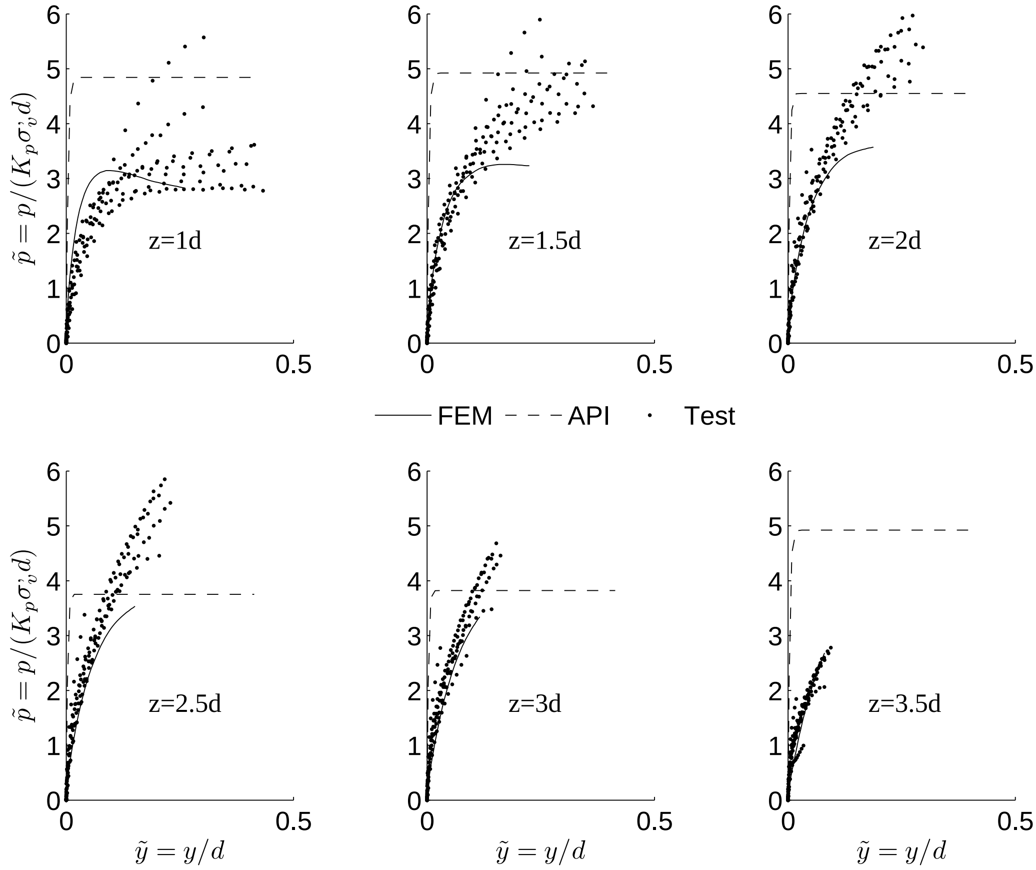

Figure 4.6: *Monotonic test results compared with FE model and API model*

response using the methodology proposed by API (2007) overestimates the initial stiffness in a high degree, the ultimate capacity is overestimated in the top levels and underestimated in the lower levels, this is clearly seen in Figure 4.6. The FE calculation predicts the stiffness of the test result in a better way than the API (2007) methodology, but it can be seen that the stiffness of the curve in the top level is too high, at the medium levels acceptable and in the bottom to low. The maximum capacity is predicted with a high degree of accuracy in the top level, but seems to be underestimated at lower levels.

The test results from the ten tests can be represented by a single set of generic curves, this has be done in Figure 4.7. It can be seen that a maximum soil resistance was only reached in the upper layer $z = 1d$, even though the pile at sand surface has been displaced more than $0.5d$. The initial slopes of the pile - soil interaction curves were all similar and are found to $\tilde{E}_{py}/K_p = 100$. A constant normalized initial stiffness is identical with the assumption proposed by API (2007). In the same way the results from the

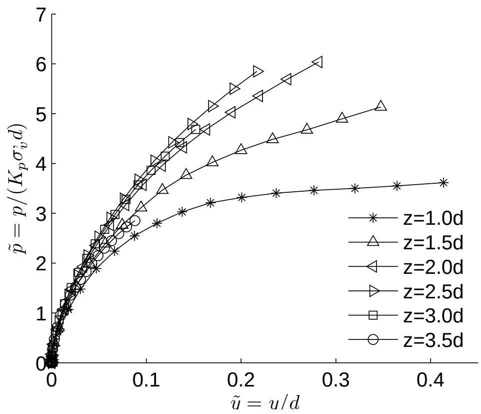

***Figure 4.7**: Generic pile - soil interaction curves from centrifuge tests*

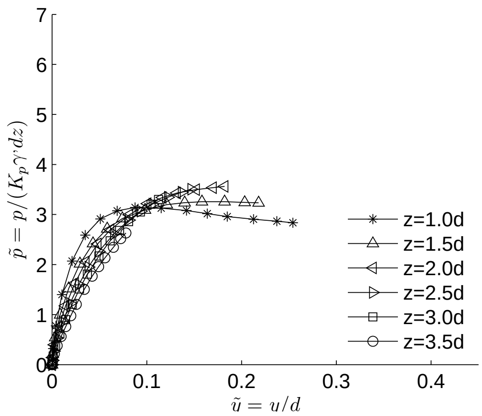

***Figure 4.8**: Pile - soil interaction curves from FE model*

FE model is shown in Figure 4.8. Here it is seen that more of the curves have reached a maximum capacity and also that the normalized stiffness is degreasing with increasing depth in contrast to the recommendation from API (2007). It should also be noticed that the maximum capacity is around 3 which is the value Broms (1964) proposed. No depths effect is here seen in contrast to the centrifuge experiment observation shown in Figure 4.4.

The magnitude of the pile-soil interaction curves from the centrifuge tests and the numerical calculations is the same. This validates in some way the results from the to methods and also the scaling from centrifuge scale to prototype scale, but the is though still a distinct difference in the responses. The results from the centrifuge is from a real physical event and the credibility of these test is therefore higher. The FE model needs to be improved in order to get better results, which can be used in the analysis of the laterally loaded monopile.

4.1.4 New monotonic pile - soil interaction model

The results from the tests were compared with methodologies of API (2007) and Kondner (1963) but here with an initial stiffness of $\tilde{E}_{py}/K_p = 100$. The two types of curves was compared and disagreements between models and results was still seen. Here is therefore introduced a new way to compute soil-pile interaction curves. It uses the formulation proposed by Kondner (1963) and the calculation of ultimate capacity is identical with API (2007), but the calculation of the empirical depth factor A, is here change in order to match the results. The calculation of A is shown in (4.2), Klinkvort and Hededal (2012b).

$$A = 0.9 + 1.1 \cdot H \tag{4.2}$$

The parameter H is a step function and controls the transition from 2 in the upper parts to 0.9 in greater depths.

$$H = \frac{1}{2} + \frac{1}{2}\tanh\left(9 - 3\frac{z}{d}\right) \tag{4.3}$$

In Figure 4.9 the new formulation is shown and compared with the formulation proposed by API (2007) and Georgiadis et al. (1992). It can be seen

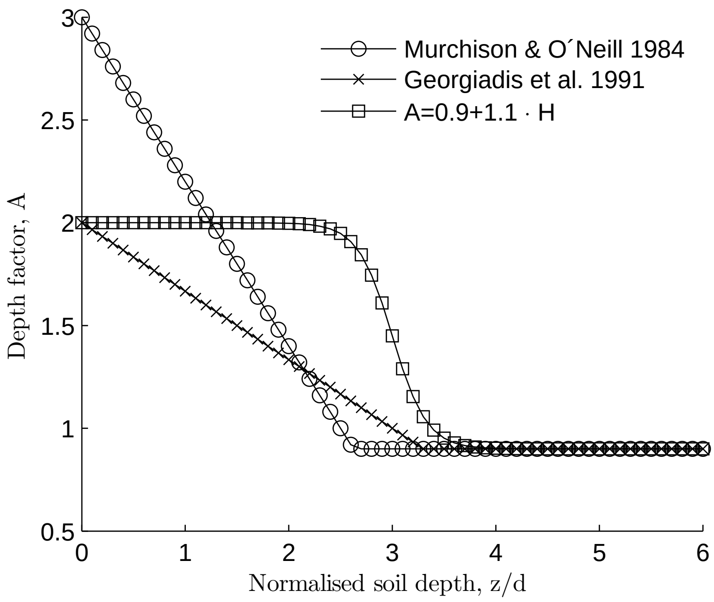

Figure 4.9*: New calculation of the empirical depth factor A*

that all of the three functions is in the same range. The formulation by Georgiadis et al. (1992) is similar to the one by API (2007) and decrease linearly to 0.9. Whereas the one showed in (4.2) has a more abrupt change from to 2 to 0.9. The centrifuge results and the new model is shown in Figure 4.10 together with the models by API (2007) and Kondner (1963) using the standard formulation of A. It can be seen on the figure that using the

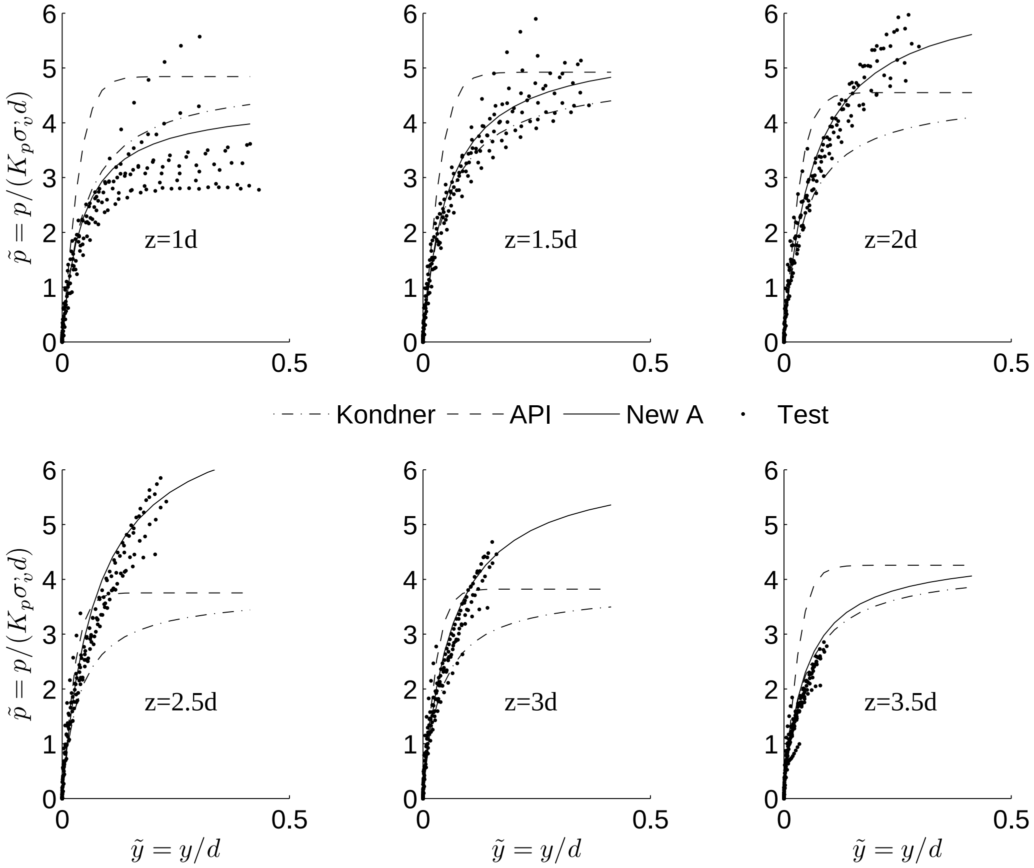

Figure 4.10: *New pile soil interaction model in comparison with test data*

standard value of A leads to overestimation of the capacity in the top layers and underestimation in the lower layers. Using the new value of A shown in (4.2) together with the hyperbolic function proposed by Kondner (1963) provides a model with a high degree of the similarity to the test observations. It is therefore recommended to use the formulation calibrated here in a ULS analysis.

4.2 Cyclic loading - total response

As a first attempt to understand the cyclic soil-pile response, a test series with focus on the overall response was carried out. First a analysis of the tests no. 54-60 was carried out, Klinkvort et al. (2011). These tests were supplemented by five extra tests and a more general analysis was carried out, Klinkvort and Hededal (2012a). Twelve cyclic tests were performed, (Test no. 54-60 & 70-74) and together with the monotonic test showed in Figure 4.1, (Test no. 28 & 53 & 66) these test were the basis in the analysis. The monotonic tests were used as a reference for the cyclic tests. First seven cyclic tests on the $d = 28mm$ pile in dry sand were performed. From these test, the non-dimensional functions was established. This was done by first changing the load amplitude of the cyclic loading (η_b), while keeping the characteristic of the cyclic loading (ζ_c) constant. Afterwards the effect of the characteristic of the cyclic loading was investigated by changing ζ_c while keeping ζ_b constant. Later, two tests on a $d = 40mm$ pile were performed to see the influence of number of cycles and three tests were used to see the influence from performing cyclic test in saturated sand. Although tests were performed on different sized piles and in dry or saturated conditions, the non-dimensional functions determined from all the tests proved representative for the entire test series.

4.2.1 Model framework

In order to investigate the accumulation of displacements and change in secant stiffness the cyclic loading is load controlled. In each load cycle the maximum and minimum value of the load ($\tilde{P}_{max,N}$, $\tilde{P}_{min,N}$) and the displacement ($\tilde{Y}_{max,N}$, $\tilde{Y}_{min,N}$) can be obtained. A schematic cyclic response is shown in Figure 4.11. The maximum displacement and the cyclic secant stiffness from each cycle can therefore be determined. The maximum displacement is found as the displacement when the load is at the maximum of each cycle and the cyclic secant stiffness is found as the slope of a straight line between the extremes for every cycle, see Figure 4.11.

Having determined the bearing capacity of the pile from a monotonic test, ($\tilde{P}_{mon}$), the cyclic loading can be described by two non-dimensional parameters, (Long and Vanneste (1994), Rosquöet et al. (2007) and LeBlanc et al. (2009)).

$$\zeta_b = \frac{\tilde{P}_{max}}{\tilde{P}_{mon}} \quad \zeta_c = \frac{\tilde{P}_{min}}{\tilde{P}_{max}} \tag{4.4}$$

The value ζ_b defines the load amplitude relative to the maximum bearing capacity, $\tilde{P}_{mon}$, and ζ_c defines the characteristic of the cyclic loading.

Displacement evolution model

The cyclic loading is described by the parameters (ζ_b, ζ_c), the maximum displacement from the number of cycle (N) may then be determined from a power function,

$$\tilde{Y}_{max,N} = \tilde{Y}_{max,1} \cdot N^{\alpha} \tag{4.5}$$

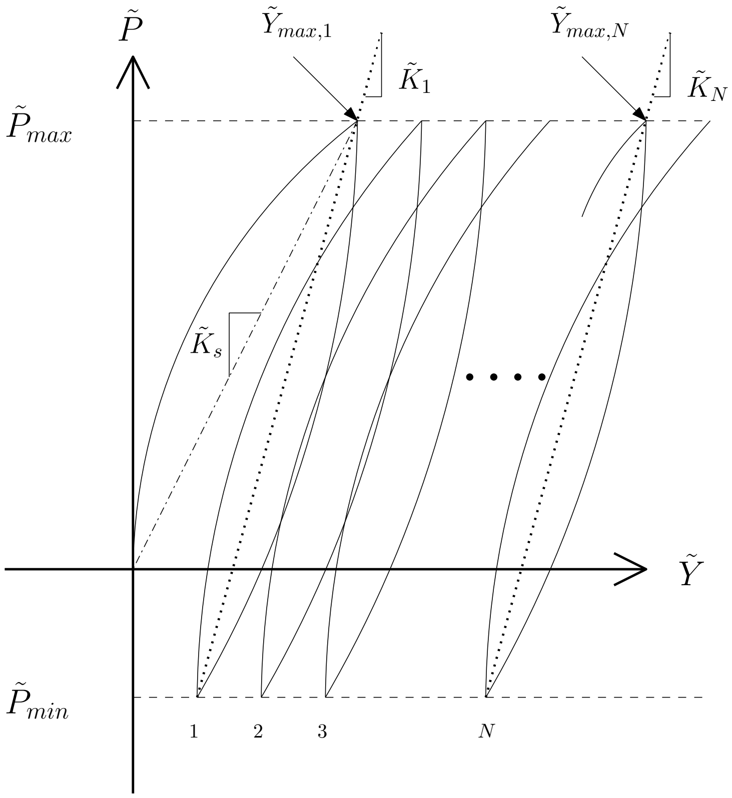

Figure 4.11*: Schematic drawing of determination of secant stiffness and maximum accumulation of displacement*

The coefficient, α is dependent both on the load characteristic described by ζ_c and the magnitude of the loading described by ζ_b. Assuming the two effects to be independent, the value of α can be calculated as a product of two non-dimensional functions.

$$\alpha(\zeta_c, \zeta_c) = T_c(\zeta_c) \cdot T_b(\zeta_b) \tag{4.6}$$

The first function, T_c, depends on the load characteristic, ζ_c, and the second function, T_b, depends on the load magnitude, ζ_b.

Secant stiffness evolution model

The cyclic secant stiffness in every cycle may be described by a logarithmic function;

$$\tilde{K}_N = \tilde{K}_1(1 + \kappa \cdot \ln(N)) \tag{4.7}$$

In (4.7), κ is the accumulation rate, $\tilde{K}_1$ is the cyclic secant stiffness for the first cycle and $\tilde{K}_N$ is the cyclic secant stiffness for cycle number N. As for the accumulation of displacements, it is chosen to describe the value of κ by two independent non-dimensional functions.

$$\kappa(\zeta_c, \zeta_c) = \kappa_c(\zeta_c) \cdot \kappa_b(\zeta_b) \tag{4.8}$$

The non-dimensional cyclic secant at the first cycle, $\tilde{K}_1$, is found using the secant stiffness of the monotonic response.

$$\tilde{K}_s(\zeta_b) = \frac{\tilde{P}_{max}}{\tilde{Y}_{max}} \tag{4.9}$$

This value is appropriately scaled by $\tilde{K}_c(\zeta_c)$ which depends on the cyclic load characteristic, i.e.

$$\tilde{K}_1(\zeta_c, \zeta_c) = \tilde{K}_c(\zeta_c) \cdot \tilde{K}_s(\zeta_b) \tag{4.10}$$

The input to the two evolution models can be established from a monotonic test combined with the non-dimensional functions, $(T_c(\zeta_c), T_b(\zeta_b)$,$\kappa_c(\zeta_c), \kappa_s(\zeta_b)$ and $\tilde{K}_c(\zeta_c), \tilde{K}_b(\zeta_b))$. These functions can be empirically determined by a series of cyclic load tests.

4.2.2 Evolution of displacements

The accumulation of displacement may be described by a power function. The maximum deflection for all cycles plotted together with the power fit is shown in Figure 4.12. It can be seen that the power fit captures the accumulation of displacement well. The results together with the non-dimensional cyclic load characteristics can be seen in Table 2 in Klinkvort and Hededal (2012b). The value of α can be calculated using two non-dimensional cyclic functions as shown in (4.6). By normalizing $T_c = 1$ for pure one-way loading, $\zeta_c = 0$, the non-dimensional function T_b can be found from a series of test where T_b is changed while $T_c = 0$.

$$\alpha(\zeta_c = 0, \zeta_b) = 1 \cdot T_b(\zeta_b) \tag{4.11}$$

When T_b is created the function T_c may be found by performing a series of test with a constant ζ_b and then dividing the results with the T_b function, i.e.

$$T_c(\zeta_c) = \frac{\alpha}{T_b(\zeta_b)} \tag{4.12}$$

The result of this analysis can be seen in Figure 4.13. It was chosen to force

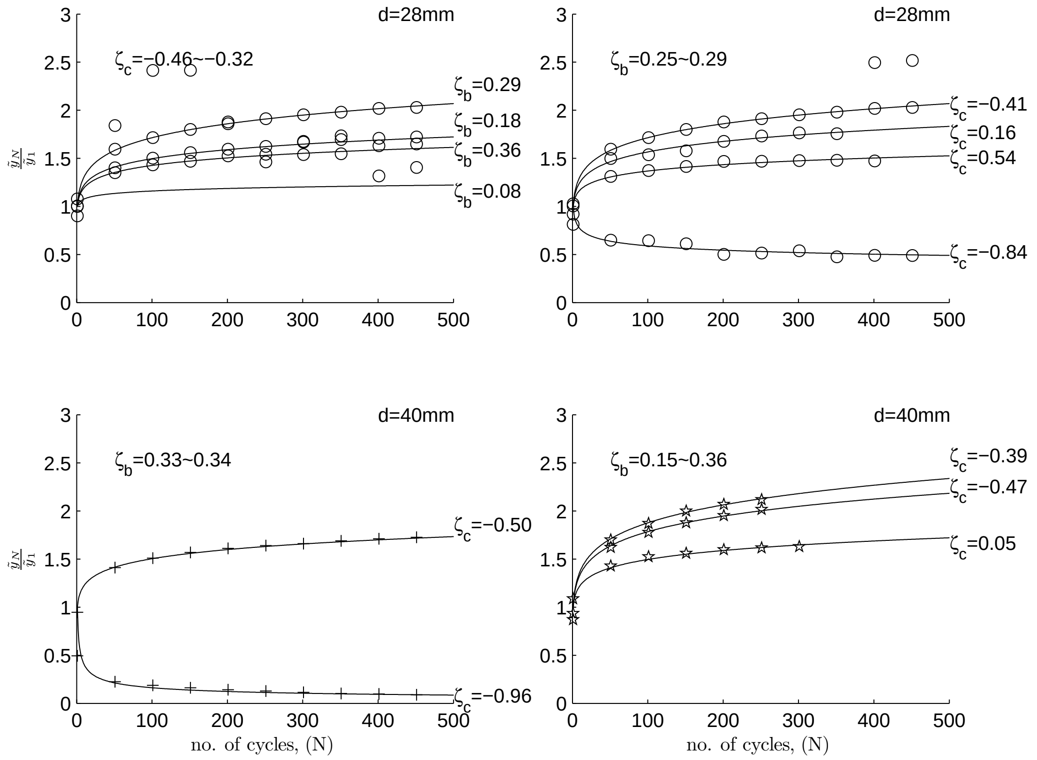

Figure 4.12: *Accumulation of displacements*

the values of T_b to be a straight line and then to plot the corresponding value of T_c. The linear dependency of the load magnitude can be seen in (4.13).

$$T_b(\zeta_b) = 0.61\zeta_b - 0.013 \tag{4.13}$$

The function T_b cannot be negative, hence cyclic loading with a small magnitude $\zeta_b \leq 0.02$, will lead to a value $T_b = 0$, implying that the pile-soil interaction is reversible and no accumulation of displacements will occur. Figure 4.13 shows results for the cyclic load characteristic function. The results seem to follow a third order polynomial, see (4.14).

$$T_c(\zeta_c) = (\zeta_c + 0.63)(\zeta_c - 1)(\zeta_c - 1.64) \tag{4.14}$$

The function secures that $\alpha = 0$ for monotonic loading, $\zeta_c = 1$. The maximum value of the function is found at $\zeta_c = -0.01$, which means that the most damaging load situation is when the monopile is loaded in a more or less pure one-way loading. When $\zeta_c \leq -0.63$ the function T_c becomes negative, which means that the accumulation of displacement is reversed and the pile moves towards its initial position. Since both dry and saturated condition

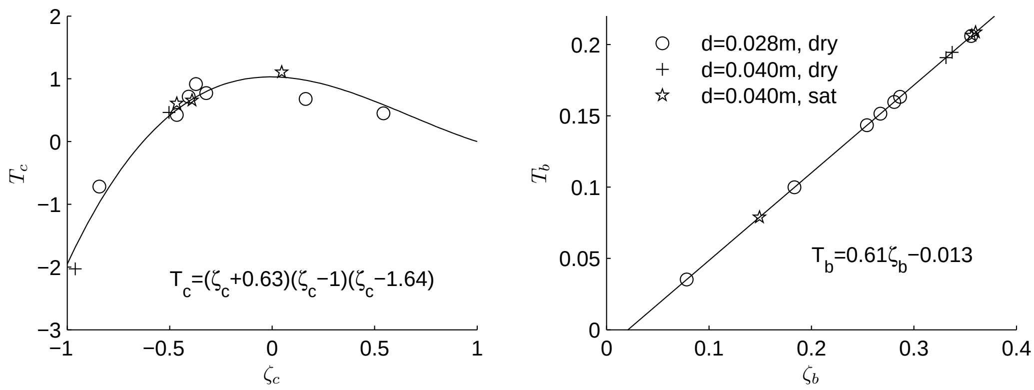

***Figure 4.13**: Non-dimensional function*

have been used in the tests, this shows that all tests are fully drained and the chosen scaling approach seems valid also for quasi static cyclic loading. From the non-dimensional functions it can be concluded that the accumulation coefficient, α is increasing with increasing magnitude of the cyclic loading, and that the most damaging cyclic load orientation is in the interval of $-0.4 \leq \zeta_c \leq 0$. The displacement for the first cycle is easily found from a monotonic test, and is only depending on the load magnitude. Having the monotonic load-displacement curve together with the non-dimensional functions shown in (4.13) and (4.14) thus makes it possible to estimate the displacement to a given number of cycles using (4.5).

4.2.3 Evolution of secant stiffness

In Figure 4.14, the secant stiffness is plotted against the number of cycles. It shows that the logarithmic function seems to describe the changes in secant stiffness reasonably. The results of the logarithmic fits can also be been seen in Table 2 in Klinkvort and Hededal (2012a). The determination of the non-dimensional functions follows the same methodology as described for the displacements. The results are shown in Figure 4.15. A linear dependency of the load magnitude is found;

$$\kappa_b(\zeta_b) = 0.05\zeta_b + 0.02 \tag{4.15}$$

(4.15) implies that an increase in the cyclic load magnitude leads to an increase in the accumulation secant stiffness accumulation rate, κ . Having determined κ_b, the values of κ_c are plotted and it is seen that a linear fit seems to capture the trend, see (4.16).

$$\kappa_c(\zeta_c) = -6.92\zeta_c + 1 \tag{4.16}$$

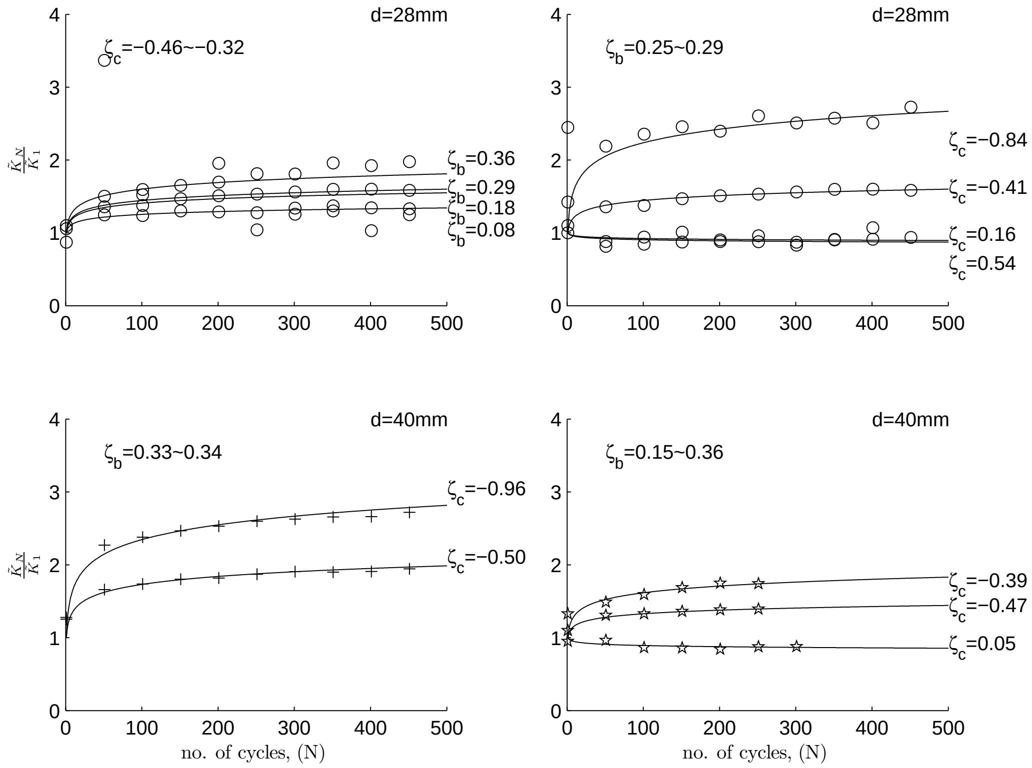

Figure 4.14: *Change in cyclic secant stiffness*

It can be seen that going from one-way to two-way loading will lead to an increasing accumulation of stiffness.

The initial cyclic secant stiffness is found by considering the results of a monotonic test and cyclic tests with varying amplitude. The function $\tilde{K}_s(\zeta_b)$ is established directly from the monotonic load-displacement curve. The function $\tilde{K}_c(\zeta_c)$ is then evaluated from the cyclic tests. The results are shown in Figure 4.16, and it can be seen that a second order polynomial describe the variation of $\tilde{K}_c(\zeta_c)$,

$$\tilde{K}_c(\zeta_c) = 1.64\zeta_c^2 + 3.27\zeta_c + 3.27 \tag{4.17}$$

From this equation, it should be recognized that the initial stiffness due to cyclic loading is stiffer than the monotonic stiffness. Depending on the characteristic of the cyclic loading, the initial cyclic secant stiffness may be 2 to 8 times the monotonic secant stiffness.

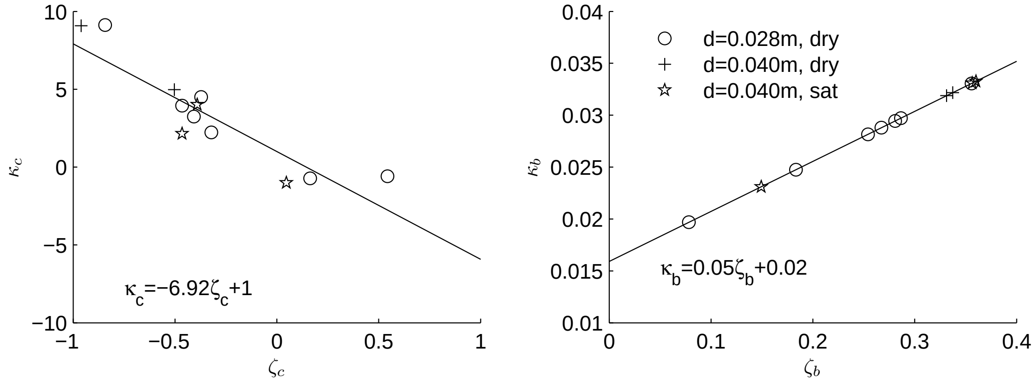

Figure 4.15: *Non-dimensional functions to calculate the cyclic stiffness accumulation rate*

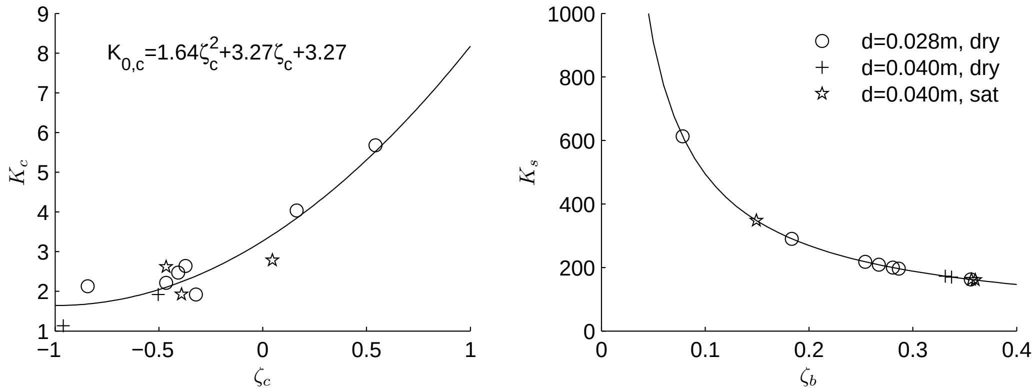

Figure 4.16: *Non-dimensional functions to calculate the cyclic initial stiffness*

4.2.4 Concluding remarks

Two key issues for the design of a monopile support for an offshore wind turbine were investigated, accumulation of displacements and the change in secant stiffness. It was clearly seen that the accumulation of displacement and secant stiffness is affected by the characteristic of the cyclic loading, and by the load amplitude. An empirically based design procedure for a monopile installed in dense saturated sand has been given, but should only be used for drained conditions. The design procedure can be applied for any load amplitude, load characteristic and number of cycles. Together with three sets of non-dimensional functions, the procedure only needs a monotonic response in order to an address the accumulation of displacement and the change in stiffness. This gives a very simple design procedure which is superior the given methodology used in the industry today. Random loading can be taken into account using the presented methodology together with rain-flow counting and Minor's rule. This methodology was demonstrated with success by Leblanc et al. (2010b).

4.3 Cyclic pile - soil interaction response

The overall response from load controlled cyclic loading was documented in the previously section. A model to predict the accumulation of displacement and the change in stiffness was given. To investigate the pile - soil interaction in more details cyclic pile - soil interaction curves were therefore generated in order to investigate the soil resistance. First four tests were performed with deformation controlled few cycles, (test no. 61-64), and afterwards force controlled test with a high number of cycles where performed (test no. 70-74).

4.3.1 Deformation controlled cyclic loading

Four deformation controlled tests were performed on the $d = 28$mm pile in order to investigate the cyclic soil resistance, (Test no. 61-64). The tests was carried out with five cycles with a maximum deformation of $Y_{max} = 0.5d$ at pile top, and then five cycles to a maximum deformation of $Y_{max} = 1.0d$. The characteristic of the cyclic loading was designed so the four test would represent different load scenarios going from pure two-way loading to a pure one-way loading. The results shown here will be from the soil layer in $z = 2d$ and the results will be plotted together with the monotonic response shown in Figure 4.2. The monotonic response from the $d = 28$mm pile will on the plot be shown as a thick dark line.

Here is only shown the result of the first tests. The observation seen in this test was general and the observation is therefore also valid for the three other cyclic load scenarios. The tests was performed with a deformation controlled loading of five cycles each loaded to $0.5d$ to each side and then five cycles with deformation of $1.0d$ to each side, (Test no. 61). This is equivalent to the non-dimensional cyclic parameter $\zeta_c = -1$. The test result can be seen in Figure 4.17. From the figure it can be seen that the first loading of the pile follows the results from the monotonic test, this is here called virgin loading. When the movement of the pile is change an elastic unloading of the pile is seen. This is followed be a small plateau where the load is more or less constant follow by a increase in resistance until the response seems to followed the opposite virgin curve again. When the pile movement is

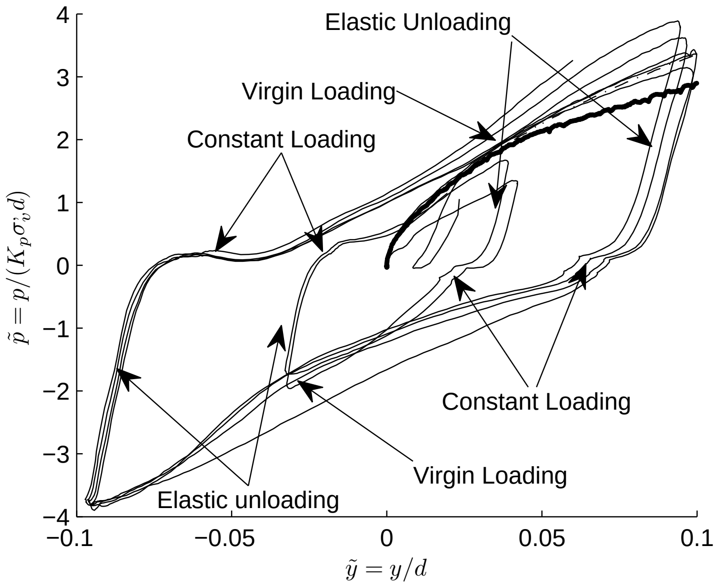

***Figure 4.17**: Cyclic non-dimensional p-y curves $\zeta_c = -1$, $z = 2d$*

returned again an elastic unloading followed by a plateau is again seen. This behavior seems to be identical for all of the five cycles. It can also be seen that the soil resistance increases due to cyclic loading.

4.3.2 Force controlled cyclic loading

Force controlled cyclic loading was applied to the $d = 40mm$ pile and the cyclic pile - soil interaction was observed for six soil depths. The loading magnitude of these piles are much smaller than the previously deformation controlled tests. Here the cyclic loading is carried out at a maximum cyclic load level of approximate 35% of the monotonic capacity, corresponding to the serviceability loading of a offshore wind turbine. Two tests are here shown to demonstrate some general observations.

Cyclic interaction curves $\zeta_c \approx -1$

Here are interaction curves from six depths observed and the interaction between soil resistance and depths can be seen. In Figure 4.18 the two-way loading test is shown, (Test nr 71). Here the force control allows the pile to accumulate displacements/rotations. From the overall observation it was seen that after one initial displacement from virgin loading, the pile is moving back against its original position. This can also be seen at Figure 4.18, here the pile - soil interaction curves from the first three cycles and after 1000

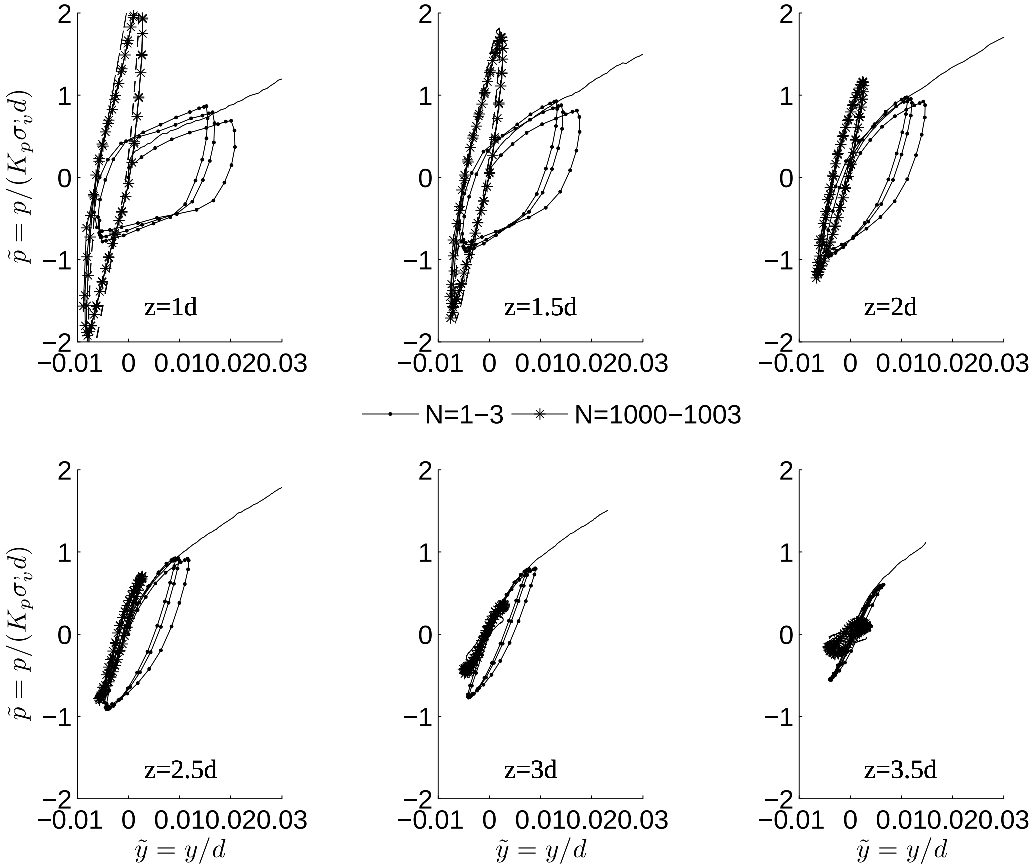

***Figure 4.18**: Cyclic non-dimensional p-y curves $\zeta_c = -1$, N=1-3 & 1000-1003*

cycles are shown. It can be seen that these curves also moves backwards like the overall response. It can also be seen that no degradation of the sand is occurring due to the cyclic loading. The capacity is due to densification getting stronger and stronger. The load carrying soil pressure is therefore also shifting so the soil in the upper parts are carrying more and more and the soil resistance mobilization in the lower layers is therefore decreasing. There is a large hysteretic behavior in the three top layers whereas the lower layers is showing a more linear and elastic behavior.

Cyclic interaction curves $\zeta_c \approx -0.5$

In Figure 4.19 the semi two-way loading test is shown, (Test no. 70). Here cycles between 1-3, 1000-1003 and 10.000-10.003 is shown. Again it can be seen that the pile starts to accumulate displacements. The pile was subjected to 10.000 of cycles and accumulation of displacements and hysteric behaviour was still seen for the top layers. Comparing the cyclic interaction curves with

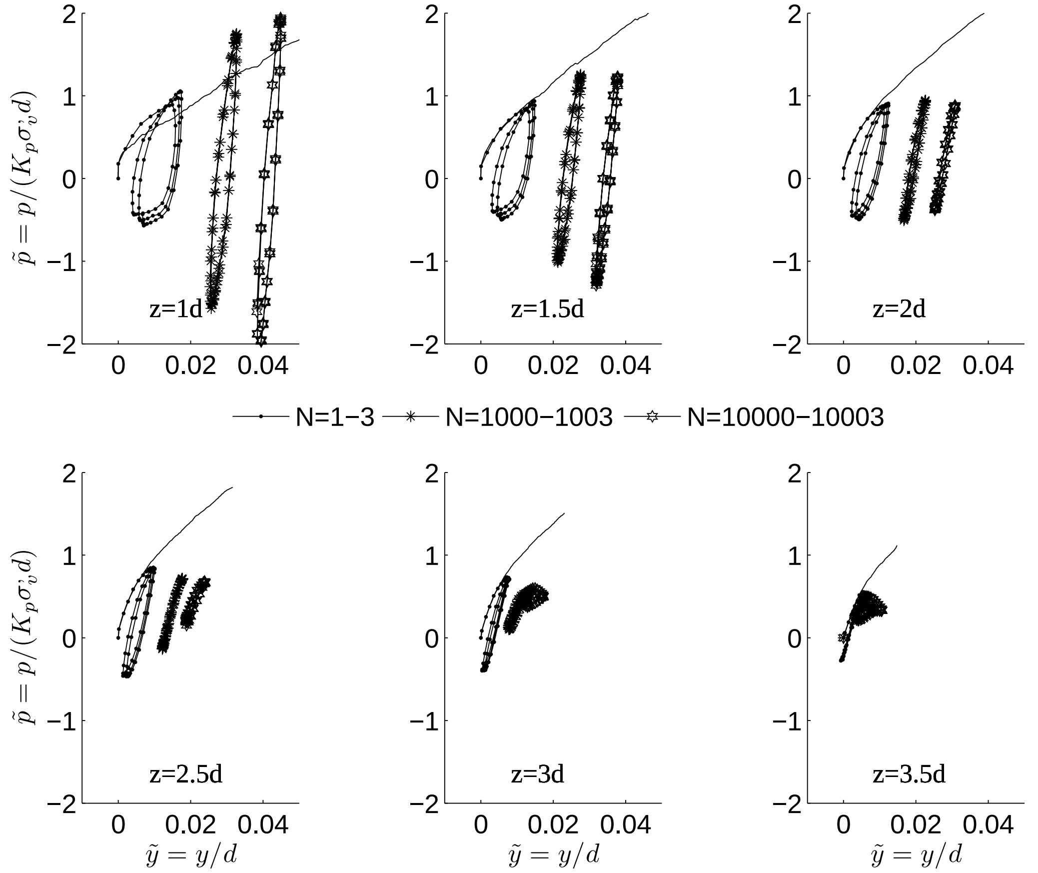

***Figure 4.19**: Cyclic non-dimensional p-y curves $\zeta_c = -0.5$, N=1-1000-10000*

the monotonic response it can be seen that the maximum soil resistance seems to follow the virgin curve. The soil layer in the top is getting stronger and stronger. This rearranges the soil resistance and the layers in the bottom therefore do not have to mobilize soil resistance in the same degree.

4.3.3 General observations

From all of the tests it was seen that the virgin loading was following the monotonic test results. It was also observed that the sand due to the cyclic loading always was the same or a bit above the monotonic response, this was also seen on the overall response in Klinkvort et al. (2010). From this it is concluded that the monotonic response can on the safe side be used as yield surface and the soil resistance in a given point is controlled by its displacement. From all the tests it can be seen that the cyclic loading seems to find a mean value where the cycles are symmetric around, and also hysterics is seen in all cycles. The unloading is always linear and the stiffness is here also always much stiffer compared to the initial stiffness of the virgin curve when the pile is unloaded. The rebuild of soil pressure after elastic unloading also seems stiffer than the initial virgin curve. From the load controlled test it was seen that the displacement and the stiffness of the pile is highly affected by the load situation. For a two-way loading situation the pile displacement moves towards its original position, whereas a one-way load situation accumulates displacements. Hysteresis was seen from both of the test . This was also the case for the test (Test no. 74) with a maximum cyclic load of only 15 % of the capacity.

4.4 Summary of pile - soil interaction results

37 tests have been performed in order to investigate the pile soil interaction. This have been done for both the overall and the pile - soil interaction responses. From the monotonic and cyclic centrifuge tests different conclusions can be drawn and are here listed:

1. The use of Rankines passive earth pressure coefficient as a normalization parameter was also seen to merge the pile-soil interaction curves into one set of generic curves.

2. No effect on the earth pressure coefficient K from load eccentricity.

3. Centrifuge and Finite element calculations shows responses in same order of magnitude but initial stiffness and capacity is different.

4. The method proposed by API (2007) was not capable to predict the monotonic centrifuge results in a sufficient degree.

5. A new formulation of the pile - soil interaction was proposed using the shape by Kondner (1963) and a re-calibration of the empirical factor A.

6. The change of displacements and secant stiffness is affected of the characteristic, the magnitude and the number of the cyclic loading

7. For the overall cyclic response, a new prediction model based on the centrifuge results was proposed.

8. For the local pile - soil interaction response, four basic behaviors was identified; Virgin loading, elastic unloading, constant loading and that the cycles seems to adjust around a mean value.

Chapter 5

Pile - soil interaction model

The observations from the centrifuge experiments are used to develop a spring element for cyclic pile-soil interaction. The spring element is used in an algorithm based on the finite element framework FemLab, (Hededal and Krenk, 1995). The model is a Winkler model where the pile is modeled as beams and the soil as a system of uncoupled non-linear cyclic springs. The response of the pile subjected to cyclic loads can then be investigated using this model. Additional a time integration algorithm was implemented in the FemLab framework based on the generalized α method to take the dynamic loading into account (Chung and Hulbert, 1993; Krenk, 1999). Here the total soil - pile - turbine interaction can be investigated; the main purpose of this model is to demonstrate how hysteretic damping can be introduced to the system using the cyclic spring formulation.

5.1 Cyclic pile - soil interaction spring

In seismic engineering, different kinds of cyclic pile - soil interaction formulations have been proposed. Boulanger et al. (1999) proposed an elasto-plastic model based on a two component set-up in which the loading response is handled by a series connection of springs - one spring handling loading (passive failure mode). Another spring handling the unloading-reloading properties while it is gradually creating a gap behind the pile. Taciroglu et al. (2006) further developed these ideas and proposed an element consisting of three components; leading-face element, rear-face element and drag-element. The two face-elements are formulated in terms of elasto-plastic springs supplemented with a tension cut-off. The drag element controls the side friction, when the pile is moving inside a cavity during unloading. In contrast to the two models by Boulanger et al. (1999) and Taciroglu et al. (2006), is here presented a model where the cyclic pile - soil interaction is incorporated into one single spring element. This makes the implementation into a standard finite element code easier. Also the formulation is based on observation from rigid pile tests which makes it more suitable for monopiles supporting wind turbines.

From the cyclic tests, basis observations of the cyclic pile - soil interaction was seen. In Figure 5.1, the test $\zeta_c = -0.5$ is shown, (Test no. 62). On top of the result is drawn three types of lines in order to show the physics of the spring model. The model consists of 3 parts, shown on the Figure 5.1

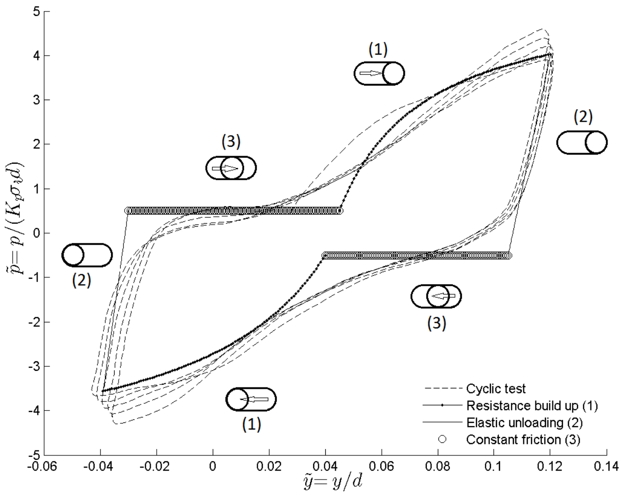

Figure 5.1: *Cyclic non-dimensional p-y curves*

as (1), (2) and (3). Firstly, a loading phase where the resistance is building up. Here the pile is pushing the soil and creating a gab behind the pile (1). Secondly, an elastic unloading phase is seen (2). Finally, a phase where the pile moves towards the initial position in the cavity created behind the pile during initial loading (3). In this phase it may be assumed that there exists a drag or friction along the side of the pile. For a cohesive soil the gab can be assume to develop between the two most extreme points of the pile movements, this was also the assumption in Hededal and Klinkvort (2010). El Naggar et al. (2005) assumes that this the gap will develop for cohesive soils, whereas for cohesionless soils, the soil will cave in and close the gap. From the centrifuge tests it can be argued that a mechanism in between these two extremes occurs. The sand will fall back, but it will not fill the gap totally. From the test it was also seen that the soil-pile interaction curves were symmetrical around the mean value of the two extremes. In this model the pile will move in the cap until reaching the mean of the two extremes, here the soil resistance starts to build up again.

In order to handle the observation seen in the centrifuge tests, the formulation presented in Hededal and Klinkvort (2010) is here modified. The modified model is basically identical to the model presented in Hededal and Klinkvort (2010), but here change with a new hardening model. This was chose in order to mimic the behavior seen in the centrifuge experiments in a better way.

Spring behavior

The current yield strength is divided into two parts; one relating the drag contribution when the pile is moving in the cavity and one relating the soil resistance build up while the pile is pushing the soil face.

$$p_u(y*) = p_u^{drag} + p_u^{face}(y*) \tag{5.1}$$

The term p_u^{drag} is the drag capacity, here assumed constant, when the pile is moving in the gap. Below this value the the spring is elastic. The second term p_u^{face} is the soil resistance build up, when the pile is in contact with the sand and pushing the face. When there is no contact, the term is zero. A schematic drawing of the model can be seen in Figure 5.2. Here a schematic representation of a cyclic curve is shown together with definitions.

Here is introduced a corrected displacement ($y*$) given as the difference between the current displacement y and the hardening parameter (α). This is done in order to capture the cyclic behavior around a mean value as seen in the experiments.

$$y* = y - \alpha \tag{5.2}$$

The hardening parameter α is given as the mean of the maximum and minimum plastic displacements as shown in Figure 5.2:

$$\alpha = \frac{y_{p,max} + y_{p,min}}{2} \tag{5.3}$$

The additional soil resistance for the face element can then be written as:

$$p_u^{face}(y*) = S(p_i)S(y * -y_{k,i})p_u^{Kondner}(y*) \tag{5.4}$$

The control of the contact is done by introducing the step function, $S(x)$. An approximation of the heavy side step function is used to control if the face element is zero or if resistance is building up. The formula for the approximation can be seen in equation (5.5).

$$S(x) = \frac{1}{1 + e^{-2\cdot\beta x}} \tag{5.5}$$

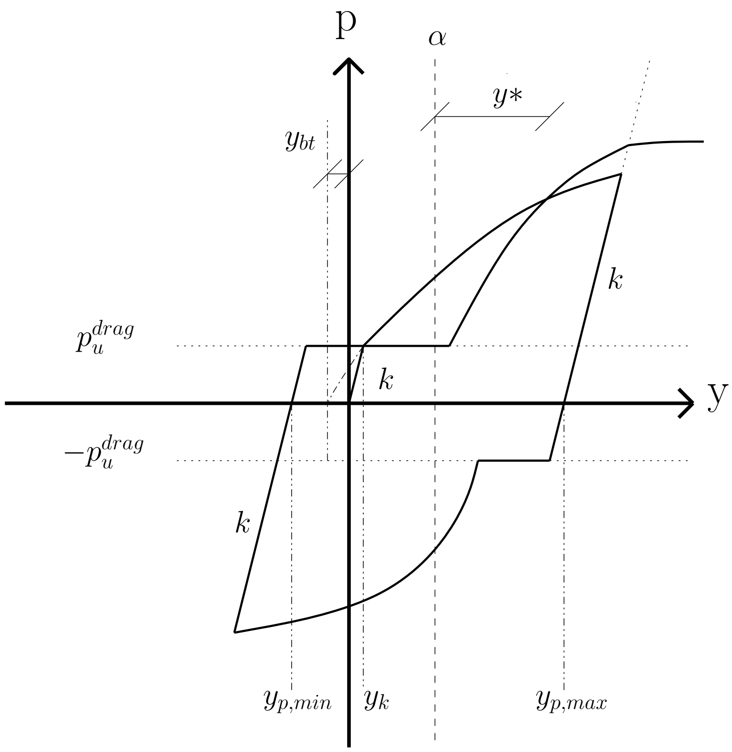

Figure 5.2: *Schematic drawing of the spring element*

The step function is zero when $x < 0$, one half when $x = 0$ and one when $x > 0$. The constant β defines the change from zero to one in the approximation. High β values gives an abrupt change whereas a smaller value will give a smoother transition from zero to one. Here is chosen to have a good approximation of the heavy side function and a value of $\beta = 1,000,000$ is used. The values used in the step function is then given as:

$$\begin{array}{lll} p_1 = p & \& \quad y_{k,1} = y_k & \text{for} \quad y* > 0 \\ p_2 = -p & \& \quad y_{k,2} = -y_k & \text{for} \quad y* < 0 \end{array} \tag{5.6}$$

From the static centrifuge tests it was seen that the monotonic response seems to follow the hyperbolic relation proposed by Kondner (1963) using a modified value of A, (4.2). This observation is used to described the virgin curve in the model.

$$p_u^{virgin} = \frac{y}{\dfrac{1}{E_{py}} + \dfrac{y}{p_{ult}}} \tag{5.7}$$

In order to implement this relation into the framework the resistance is split into a drag contribution and a face loading contribution.

$$p_u(y*) = p_u^{drag} + p_u^{face}(y*) \tag{5.8}$$

The drag contribution is a constant value and defined as a input parameter. The face element should follow the virgin curve, when the element is loaded first time ($y_{p,min} = 0$), From (5.2) and (5.3) the displacement y for virgin loading can then be defined as:

$$
\begin{aligned}
y* &= y - \alpha = y - \frac{1}{2}(y - \frac{p}{k}) \\
2y* &= 2y - y + \frac{p}{k} \\
y &= 2y * - \frac{p}{k}
\end{aligned}
\tag{5.9}
$$

From Figure 5.2 it can be seen that the virgin curve has a artificial starting point this distance has to be added to the displacement in order to capture the correct virgin curve. The displacement used in the Kondner (1963) formulation is therefore written as:

$$
y = 2y * - \frac{p}{k} + y_{bt} \tag{5.10}
$$

The artificial starting point is calculated as:

$$
y_{bt} = \frac{p_u^{drag}}{E_{py} \cdot (1 - \frac{p_u^{drag}}{p_{ult}})} - \frac{p_u^{drag}}{k} \tag{5.11}
$$

This is used together with the virgin curve model found from the monotonic test shown in (5.12). Remembering to take the drag contribution into account, the face element is then defined as:

$$
p_u^{virgin}(y*) = \frac{2y * - \frac{p}{k} + y_{bt}}{\frac{1}{E_{py}} + \frac{2y * - \frac{p}{k} + y_{bt}}{p_{ult}}} - p_u^{drag} \tag{5.12}
$$

The establishment of the cyclic pile-soil interaction spring element is thereby carried out. The only extra input parameter compared to the monotonic calculation is the size of the drag contribution and the elastic loading-unloading stiffness. The formulation used here is not strict in terms of elasto plastic modelling, because the model can build up soil pressure without any hardening. This discrepancy is chosen in order to represent the observations seen in the experiment.

In Figure 5.3 a schematic drawing of the spring element behavior is shown. First time the element is loaded the element will follow the virgin curve, as seen in the monotonic tests. Here the element "pushes" the yield surface and

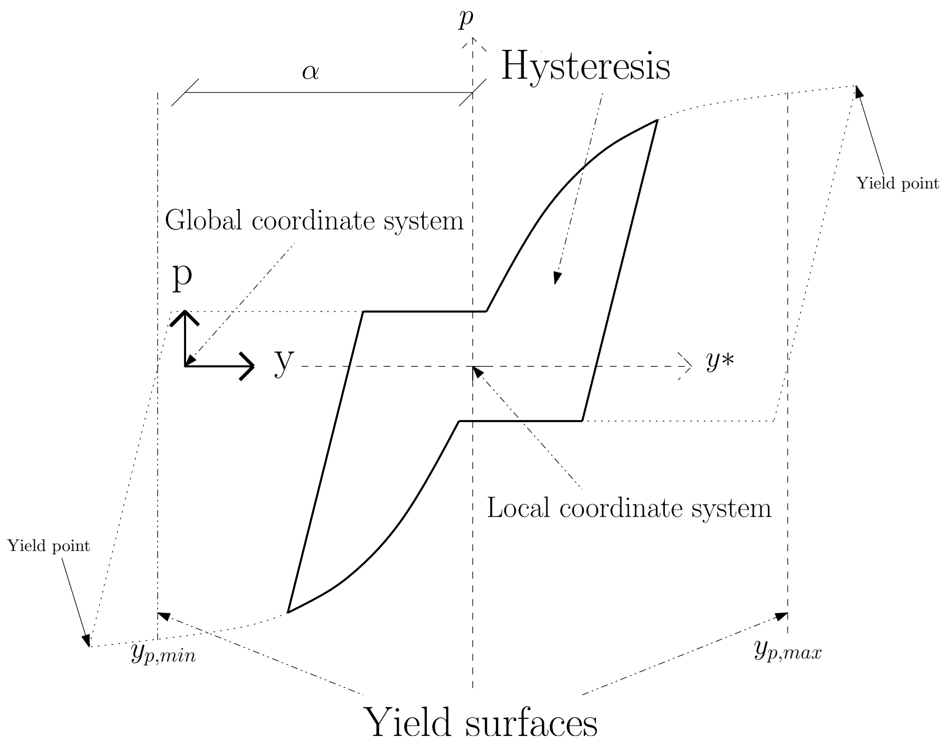

Figure 5.3: *Schematic demonstration of the cyclic spring*

the hardening parameter is activated. When the element is working "inside¨ ¨ the yield surface, the element is symmetrical around a local coordinate system as shown in Figure 5.3. Here the hysteretic behavior can develop with out any hardening. When the element "pushes" to the yield point again the increase in soil pressure will again follow the virgin curve but with a displaced initial start. There is special two phenomenons of this model which is important to realise; First, even though the element is moving inside the yield surface the pile - soil response having a hysteretic behavior. Secondly, the soil resistance can also be larger than defined by the virgin curve, but never larger than the ultimate capacity.

5.1.1 Calibration and demonstration of response

The cyclic spring model have four input parameters, elastic stiffness k, initial stiffness of virgin curve E_{py}, maximum capacity p_u and friction capacity p_u^{drag}. The stiffness of the virgin curve and the maximum capacity can be found using e.g. the API (2007) recommendation. From the cyclic tests it was seen that friction capacity was in the range of 10% of the maximum capacity. Here is therefore used $p_u^{drag} = 0.1 \cdot p_u$. The elastic unloading stiffness was seen to be approximate 5 times stiffer than the virgin curve, here is therefore used $k = 5 \cdot E_{py}^{model}$. The cyclic interaction model can then be used with the same input parameters as a monotonic calculation. To demonstrate the performance of the cyclic spring, the response is compared with results from four deformation controlled tests, (Test nr 61-64). In Figure 5.4 the response

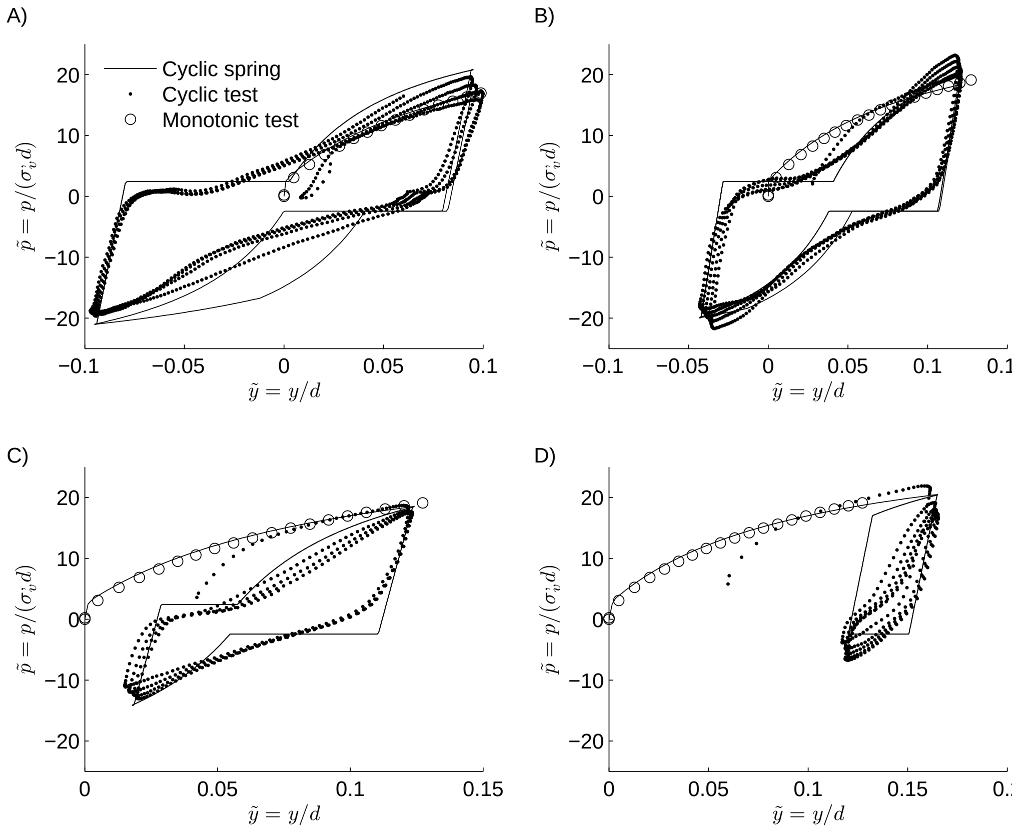

***Figure 5.4**: Demonstration of the cyclic spring, d=3.2m & z=2d & $\phi = 42^o$*

of the cyclic spring and the test results is seen. As described above the model works with two different stiffness' and due to the initial stiff response the stiffness of the virgin curve is reduced to 60% of the initial stiffness found from monotonic tests $E_{py}^{model} = 0.6 \cdot E_{py}^{test}$. This is done in order to follow the virgin curve from the tests. With this reduction the virgin curve of the model seems to follow the monotonic test results. The elastic unloading also seems to predict the test results with a high degree of accuracy for all the tests. The model has a constant friction term and from the test results it can be seen that accuracy is acceptable, but that a constant value maybe is too simple. From the three first load scenarios the model perform very well, but for the last load scenario shown in the low right corner in Figure 5.4, the model shows a to stiff reloading response and a to large hysteresis. In general the model seems to catch the important observation seen from the centrifuge tests on element level.

To observed the behavior of the cyclic spring element in greater details, the pile - soil interaction spring is implemented in a cyclic quasi-static finite element analysis. The aim of this calculation is to compare the pile - soil interaction model with a cyclic centrifuge experiment. The pile is modeled as a solid steel pile with a diameter of d = 3m, load eccentricity of $l_e = 15d = 45$m and a penetration of $l_L = 6d = 18$m. The soil is uniform sand with a relative density of $I_D = 0.9$. The corresponding angle of friction is calculated using the expression by Bolton (1986) showed in (3.15). There is full similarity between the centrifuge and numerical models. The stiffness of the monotonic response was found to be $\tilde{E}_{py}/K_p = 100$, and the stiffness of the virgin curve and the elastic unloading reloading stiffness is fund as described above. From the centrifuge tests it was seen that the overall dis-

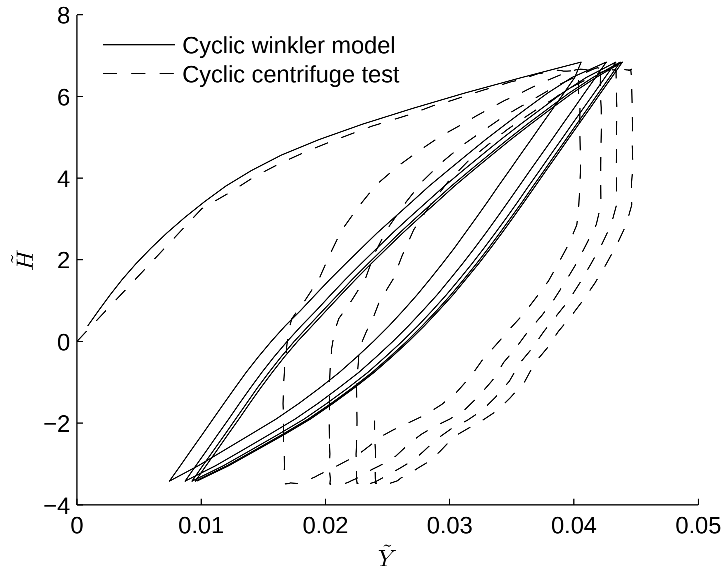

Figure 5.5: *Comparison of the centrifuge test and Winkler model with the cyclic spring, for the overall response*

placements and secant stiffness was changing due to cyclic loading, and was dependent of the characteristic of the loading and the number of cycles. The effect from number of cycles, is not caught by the numerical model, and here is therefore only shown the first couple of cycles.

To demonstrate the response of the model one simulation have been carried out and compared with the centrifuge results in test nr 71. The simulation was carried out with five load controlled cycles corresponding to the test 71. The total response of the first couple of cycles is shown in Figure 5.5. Here it can be seen that the model follows the virgin curve with a high degree of accuracy. When the load is reversed the model shows a much softer response than seen in the tests. Here it should be remembered that the deflection in the tests is measured with a mechanical potentiometer. If there is just a small clearance in the contact between the pile and potentiometer this will lead to a too stiff unloading. The small increase in deflection after load reversal indicates this. At the end of the half cycle the model under predicts the displacement a bit. The overall response seems though to be simulated acceptable. The hysteresis seen in the model test is here larger than the model simulation. This shows that the model will underestimate the damping in the soil.

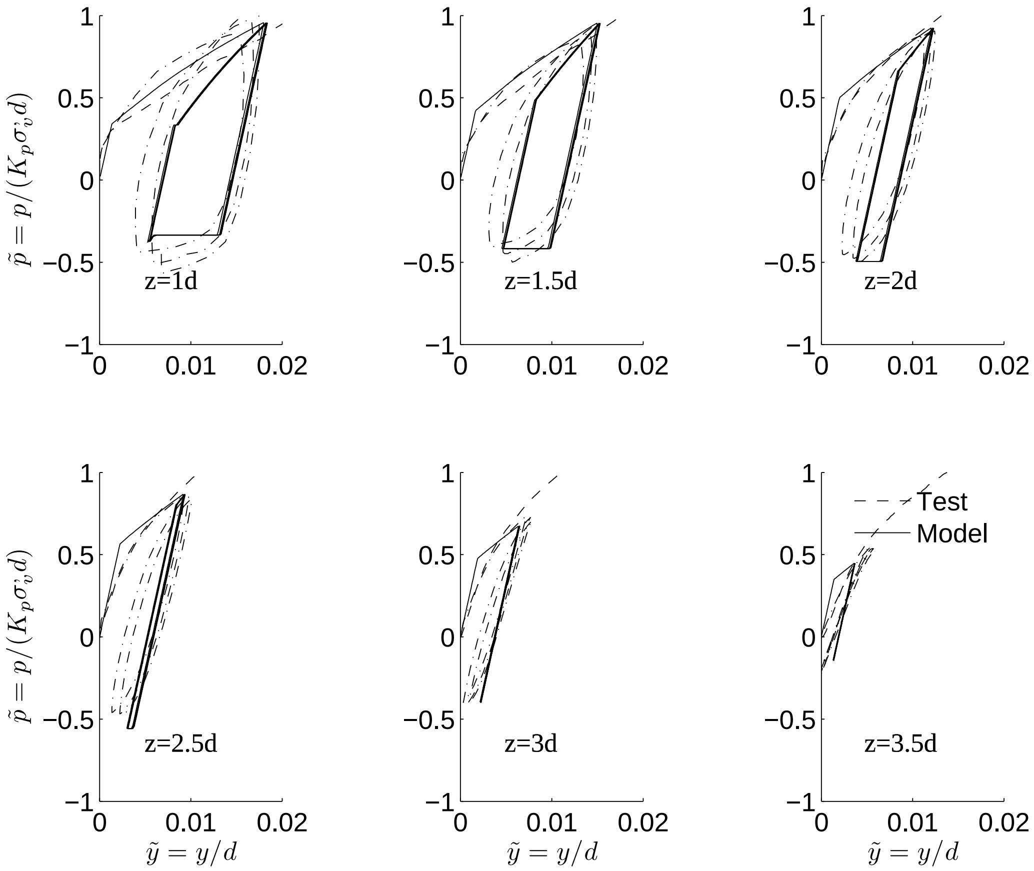

Figure 5.6*: Comparison of the centrifuge test and Winkler model with the cyclic spring, for the local response*

The pile - soil interaction curves previously shown in in Figure 4.19 is here again shown together with the results from the numerical simulation, the results can be seen in Figure 5.6.In the six soil layers a good simulation of the pile - soil interaction is seen. It is though seen that the cyclic spring element does not change in the same degree as seen in the tests. The hysteresis area seen in the tests changes shapes due to the increase in capacity of the sand and the response is also getting stiffer. A qualitative assessment indicates that the hysteretic area is more or less constant.

The prediction of the accumulation of displacement and the change in secant stiffness is not modeled sufficiently accurate by the cyclic model. It is therefore recommended to use the overall response model for the total response in order to address accumulation of displacements.

5.2 Dynamic model

The cyclic spring represents the hysteretic behaviour seen in the centrifuge experiments. This was shown in Figure 5.4 and 5.6. The hysteretic behaviour represents friction damping in the soil and this parameter can be very difficult to access. To give an estimate of the soil damping in the sand the finite element framework FemLab was extended with a time integration scheme.

The time integration scheme uses the generalized α procedure, described in e.g. Krenk (1999) and Krenk (2009). In this methodology both the acceleration and the force term are formed by weighted means between t_n and t_{n+1}, Chung and Hulbert (1993). The basis of the α procedure is the Newmark (1959) formulation, which uses a γ and a β for forward weighting. The generalized α method introduces two additional parameters α_m and α_f. The parameter α_m describes the relative weight of the old inertia term, and the parameter α_f describes the relative weight of the old force term. In the dynamic calculations presented in this thesis the values of these parameters are $\alpha_m = \alpha_f = \gamma = 1/2$ and $\beta = 1/4$.

Foundation and wind turbine is modelled as a beam and the cyclic spring formulation is used for the soil. A simple model of a Horns Rev wind turbine is used, Figure 5.7, a sketch of the simplification can be seen in Figure 5.8. Here the pile is penetrated 24 meter in the sand and the structure above is modeled as a beam with a constant cross section, and thereby also constant mass distribution and stiffness. The nacelle is located 80 meters above sand surface and has a weight of 106 ton. The size of the stiffness and masses corresponds with the one reported in Augustesen et al. (2009). The structure above sand surface is modelled as 40 Bernoulli Euler beam elements with a distributed mass. The structure under sand surface is modelled as 24 Bernoulli Euler beam elements with a distributed mass. At each node in the soil, a spring is attached.

Figure 5.7: *Photo of the Horns rev wind turbine*

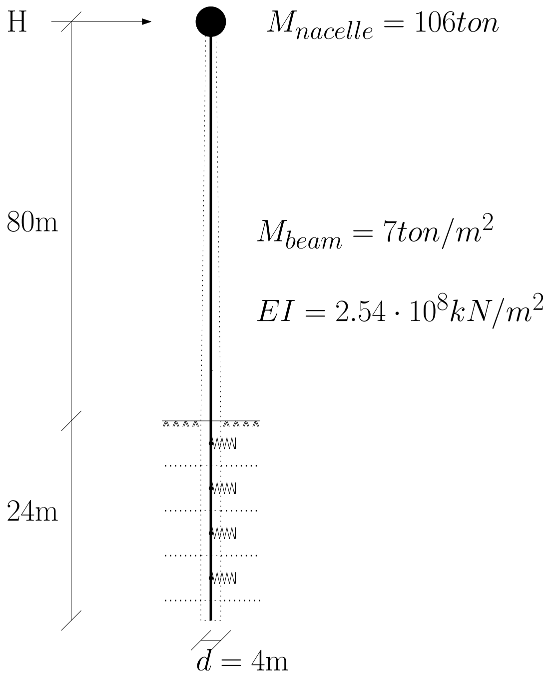

Figure 5.8: *Sketch of numerical model*

5.2.1 Validation of dynamic model

The general α procedure introduces some beneficial numerical high frequency damping into the model. To investigate the numerical damping in the algorithm a free decay test with elastic springs was performed. No viscous damping is applied the model and the numerical damping is therefore the only damping contribution here.

The free vibration of the first mode of the model shown in Figure 5.8 can also be threaded as a single degree of freedom (SDOF) system. The displacement response of the nacelle is therefore compared to the analytical solution of a single degree of freedom system. The free response of a undamped single degree of freedom system can be given as:

$$\ddot{x} + \omega_o^2 x = 0 \tag{5.13}$$

The homogeneous solution to the free oscillations, Chopra (2007) is given entirely in terms of the initial conditions as:

$$\begin{aligned} x &= x_0 \cos(\omega_0 t) + \dot{x}\omega_o^{-1} \sin(\omega_0 t) \\ \dot{x} &= -x_0\omega_0 \sin(\omega_0 t) + \dot{x} \cos(\omega_0 t) \end{aligned} \tag{5.14}$$

It can be seen that the solution given in (5.14) is calculate entirely in terms of the initial conditions. The solution to the undamped vibration therefore only needs the natural angular frequency and the initial displacement and velocity as input parameters. By solving the Eigen value problem of the multi degree of freedom (MDOF) system the initial Eigen frequency of the combine soil - monopile - turbine structure was performed and the first natural Eigen frequency was found to $f = 0.37hz$. This place the structure in the soft-stiff region with a first Eigen frequency between 1P and 3P as shown in Figure 1.4. This is used as input parameter in the calculation of the SDOF system together with the displacement at the point where the force is removed. At this point the loading is very slow and the velocity of the displacements is set as zero. In this analysis elastic springs was used. The results of the analysis

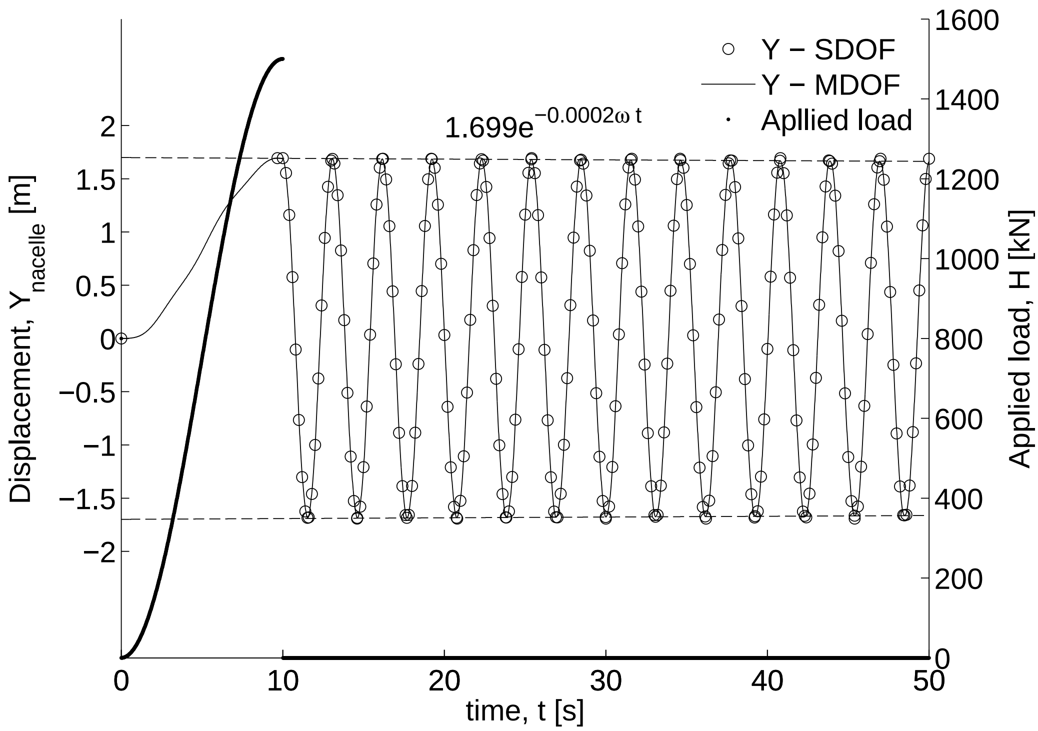

***Figure 5.9**: Free decay modelling of Horns Rev 2 wind turbine with elastic springs*

are shown in Figure 5.9. The force is applied in steps and is maximum after 10 seconds at this time the force is removed and the structure is free to vibrate. The applied load and the displacement of the nacelle is shown in Figure 5.9. The responses of the MDOF and SDOF simulations shows identical responses which validates the dynamic FE model and shows that the numerical high frequency damping is neglectable for the first vibration mode.

5.2.2 Estimation of soil damping

In the fatigue analysis of a wind turbine damping plays a huge role and is often critical for offshore wind turbines, Andersen et al. (2012). The fatigue analysis is carried out using an aero elastic code (e.g. Flex5 - Øye (1996) or HAWK2 - Larsen and Hansen (2007)) where soil damping often is introduces as a viscous damping. Soil damping consist of two parts; one from radiation viscous damping and one from friction in the soil. For sand the main damping contribution is from friction, Bolton and Wilson (1990). The soil damping is difficult to access, but several studies shows that the soil damping is higher than expected, e.g. Tarp-Johansen et al. (2009); Versteijlen et al. (2011); Devriendt et al. (2012).

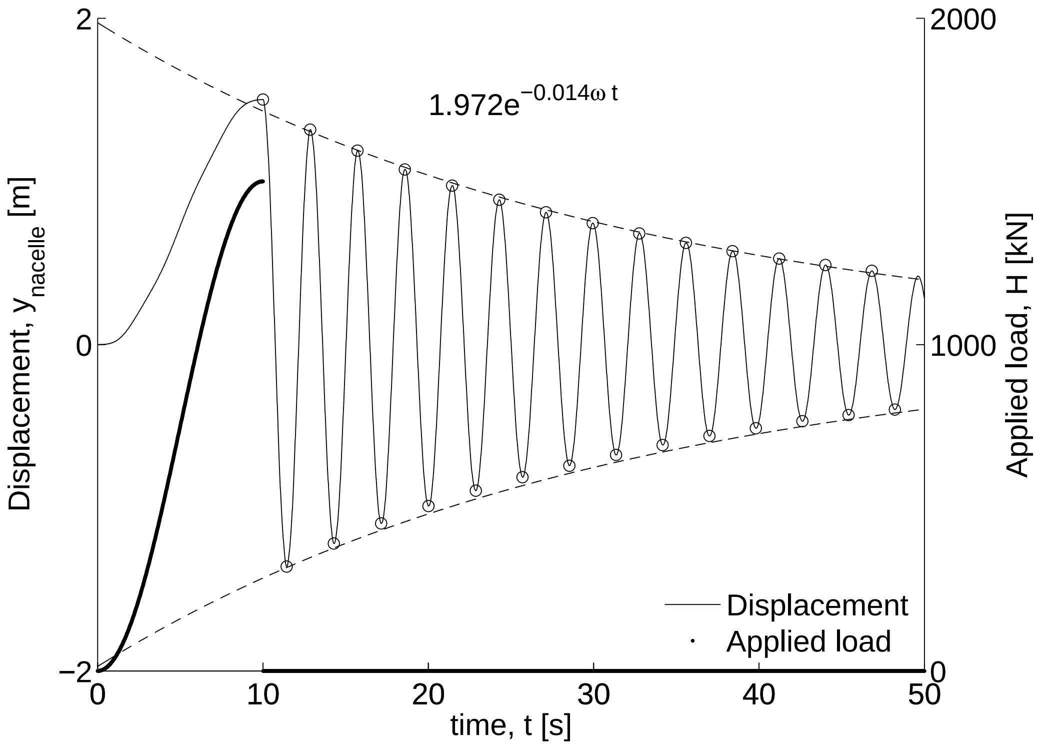

Figure 5.10: *Free decay modelling of Horns Rev 2 wind turbine*

To demonstrate how the pile - soil interaction spring element introduces soil damping to the entire wind turbine structure a series of free decayed tests have been simulated. Using a free decay test with the cyclic spring element a good indication of the damping in the soil can be given. Soil properties identical with the sand used in the centrifuge is used. Input parameter to the cyclic spring element is found as describe above. Here is though used a initial subgrade modulus as proposed by API (2007), shown in Figure 2.3 and is found to $k = 40000kN/m^2$ for a sand with a relative density of $D_r = 0.9$.

In total 6 simulation was carried out, in Figure 5.10 the response from the test where the pile is loaded to 1500kN and afterwards released to vibrated can be seen.

To estimate the damping of the first mode the displacement at the first cycle and the displacement after ten cycler is used to calculate a mean logarithmic decrement. This is done as:

$$\delta = \frac{1}{10} ln\left(\frac{Y_1}{Y_{1+11}}\right) \tag{5.15}$$

From the figure it can be seen that the displacement is decreasing due to the damping. The results from the six tests is shown in Table 5.1. From

***Table 5.1**: Logarithmic decrement from free decay simulations*

P_{max} $[kN]$	Y_{max} $[m]$	$y_{surface}$ $[m]$	element $[-]$	Y_1 $[m]$	Y_{11} $[m]$	δ $[\%]$
1500	1.6990	0.0668	elastic	1.4095	1.4015	0.06
1500	1.4932	0.0386	cyclic	1.3228	0.5741	8.3
1000	0.9790	0.0233	cyclic	0.8765	0.4026	7.8
500	0.4768	0.0098	cyclic	0.4355	0.2309	6.3
250	0.2330	0.0041	cyclic	0.2194	0.1434	4.3
125	0.1146	0.0018	cyclic	0.1118	0.0933	1.8

Table 5.1 it can be seen that the response from the simulation with elastic springs shown in Figure 5.9 has a small amount of numerical damping 0.06%. This is so small that it is neglectable. It is also clearly seen that, that the damping is dependent of the size of the displacements. Large displacements gives large damping and small displacements gives small damping. This is not a surprise and just shows that using a constant damping in the soil is a to simplified model.

In Figure 5.11 the results from Table 5.1 is shown. It is seen that using a logarithmic function the damping decrement can be estimated just knowing the pile displacement at sand surface with a good accuracy. This model can be used to estimate the equivalent viscous damping for the first mode and use this in the a aero elastic code.

The optimal solution is to implement the cyclic spring directly in a aero elastic code. Here the friction based damping is introduce in a more realistic way.

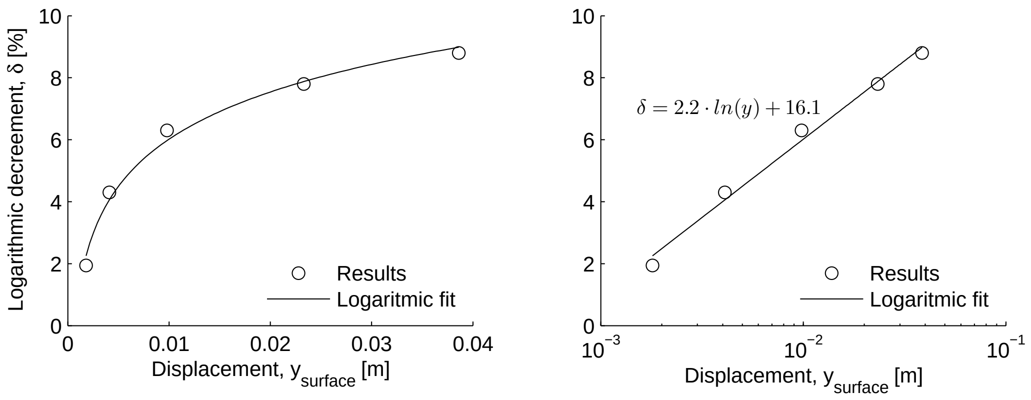

Figure 5.11: *Logarithmic decrement as a function of displacement*

5.3 Summary of pile - soil interaction model

A cyclic spring element have been developed and implemented in a quasi static cyclic code and also a dynamic code. The spring element have been calibrated against deformation controlled and load controlled tests. In the dynamic code the element have been used to estimate the soil damping which arising from friction. From calibration and the demonstration of the spring element different conclusions can be drawn and are here listed:

1. The cyclic spring element only needs 4 parameters which is reduced to two with the current calibration.
2. The cyclic spring element represents the initial hysteresis seen in centrifuge experiments.
3. The change of secant stiffness and accumulation of displacement is not modelled with a sufficient accuracy.
4. In a dynamic analysis the element can be used to estimate the soil damping

Chapter 6

Discussion

Offshore monopiles are situated in saturated soil conditions. The centrifuge test series was primarily carried out in dry dense sand. Choosing an effective stress scaling approach enables to model piles situated in saturated conditions using dry sand. This was demonstrated by four monotonic tests. A direct comparison between cyclic tests performed in dry and saturated conditions was not carried out, but looking at the non-dimensional functions derived from testing in dry and saturated condition, no difference was registered. The scaling approach therefore seems valid. It is important to recognize that the results only are valid for drained loading conditions. Testing in water saturated sand does not represent full scale drainage which means that the water flow in the centrifuge setup is occurring η times faster compared to the prototype and it is therefore unlikely that pore pressures can build up at the current rate of loading. The possible accumulation of pore pressure therefore has to be studied in more details.

6.1 Monotonic loading

In the design of a monopile supporting an offshore wind turbine, the initial stiffness and the maximum bearing capacity are important design parameters for a monotonic load situation. The design methodology used today relies on empirical tests on slender piles. From these tests, pile - soil interaction curves were deducted and are today used also for large diameter, stiff monopiles. The validity of the extrapolation of these curves seems to lack a scientific justifications.

The diameter effect cannot be investigated in a centrifuge experiment, simply because this type of experiment uses a scaled down model. A possible effect from using large diameter piles can only be investigated using prototype dimensions. In a given situation where full scale tests have to be compared, it is important to to have full similarity between the tests.

In full scale tests on large diameter laterally loaded monopiles, not only the diameter but also the stress level are increased compared to the original tests. Five centrifuge tests were performed on one model monopile subjected to increasing stress levels. From the tests it was clearly seen that by taking the stress dependent soil behaviour into account with a simple normalization, the stress level did not affected the normalized response. The normalized result from one centrifuge test can then be compared to a pile with any given diameter. Using the proposed normalization the effect from both diameter and stress level can be decoupled and a possible diameter effect can then be investigated in a full scale test.

Normalized pile - soil interaction curves from centrifuge tests with different load eccentricities were also compared, and the results from the tests showed a high degree of similarity regardless of the load eccentricity. It was therefore possible to relate all the different tests to one generic pile - soil interaction model no matter the load eccentricity. It therefore seems like the change in bending moment to shear force ratio does not affect the pile - soil interaction.

6.1.1 Initial stiffness

There is a wide consensus that the stiffness of sand found in a triaxial test can be described by a power law. This was also seen in (3.16). As a first approximation it is therefore also natural to try to convert the observation seen in the triaxial test to the pile - soil interaction. In this perspective the linear increase of the initial stiffness therefore seems too simple and should instead follow the power law seen in the triaxial test. This has also been tried in this thesis, but no correlation between triaxial and centrifuge results could be given. It can be hard to address the exact reason why there exist a disagreement between triaxial tests and the results from the centrifuge, but it could be related to difference in stress states and complex pile - soil interaction.

Here it is proposed to calculate the initial stiffness using the effective stress level; this enables the calculation of E_{py} with only one initial subgrade modulus function which is valid both for dry and saturated sand. Having an effective density of $10kN/m^3$ leads to an initial subgrade modulus of $k = 5000kN/m^3$, which is significantly smaller than the proposed value of, $k = 40000kN/m^3$. The initial stiffness is affected by the installation procedure and pile installed in-flight at the right stress level would have a larger stiffness. The value found from this study is very small but it is confirming the order of magnitude seen in other centrifuge tests. From the tests presented in this thesis the linear increase with depth above a point of 3.5d is clear, whereas the order of magnitude of the initial subgrade modulus needs to be investigated further.

6.1.2 Maximum bearing capacity

From the centrifuge tests it was clear that the ultimate capacity is not well predicted by non of the methodologies, (Broms (1964) Hansen (1961) or API (2007)).

In the formulation of the ultimate capacity by API (2007) the minimum value of the theoretical calculation of failure in shallow or greater depth is used. For monopiles supporting offshore wind turbines installed in dense sand, the piles are all relative short and the ultimate capacity is thus always calculated as the shallow failure. The failure mechanism is therefore not correct and the value of A plays a huge role.

The use of an empirical factor in the calculation of the ultimate capacity clearly shows that the theoretical assumption lacks accuracy. Here is chosen to use a pragmatic approach with calibration of this factor to the tests. It would thus be preferable to develop a theoretical approach where an empirical factor is avoided. In this perspective the formulation by Hansen (1961) seems to be a better choice. Here is not used an empirical factor and the formulation secures a failure transition from shallow to greater depth. No clear conclusions can though be drawn from this study and it has to be investigated further.

6.2 Cyclic loading

A simple framework for the predication of displacements and secant stiffness has been proposed. This framework was calibrated by a set of centrifuge tests in order to determine a set of non-dimensional functions. The centrifuge tests represent simplifications of the complex soil - water - structure - wind interaction problem and these simplifications are discussed in connection with offshore prototype monopile conditions.

The main part of the tests in this study involved 250-500 load cycles. Three tests were performed with more than 500 cycles; one test with 1000 cycles on the $d = 28mm$ pile and two tests on the $d = 40mm$ pile with respectively 3000 and 10000 numbers of cycles. From these tests it was seen that accumulation of displacement and secant stiffness was well described with the predictions based on the first 500 cycles. It therefore seems reasonable to use the results for up to 10000 cycles. This is still below the number of cycles for the fatigue limit state ($N = 10^7$), but it is an improvement compared to the original design method which is based on tests with fewer than 50 cycles.

In general, the model framework is similar to the one proposed by LeBlanc et al. (2010a), but differences between the models are seen. One of the main findings from the 1g experiments was that the most damaging load situation was for two-way loading, i.e. $\zeta_c = -0.6$. The present centrifuge test series does not show this trend, instead it indicates that one-way loading, $\zeta_c = 0$, is the most damaging one. From the tests by LeBlanc et al. (2010a) accumulation of rotation was seen regardless of the characteristic of the loading. This is also in contrast to the observation done in this study, where it was seen that the pile starts to move back against its initial position for pure two-way loading. This observation was also done by Rosquoët et al. (2010) who performed centrifuge tests on long slender piles. One explanation of these disagreements can be the fact that the tests performed by LeBlanc et al. (2010a) was carried out in loose sand in order to model the maximum angle of friction correctly. The sand in the 1g experiments thus most likely starts to compact when loaded. Tests performed in a centrifuge model stresses and relative densities correctly, so the dilatant behaviour of sand is therefore better accounted for.

The correct modelling of stresses together with the chosen simplification indicates that the findings from the study in this thesis is reliable and can be used in the predications of prototype monopiles.

6.3 Cyclic spring model

A simple cyclic spring element has been presented and the performance of the element has been compared with results from centrifuge experiments. The element predicts the hysteresis seen on element level in an acceptable way but does not predict the accumulation of displacements and change in secant stiffness as seen in the experiments. Soil damping from friction is hard to address and is also depending on the magnitude of the loading, Hald et al. (2009). The spring element takes this into account and it was shown from simple free decay tests to add a logarithmic decrement of 1-8% of soil damping of the first natural vibration mode. This is in accordance with the observation seen in Versteijlen et al. (2011).

Soil damping is especially important in the fatigue analysis and it is believed that applying this cyclic element in a aero elastic calculation will reduce the resonance loads. Especially when the waves and wind is misaligned and the aerodynamic damping is small, Schløer et al. (2012). With reduction in loads the material used in the monopile can be reduced, making the monopile cheaper. This of course has to be validated by simulations.

The spring element still needs some improvements in order to handle the accumulation of deflection and the change in secant stiffness as observed in the centrifuge.

Chapter 7

Conclusions

In this thesis the response of a laterally loaded pile has been investigated. The investigation has been carried out with the application as supporting structure for an offshore wind turbine in mind. To narrow down the scope only a pile installed in homogenously saturated sand has been investigated and the possible accumulation of the pore pressure has been deliberately neglected. Hence, only the drained case is investigated here.

The design of a monopile supporting an offshore wind turbine is carried out in different design limit states. Through this thesis, design methodologies have been presented which can be used for a better technical solution for a monopile supporting an offshore wind turbine.

The scientific validation of this methodology is based on a set of 74 different centrifuge experiments on laterally loaded model piles. About half of the tests have been used in order to investigate the transformation of centrifuge results to prototype scale. This has primarily been carried out using the "Modelling of Models" technique. Scale effects were identified and a centrifuge modelling procedures were developed in order to have a reliable modelling technique.

With a reliable modelling technique established, the pile - soil interaction was investigated with a range of monotonic and cyclic centrifuge tests. The ultimate limit state was investigated by a series of monotonic tests. From the observation seen in these test, a formulation of the monotonic pile-soil interaction was given. This formulation can be used in a standard Winkler model and predicts the displacement from a given lateral load. The serviceability limit state has been investigated by a series of cyclic load tests. From these test, a model to predict the overall displacement and secant stiffness of the foundation from cyclic loading has been proposed. The model only needs a monotonic test as input parameter, which can be found using the Winkler approach described above.

A cyclic spring element has been developed and can be used in monotonic, cyclic and dynamic calculation. This is needed in the design of the fatigue limit states. The spring element has been developed from cyclic centrifuge test observations and describes the cyclic pile - soil interaction. The element predicts the hysteresis seen in the different soil layers acceptably, but does not catch the accumulation of displacement and change in secant stiffness seen in the centrifuge experiments.

It is here recommended that the cyclic spring element is implemented in an aero elastic code. This code can be used in the fatigue analysis and in the load analysis. When this analysis is carried out, the monotonic model can be used to calculate a static response and the cyclic model for overall displacements can be used to estimate the permanent displacements. The design limit states can thereby all be handled with models developed in this thesis.

Outlook

Doing the three years of my Ph.D. studies, I have gained an in sight in a complex soil - structure interaction problem. With the centrifuge setup as my main investigation tool I have tried to identify different important parameters for the interaction problem of a laterally loaded pile. This outlook tries to describes my current understanding of the interaction problem and especially in which direction further investigations should be performed in.

A large part of my project has been about the centrifuge methodology and how to transfer these results to a prototype scale. This can be done by a dimensional analysis and is not only a tool for scaling of results, but also a tool which should be used in order to understand scaling problems. From industry and research communities concerns about the use of pile - interaction curves for large diameter piles have been given, this is known as the diameter effect. Through my three years of work I have not seen a paper where the diameter effect has been threatened and full similarity has been kept between the investigated models. It is therefore very difficult to know if such an effect is existing. It is my belief that a finite element calculation can not capture a possible diameter effect. This was also illustrated in this thesis by having identical normalised response from two simulations of laterally loaded piles in two different scales. I therefore only see, the use of full scale testing in order to document a possible diameter effect.

Pore pressure accumulation is also a factor that needs to be investigated. If a possible pore pressure accumulation have to be investigated in a centrifuge, both loading frequency and permeability have to be scaled with the increase in gravity in order to achieve full similarity with prototype. The permeability can be decreased by changing the liquid used in the centrifuge test to e.g. silicon oil. The loading frequency is hard to scale and with the current setup at DTU I do not think it is possible to perform loading at this frequency. I think the solution for this is to perform centrifuge test in oil saturated sand with a load frequency as high as possible. The results from these tests should then be calibrate against a cyclic numerical model. The numerical model can then be used for the final scaling of the observation.

The numerical model should be cable of handling the interaction between structure soil and water.

The centrifuge tests performed during this thesis have all been carried out with the focus on initial stiffness and maximum capacity. This has implied that a solid pile has been used in order to capture the soil failure. The initial stiffness of the pile - soil response is for wind turbines more crucial than the ultimate capacity. I will recommend that a hollow pile is used in the further centrifuge tests. The installation force for a hollow pile is smaller and the softer response will help the interpretation of the initial stiffness. The focus should be the initial stiffness and the the displacement magnitude should be very small $y < 1/100d$. With a pile with a diameter of $d = 40mm$ this leads to maximum deformations at sand surface of $y < 0.4mm$. This set some demands on the displacement measurements.

The installation of the pile at the correct stress level has been shown in thesis to be important for the lateral response. The a load setup with in-flight installation at the correct stress level and laterally load testing without stopping the centrifuge is needed. The installation of the pile and afterwards laterally loading of pile also leads to smaller manual work with the setup after the pile is installed and thereby also smaller disturbance of the soil package. The demand from installation and laterally loading in one take and the precision of the deflection measurements leads to that two new contact less measurement devices is needed. Here laser LVDT's would be the obvious choice.

This thesis have been concerning centrifuge modelling, I have briefly in thesis and here in the outlook discussed the used of other methodologies. I think it is important to remember that no methodology is perfect and for reliable research different methodologies should always be used.

Lyngby, the 29$^{\text{th}}$ of June 2012

Rasmus Tofte Klinkvort

Bibliography

K. Abdel-Rahman and M. Achmus. Finite element modelling of horizontally loaded monopile foundations for offshore wind energy converters in germany. In *International Symposium on Frontiers in Offshore Geotechnics (ISFOG)*, 2005.

M. Achmus, Y.-S. Kuo, and K. Abdel-Rahman. Behavior of monopile foundations under cyclic lateral load. *Computers and Geotechnics*, 36(5):725–735, 2009. M3: 10.1016/j.compgeo.2008.12.003.

International Energy Agency. *Energy Technology Perspectives 2008: Scenarios and Strategies to 2050.* Organisation for Economic Co-operation and Development, Jul 08 2008. ISBN 9789264041424.

International Energy Agency. *Energy Technology Perspectives 2010.* Organisation for Economic Co-operation and Development, Jul 01 2009. ISBN 9789264085978.

L. V. Andersen, M. J. Vahdatirad, M. T. Sichani, and J. D. Sørensen. Natural frequencies of wind turbines on monopile foundations in clayey soils - a probabilistic approach. *Computers and Geotechnics*, 43:1–11, 2012.

API. *API RP 2A-WSD Recommended practice for planning, designing, and constructing fixed offshore platforms - Working stress design*, 2007.

S. A. Ashford and T. Juirnarongrit. Evaluation of pile diamter effect on initial modulus of subgrade reaction. *Journal of geotechnical and geoenvironmental engineering*, 129:234–242, 2003.

A. H. Augustesen, K. T. Brødbæk, M. Møller, S. P. H. Sørensen, L. B. Ibsen, T. S. Pedersen, and L. Andersen. Numerical modelling of large-diameter steel piles at Horns Rev. In *Proceedings of the Twelfth International Conference on Civil, Structural and Environmental Engineering Computing*, 2009.

S. Bhattacharya, D. Lombardi, and D. M. Wood. Similitude relationships for physical modelling of monopile-supported offshore wind turbines. *International Journal of Physical Modelling in Geotechnics*, 11:58 –68, 2011.

M. D. Bolton. Strength and dilatancy of sands. *Geotechnique*, 36(1):65–78, 1986.

M. D. Bolton and J. M. R. Wilson. Soil stiffness and damping. *Structural Dynamics*, 1:209–216, 1990.

R. W. Boulanger, C. J. Curras, B. L. Kutter, D. W. Wilson, and A. Abghari. Seismic soil-pile-structure interaction experiments and analysis. *Journal of Geotechnical and Geoenvironmental Engineering*, 125:750–759, September 1999.

J.-L. Briaud, T. D. Smith, and B. J. Meyer. Using the pressuremeter curve to design laterally loaded piles. *Proceedings - Annual Offshore Technology Conference*, 1:495–502, 1983.

B. Broms. Lateral resistance of piles in cohesionless soils. *ASCE – Proceedings – Journal of the Soil Mechanics and Foundations Division*, 90:123–156, 1964.

A. K. Chopra. *Duynamics of structures - Theory and applications to earthquake engineering.* Prentice Hall, 2007.

J. Chung and G. M. Hulbert. A time integration algorithm for structural dynamics with improved numerical dissipation: The generalized-alpha method. *Journal of applied mechanics*, 60(2):371–375, 1993. ISSN 15289036.

W. H. Craig. Installation studies for model piles. *Proceedings of a Symposium on the Application of Centrifuge Modelling to Geotechnical Design.*, pages 441–456, 1985.

P. Cuéllar, M. Baeßler, and W. Rücker. Ratcheting convective cells of sand grains around offshore piles under cyclic lateral loads. *Granular Matter*, 11(6):379–390, 2009. M3: 10.1007/s10035-009-0153-3.

C. Devriendt, P. J. Jordaens, G. D. Sitter, and P. Guillaume. Damping estimation of an offshore wind turbine on a monopile foundation. In *EWEA*, 2012.

DNV. *Design of offshore wind turbine structures*, volume DNV-OS-J101. Det norske Veritas, 2011.

DNV and RISØ. *Guidelines for Design of Windturbines*, 2001.

G. J. Dyson and M. F. Randolph. Monotonic lateral loading of piles in calcareous sand. *Journal of Geotechnical and Geoenvironmental Engineering*, 127(4):346–352, 2001. M3: 10.1061/(ASCE)1090-0241(2001)127:4(346).

M. H. El Naggar, M. A. Shayanfar, M. Kimiaei, and A. A. Aghakouchak. Simplified bnwf model for nonlinear seismic response analysis of offshore piles with nonlinear input ground motion analysis. *Can. Geotech. J.*, 42 (2):365–380, 2005. ISSN 12086010.

C.-C. Fan and J. H. Long. Assessment of existing methods fro predicting spoil response of laterally loaded piles in sand. *Computers and Geotechnics*, 32: 274–289, 2005.

L. D. Fuglsang and J. Nielsen. Danish centrifuge hardware and usage. *Centrifuges in Soil Mechanics*, pages 93–95, 1988.

L. D. Fuglsang and N. K. Ovesen. The application of the theory of modelling to centrifuge studies. *Centrifuges in Soil Mechanics*, pages 119–138, 1988.

J. Garnier, C. Gaudin, S. M. Springman, P. J. Culligan, D. Goodings, D. Konig, B. Kutter, R. Phillips, M. F. Randolph, and L. Thorel. Catalogue of scaling laws and similitude questions in geotechnical centrifuge modelling. *International Journal of Physical Modelling in Geotechnics*, 7 (3):1–23, 2007.

C. Gaudin, F. Schnaid, and J. Gamier. Sand characterization by combined centrifuge and laboratory tests. *International Journal of Physical Modelling in Geotechnics*, 5:42–56, 2005.

M. Georgiadis, C. Anagnostopoulos, and S. Saflekou. Centrifugal testing of laterally loaded piles in sand. *Canadian Geotechnical Journal*, 29(2): 208–216, 1992.

T. Hald, C. Mørch, L. Jensen, C. L. Bakmar, and K. Ahle. Revisiting monopile design using p-y curves. results from full scale measurements on Horns Rev. *Proceedings of European Offshore Wind 2009 Conference*, 2009.

J. B. Hansen. Ultimate resistance of rigid piles against transversal forces. *Geoteknisk Institut – Bulletin (Danish Geotechnical Institute – Bulletin)*, 1(12):5–9, 1961.

O. Hededal and R. T. Klinkvort. A new elasto-plastic spring element for cyclic loading of piles using the p-y curve concept. *Numerical Methods in Geotechnical Engineering : NUMGE 2010*, pages 883–888, 2010.

O. Hededal and S. Krenk. Femlab, matlab toolbox for the finite element method. Aalborg University, May 1995.

M. Hetenyi. *Beams on Elastic Foundation: Theory with Applications in the Fields of Civil and Mechanical Engineering.* University of Michigan Press, 1946.

M. Jacobsen. *New oedometer and new triaxial apparatus for firm soils.* Geoteknisk Institut, 1970.

B. T. Kim, N.-K. Kim, W. J. Lee, and Y. S. Kim. Experimental load-transfer curves of laterally loaded piles in nak-dong river sand. *Journal of Geotechnical and Geoenvironmental Engineering*, 130(4):416–425, 2004. M3: 10.1061/(ASCE)1090-0241(2004)130:4(416).

R. T. Klinkvort and O. Hededal. Lateral response of monopile supporting an offshore wind turbine. Submitted for publication, 2012a.

R. T. Klinkvort and O. Hededal. Monotonic soil-structure interaction of monopile support for offshore wind turbines. Submitted for publication, 2012b.

R. T. Klinkvort, C. T. Leth, and O. Hededal. Centrifuge modelling of a laterally cyclic loaded pile. *Physical Modelling in Geotechnics*, pages 959–964, 2010.

R. T. Klinkvort, O. Hededal, and M. Svensson. Laterally cyclic loading of monopile in dense sand. *Proceedings of the 15th European Conference on Soil Mechanics and Geotechnical Engineering*, 2011.

R. T. Klinkvort, O. Hededal, and S. Springman. Scale effects in centrifuge modelling of monopiles. Submitted for publication, 2012.

R.T. Klinkvort and O. Hededal. Centrifuge modelling of offshore monopile foundation. *Frontiers in Offshore Geotechnics II*, pages 581–586, 2010.

R. L. Kondner. Hyperbolic stress-strain response; cohesive soils. *ASCE – Proceedings – Journal of the Soil Mechanics and Foundations Division*, 89: 115–143, 1963.

S. Krenk. Dynamic analysis of structures - numerical time integration. Technical report, Course on Non-Linear Analysis of Frame Structursc, 1999. Course on Non-Linear Analysis of Frame Structurs, 1999.

S. Krenk. *Non-linear Modeling and Analysis of Solids and Structures*. Cambrigde University Press, 2009.

H. L. Langhaar. Dimensional analysis and theory of models. Technical report, John Wiley & Sons, 1951.

T. J. Larsen and A. M. Hansen. *How 2 HAWC2, the user's manual*, 2007.

C. LeBlanc, G. T. Houlsby, and B. W. Byrne. Response of stiff piles in sand to long-term cyclic lateral loading. *Geotechnique*, -:–, 2009.

C. LeBlanc, G. T. Houlsby, and B. W. Byrne. Response of stiff piles in sand to long-term cyclic lateral loading. *Geotechnique*, 60(2):79–90, 2010a. M3: 10.1680/geot.7.00196.

C. Leblanc, B. W. Byrne, and G. T. Houlsby. Response of stiff piles to random two-way lateral loading. *Geotechnique*, 60(9):715–721, 2010b. M3: 10.1680/geot.09.T.011.

K. Lesny and J. Wiemann. Finite-element-modelling of large diameter monopiles for offshore wind energy converters. In *Geo Congress*, 2006.

C. T. Leth, A. Krogsbøll, and O. Hededal. Centrifuge facilities at danish technical university. In *15th Nordic Geotechnical Meeting*, 2008.

Z. Li, S. K. Haigh, and M. D. Bolton. Centrifuge modelling of mono-pile under cyclic lateral loads. *Physical Modelling in Geotechnics*, pages 965–970, 2010.

J. H. Long and G. Vanneste. Effects of cyclic lateral loads on piles in sand. *Journal of Geotechnical Engineering*, 120:225–244, 1994.

B. McClelland and J. A. Focht. Soil modulus for laterally loaded piles. *American Society of Civil Engineers – Proceedings – Journal of the Soil Mechanics and Foundations Division*, 82, 1956.

G. G. Meyerhofs, K. Mathur, and A. J. Valsangk. Lateral resistance and deflection of rigid walls and piles in layered soils. *CAN. GEOTECH. J.*, 18:159–170, 1981.

J. M. Murchison and M. W. O'Neill. Evaluation of p-y relationships in cohesionless soils. In *Proc., Symposium of Analysis and Design of Pile Foundations, ASCE, San Fransisco*, pages 174–191, 1984.

N. M. Newmark. Method of computation for structural dynamics. *ASCE – Proc (J Eng Mechanics Div)*, 85:67–94, 1959.

G. Norris and P. Abdollaholiaee. Bef - studies with the strain wedge model. part a. *Proceedings of the 1990 Annual Symposium on Engineering Geology & Geotechnical Engineering*, pages 13A.1–13A16, 1990.

I. L. Nunez, R. Phillips, M. F. Randolph, and B. D. Wesselink. Modelling laterally loaded pile in calcareous sand. *Centrifuge 88*, pages 353–362, 1988.

N. K. Ovesen. Centrifugal testing applied to bearing capacity problems of footings on sand. *Geotechnique*, 25(2):394–401, 1975.

F. Parker and L. Reese. Experimental and analytical study of behavior of single piles in sand under lateral and axial loading - research report no. 117-2. Technical report, Center for Highway Research, The University of Texas, 1970.

M. J. Pender, D. P. Carter, and S. Pranjoto. Diameter effects on pile head lateral stiffness and site investigation requirements for pile foundation design. *Journal of Earthquake Engineering*, 11(1), 2007. SP:.

P. Peralta and M. Achmus. An experimental investigation of piles in sand subjected to lateral cyclic experiments. In *Physical Modelling in Geotechnics*, 2010.

H. Poulos and T. Hull. The role of analytical geomechanics in foundation engineering. *Foundation Engineering: Current principles and Practices, ASCE, Reston*, 2:1578–1606, 1989.

M. F. Randolph. Science and empiricism in pile foundation design. *Geotechnique*, 53(10):847–875, 2003. M3: 10.1680/geot.53.10.847.37518.

L. C. Reese and . F. Van Impe. *Single Piles and Pile Groups Under Lateral Loading*. A. A. Balkema, 2001.

L. C. Reese and H. Matlock. Non-dimensional solutions for laterally-loaded piles with soil modulus assumed proportional to depth. In *Proceedings of eighth Texas Conference on Soil Mechanics and Foundation Engineering*, 1956.

L. C. Reese, W. R. Cox, and F. D. Koop. Analysis of laterally loaded piles in sand. In *Offshore Technology Conference*, 1974.

D. Remaud. *Pieux sous charges latérales: Etude Experimentale de l'effect de groupe*. PhD thesis, Ecole Centrale de Nantes, 1999.

F. Rosquöet, L. Thorel, J. Garnier, and Y. Canepa. Lateral cyclic loading of sand-installed piles. *Soils and Foundations*, 47, no 5:821–832, 2007.

F. Rosquoët, L. Thorel, J. Garnier, and M. Khemakhem. P-y curves on model piles: Uncertainty identification. In *Physical Modelling in Geotechnics*, pages 997–1002, 2010. ISBN 978-0-415-59288-8.

S. Schløer, H. Bredmose, H. B. Bingham, and J. T. Larsen. Effects from fully nonlinear irregular wave forcing on the fatique life of an offshore wind turbine and its monopile foundation. In *Proceedings of the ASME, International Conference on Ocean, Offshore and Artic Engineering, OMAE*, 2012.

A. N. Schofield. Cambridge geotechnical centrifuge operations. *Geotechnique*, 30(3):227–268, 1980.

R. F. Scott. Analysis of centrifuge pile tests: Simulation of pile driving. Research report, american petroleum institut osapr project 13, California Institute of Technology, 1980.

T. D. Smith. Pile horizontal soil modulus values. *Journal of Geotechnical Engineering*, 113(9):1040–1044, 1987.

S.P.H. Sørensen, K. T. Brødbæk, M. Møller, A. H. Augustesen, and L. B. Ibsen. Evaluation of the load-displacement relationships for large-diameter piles in sand. In *Proceedings of the Twelfth International Conference on Civil, Structural and Environmental Engineering Computing*, 2009.

M. Svensson. Load amplitude effects on cyclically loaded monopile. Master's thesis, Technical University of Denmark, 2010.

E. Taciroglu, C. Rha, and J. W. Wallace. A robust macro element model for soil pile interaction under cyclic loads. *Journal of geotechnical and geoenvironmental engineering*, Vol. 132(No. 10):p. 1304–1314, October 2006.

N.J. Tarp-Johansen, L. Andersen, E. Damgaard, B. Kallesøe, and Sten Frandsen. Comparing sources of damping of cross-wind motion. In *European Offshore Wind*, 2009.

R. N. Taylor. *Centrifuges in modelling: principles and scale effects*. Blackie Academic & Professional, 1995.

K. Terzaghi. Evaluation of coefficients of subgrade reaction. *Geotechnique*, 5(4):297–326, 1955.

J. Ubilla, T. Abdoun, and T. Zimmie. Application of in-flight robot in centrifuge modeling of laterally loaded stiff pile foundations. *Physical Modelling in Geotechnics*, 1:259–264, 2006.

W.G. Versteijlen, A. Metrikine, J.S. Hoving, E.H. Smidt, and W.E. De Vries. Estimation of the vibration decrement of an offshore wind turbine support structure caused by its interaction with soil. In *Proceedings of the EWEA Offshore 2011 Conference, Amsterdam, The Netherlands*, 2011.

D. M. Wood. *Geotechnical modelling*. Spon Press, 2004.

K. Yang and R. Liang. Methods for deriving p-y curves from instrumented lateral load test. *Geotechnical testing journal*, 30:1–8, 2006.

S. Øye. Flex4 simulation of wind turbine dynamics. In *28th IEA Meeting of Experts, Concerning State of the Art of Aeroelastic Codes for Wind Turbine Calculationsn.*, 1996.

V. Zania and O. Hededal. The effect of soil-pile interface behaviour on laterally loaded piles. In *Proceedings of the Thirteenth International Conference on Civil, Structural and Environmental Engineering Computing*, 2011.

V. Zania and O. Hededal. Friction effects on lateral loading behavior of rigid piles. In *GeoCongress 2012 - State of the Art and Practice in Geotechnical Engineering*, 2012.

L. Zhang, F. Silva, and R. Grismala. Ultimate lateral resistance to piles in cohesionless soils. *Journal of Geotechnical and Geoenvironmental Engineering*, 131(1):78–83, 2005. M3: 10.1061/(ASCE)1090-0241(2005)131:1(78).

Part II

Papers

Paper I

"Centrifuge modelling of offshore monopile foundation"

R.T. Klinkvort & O. Hededal

Published in: *Frontiers in Offshore Geotechnics II, 2010*

Frontiers in Offshore Geotechnics II – Gourvenec & White (eds)

Centrifuge modelling of offshore monopile foundation

R.T. Klinkvort & O. Hededal
Technical University of Denmark, Copenhagen, Denmark

ABSTRACT: Today one of the most used concepts for wind turbine foundation is the monopile. The foundation concepts for these monopiles on deeper water is uncertain and consequently the design needs to be conservative leading to uneconomic designs. This paper describes a total number of 6 static and 5 cyclic centrifuge tests on a laterally loaded monopile in dry sand. The prototype dimension of the piles was modelled to a diameter of 1 meter and penetration depth on 6 meter. The test series were designed in order to investigate the scaling laws in the centrifuge both for monotonic and cyclic loading. It was not possible in the tests to reproduce the same prototype response for both the monotonic and the cyclic loading. It was not clear if this scatter in prototype data was due to normal measurement uncertainties or if the response is depending on the scaling factor.

1 INTRODUCTION

Single large diameter tubular steel piles commonly denoted monopiles is today a very used foundation method for offshore wind turbines. The design of these monopiles is commonly based on the theory of laterally loaded piles which relies on empirical data originated from the oil and gas industry, Reese and Matlock (1956) & McClelland and Focht (1958). The lateral capacity is determined by modelling the pile as a beam and the soil as a system of uncoupled springs, this is known as a Winkler model. The springs are described by p-y curves defining the load-displacement relationship for the interaction between soil and pile, API (1993). The formulation of these curves was originally calibrated to slender piles, but is today even used for design of large diameter monopiles with a slenderness ratio L/D as low as 5. The monopiles used for wind turbine foundations thus act as stiff piles. Therefore it is relevant to investigate the behavior of stiff piles in more detail. The tests series presented in this paper is an initial program that intends to investigate the response of model monopiles subjected to different artificial gravities in a centrifuge. The concept called modelling of models is used to investigate the response from five different piles which are scaled to the same prototype dimensions.

2 CENTRIFUGE MODELLING

When performing centrifuge tests an artificial gravity is applied to a model test setup. This is done to ensure that the stress field in the model is similar to the stress field in the prototype. This is important in model testing due to the non-linearity of the stress-strain relations of soils. To apply the artificial gravity the model is placed at the end of a rotating arm. The acceleration in a specified point in the model is given by the angular rotation speed (ω) and the distance (R) from the rotational axis. The ratio between gravity (g) and artificial gravity is described by the gravity scale factor (N).

$$N = R\omega^2/g \tag{1}$$

In centrifuge modelling two key issues are represented, the scaling laws and the scaling errors.

2.1 *Scaling laws*

To transform results from test carried out on models to prototypes the dimensional analysis can be used, Langhaar (1951). The foundation for the dimensional analysis is Buckingham's Π theorem. From this, dimensionless parameters can be determined. These dimensionless parameters have to be the same for the prototype and the model to have full similarity. If all governing laws of similitude are in place a true model is obtained. This implies that stresses and strains are scaled by a factor of 1, deflection and lengths is scaled by a factor of N, forces are scaled by a factor of N^2 and so on; see e.g. Taylor (1995).

2.2 *Scale effects*

In physical modelling it is seldom possible to produce a model where all details of the model is scaled correctly in the prototype. Therefore some approximations have to be made. These differences are called scale effects and are important to be aware of when the test results are interpreted. Model studies are not perfect and it is important to understand this. Two main effects will be presented here. The first is the stress distribution. Looking at Equation 1 on the preceding page it can be seen that the applied gravity is depending on the distance to the rotational axis.

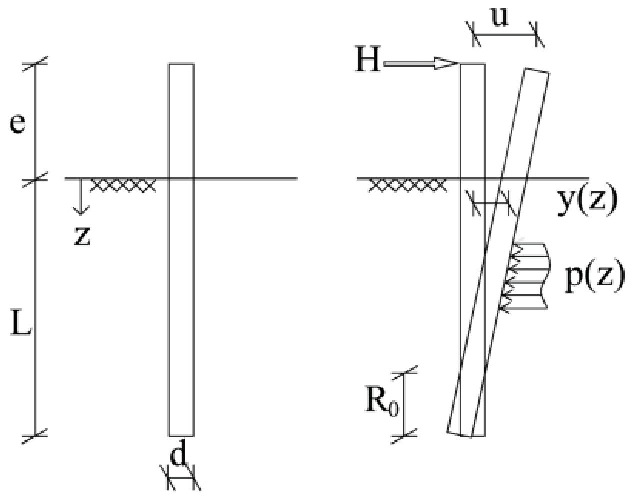

Figure 1. Sketch of pile.

This distance will increase through the model. In the prototype the stresses will increase linearly due to the constant gravity field, whereas the stresses in the model will increase parabolically. To minimize this error the radius is defined from center to a depth of 2/3 of the pile penetration depth, Stuit (1995).

When performing centrifuge modelling it is not possible to scale the sand grain diameter correctly, since this will imply a difference in friction angle and cohesion. Therefore, when considering bearing capacity, it is most often necessary to use the same sand in the model as in the prototype. This causes the sand grains to be scaled by a factor of N in the model. This is known as the particle size effect. The grain size effect has been investigated with "modelling of models". Particle size effect has been tested for laterally loaded piles by Hoadley et al. (1981) and they found that a "model diameter/ grain size diameter" ratio of 50 and above gave a good agreement. Remaud et al. (1998) found that a ratio over 60 was enough to avoid particle size effects. Both of these studies were performed on long slender piles. Nunez et al. (1988) performed modelling of models on tension piles. They found that the smaller piles tested at high accelerations gave consistently higher capacity than larger piles tested at smaller accelerations. They explain this difference with installation effects and differences in wall thickness and conclude that the effect from particle size is not significant.

3 EXPERIMENTS

As the first of a larger test series on monopiles a series of modelling of models have been performed to analyze the response of a monopile in relation to the applied gravity. The test program was performed on five solid steel piles with a diameter between 16–40 mm and penetration depths between 96–240 mm which were all scaled to a prototype pile with a diameter of $d = 1$ m and penetration depth $L = 6$ m.

In figure 1 a sketch of the test pile can be seen. In Table 1 the dimension of the five piles and the scaling factor is shown. This should scale all the piles to the same prototype pile.

Table 1. Dimensions and scaling factor for the piles.

d [mm]	e [mm]	L [mm]	N [–]
16	40	96	62.5
22	55	132	45.5
28	70	168	35.7
34	85	204	29.4
40	100	240	25

Table 2. Classification parameters for the Fontainebleau sand.

Specific gravity of particles	G_s	2.646
Minimum void ratio	e_{min}	0.548
Maximum void ratio	e_{max}	0.859
Average grain size	d_{50}	0.18
Coefficient of uniformity	C_u	1.6

Table 3. Void ratio for the different tests.

d [mm]	16	22	28	34	40
Monotonic	0.58/0.57	0.58	0.57	0.59	0.56
Cyclic	0.59	0.56	0.56	0.58	0.55

All monotonic and cyclic tests were performed in dry Fontainebleau sand. Leth et al. (2008) has collected classification parameters for the Fontainebleau sand which can be seen in table 2 on the next page. The average grain size of the Fontainebleau sand is 0.18 mm. With pile diameter ranging from 16 mm to 40 mm this leads to a "model diameter/ grain size diameter" ratio ranging from 88 to 189.

The centrifuge at DTU uses a spot pouring hopper (SPH) for the preparation of the sand sample. Due to the geometry of the container and pile the sand is prepared using a circular travelling loop as described in Zhao et al. (2006). The sand is installed in a container with a inner diameter of 50 cm and a height of 49 cm. A new sample is prepared for each of the tests. CPT tests have been carried out to validate the pouring method. All these CPT tests showed the soil sample has a good homogeneity in the container.

After the sand is prepared, the pile is installed at 1 g. It must be expected that the sand is compacted in a higher degree around the pile, for large piles than for small piles. When the tests are carried out it must be expected that the stresses in the sand is so high that potential preconsolidated areas disappears. Installing the pile at 1 g. is therefore intended to minimize the effects from the installation.

A total of 11 centrifuge tests have been performed: six monotonic and five cyclic. For all the tests the relative density was found to vary in the range 0.8–0.94. A table with the different void ratios can be seen in table 3 on the following page. The relative densities

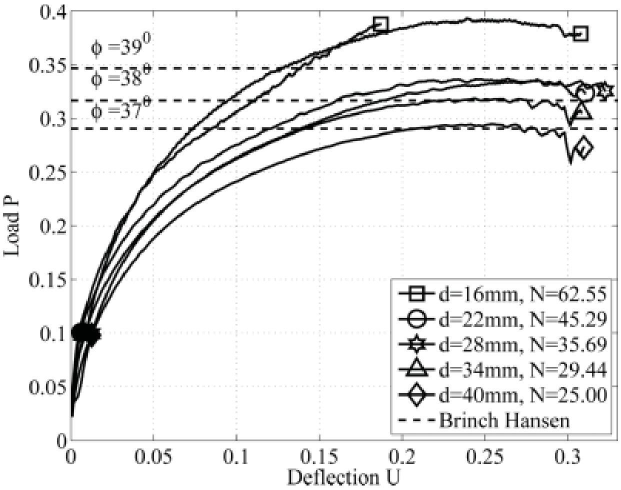

Figure 2. Normalized plot with the five static tests.

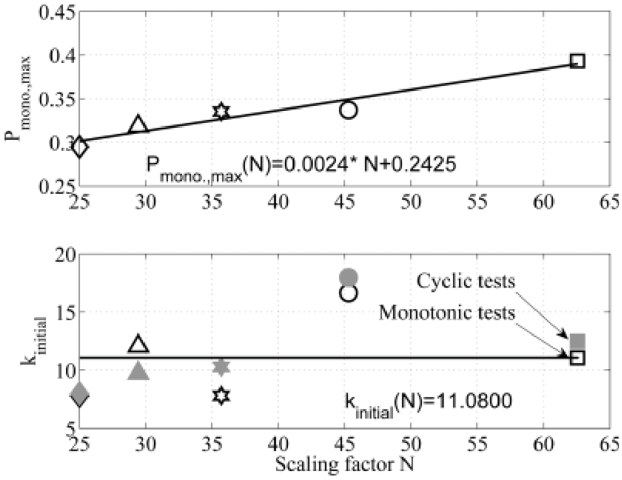

Figure 3. Normalized plot bearing capacity and initial stiffness as a function of the scaling factor.

are calculated by knowing the weight and the volume of the sand sample. The average value for both the static and cyclic tests is for the relative density $I_D = 0.924$ and a void ratio of $e = 0.57$ leading to a triaxial frictional angle of $\phi = 38°$.

3.1 *Monotonic tests*

The force and deflection is normalized, to compare the general pile behavior. On the y-axis the normalized force is plotted. This is found as shown in equation 2.

$$P = \frac{H}{\gamma \cdot L^3} \tag{2}$$

On the x-axis the normalized deflection is plotted. This is shown in equation 3

$$U = \frac{u}{L} \tag{3}$$

In figure 2 the observation of the monotonic loading can be seen. Remember that all the test is scaled to same prototype and the response from the different tests should be identical. However a variation in the results can be seen. The test performed at 62.5 g showed a significantly high bearing capacity therefore a second test on the $d = 16$ mm was performed to validate the response. The second test confirmed the response.

Interpretation method 1: Looking at figure 2 you could say that the pile with a diameter of $d = 16$ mm shows a much higher capacity than the other piles and thereby indicates that the pile diameter particle diameter is too small. If this pile is neglected an acceptable scatter of the results is obtained. From this a bearing capacity for the prototype pile could be expected to be $P_{max} \approx 0.32$. This will be called interpretation method 1. On figure 2 the bearing capacity according to Hansen (1961) is shown for three different frictional angles. This indicates small change in frictional angle can be the reason for this scatter. On the other hand using the result from the pile with a diameter of $d = 16$ mm it can be seen that the maximum bearing capacity is increasing with the applied gravity. This could indicate that the linear scaling which is assumed is problematic.

Interpretation method 2: The maximum bearing capacity and the initial stiffness is plotted on figure 3 against the scaling factor. The maximum capacity is found as the maximum value found on figure 2 and the initial stiffness is found at the point where the applied load is $P = 0.1$. This is shown on figure 2 as the black markings. From figure 3 it seems to be a clear linear relationship between the maximum bearing capacity and the scaling factor. Looking at the initial stiffness of the load deflection response no clear relationship is seen. The variance of the stiffness could though indicate that a constant stiffness from the tests could be expected. Here is also plotted the initial stiffness found from the cyclic testing which support this conclusion.

Four of the piles were mounted with measuring of the pile head rotation, if the pile is assumed to behave as a rigid pile, the pile movement can be described according to equation 4.

$$y(z) = u - \theta(e + z) \tag{4}$$

The assumption of the pile behaves like a rigid pile is satisfied according to Poulos and Hull (1989) if the stiffness of the sand is lesser than $E_s = 35$ MPa. If the pile should act as a slender pile then the soil stiffness should be over $E_s = 3090$ MPa. Even if the stiffness of the sand is larger than 35 MPa it is expected that the pile will be located close to the rigid boundary. Therefore it is assumed that the pile behaves as a stiff pile. From this assumption the point of rotation can be found knowing the deflection of the pile u and the rotation θ. The normalize point of rotation measured from pile tip is plotted in figure 4. Due to practical reasons the rotation of the 16 mm pile could not be measured. All the piles shows that the normalized point of rotation is located below the pile tip at initial deflection and the pile is therefore sheared through the sand. After some deformation the rotation point moves up and is located

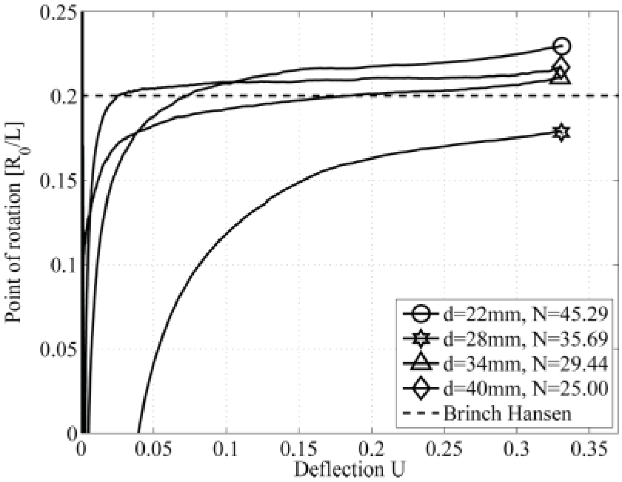

Figure 4. Point of rotation.

in the pile where it is stabilized until failure. From figure 4 no clear relation between normalized point of rotation and scaling factor can be seen. It seems like for all the piles that the rotation point stabilizes around a value of 0.22 except the pile with a diameter of $d = 28$ mm which haves a lower rotation point that the others. Using the theory of Hansen (1961) the rotation point is calculated to 0.2 which is close to the observation. It seems like all the piles is moving in the same manner.

3.2 *Cyclic tests*

The cyclic tests were performed with 500 force controlled cycles. To investigate the effects from cyclic loading this paper uses a method describe in LeBlanc (2009) to described the cyclic loading. The load characteristics are denoted ζ_b and ζ_c. They are determined as shown in equation 5.

$$\zeta_b = \frac{P_{max}}{P_{monotonic}} \qquad \zeta_c = \frac{P_{min}}{P_{max}} \tag{5}$$

Here P_{max} and P_{min} are the maximum and minimum applied force in the cyclic loading. $P_{monotonic}$ is the maximum bearing capacity found from the corresponding monotonic test.

The amount of the applied load depends on the interpretation of the monotonic test. The cyclic loading was performed as individual tests, with five different maximum capacities according to the monotonic tests shown on figure 2 on the preceding page. It was the intension to perform the cyclic test with a $\zeta_b = 0.40$ and a $\zeta_c = 0$ but due to the control system it has not been possible to perform tests with exactly the same load characteristics. However the load characteristics can also be calculated assuming a constant bearing capacity for the monotonic tests. The characteristics of the cyclic loading for the tests series for the two types of interpretation can be seen on Figure 4. For the cyclic loading the accumulation of deflection and the change in secant stiffness is calculated. This is done as showed on figure 5. For every cycle the maximum and minimum values of load and the deflection is found. From this the average deflection can be calculated as shown in equation 6 and the secant stiffness can be calculated as shown in equation 7.

Table 4. Load characteristics for the cyclic tests.

N	$P_{mono.,1}$	$P_{mono.,2}$	$\zeta_{b,1}$	$\zeta_{b,2}$	ζ_c
62.6	0.32	0.39	0.53	0.44	−0.04
45.3	0.32	0.34	0.52	0.49	−0.05
35.7	0.32	0.34	0.44	0.44	−0.02
29.4	0.32	0.32	0.41	0.42	−0.02
25.0	0.32	0.29	0.41	0.44	−0.10

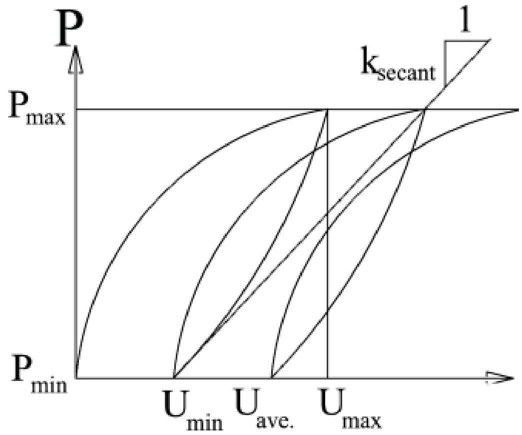

Figure 5. Schematic illustration of average deflection and secant stiffness.

$$U_{average} = \frac{U_{max} + U_{min}}{2} \tag{6}$$

$$K_{secant} = \frac{P_{max} - P_{min}}{U_{max} - U_{min}} \tag{7}$$

The best fit to the accumulation of deflection was done with a power fit as proposed by Long and Vanneste (1994), cf. equation 8.

$$U_{average}(n) = u_0 \cdot n^{\alpha} \tag{8}$$

Here u_0 is the accumulated deflection at the first cycle and α is an empirical coefficient which controls the shape of the curve. n is the number of cycles. The accumulated deflection for a given cycle is defined as the average value for the cycle. The values of the coefficient to the proposed formula can be seen in Table 5. If interpretation method 1 is used the accumulation depends on the load characteristic. ζ_c is nearly constant for all the tests expect test on $d = 40$ mm. It must therefore be expected to see a relation between ζ_b and the coefficient to the power fit. A linear relationship is assumed which leads to the following equations.

$$u_0(\zeta_b) = 0.0300 \cdot \zeta_b + 0.0002 \tag{9}$$

$$\alpha(\zeta_b) = 0.3170 \cdot \zeta_b + 0.1585 \tag{10}$$

Table 5. Empirical constant for accumulation of the deflection from the cyclic testing.

d	u_0	α
16	0.016	0.324
22	0.015	0.315
28	0.010	0.339
34	0.015	0.245
40	0.012	0.256

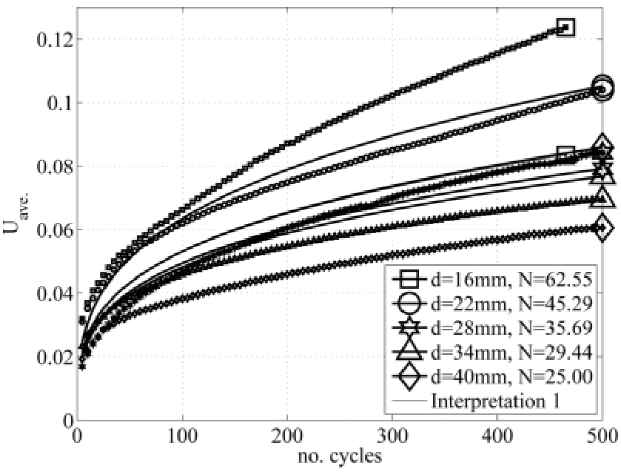

Figure 6. Accumulation of average deflection with interpretation method 1 prediction.

If on the other hand interpretation method 2 is used a linear relationship between the coefficients for the power fit and the scaling factor can be assumed. This leads to following equations.

$$u_0(N) = 0.0001 \cdot N + 0.0096 \tag{11}$$

$$\alpha(N) = 0.0018 \cdot N + 0.2266 \tag{12}$$

On figure 6 the accumulation of the deflection for cyclic testing is seen. Here is also shown the prediction as proposed in equation 8 for the interpretation methods 1. The prediction for the interpretation methods 2 can be seen in Figure 7. None of the methods give good predictions, but it seems that interpretation method 2 is the best. It should again be noted that the cyclic loading is performed according to the maximum bearing capacity found from the monotonic tests. This means that the piles are not loaded to the same prototype loads. The maximum prototype load for the small pile with the large scaling factor is therefore larger than the large pile with the small scaling factor.

Lin and Liao (1999) proposed a logarithmic fit to the change in secant stiffness as shown in equation

$$K_{secant}(n) = k_0 + \kappa \cdot ln(n) \tag{13}$$

Here k_0 is the secant stiffness at the first cycle and κ is an empirical coefficient which control the shape of the curve. n is the number of cycle. A formulation like

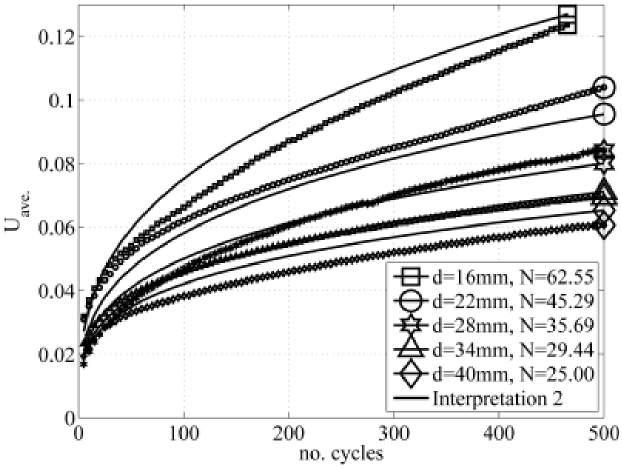

Figure 7. Accumulation of average deflection with interpretation method 2 prediction.

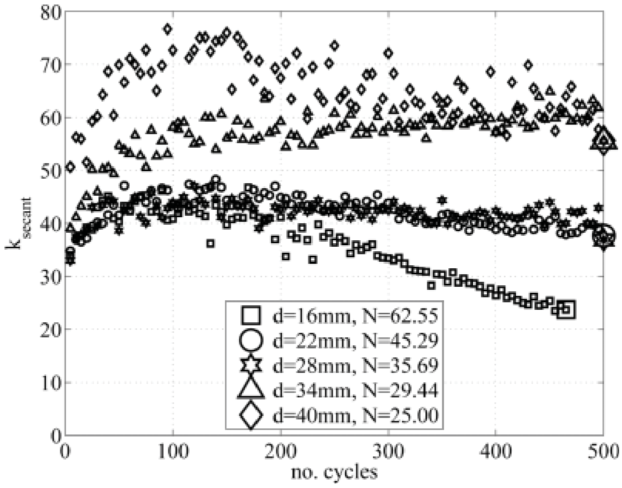

Figure 8. Change in secant stiffness.

this fits the first 100 cycles for the 5 cyclic tests, but as it can be seen in Figure 8 the secant stiffness starts to decrease or stabilize after 100 cycles. It has not been possible to fit the entire number of cycles cyclic. Looking at Figure 8 it can be seen that the secant stiffness is changing from test to test. The secant stiffness is large for the large piles and smaller for the small piles. The explanation for the difference can again be explained for interpretation method 1 as high ζ_b values gives small secant stiffness. Using method 2 high scaling factor gives high secant stiffness. No clear dependency is seen for the two interpretation methods.

4 CONCLUSIONS

A test series of modelling of models have been performed for both monotonic and cyclic loading. It has not been possible for the two loading types to reproduce exactly equal prototype response. The results have been analyzed in two ways; one as a normal scatter in the response, and one using a dependency of the scaling factor. It seems like the scaling factor affects the results but it is not clear. Nunez et al. (1988) reports also higher capacity for the small piles tested at high g levels and more tests have to be conducted. The fact that the piles in this test series are acting as stiff piles could be an explanation of the difference from previously modelling of models tests. More tests have to be conducted in order to clarify the scaling laws for these stiff laterally loaded piles.

REFERENCES

API (1993). *Recommended Practice For Planning, Designing and Construction Fixed Offshore Platforms* – Load and Resistance Factor Design. American Petroleum Institute.

Hansen, J. B. (1961). The ulitimate resistance of rigid piles against transversal forces. *Danish Geotechnical Institute, Copenhagen, Denmark Bulletin NO. 12*, 5–9.

Hoadley, P. J., Y. O. Barton, and R. H. G. Parry (1981). Cyclic lateral load on model pile i a centrifuge. In *Proceedings of the Tenth International Conference on Soil Mechanics ans Foundation Engineering*, Volume Vol. 1.

Langhaar, H. L. (1951). Dimensional analysis and theory of models. Technical report, John Wiley & Sons.

LeBlanc, C. (2009). *Design of Offshore Wind turbine Support Structures*. Ph. D. thesis, Aalborg University.

Leth, C. T., A. Krogsbøll, and O. Hededal (2008). Centrifuge facilities at danish technical university. In *15th Nordic Geotechnical Meeting*.

Lin, S. S. and J. C. Liao (1999). Permanent strains of piles in sand due to cyclic lateral loads. *Journal of Geotech. and Geoenv. Engng. 125 No. 9*, 798–802.

Long, J. H. and G. Vanneste (1994). Effects of cyclic lateral loads on piles in sand. *Journal of Geotechnical Engineering 120*, 225–244.

McClelland, B. and J. A. Focht (1958). Soil modulus for laterally loaded piles. *Journal of the soil mechanics and foundations division – Proceedings of the American Society of Civil Engineers* -, 1–22.

Nunez, I. L., P. J. Hoadley, M. F. Randolph, and J. M. Hulett (1988). Driving and tension loading of piles in sand on a centrifuge. In *Centrifuge 88*.

Poulos, H. and T. Hull (1989). The role of analytical geomechanics in foundation engineering. *Foundation Engineering: Current principles and Practices, ASCE, Reston 2*, 1578–1606.

Reese, L. C. and H. Matlock (1956). Non-dimensional solutions for laterally loaded piles with soil modulus assumed proportional to depth. *Proceedings of the 8th Conference on Soil Mechanics* -, 1–41.

Remaud, D., J. Garnier, and R. Frank (1998). Pieux sous charges lat'erales: étude de léffect de groupe. *5. Journées Nationales Génie Civil Génie Côtier, Toulon*, pp. 369–376.

Stuit, H. G. (1995). *Sand In The Geotehcnical Centrifuge*. Ph. D. thesis, Technische Universiteit Delft.

Taylor, R. N. (1995). *Centrifuges in modelling: principles and scale effects*. Blackie Academic & Professional.

Zhao, Y., K. Gafar, M. Elshafie, A. Deeks, J. Knappett, and S. Madabhushi (2006). Calibration and use of a new automatic sand pourer. In *Physical modelling in Geotechnics, 6th ICPMG '06*, pp. p. 265–270.

Paper II

"Scale effects in centrifuge modelling of monopiles"

R. T. Klinkvort, O. Hededal & S. Springman

To be submitted for publication -, *2012*

Scale effects in centrifuge modelling of monopiles

Rasmus Tofte Klinkvort[1], Ole Hededal[2] and Sarah Springman[3]

1) Ph.D. research student, Dept. of Civil Engineering, Technical University of Denmark, Sec. of Geotechnics and Soil Mechanics, Brovej Building 118, 2800 Kgs. Lyngby, Denmark. Phone: (+45) 25 38 78 13, rakli@byg.dtu.dk.

2) Associate Professor, Dept. of Civil Engineering, Technical University of Denmark, Sec. of Geotechnics and Soil Mechanics, Brovej Building 118, 2800 Kgs. Lyngby, Denmark. Phone: (+45) 45 25 50 20, olh@byg.dtu.dk.

3) Professor, Institute for Geotechnical Engineering, Swiss Federal Institute of Technology – Zurich , Sec. of Geotechnics, HIL C13.1, 8093 Zurich, Switzerland. Phone: +41 (44) 633 38 05, sarah.springman@igt.baug.ethz.ch

Keywords: *Centrifuge modelling, Foundations, Piles and piling, Sands, Renewable energy.*

Date written: Thursday, June 28, 2012

Date revised: -

Number of words: 5055 (without abstract, tables, figure and references)

Number of pages: 25

Number of figures: 10

Number of tables: 4

Abstract

Offshore wind turbine generating capacity is increasing and new wind farms are being constructed in deeper and deeper waters. A reformulation of the design concept based on rigid piles is needed if the monopile foundation concept is to succeed into deeper waters. Centrifuge modelling offers a tool for testing monopiles, and this paper deals with three different important issues for centrifuge testing on monopiles for offshore wind turbines. A series of centrifuge model tests of laterally-loaded stiff monopiles has been conducted on cylindrical model piles installed at 1g and in-flight and also on conical model piles installed in-flight. All model tests were performed in normally consolidated dense dry sand, simulating drained condition. The tests showed three important issues for centrifuge modelling of monopiles for offshore wind turbines. First, to avoid any grain-size effect, the ratio between average grain-size and pile diameter has to be larger than 88. Secondly, the non-linear stress distribution which is often neglected has to be taken into account in the analysis of the lateral response. Finally, the tests confirm that both stiffness and strength increase using in-flight installation but it also shows that in-flight installation is needed to avoid any scale effects.

Introduction

Offshore wind turbine generating capacity is increasing and new wind farms are being constructed in deeper and deeper waters. A popular foundation concept for offshore wind turbines is the monopile. A monopile foundation is a large diameter hollow steel pile, which is driven into the soil. Lateral loads, characterised by large eccentricity, are transferred to the foundation from the wind turbine. With a penetration depth of 5-6 times the diameter, monopiles act in a rigid manner when subjected to lateral loads. The design formulation used today is calibrated for slender piles but is still used for rigid monopiles. A reformulation of the design concept based on rigid piles is needed if this foundation concept is to succeed in deeper waters. This is the justification for current research on monopiles. In this context, centrifuge modelling offers a low-cost tool, compared to prototype testing, which if handled correctly makes it possible to scale model observations to prototype. The centrifuge modelling technique has with success been used for a number of offshore foundation problems, and has been used in order to establish design procedures for range of different problems (e.g. Bienen, Cassidy & Gaudin (2009), Cassidy, Randolph & Byrne (2004) & De Nicola, Randolph (1999)). For lateral loaded piles scale effects have been investigated by Nunez et al. (1988) and Remaud (1999) in order to develop a reliable modelling technique, but these investigations have been for long slender piles. No investigation of scale effects seems to have been carried out for rigid monopiles loaded with a high moment to shear ration. Therefore an investigation of the scaling issues for a monopile has been performed in this study, and with the conclusions from the investigation a centrifuge modelling methodology has been established where model observations can be used in the analysis of a prototype monopile. The investigation have been based on a modelling technique where using different sizes of piles and stress distributions all simulating same prototype response, scale effects can be identified. This is known as modelling of models, (Ovesen 1975) and is in this paper used for five different sized piles. This paper deals with three different important aspects when performing centrifuge modelling of laterally loaded monopiles for offshore wind turbines. The issues are the scaling of grain-sizes, installation and g-field.

Scale effects in the centrifuge

To transform results from model scale to prototype scale dimensional analysis can be used. To establish the analysis the important phenomena's have to be known in order to determine the governing parameters. The governing parameters have been established looking at the similar problem for laterally loading of piles, e.g. Hansen (1961) and Randolph (1981). In this analysis we assume quasi static laterally loading of the monopile, no pore pressure build up, the problem can therefore be analysed as an effective stress problem. The result of a dimensional analysis can then be written in a form where the normalised applied load is a function of a set of non-dimensional ratios, (Langhaar (1951), Fuglsang, Ovesen (1988) and Wood (2004)).

$$\frac{H}{\gamma'\cdot d^3} = f\left(\frac{Y}{d},\frac{l_L}{d},\frac{l_e}{d},\frac{E_s l_L{}^4}{E_p I_p},\frac{d}{d_{50}},\frac{q_c-\gamma\cdot z}{\gamma'\cdot z},\phi'\right) \qquad (1)$$

These non-dimensional ratios have to be identical in model and prototype scale in order to avoid scale effects.

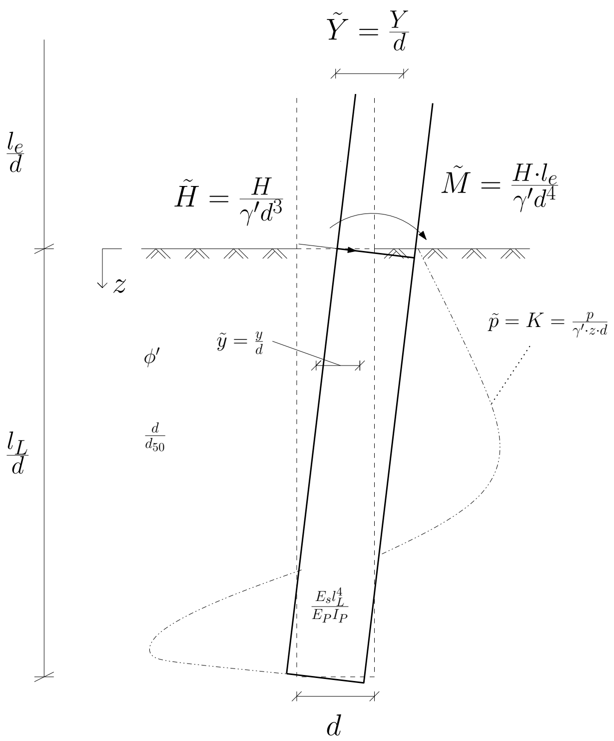

Figure 1 Sketch of non-dimensional lateral loaded pile

A sketch of a laterally loaded pile with dimension is seen in Figure 1, here the definition of the different parameters can be seen. The dimensions of the pile ($l_L / d, l_e / d$) are scaled with the length scale ratio $N_s = d_p / d_m$ (ratio between prototype and model diameter) and having same material and stress field in model and prototype the non-dimensional stiffness ratio $E_s l_L^4 / E_p I_p$ is also easily obtained. Using identical soil in model and prototype, leads to a scaling problem for the size of the grains. The use of identical soil is carried out to ensure identical mechanical behaviour in model and prototype. The soil resistance is a combination of pressure and friction, (Briaud, Smith & Meyer 1983) and (Smith 1987). A minimum ratio between in this case pile diameter and average grain-size diameter d / d_{50} is therefore needed to ensure that the soil behaves in a consistent manner at all geometrical scales, (Ovesen 1975). This insures that the pressure is modelled correctly, the friction is on the other hand difficult to model correctly due to the difference in roughness and grain size, and this often leads to scale effects, (Garnier, Konig 1998).

For axially loaded piles, in-flight installation is important for the vertical response. Several studies have shown that the installation method is important for the lateral response as well (Craig 1985, Dyson, Randolph 2001). The majority of centrifuge tests on laterally loaded monopiles are though still performed on piles installed at 1g, e.g. Remaud (1999), Ubilla, Abdoun & Zimmie (2006) and Li, Haigh & Bolton (2010). The process under pile installation is complex and involves movement of the sand grains and also sand crushing, (Randolph, Dolwin & Beck 1994), (De Nicola, Randolph 1999), (McDowell, Bolton 2000), (White, Bolton 2004), (White, Lehane 2004) and (Weber et al. 2010). The non-dimensional installation stress, $\tilde{Q} = \left(q_c - \gamma \cdot z\right) / \left(\gamma' \cdot z\right)$ therefore have to have similarity with prototype in order to model these effects correctly.

To achieve identical stress level compared to prototype, the model is placed in a centrifuge to increase the acceleration gravity. The increase in gravity can be calculated using equation 1. See e.g. (Schofield 1980).

$$\eta = \frac{\omega^2 R}{g} \qquad (2)$$

where ω is the angular frequency of the centrifuge, R is the radius of the rotation measured to a selected point of reference and g is the earth's gravity. It can be seen from Equation 1 that the increase in gravity is increasing with the radius. This implies the soil density is increasing with depth. The soil stresses in prototype is increasing linearly and an effective radius $R_e = R_t + l_L/3$ corresponding to 1/3 of pile penetration was chosen so soil stresses in model and prototype was identical at a depth of 2/3 of the pile penetration. This was chosen to minimize the stress error (Taylor 1995) . The vertical stress can be calculated as shown in Equation 2. This takes the non-linear distribution into account.

$$\sigma_v \approx \rho \cdot \varpi^2 \cdot z \cdot (R_t + \frac{z}{2}) \qquad (3)$$

The soil stresses in prototype and in the centrifuge model are therefore not exactly identical. The height of the centrifuge soil model introduces a parabolic non-linear increase in soil stresses. In comparison with the linear increase that is assumed to occur to the prototype. This implies small stress errors between model and prototype. The error is often not larger than 2-3 % and is therefore usually neglected (Schofield 1980).

The three issues presented above can be studied by performing centrifuge tests on different sized model piles with a stress distribution corresponding to the same prototype. This is called "modelling of models". This technique has been used before for laterally loaded piles e.g. (Barton 1985), (Nunez et al. 1988), (Terashi 1989) and (Remaud 1999) . Still in these cases only the grain-size effect where investigated. Monopiles for wind turbines are different from normal laterally loaded piles because these monopiles are rigid piles subjected to a high ratio between bending moment and shear force. According the scaling catalogue from "TC2 –Physical Modelling in Geotechnics" (Garnier et al. 2007), no grain size effect was detected in "modelling of models" if the ratio between pile diameter and average grain size was larger than 45 (Nunez et al. 1988) or 60 (Remaud 1999) for laterally loaded piles. Both of these tests were performed on long slender piles and the results from these tests should be used with caution for short stiff piles. (Klinkvort, Hededal 2010) performed "modelling of models" on five stiff monopiles with ratios between pile diameter and average grain size all larger 88. All piles were installed at 1g and here a relationship between stiffness/strength and applied gravity was reported, indicating scale effects.

Experimental method

The centrifuge experiments were carried out in a beam centrifuge at the Technical University of Denmark (DTU). The centrifuge, Figure 2, has a radius of 1.7m to the swing and 0.521m from the swing to the sand surface, this sums up to a rotation radius to the sand surface of R_t=2.221m. At the swing a circular strong box is placed and on top of this a load actuator is mounted. The maximum payload of the strongbox and load actuator is 100 gton.

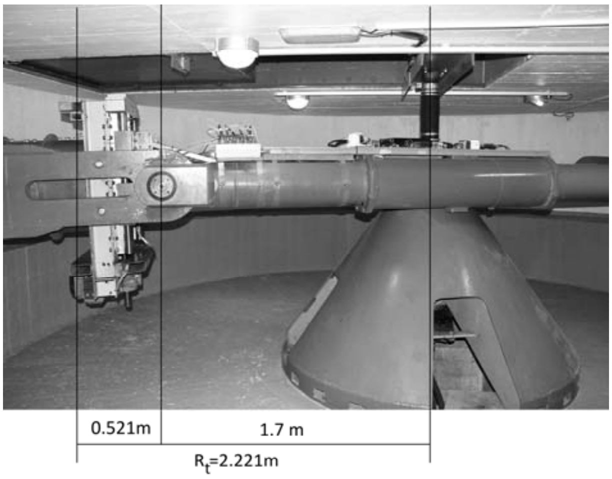

Figure 2 Photo of the beam centrifuge at DTU used for testing

A multipurpose load actuator was mounted on the strongbox container to apply load to the pile. The load setup allows different kinds of tests with only small changes. The setup consists of a tower which can be moved back and forth perpendicular to the soil surface. A jack can be mounted between two columns in the tower for CPT tests and for the installation of piles. The jack has a capacity of 20kN operates at speed of 2mm/s with and a maximum stroke of 250 mm. For laterally loading of piles a beam can be mounted in the tower. The tower is controlled through a feedback loop and deformation or loading speeds applied by the user can be defined.

The vertical load actuator, here worked one-way, and applies vertical load to the pile until a penetration of 6d was reached. After pile installation the vertical jack was removed and the lateral beam was mounted. A sketch of the lateral load actuator and the circular strongbox can be seen Figure 3. The diameter of the circular strongbox is d_b=0.52m and the height of the sand layer is h_z=0.388m. The lateral load was applied to the pile head through a hinge connected to a load cell with a capacity of 2kN. The lateral displacement and the rotation of the pile head was measured by three potentiometers, see Figure 3.

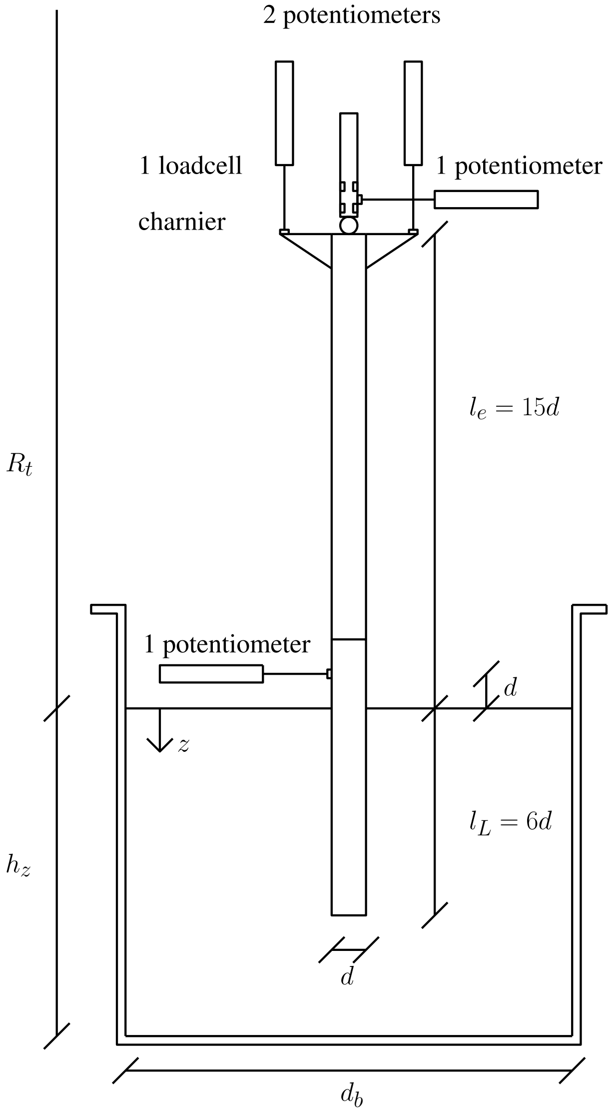

Figure 3 Sketch of the lateral load setup

One additional displacement measurement close to the sand surface was carried out using a potentiometer. The laterally loading of the piles was controlled so a deformation of 0.5d at the potentiometer close to the sand surface took 30 sec. All potentiometers and strain-gauge based load cells were calibrated before and after the tests and showed a high degree of identical linearity.

The setup provides a flexible solution but for the piles installed in-flight the centrifuge has to be stopped for the removal of the jack and remounting of the beam for lateral loading. The sand package is affected of this load cycle and leads to a densification of the sand. (Leth 2011) showed using the DTU centrifuge that the sand surface will displace around 0.2mm for a density and load cycle similar to one used in this paper.

The procedure for pile testing for the piles installed in-flight (IF) was as follows: The soil sample is prepared using a spot pouring hopper and dry pluvation. The package is then mounted in the centrifuge swing. The gravity in the centrifuge is then increased to the level for the given pile and the pile is installed. The levels can be seen in Table 4. The centrifuge is then stopped and the beam for lateral loading is mounted together with extension piece, load cell and potentiometers. The centrifuge is again spun up to the given gravity and the monotonic lateral load test is then performed. The test procedure for the piles with 1g installation is quite similar but here the pile is installed at 1g after the first spin up of the centrifuge to the required g-level, so there always is one loading cycle. A schematic presentation of the procedure is seen in Table 1.

	IF Insta.	**1g Insta.**	
N g consolidation	X	X	
N g installation	X		Centrifuge
1 g installation		X	stop
N g test	X	X	

Table 1 Centrifuge testing procedure

The test series consisted of 5 monotonic tests with 1g installation on cylindrical piles, 5 monotonic tests with in-flight installation on cylindrical piles and 4 tests performed on in-flight installed piles with a conical shape. The conical shaped piles were created with a circular decreasing cross section, with the largest diameter at the sand surface. The test program is shown in Table 4 here dimension, the increase in acceleration, laterally loading speeds and the relative density used in the different tests can be seen.

The tests were carried out on solid steel piles at a stress distribution identical to a prototype dimension of d=1m in dry sand. For all the tests the penetration and load eccentricity was kept constant to, l_L=6d and

l_e=15d. The choice of using solid steel piles which do not reflect a real monopile of a wind turbine was made to ensure that the tested pile would be completely rigid and that the stiffness of the pile was known. Four conical piles were designed, to take account of the stress errors. The increase in gravity in the sand sample is not constant due to the increase in centrifuge radius down with the depth in the sand sample. This will introduce a non-linear stress distribution and it is therefore not possible to model the linear increase seen in the prototype. The error is small but is taken into account here by the use of conically shaped piles. The idea is that the pile is wider in the part where the stresses are too small and the diameter is smaller in the part where the stresses are too high. Full similarity for the forces acting on the different piles is achieved when the stresses are integrated over the width of the pile.

Additionally, one in-flight and one 1g tests was performed using a CPT penetrometer, (Leth 2011) here mounted with a flat tip to investigate the installation procedure in more detail.

Experimental results

Sand properties

The centrifuge experiments were carried out in dry Fontainebleau sand, which is an uniform silica sand from France and consists of fine and rounded particles. The classification data can be seen Table 2, (Leth 2011).

Specific gravity of particles [g/mm^3]	G_s	2.644
Minimum void ratio	e_{min}	0.532
Maximum void ratio	e_{max}	0.851
Average grain size [mm]	D_{50}	0.21
Coefficient of uniformity	C_U	1.6

Table 2 Classification data for Fontainebleau sand

From Table 4 the average relative density for the different tests is shown. The average relative density is found from the total weight and volume of the sand sample. There is a slight change in the density between the different tests but it is believed that this change in relative density, not will affect the results.

Triaxial testing has been performed to obtain mechanical properties of the sand. Five isotropic consolidated drained triaxial tests were performed on Fontainebleau sand with a relative density of 0.9. The triaxial tests were carried out with smooth end platens, deformations measured within the triaxial chamber and with sample dimensions of HxD=70x70mm, (Jacobsen 1970). The maximum angle of friction and the maximum angle of dilation were determined from these tests and are shown in Table 3.

q' [kPa]	**p' [kPa]**	**ϕ'_{max} [^{o}]**	**ψ'_{max} [^{o}]**
66	38	42.3	16.9
120	70	41.8	16.8
220	133	40.3	14.9
495	315	38.5	13.8
920	607	37.2	12.7

Table 3 Triaxial data at failure

The maximum angle of friction from these triaxial tests correspond well with the predictions made by (Bolton 1986) using a critical state angle of φ'_{cr}=30^o. The critical state angle of friction was not measured and was therefore chosen in order to fit the results. In another study by (Gaudin, Schnaid & Gamier 2005) Fontainebleau sand was also tested here the critical state angle was determined to be identical the value chosen here.

$$\varphi'_{\max} \approx \varphi'_{cr} + 3\left(D_r\left(10 - \ln(p')\right) - 1\right) \qquad (4)$$

The triaxial tests showed that both the maximum angle of friction and the angle of dilation are a function of the relative density and the mean pressure in the sand.

Centrifuge tests

15 centrifuge tests were carried out. The dimensions and effective scaling factors for the different piles can be seen in Table 4. Model dimensions of the model pile are given together with the corresponding effective scaling factor (η), lateral load velocity (v) and average relative density (D_r) achieved in the tests.

Test ID	d [mm]	l_L [mm]	l_e [mm]	η [-]	v [mm/s]	D_r [%]
T-01	11.2	250	-	89.3	-	84
T-01	11.2	250	-	1	-	84
T-02	16	96	240	62.5	0.266	92
T-03	22	132	330	45.5	0.366	84
T-04	28	168	420	35.7	0.466	86
T-05	34	204	510	29.4	0.566	89
T-06	40	240	600	25.0	0.666	89
T-07	16	96	240	62.5	0.266	90
T-08	22	132	330	45.5	0.366	86
T-09	28	168	420	35.7	0.466	84
T-10	34	204	510	29.4	0.566	96
T-11	40	240	600	25.0	0.666	89
T-12	22.4-21.8	132	330	45.5	0.366	84
T-13	28.7-27.7	168	420	35.7	0.466	90
T-14	35.0-33.5	204	510	29.4	0.566	91
T-15	41.4-39.3	240	600	25.0	0.666	84

Table 4 Dimensions and scale factors for the test piles

Pile installation

The resistance to pile installation is affected by the tip resistance and the friction along the pile. A CPT mini penetrometer was mounted with a flat tip to simulate pile installation. The mini penetrometer is 300mm long and has a diameter of 11.3mm, and mounted with strain-gauge bridges for measurements of tip resistance, tip + friction resistance, measured on a section directly behind the tip, and also pore pressures can be measured behind the tip, (Leth 2011). The mini penetrometer is subjected to a stress field identical with a prototype diameter of 1m in dry sand and in this analysis we compare the tip resistance with the total driving stress.

The driving stress q_p is found as the driving force F divided by the pile area. Tip resistance q_c is found as the force at pile tip divide by pile area. The results from driving stress and tip resistance can be seen in Figure 4.

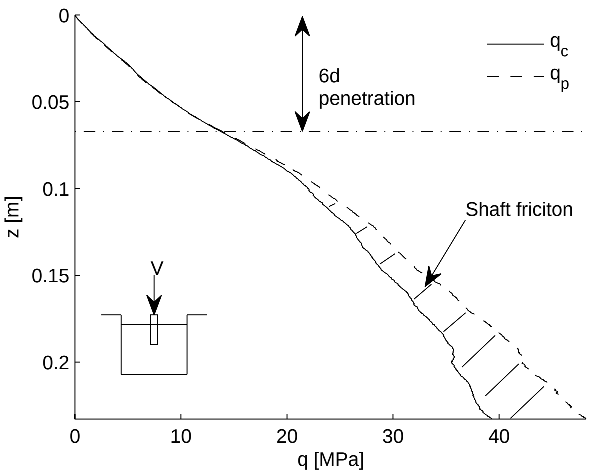

Figure 4 Installation resistance of CPT with flat tip

The force acting on the pile for 1g installation was too small to give meaningful results and is therefore not shown. The driving stress and the tip stress are identical to approximately 100 mm depth in the soil sample, before any shaft friction is mobilised, and the rate of increase of the tip resistance is decreasing below this depth. This is probably due to a change from a shallow failure mechanism in the upper part of the pile penetration to a combined failure mode in end bearing and shaft friction in the deeper part of the pile penetration, (Lau, Bolton 2011). The shallow failure is related to a mechanism similar to one known from bearing capacity theory with rupture lines going from pile tip to sand surface; (Vesic 1963) calls this general shear failure. The failure at greater depth is related to a combination of grain crushing, spherical followed by cylindrical cavity expansion, and is interpreted by (Vesic 1963) as a local shear failure. At a depth of 62.7 mm a horizontal line is shown at Figure 4 to indicate the depth of 6 pile diameters. This corresponds to the penetration depth of the piles for this investigation. This suggests that for pile installation to maximum a depth of 6d the shaft friction have not been mobilised sufficient. It therefore seems as a valid approximation to assume that q_c and q_c is identical. This enables the calculation of the pile tip stress as:

$$q_c \approx q_p = \frac{F}{\pi/4 \, d^2} \qquad (5)$$

This approximation is used in the entire test series in the analysis of pile installation.

1g pile installation

The force measured during 1 g installation is plotted, In Figure 5. The data was logged continuously at a sampling frequency of 10 Hz for all the tests. The installation resistance curves for the different piles show increasing resistance with depth and are all quite smooth, indicating that the soil sample was homogenous for all the tests. Surface heave was seen around the pile for all the piles installed at 1g. Circular rupture lines were seen on the surface, especially for the larger piles. The stress state for 1 g installed piles is low, which

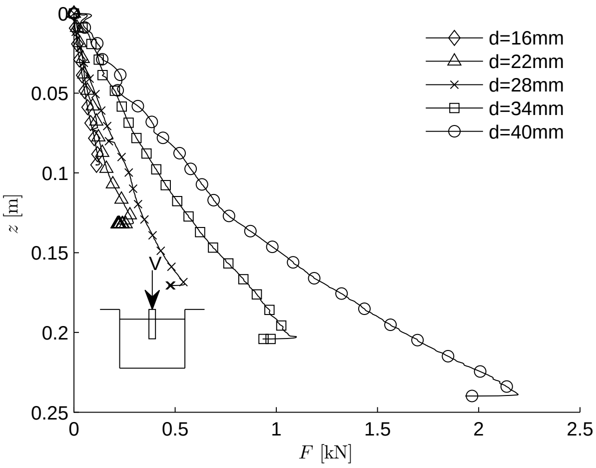

Figure 5 Installation of piles at 1g

leads to high a degree of dilatancy and volume change for dense sands. This was e.g. observed from the five triaxial test performed in connection with this study, and the surface heave is believed to be closely related to this fundamental sand behaviour.

In-flight installation

The force required to install the piles in-flight is shown in Figure 6. Here too the curve shows increase in load with depth and the results implies that a homogenous sample has been prepared. The required installation force, not shown here, for the piles with a conical shape are similar, but are approximate 5% smaller compared to those obtained for the cylindrical piles. No surface heave was observed in soil around piles installed in-flight; confirming the hypothesis of the surface heave at 1g installation is related to dilantancy of the sand. All piles were installed at the same stress levels. The pile tip stress is here around 10

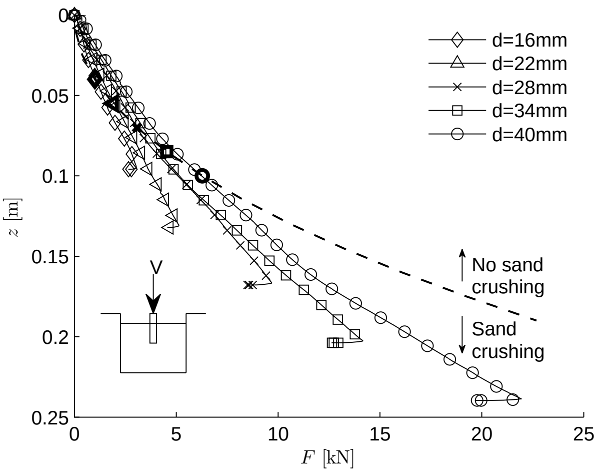

Figure 6 Installation of piles in-flight

times larger compared to the 1g installed pile. (McDowell, Bolton 1998) showed that the tensile strength of sand grains can be exceeded under compression, and also crushing of grains was reported to occur at a pile tip stress of 5 MPa (Yang et al. 2010). It must be expected that crushing of the sand grains can occur under pile installation. From the in-flight installed piles a pile tip stress of 5 MPa is reached approximately 2.5 pile diameters down in the soil and under this level. The zone is shown on Figure 6 as a dashed line.

A normalization procedure is used to interpret the pile installation further. The pile installation is normalized as proposed by (Bolton, Gui & Phillips 1993) for interpretation of CPT tests. The tip stress is normalized with soil stresses and the depth z is normalized with the diameter.

$$\tilde{Q} = \frac{q_c - \sigma_v}{\sigma'_v} \tag{6}$$

$$\tilde{Z} = \frac{z}{d} \tag{7}$$

The vertical stress is found using equation 2 under in-flight installation and is defined as shown in equation 8 for 1-g installation.

$$\sigma_v = \rho \cdot g \cdot z \qquad (8)$$

The total stresses are equal to the effective stresses for the dry sand. With the normalisation procedure it is possible to compare the installation procedures at 1g and in-flight. The comparison is shown in Figure 7 here it is seen that that 1g installations produce a large scatter in the normalised tip stress. This is due to the very low mean stress during installation. With a very small value of vertical stress the data acquisition also becomes less precise.

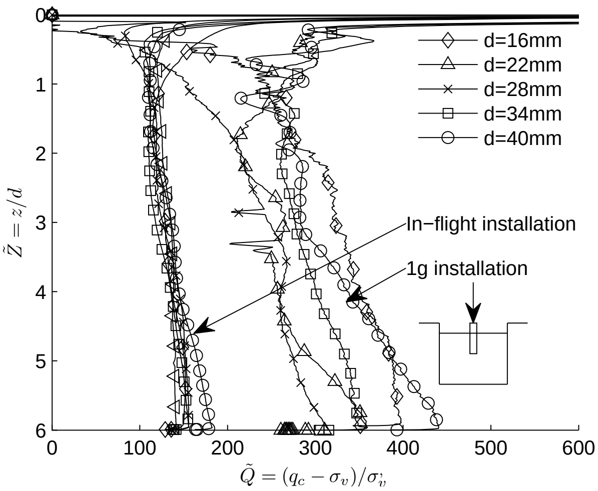

Figure 7 Normalisation of pile installation

Normalization of the tip stress indicates that no scale effects are here apparent for the in-flight installation. Only a difference of 5% and no clear tendency of pile diameter effect is seen in contrast to this a clear scale effect is seen for the 1g installation.. (Borghi et al. 2001) reported effects from the diameter on the pile tip stress for in-flight installed piles. The effect from diameter was explained with an increase in pile tip stress for smaller piles due to a larger frictional force. The results here do not show any sign of this effect which indicates that the assumption of small friction is valid. The increase in normalised pile tip stress indicates that a critical depth was not reached and the assumption of a shallow failure therefore seems appropriate.

Lateral loading

After installation, the piles were loaded laterally and both deflection and force is here normalised, according to the dimensional analysis shown in equation 1. The deflection, Y measured one diameter above the sand surface is normalised with the pile diameter, d.

$$\tilde{Y} = \frac{Y}{d} \tag{9}$$

The force H applied 15 pile diameters above the sand surface is normalised by the in-flight effective bulk unit weight and the diameter.

$$\tilde{H} = \frac{H}{\gamma' \cdot d^3} \tag{10}$$

Grain-size effect

The results of the lateral loading for the cylindrical piles installed at 1g can be seen in Figure 8. The response is significantly different for the d=16mm pile compared to the others, showing high initial stiffness before approaching a failure plateau that was higher than the other piles.

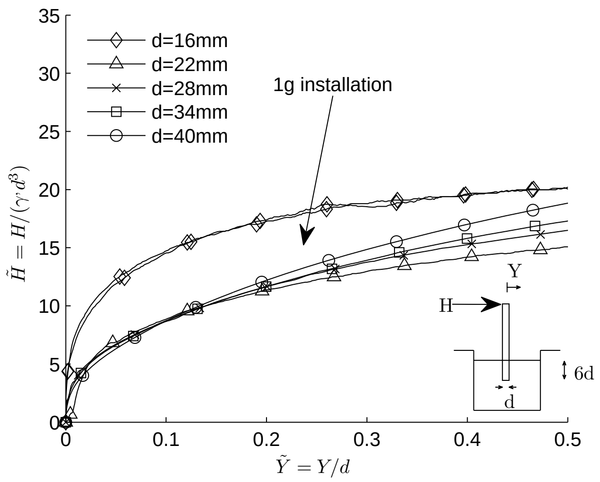

Figure 8 Lateral loading of cylindrical piles 1g installation

The test was therefore repeated and identical results were obtained. This is clearly an outlier and it is concluded that the ratio between diameter of the pile and diameter of average grain size $d/d_{50}=88$ is too small, which leads to a grain size effect. This ratio is 30% higher than reported by (Remaud 1999). The response is more or less identical until a normalised deflection of 0.1 is reached for the four other piles, for larger deflection the load-deflection curves start to deviate. The capacity of the piles with large diameter increases more rapidly than the piles with smaller diameter and the difference at a deflection of 0.5 d is about 25% between the d=22mm and d=40mm piles, indicating scale effects.

Installation effect

The same five piles were tested with the in-flight installation procedure, and the load-deflection curves are shown in Figure 9.

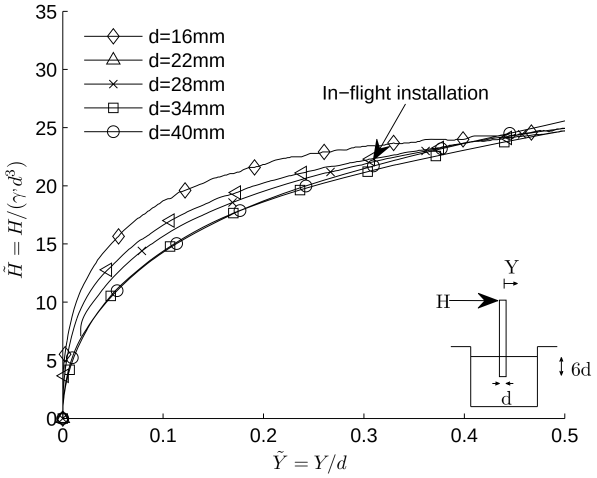

Figure 9 Lateral loading of cylindrical piles

The response from the 16mm diameter pile shows again a high initial stiffness and approaches a failure plateau at large deflection, even though the tendency is not that clear, it is still concluded that the pile is to small. The response for the rest of the in-flight installed piles seems more identical than the piles installed at 1g, but a scale effect is still seen with larger initial stiffness's for the smallest piles.

The lateral response of the 1g - and in-flight installed piles can be seen in Figure 8 and Figure 9 whereby the piles installed in-flight shows a larger initial stiffness and higher normalised bearing capacities than the piles installed at 1g. This is in agreement with the observations made by (Craig 1985) and (Dyson, Randolph 2001).

g-field effect

To investigate the influence of g-field, conical shaped piles were designed to counteract the change in g-field with depth, and the load deflection curve is plotted in Figure 10.

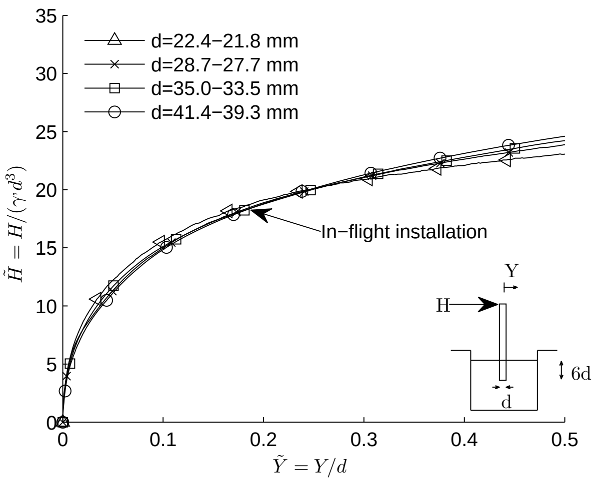

Figure 10 Lateral loading of conical monopiles

Here only four piles was created, because it was concluded that the d=16m pile was too small. A very good agreement between the normalized load-deflection results was achieved. The stiffness of the larger piles increases more rapidly, than the smaller piles, but the effect almost negligible. This demonstrates that it is possible to model same normalised response using different sized piles.

Discussion

The centrifuge tests represent simplifications of the complex wind-water-structure-soil interaction problem for a monopile supporting an offshore wind turbine and some of these simplifications are here discussed.

First of all, an offshore monopile is situated in saturated soil conditions. The centrifuge test series was carried out in dry dense sand. Choosing an effective stress scaling approach enables piles to be modelled as situated in saturated conditions using dry sand. This modelling technique was also used by (Li, Haigh & Bolton 2010). In the investigation of scale effects this simplification seems to be appropriate and the observation seen in dry condition is also believed to be present in the drained saturated condition.

The stress field applied to the piles corresponds to a stress for a prototype pile with a diameter of d=1m. This stress distribution is therefore smaller compared to the prototype case where pile diameters of 5-6 meters are seen. Even though the tests here are performed at a lover stress field it is believed that the observation deen here is also valid for a higher stress field.

This study shows that, the ratio between pile diameter and average grain size has to be above 88 for a smooth stiff pile to avoid grain size scale effects. This is nearly 30 % more than recommended by (Garnier et al. 2007) which is based on tests on slender piles. One reason for this increase in ratio could be the fact that the stiff piles load the sand over the whole length of the pile, which is not the case for a slender pile. The ratio between grain size and pile diameter is therefore more important for stiff piles than for slender piles.

The maximum angle of friction and the dilation angle determined from triaxial testing where seen to be controlled by the stress level. This implies that the sand surrounding the piles installed at 1g is subjected to larger dilation than piles installed in-flight, e.g. seen as surface heave around the piles. Both (Craig 1985) and (Dyson, Randolph 2001) report an effect from the in-flight installation but in the literature it does not seem to be a common procedure for monopiles. The driving force for the installation of these large diameter piles is probably the reason for this choice. This study shows that not only the stiffness and the strength are smaller using 1g installation. It also finds that the piles are showing scale effects due to the lack of stress similarity during installation. It is therefore important to perform the installation under soil stresses corresponding to prototype.

A scale effect was seen even for the piles installed in-flight. The explanation for this is suggested to be the non-linear stress distribution, which is not identical for the different tests. This was investigated with conical shaped piles to take account for the non-linear stress distribution. The conical piles can be view as tapered piles with a small taper angle. (El Naggar, Sakr 2000) performed centrifuge tests with tapered piles and showed that the axial response was increasing using tapered piles. Comparing the installation of the conical piles with the cylindrical ones shoved a slightly smaller installation force for the conical piles. This is in contrast to the observation seen in (El Naggar, Sakr 2000) and it is believed in this research to be related to the very low taper angle used. The influence of the taper angle is therefore neglect able and the installation force is smaller due to a smaller pile tip. The effect from using conical piles seems only to affect the lateral response. The lateral response using conical shaped showed out to having almost identical normalized load-deflection responses. The results supported the hypothesis of the influence of the stress distribution on the lateral response.

Conclusions

The centrifuge modelling technique has with success been used for a number of offshore foundation problems, and it therefore also seems appropriate to use the technique to investigate the lateral response of offshore monopiles for wind turbines. For lateral loaded piles scale effects have been investigated in order to develop a reliable modelling technique before, but these investigations have been for long slender piles. For rigid monopiles no investigation of scale effects seems to have been carried out. This research demonstrated have the concept of modelling of models can be used in order to establish a centrifuge modelling procedure where model observations can be used in the analysis of a prototype monopile.

Using five different sized 1g installed piles one attempt to model the same lateral normalised response was performed. The result of the tests showed different normalised responses, and thereby indication of scale effects. Here special the smallest pile with a pile diameter of d=16mm was showing a different response compared to the other piles and indicated that the ratio between pile diameter and average grain size was too small.

The same five pile used again but this time the piles was in-flight installed. Still scale effects were seen in the normalised lateral response. The smallest pile with a pile diameter of d=16mm showed a response comparable with the one for 1g installation, and it was concluded that the pile was too small. The tests show that the initial stiffness and the maximum bearing capacity were increased with in-flight installation of monopiles, conforming results seen before.

As a third attempt to perform a successful modelling of models test series, conical piles were used. Using conically shaped piles to counteract the effect of the non-linear stress distribution, full similarity of the force acting on the piles can be achieved. The normalised lateral responses showed nearly identical responses and it was therefore possible to model the same prototype behaviour with different pile sizes. The assumption of a linear stress distribution should be used with care.

The test series shows that for centrifuge modelling of monopiles the ratio of pile diameter to average grain size, the non-linear stress distribution and the installation process are key modelling parameters. With due consistency of these effects, it is possible to scale centrifuge results of rigid monopiles to prototype scale.

References

Barton, Y.O. 1985, "RESPONSE OF PILE GROUPS TO LATERAL LOADING IN THE CENTRIFUGE", *Proceedings of a Symposium on the Application of Centrifuge Modelling to Geotechnical Design.* pp. 457-473.

Bienen, B., Cassidy, M.J. & Gaudin, C. 2009, "Physical modelling of the push-over capacity of a jack-up structure on sand in a geotechnical centrifuge", *Canadian Geotechnical Journal,* vol. 46, no. 2, pp. 190-207.

Bolton, M.D. 1986, "Strength and dilatancy of sands", *Geotechnique,* vol. 36, no. 1, pp. 65-78.

Bolton, M.D., Gui, M.W. & Phillips, R. 1993, "Review of Miniature Soil Probes For Model Tests", *Eleventh Southeast Asian Geotechnical Conference.*

Borghi, X., White, D.J., Bolton, M.D. & Springman, S. 2001, "Empirical pile design based on cone penetrometer data: an explanation for the reduction of unit base resistance between CPTs and piles", *Proceedings of the 5th International Conference on Deep Foundation Practice.*

Briaud, J., Smith, T.D. & Meyer, B.J. 1983, "USING THE PRESSUREMETER CURVE TO DESIGN LATERALLY LOADED PILES", *Proceedings - Annual Offshore Technology Conference,* vol. 1, pp. 495-502.

Cassidy, M.J., Randolph, M.F. & Byrne, B.W. 2004, "A comparison of the combined load behaviour of spudcan and caisson foundations on soft normally consolidated clay", *Geotechnique,* vol. 54, no. 2, pp. 91-106.

Craig, W.H. 1985, "Installation studies for model piles", *Proceedings of a Symposium on the Application of Centrifuge Modelling to Geotechnical Design.*,pp. 441-456.

De Nicola, A. & Randolph, M.F. 1999, "Centrifuge modelling of pipe piles in sand under axial loads", *Geotechnique,* vol. 49, no. 3, pp. 295-318.

Dyson, G.J. & Randolph, M.F. 2001, "Monotonic lateral loading of piles in calcareous sand", *Journal of Geotechnical and Geoenvironmental Engineering*, vol. 127, no. 4, pp. 346-352.

El Naggar, M. & Sakr, M. 2000, "Evaluation of axial performance of tapered piles from centrifuge tests", *Canadian Geotechnical Journal,* vol. 37, no. 6, pp. 1295-1308.

Fuglsang, L.D. & Ovesen, N.K. 1988, "The application of the theory of modelling to centrifuge studies", *Centrifuges in Soil Mechanics,* , pp. 119-138.

Garnier, J., Gaudin, C., Springman, S.M., Culligan, P.J., Goodings, D., Konig, D., Kutter, B., Phillips, R., Randolph, M.F. & Thorel, L. 2007, "Catalogue of scaling laws and similitude questions in geotechnical centrifuge modelling", *International Journal of Physical Modelling in Geotechnics,* vol. 7, no. 3, pp. 1-23.

Garnier, J. & Konig, D. 1998, "Scale effects in piles and nails loading tests in sand", *Centrifuge 98,* vol. 1, pp. 205-210.

Gaudin, C., Schnaid, F. & Gamier, J. 2005, "Sand characterization by combined centrifuge and laboratory tests", *International Journal of Physical Modelling in Geotechnics,* vol. 5, pp. 42-56.

Hansen, J.B. 1961, "Ultimate resistance of rigid piles against transversal forces", *Geoteknisk Institut -- Bulletin (Danish Geotechnical Institute -- Bulletin)* , no. 12, pp. 5-9.

Jacobsen, M. 1970, *New oedometer and new triaxial apparatus for firm soils,* Geoteknisk Institut.

Klinkvort, R.T. & Hededal, O. 2010, "Centrifuge modelling of offshore monopile foundation", *Frontiers in Offshore Geotechnics II*, pp. 581-586.

Langhaar, H.L. 1951, *Dimensional Analysis and Theory of Models,* Chapman & Hall, London.

Lau, C.K. & Bolton, M.D. 2011, "The bearing capacity of footings on granular soils. I: Numerical analysis", *Geotechnique,* vol. 61, no. 8, pp. 627-638.

Leth, C.T. 2011, *Centrifuge modelling of large diamter pile in sand subject to lateral loading*, DTU Civil Engineering, http://www.byg.dtu.dk/Publikationer/Byg_rapporter.aspx.

Li, Z., Haigh, S.K. & Bolton, M.D. 2010, "Centrifuge modelling of mono-pile under cyclic lateral loads", *Physical Modelling in Geotechnics*, pp. 965-970.

McDowell, G.R. & Bolton, M.D. 2000, "Effect of particle size distribution on pile tip resistance in calcareous sand in the geotechnical centrifuge", *Granular Matter,* vol. 2, no. 4, pp. 179-187.

McDowell, G.R. & Bolton, M.D. 1998, "On the micromechanics of crushable aggregates", *Geotechnique,* vol. 48, no. 5, pp. 667-679.

Nunez, I.L., Phillips, R., Randolph, M.F. & Wesselink, B.D. 1988, "Modelling laterally loaded pile in calcareous sand", *Centrifuge 88,* , pp. 353-362.

Ovesen, N.K. 1975, "Centrifugal testing applied to bearing capacity problems of footings on sand", *Geotechnique,* vol. 25, no. 2, pp. 394-401.

Randolph, M.F. 1981, "Response of flexible piles to lateral loading", *Geotechnique,* vol. 31, no. 2, pp. 247-259.

Randolph, M.F., Dolwin, J. & Beck, R. 1994, "Design of driven piles in sand", *Geotechnique,* vol. 44, no. 3, pp. 427-448.

Remaud, D. 1999, "Pieux sous charges latérales: étude expérimentale de l'effet de groupe", *Ph.D. thesis,* .

Schofield, A.N. 1980, "Cambridge geotechnical centrifuge operations", *Geotechnique,* vol. 30, no. 3, pp. 227-268.

Smith, T.D. 1987, "PILE HORIZONTAL SOIL MODULUS VALUES", *Journal of Geotechnical Engineering,* vol. 113, no. 9, pp. 1040-1044.

Taylor, R.N. 1995, *Geotechnical centrifuge technology,* Blackie Academic, London.

Terashi, M. 1989, "Centrifuge modeling of a laterally loaded pile", *Proceedings of the International Conference on Soil Mechanics and Foundation Engineering,* vol. 2, pp. 991-994.

Ubilla, J., Abdoun, T. & Zimmie, T. 2006, "Application of in-flight robot in centrifuge modeling of laterally loaded stiff pile foundations", *Physical Modelling in Geotechnics,* vol. 1, pp. 259-264.

Vesic, A.B. 1963, "Bearing capacity of deep foundations in sand", *National Research Council -- Highway Research Board -- Research Record,* , no. 39, pp. 112-153.

Weber, T.M., Plotze, M., Laue, J., Peschke, G. & Springman, S.M. 2010, "Smear zone identification and soil properties around stone columns constructed in-flight in centrifuge model tests", *Geotechnique,* vol. 60, no. 3, pp. 197-206.

White, D.J. & Bolton, M.D. 2004, "Displacement and strain paths during plane-strain model pile installation in sand", *Geotechnique,* vol. 54, no. 6, pp. 375-397.

White, D.J. & Lehane, B.M. 2004, "Friction fatigue on displacement piles in sand", *Geotechnique,* vol. 54, no. 10, pp. 645-658.

Wood, D.M. 2004, *Geotechnical Modelling - applied geotechnics volume 1,* 1st edn, Spon Press, Great Britain.

Yang, Z.X., Yang, Z.X., Zhu, B.T., Foray, P., Jardine, R.J., Zhu, B.T., Foray, P. & Tsuha, C.H.C. 2010, "Sand grain crushing and interface shearing during displacement pile installation in sand", *Geotechnique*, vol. 60, no. 6, pp. 469-482.

Paper III

"Monotonic soil-structure interaction of monopile support for offshore wind turbines"

R. T. Klinkvort & O. Hededal

Submitted for publication -, *2012*

Monotonic soil-structure interaction of monopile support for offshore wind turbines

Rasmus Tofte Klinkvort and Ole Hededal

Abstract: Currently monopiles is the preferred foundation solution for offshore wind turbines. The design of these monopiles relies on empirical data from tests performed on long slender small diameter piles loaded predominantly in shear. In contrast, a monopile is a large diameter relatively short pile, where load is applied with a large eccentricity. With centrifuge tests as the basis, this paper discusses the effects on the non-linear soil-pile interaction in sand from changing the stress level and the load eccentricity. Hence, a test series was carried out to simulate idealised load situations for monopiles supporting an offshore wind turbine. Centrifuge tests were performed on model monopiles subjected to stress levels equal to prototype monopiles with a diameter ranging from 1-5 meters. It was possible to merge these tests into one general response using Rankine's passive earth pressure coefficient as a normalisation parameter. The effect of load eccentricity was investigated by considering five different eccentricities. The main conclusions from these tests were, the initial stiffness of the soil-pile response was increasing linearly and ultimate soil resistance seemed unaffected by the load eccentricity, which is in agreement with the current design methodology. The size of the ultimate soil resistance, the magnitude of the stiffness and the shape of the soil-pile interaction were all different from the current design methodology.

Key words: Monopiles, Monotonic loading, Centrifuge modelling, p-y curves, Sand, Initial stiffness, Ultimate capacity.

1. Introduction

Monopiles are today one of the most popular foundation methods for offshore wind turbines. These piles are often installed in dense sand at water depths ranging from 10-30 meters. A monopile is a single, large diameter tubular steel pile driven 5 to 6 times its diameter into the seabed. The diameter of the piles ranges from 4-6 meters. Monopiles for wind turbines are affected by lateral loads from waves and wind, which subject the pile at seabed level to shear forces and moments corresponding to the load eccentricity; this is illustrated at Figure 1. Today, the design of monopiles is carried out by modelling the pile as a beam and the soil as a system of uncoupled non-linear springs, (API 2007). This method has successfully been used in pile design for offshore oil and gas platforms. The design methodology originates from tests on long slender piles with a small load eccentricity, (Reese and Matlock 1956; McClelland and Focht 1956). Even though this methodology was originally calibrated to slender piles, it is today used for design of large diameter rigid monopiles. Still, the methodology lacks of scientific justification and a better understanding of rigid piles is needed. This is the motivation for current research on monopiles. In this context, centrifuge modelling offers a low-cost tool, compared to prototype testing, and if handled correctly makes it possible to scale model observations to prototype. The centrifuge modelling technique have successfully been used for a number of offshore foundation problems to establish design procedures e.g. (Bienen, Cassidy, and Gaudin 2009; Cassidy, Randolph and Byrne 2004; De Nicola and Randolph 1999).

Fig. 1. Non-dimensional dimensions of a typical offshore wind turbine

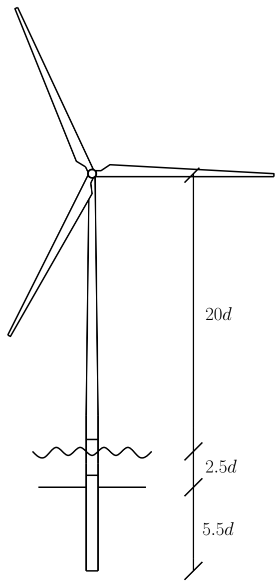

In order to understand the behaviour of a pile, it is important to recognize the stresses acting on the pile. When a pile is moved in a soil continuum, passive earth pressure will act in front of the pile, friction on the side of the pile and active pressure will load the back of the pile. The sum of these components will resist the pile movement. These are three independent forces acting on the pile, but as a simplification the three forces can be combined into one resulting force over the

Received . Revision received . Accepted . Revision accepted .

Rasmus Tofte Klinkvort. Dept. of Civil Engineering, Technical University of Denmark, Sec. of Geotechnics and Geology, Brovej Building 118, 2800 Kgs. Lyngby, Denmark
Ole Hededal. Dept. of Civil Engineering, Technical University of Denmark, Sec. of Geotechnics and Geology, Brovej Building 118, 2800 Kgs. Lyngby, Denmark

DOI: 10.1139/

pile width, (Briaud, Smith and Meyer 1983; Smith 1987). The soil resistance can as a simplification be described as the effective vertical stress (σ'_v) in a given depth, which is found as the effective unit weight (γ') , multiplied the depth in the soil (z), integrated over the diameter of the pile (d), multiplied by an earth pressure coefficient (K) representing the mobilised resistance.

$$p \approx K \cdot \sigma'_v \cdot d \tag{1}$$

It is important to recognise that the earth pressure coefficient, K, here incorporates the friction on the side of the pile and is therefore the sum of active soil pressure, passive soil pressure and side friction. This modulus approach is used by different researcher's e.g. (Brinch Hansen 1961 ; Broms 1964; Briaud, Smith and Meyer 1983; API 2007).

The earth pressure coefficient is a function of a set of parameters depending on the soil behaviour (ϕ', E_s), pile material $(\delta, E_p I_p)$, pile geometry $(\frac{z}{d})$, pile installation $(Inst.)$ and degree of mobilisation $(\frac{y}{d})$. For a rigid monopile this can be written as:

$$K = f\left(\phi', E_s, \delta, E_p I_p, \frac{z}{d}, Ins., \frac{y}{d}\right), \tag{2}$$

The soil-pile interaction is thus a function of the degree of mobilisation controlled by the normalised displacement of the pile. Especially, the initial stiffness of this function and the ultimate capacity has been investigated by different authors and the conclusions of the findings are contradictory. The ultimate capacity was studied by Zhang, Silva and Grismala 2005 who collected data from 17 different tests; both centrifuge and full scale. They presented a method to determine the ultimate capacity of a pile by using Rankines passive soil pressure coefficient squared for the ultimate soil pressure. The initial stiffness was investigated by Fan and Long 2005 and Ashford and Juirnarongrit 2003,they agreed with the original assumption by Terzaghi 1955, that there is no effect from the diameter on the initial stiffness of the p-y curves. This is also the conclusion by Pender, Carter and Pranjoto 2007 who compared a series of full scale test and states that the apparent diameter size effect is a consequence of the distribution of the soil modulus. On the other hand numerical modelling by Lesny and Wiemann 2006 and Sorensen et al. 2009 suggest an effect of changing the diameter on the initial stiffness of the p-y curves.

The general tendency of the research performed on monopiles is that the current design values of the initial stiffness are too large, e.g. (Rosquot et al. 2007; Lesny and Wiemann 2006; Abdel-Rahman and Achmus 2005; Augustesen et al. 2009. The problem with these findings is that they are not in agreement with the findings from full scale monitoring on monopiles which states that the recommenced value is too small, (Hald et al. 2009).

The purpose of this paper is to investigate the earth pressure coefficient (K) both in terms of initial stiffness, ultimate capacity and shape. The investigation is performed with the application for wind turbine foundation in mind. This means that the tests are performed on rigid piles with a high load eccentricity and a stress distribution corresponding to piles with diameters ranging from 1 to 5 meters. This is in both cases in contrast to the tests that the current practice relies on.

2. Soil-pile interaction

The formulation of the soil-pile interaction used in the analysis of laterally loaded piles have been given special attention since the development of the semi-empirical based method was developed in the 1950^{ies}. A number of different proposals describing the soil-pile interaction have been given, e.g. (Reese, Cox and Koop 1974; Murchison and O'Neill 1984; Norris 1986; Wesselink et al. 1988; Georgiadis, Anagnostopoulos and Saflekou 1992). All of these studies have been on long slender piles.

Here is presented two methods to calculate the pile-soil interactions. The first one, is the API 2007 design method and is based on the formulation proposed by Murchison and O'Neill 1984. The second one, is based on the hyperbolic stress strain response proposed by Kondner 1963. This method was found to be superior to the other methods in the prediction of experiments on laterally loaded piles Georgiadis, Anagnostopoulos and Saflekou 1992 and Kim et al. 2004.

The modulus approach shown in eq. 1 is the basic framework and the original formulations are therefore rewritten to be expressed as an earth pressure coefficient. For both of the methods the soil-pile interaction is a function of initial stiffness, maximum capacity and pile displacement. The calculations of these values are here identical for the two methods and the recommendations from API 2007 is here used. The initial stiffness is given by the subgrade modulus (k) multiplied the depth in the soil (z), and is assumed to increase linear with depth, this is normalised with the vertical effective stress.

$$\tilde{E}_{py} = \frac{k \cdot z}{\sigma'_v} \tag{3}$$

Reese, Cox and Koop 1974 proposed a methodology to calculate the ultimate capacity K_{ult} using plasticity theory;

$$K_{ult} = A \cdot \min \begin{cases} (C_1 \cdot \frac{z}{d} + C_2) & \text{shallow depth} \\ C_3 & \text{great depth} \end{cases} \tag{4}$$

Here the coefficients C_1, C_2 and C_3 is found by plasticity theory and is only dependent of angle of friction. The value of K_{ult} is found as the minimum value of the expressions showed in eq. 4. Where the upper expression defines a failure in shallow depths and the lower is failure in great depth. A is an empirical constant which was used to fit the original test results with theory. For monotonic loading $A = \left(3.0 - \frac{0.8X}{D}\right) \geq 0.9$.

The formulation of the non-linear soil-pile interaction spring, also known as the p-y relationship, is expressed by a hyperbolic tangent function in the API 2007 method. Here shown in the normalised form as the earth pressure coefficient.

$$K = K_{ult} \cdot \tanh\left[\frac{k \cdot z}{\sigma_v} \cdot \frac{1}{K_{ult}} \cdot \frac{y}{d}\right] \tag{5}$$

Alternatively, the hyperbolic equation proposed by Kondner 1963 may be used:

$$[6] \qquad K = \frac{y/d}{\dfrac{\sigma_v}{k \cdot z} + \dfrac{1}{K_{ult}} \cdot \dfrac{y}{d}}$$

The two formulations have identical initial stiffness and ultimate asymptotic capacity but the shape of the functions are different. The applicability of the two formulations will be part of the analyses based on the results from the performed centrifuge tests.

3. Experimental Methodology

A centrifuge test program was designed to investigate the stress level and the load eccentricity effects for a monopile supporting a wind turbine installed in sand, see Table 1. The penetration depth of the pile was for the entire test series kept constant to $l_l = 6d = 240mm$. Ten test were performed; five test in dry sand with a constant load eccentricity of $l_e = 15d = 600mm$ and stress distributions identical with a prototype pile with diameter ranging from d=1m - 5m, and five test in saturated sand with load eccentricities ranging from $l_e = 8.25d - 17.25d = 330 - 690mm$. The pile was loaded at the pile top and the deflection of the pile was measured $2d$ above the sand surface. The centrifuge experiments were carried out using the centrifuge at the Technical University of Denmark. The centrifuge is a beam centrifuge with a radius of $1.7m$ to the swing. In the swing a circular strongbox is placed and the distance from the swing to the sand surface is 0.521 m, (Fuglsang and Nielsen 1988a). A sketch of the basic pile setup ($l_e = 15d$) for laterally loading of a strain-gauge mounted monopile can be seen in Fig. 2. The strong box have a diameter of $d_b = 500mm$ and the height of the sand sample is $h_z = 388mm$. Centrifuge modelling theory is today standard procedure and can be seen in e.g. (Schofield 1980; Fuglsang and Ovesen 1988b).

All piles were installed in-flight, but at a stress level three times smaller than the level at which the monotonic test was performed. This was done due to a 20 kN limit on the jack. The installation at a lower stress level will lead to a softer response; this was demonstrated in Dyson and Randolph 2001, but the effect from a lower installation stress will affect the piles in the same degree and the results are therefore comparable. Pilot test carried out prior to the present study demonstrates that this would not be the case if the pile was installed at 1g. The procedure for the test sequence was to spin the centrifuge up and install the pile. Then the centrifuge has to be stopped to remove the jack and then mount the lateral loading equipment. Afterwards the centrifuge was accelerated again, to a given soil stress level and the monotonic lateral test was performed. It is assumed that the effect of this procedure is negligible.

The pile used in the tests is a solid steel pile with a diameter of $36mm$. Strain-gauges are glued to the pile and protected by a $2mm$ epoxy coating. This leads to a total model pile diameter of $40mm$. 20 strain-gauges are mounted on the pile to form 10 half-bridges for moment measurements. The strain-gauge bridges are spaced with half diameter spacing, starting with a bridge at the sand surface, see Fig. 2. The moment distribution measured in the half-bridges was fitted to a 6th order polynomial function by least square regression. From this it was possible to generate p-y curves from the moment distribution. While the deflection of these p-y curves were well described it is important to remember that the soil resistance can be affected by uncertainties of up to 35%, (Rosquot, Garnier and Khemakhem 2010). Hence, care needs to be taken in the deduction of the resistance and displacements. The soil resistance was found by differentiation of the moment distribution twice, and the pile displacement was found by an integration of the moment distribution twice. The p-y curves are very sensitive to the fitting and even small changes in the moment polynomial will due to the double differentiation, change the soil resistance significantly. To avoid effects from boundaries, it was here chosen only to use strain-gauge level $z = 1d - 3.5d$ to generated p-y curves. This ensures that at least two extra moment measurements on both sides of a given strain-gauge bridge were used.

Fig. 2. Sketch of the test setup

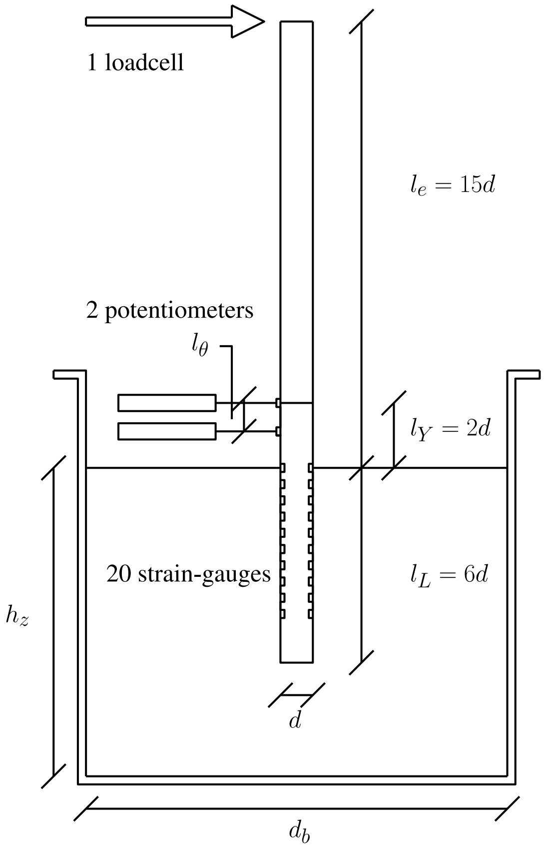

Table 1. Test program

Tests	Scaling factor N	Increase in gravity η	Diameter d [-]	l_e $[d]$	l_L $[d]$	γ' $[kN/m^3]$	I_D $[-]$	ϕ' $[^0]$	Saturated sand
1	25	15.5	0.04	15	6	16.7	0.93	46.3	No
2	50	31.1	0.04	15	6	16.6	0.93	44.2	No
3	75	46.6	0.04	15	6	16.5	0.89	42.3	No
4	100	62.1	0.04	15	6	16.4	0.86	41.0	No
5	125	77.7	0.04	15	6	16.8	0.89	40.9	No
6	75	75	0.04	8.25	6	10.3	0.88	42.2	Yes
7	75	75	0.04	10.50	6	10.4	0.93	43.0	Yes
8	75	75	0.04	12.75	6	10.2	0.87	42.0	Yes
9	75	75	0.04	15.00	6	10.2	0.87	42.0	Yes
10	75	75	0.04	17.25	6	10.2	0.86	42.0	Yes

4. Results

4.1. Sand properties

The centrifuge experiments were carried out in Fontainebleau sand - a uniform silica sand from France - which consists of fine and rounded particles. The classification data can be seen in Table 2, (Leth 2011). Triaxial tests were performed to obtain mechanical properties of the sand. A total of 9 trixial tests have been performed, five tests under saturated conditions and four under dry conditions. All tests with a relative density of, $I_D = 0.9$. The dry and saturated triaxial tests show that maximum angle of friction, (ϕ'_{max}) is a function of the relative density and the effective stress. This is in contrast to the method by API 2007 which states that maximum angle of friction only is a function of the relative density. The maximum angle of friction from these triaxial tests correspond well with the predictions done by Bolton 1986 using a critical state angle of $\phi'_{cr} = 30^o$.

Table 2. Classification parameters for the Fontainebleau sand

Specific gravity of particles	G_s	2.646
Minimum void ratio	e_{min}	0.548
Maximum void ratio	e_{max}	0.859
Average grain size	d_{50}	0.18
Coefficient of uniformity	C_u	1.6

[7] $$\phi_{max} = \phi_{cr} + 3 \cdot (I_D(10 - In(p')) - 1)$$

The mean effective stress p' was in the centrifuge tests calculated as:

[8] $$p' = \frac{1}{3}(1 + 2K_0)\sigma'_v \ , K_0 = 1 - \sin\phi'$$

The sand was prepared in the centrifuge container by dry pluvation using a single spot hopper. An average relative density was then calculated from the weight of the sand sample. A representative angle of friction was calculated using Eq. 7 and Eq. 8. The reference pressure p' was found at a soil depth of $z = 2/3l_L$. At this depth full similarity of soil stresses between model and prototype was achieved. The achieved relative density, effective density and representative angle of friction can be seen in Table 1.

4.2. Centrifuge results

4.2.1. Scaling approach

The scaling approach is carried out so tests in dry conditions can be interpreted as if they were performed in saturated conditions. The goal is to achieve identical effective stress distribution in the dry model $(\sigma'_{v,m})$ and the saturated prototype $(\sigma'_{v,p})$. This can be written as:

[9] $$\sigma'_{v,p} = \gamma'_{sat} \cdot z_p = \eta \cdot \gamma'_{dry} \cdot z_m$$
$$\Rightarrow \ \eta = \frac{\gamma'_{sat} \cdot z_p}{\gamma'_{dry} \cdot z_m} = \frac{\gamma'_{sat}}{\gamma'_{dry}} \cdot N_s$$

Here it can be seen that by increasing the gravity with η identical soil stresses can be achieved in a dry sample compared to a saturated sample for which that gravity is increased by N. The increase in gravity η and the geometrical scaling factor $N = z_p/z_m$ are here not identical. This can be achieved by performing tests at a deformation rate at which no excess pore pressure will develop. This modelling technique was used by Li, Haigh and Bolton 2010 and here it is confirmed by comparing the results from two tests performed in dry and saturated conditions. The result are compared for the two tests with a load eccentricity $l_e = 15d$ with a stress level corresponding to a 3 meter in pile diameter. The results in model scale can be seen in Figure 3. The response of the two tests shows identical responses. This confirms the scaling approach and the test series are comparable in both dry and saturated sand.

4.2.2. Stress level

To investigate the stress level effect, five different tests with stress levels corresponding to offshore monopiles ranging from 1 to 5 meters in diameter were performed. The results are here presented in non-dimensional terms. The global force (H) is

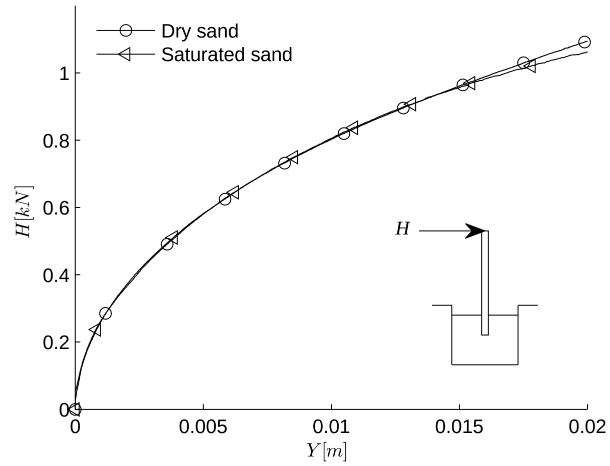

Fig. 3. Comparison of modeling approach, $l_e = 15d$

normalised with the effective density γ' (under centrifuge testing at η g), and the diameter of the pile d.

[10] $$\tilde{H} = \frac{H}{\gamma' d^3}$$

The overall displacement (Y) measured $l_Y = 2d = 80mm$ above the sand surface is normalised with the diameter of the pile.

[11] $$\tilde{Y} = \frac{Y}{d}$$

The overall load - displacement response can be seen in Figure 4 from test 1-5. Here it is seen, that the pile subjected to the smallest stress level has the highest non-dimensional bearing capacity. The pile with the second lowest stress level has the second highest bearing capacity, whereas it seems that the last three piles have identical non-dimensional responses. From the triaxial tests it was seen that the angle of friction was dependent on pressure and for the entire test series a representative angle of friction was calculated using the average relative density and the pressure calculated at a pile depth at 2/3 of the total length. This was shown in Table 2. Here it can be seen that the tests performed at low stress levels have a higher mobilized angle of friction.

Fig. 4. Normalised load deflection response, $l_e = 15d$

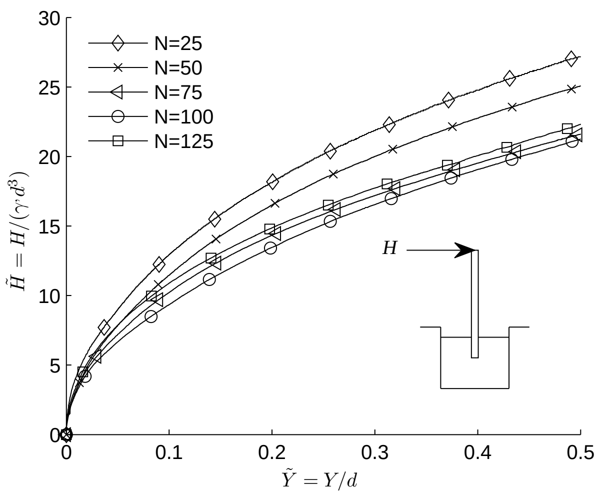

We choose to introduce Rankine's passive earth pressure coefficient.

[12] $$K_p = tan^2(45 + \phi'/2)$$

The non-dimensional load can be redefined to be:

[13] $$\tilde{P} = \frac{\tilde{H}}{K_p} = \frac{H}{K_p \gamma' d^3}$$

In Fig. 5 the overall response from test 1-5 with the new normalization is shown. Here the responses from the five different tests merge into one single characteristic curve. This indicates that the effect from stress level can as a simplification be taken into account only through the angle of friction.

Fig. 5. Load deflection response normalized with the Rankine earth pressure coefficient, le=15d

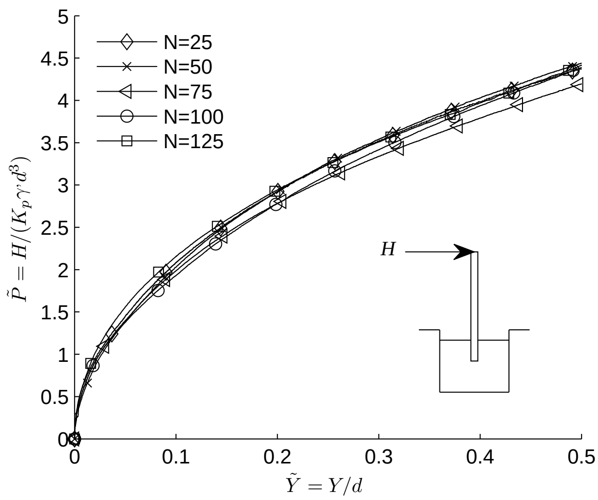

The generated p-y curves from the moment distribution are also normalised and again the Rankine coefficient is used.

[14] $$\tilde{p} = \frac{\tilde{p}}{K_p} = \frac{1}{K_p}\frac{p}{\sigma'_v d}$$

We here recognize the normalised pressure as the earth pressure coefficient introduced in Eq. 1 divided by Rankine's passive earth pressure coefficient. The normalized p-y curves from the five different tests are shown in Fig. 6. Here normalized p-y curves from the six different levels are shown separately. It is seen that the normalized p-y curves from the six different levels show the same high degree of similarity as was found for the overall response. Hence, it may be concluded that the normalized p-y responses have similar normalized behavior no matter of the stress level. It is seen that the stress level can be

Fig. 6. p-y curves for test with different stress distributions, $l_e = 15d$

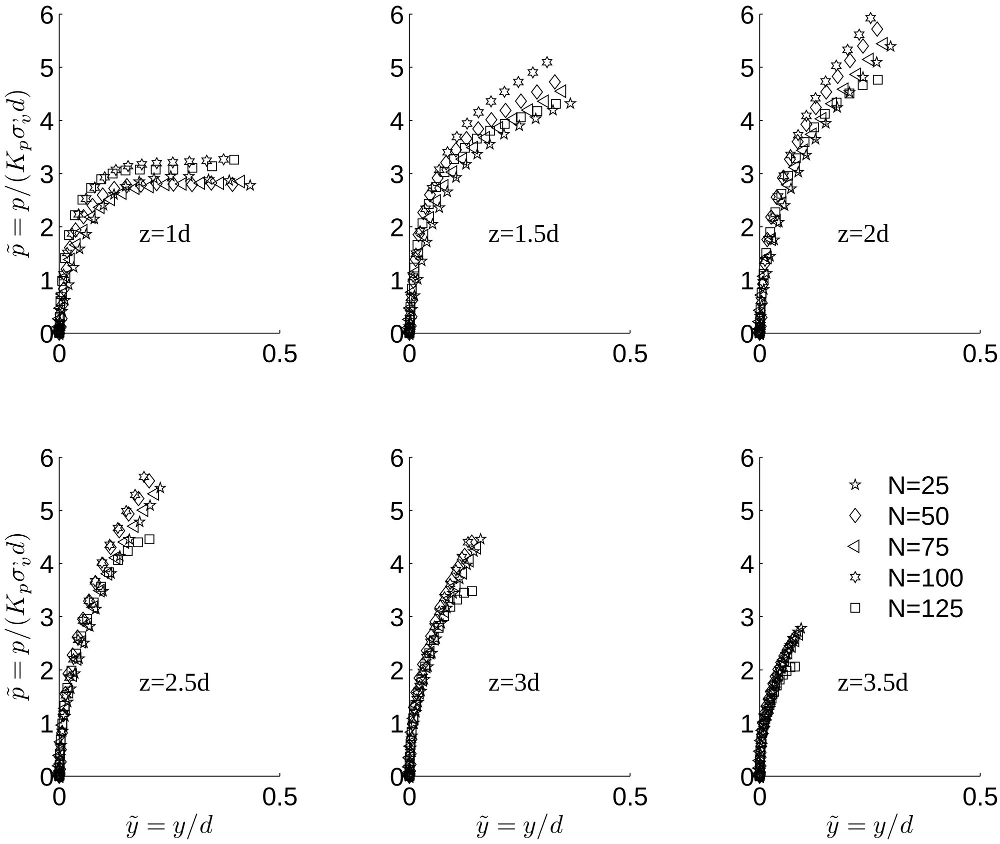

taken into account normalizing the results only using the angle of friction. These curves can then be used for any given prototype stress level, when the stress level effect is taken into account. In contrast to the API 2007 method, we use a different normalization in order to take the stress dependent maximum angle of friction into account.

4.2.3. Load eccentricity effect

The effect from load eccentricity was investigated by comparing five tests performed on piles with a stress distribution identical with a 3 meter in diameter prototype but with different load eccentricities. The five tests were all performed in water saturated sand and on a pile with load eccentricities ranging from $l_e = 8.25d - 17.25d = 330 - 690mm$. Using the normalisation strategy described in Eq. 14 the results from the five tests is shown in Fig. 7. As for the five tests with different stress distributions the results from changing the load eccentricity is shown for the six strain-gauge levels. The responses are similar no matter of the load eccentricity. Scatter is seen in the results but no systematic error is observed and with the increasing soil stress in the depth the curves seems to collapse. It is therefore concluded from these tests that the soil-pile interaction did not change in the five tests. This is identical with the assumption recommended by API 2007.

4.2.4. Generic soil-pile interaction

From the tests it was seen that using the chosen normalisation the effect from stress distribution and load eccentricity can be taken into account. The normalised response can therefore be used in the range of piles with diameter of 1-5 meters and different load eccentricities. Generic normalized p-y curves representative for the ten performed tests are shown in Fig. 8. It can be seen that a maximum soil resistance was only reached in the upper layer $z = 1d$, even though the pile at sand surface has been displaced more than $0.5d$. The initial slopes of the p-y curves were all similar and are found to $\tilde{E}_{py}/K_p = 100$.

5. Discussion

In the design of a monopile supporting an offshore wind turbine, the initial stiffness and the maximum bearing capacity of the pile foundation are important design parameters for a monotonic load situation. The design methodology used today relies on empirical tests on slender piles. From these tests, p-y curves were deducted and are today used also for large diameter, stiff monopiles. The validity of the extrapolation of these p-y curves to the design of monopiles seems to lack a scientific justification. This paper has investigated two effects in this perspective, the stress level and the load eccentricity effects.

Eq. 1 shows the maximum soil resistance is dependent on the pile diameter and the stress level. This research demon-

Fig. 7. Normalized p-y curves for tests with different load eccentricities

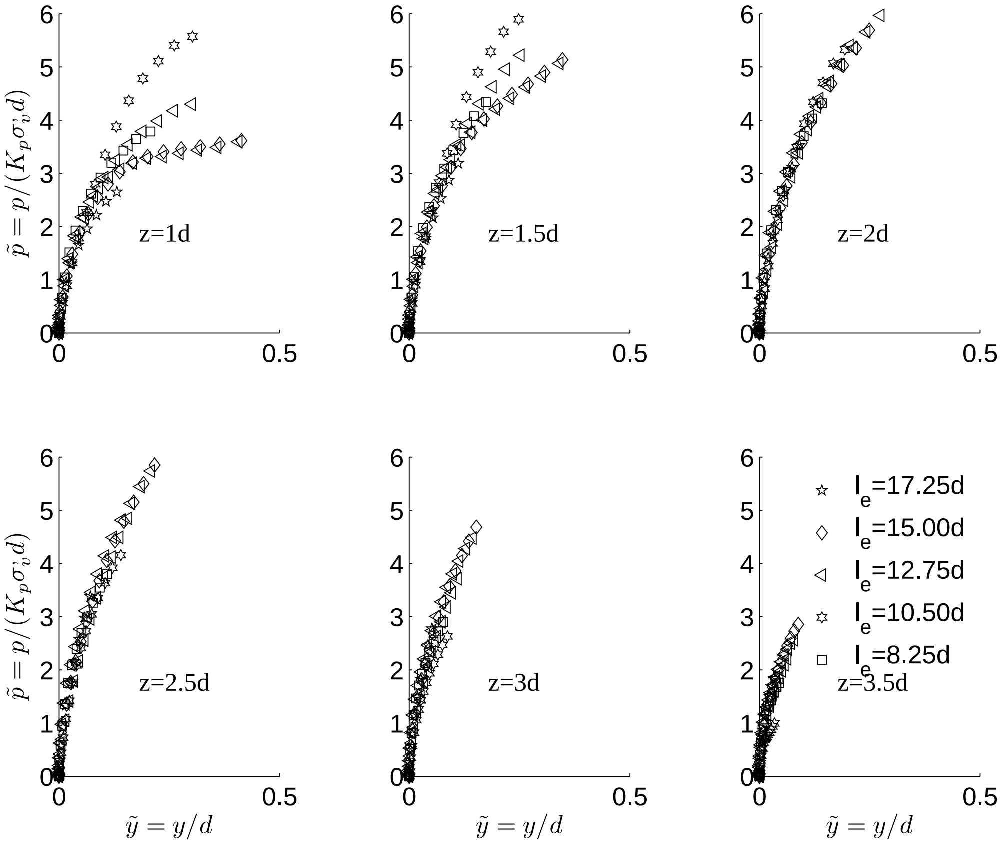

Fig. 8. Normalised general p-y curves for a pile ranging load eccentricities $l_e = 8.25 - 17.25d$ and a diameter ranging from 1-5 m

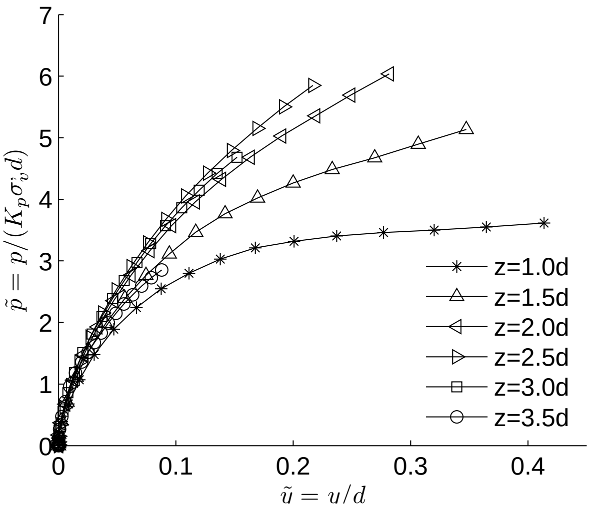

strates that the stress level depending soil behavior can be taken into account by a simple normalisation using the passive Rankine earth pressure coefficient. The effect from changing the diameter of a monopile is still unknown. In a full scale test of a monopile, both the stress level and the pile diameter are increased, compared to the original tests, from e.g. (Murchison and O'Neill 1984). Our research shows that results from a full scale test will not be affected by the stress level if this is taken correctly into account, and a possible diameter effect can thereby be identified.

One could argue that tests performed in dry sand do not represent prototype behaviour for offshore monopiles, but if no pore pressure develops the response of the pile is determined by the effective stresses. This was demonstrated by comparing one tests performed in saturated sand with a test performed in dry sand, shown in Fig. 3. The scaling approach described in Eq. 9 was used, and the responses from the tests were identical in model scale, which confirms the scaling procedure.

This research shows that for the investigated stress levels and for a range of different load eccentricities, the initial stiffness of the p-y curves increases linearly as proposed by API 2007. The corresponding stiffness found from the tests using a representative angle of friction of $\phi' = 42^o$ can therefore be written as:

$$[15] \qquad \begin{aligned} E_{py} &= \tilde{E}_{py} \cdot K_p \cdot \sigma_v' \\ &= 100 \cdot tan^2(45^o + 42^o/2) \cdot \gamma' \cdot z \\ &\approx 500 \cdot \gamma' \cdot z \end{aligned}$$

We propose to calculate the initial stiffness using the effective stress level; this enables the calculation of E_{py} with only one initial subgrade modulus function which is valid both for dry and saturated sand. Having an effective density of $10kN/m^3$

leads to an initial subgrade modulus of $k = 5000 kN/m^3$, which is significantly smaller than the proposed value of, $k = 40000 kN/m^3$ of API 2007. The initial stiffness is affected by the installation procedure and piles installed in-flight at the right stress level would have a larger stiffness. The value found from this study is very small but it is confirming the order of magnitude seen in other centrifuge tests e.g. (Remaud 1999) and (Klinkvort, Leth, and Hededal 2010). From the tests presented in this paper the linear increase with depth is clear, whereas the order of magnitude of the initial subgrade modulus needs to be investigated further.

In the data from the original tests on long slender piles, presented in Murchison and O'Neill 1984 all tests sites were presented by one characteristic angle of friction. Bolton 1986 showed that the angle of friction is dependent on both the relative density and the mean soil pressure. For a homogenous sand sample with a constant relative density, the angle of friction is therefore not constant. The determination of the empirical factor A is therefore due to this probably defined from an assumption that the soil has a constant angle of friction. In Fig. 9 all test data is shown together with the two soil-pile interaction models shown in Eq. 5 and Eq. 6. From the tests it was seen that the normalised initial stiffness was 100 and is therefore used in the models. The ultimate capacity is here calculated using Eq. 4 for both of the models, and, Eq. 7 has been used to calculate the angle of friction for every soil layer. Looking at Fig. 9 it can be seen that the initial stiffness of the two models is well described. The tangential hyperbolic function used in the API 2007 method is though very straight and it starts to deviate the data points early. On the contrary, the hyperbolic function seems to match the measurements in a larger range. The maximum capacity is overestimated in the upper soil layer $z = 1d$, it is reasonable estimated in the soil layer $z = 1.5d$ and it is underestimated in the soil layers from $z = 2 - 3d$.

It is clear that the ultimate capacity is not well predicted, and that all these layers are heavily influenced on the maximum capacity by the empirical parameter A. If one chose to use the assumption of the ultimate capacity shown in Equation 4 a reformulation of the empirical parameter A is needed. To give a better estimate of soil-pile interaction seen in the test, here is chosen to reformulate the parameter A. The step function is here used to give the transition from a value of 2 in the upper layers to a value of 0.9 in the lover layers.

[16] $$A = 0.9 + H \cdot 1.1$$

[17] $$H = \frac{1}{2} + \frac{1}{2} tanh\left(9 - 3\frac{z}{d}\right),$$

The hyperbolic function shown in Eq. 6 is used together with the new value of A, shown in Eq. 16. The results are shown in Fig. 9 and here it can be seen that the new model still overpredicts the maximum capacity in the $z = 1d$ layer but only to a minor degree and in the rest of the layers, there seems to be a good agreement.

In Figure 10 different depth factors are plotted. Here is shown the proposed function by Murchison and O'Neill 1984 and recommended by API 2007, the proposed function by Georgiadis, Anagnostopoulos and Saflekou 1992 determined from centrifuge test and the one proposed in Eq. 16. The high start

Fig. 10. Comparison of depth factor

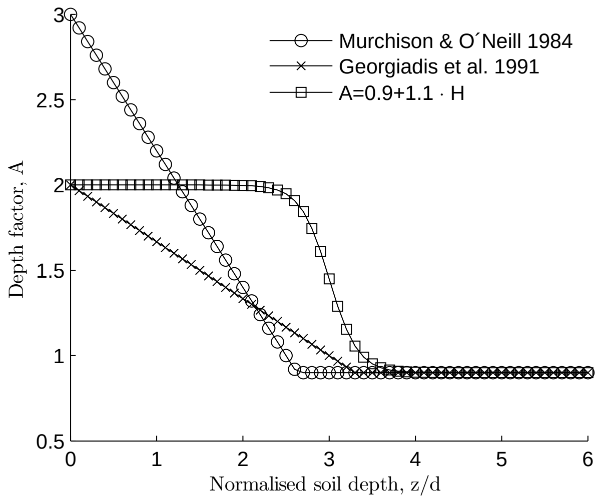

value used in the Murchison and O'Neill 1984 could be addressed to the stress dependent angle of friction. If this is not taken into account, this leads to the use of a too small angle of frictions in the top layers and thereby a high value of A. Nevertheless the inconsistency in the empirical formulation of the empirical depth factor A clearly shows that the formulation of A is site dependent. One therefore has to be very careful when a formulation of A is used on locations different from the place where it was original determined.

In the formulation of the ultimate capacity shown in Eq. 4 the minimum value of the theoretical calculation of failure in shallow or great depth is used. For monopiles supporting offshore wind turbines installed in dense sand the piles are all relative short and the ultimate capacity is thus always calculated as the shallow failure. The failure mechanise is therefore not correct and the value of A plays a huge role. The formulation, shown in Eq. 16, uses a step function and therefore has a steep transition from one value to another. This could indicate the transition from a shallow failure mechanism to a deep failure mechanism. Looking at Fig. 10 it can be seen that transition is about a depth of $3.5d$, and with a rotation point of the pile located around a depth of $4.5d$, it could be argued to use a deep failure mechanism which is closely related to the rotation point of the pile in the lower part. The use of an imperial factor in the calculation of the ultimate capacity clearly shows that the theoretical assumption lacks accuracy. Here is chosen to use a pragmatic approach with calibration of this factor to the tests. It would though be preferable to develop a theoretical approach where an empirical factor is avoided. No clear conclusions can though be drawn from this study and it has to be investigated in more details.

Fig. 9. Comparison of the effect from load eccentricity on the normalized p-y curves

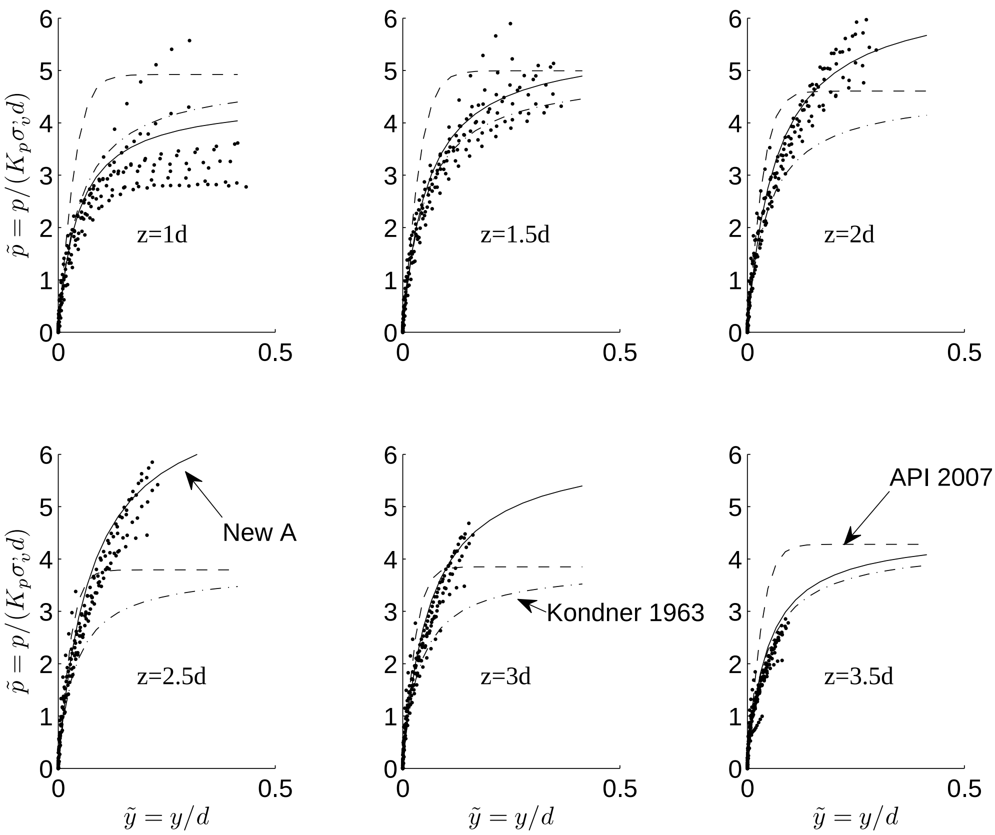

6. Conclusion

Ten centrifuge tests have been used to demonstrate the effect from changing the stress level and the load eccentricity for a monopile installed in sand supporting an offshore wind turbine. Five centrifuge tests were performed on model monopiles subjected to stress levels equal to prototype monopiles with a diameter ranging from 1-5 meters. From the tests it was clearly seen that by taking the different angle of frictions into account as a simple normalisation, the stress level did not affect the normalised response. This enables that the normalised result from 1 centrifuge test can be compared to a monopile with a diameter ranging from 1 to 5 meter.

Normalised p-y curves from tests with different load eccentricities were also compared, and it was here also seen the results from the test shoved a high degree of similarity no matter of the load eccentricity. It was therefore possible to relate all of the ten different tests to one generic soil-interaction model. The model has a constant normalised initial stiffness in accordance with the recommendations in API 2007. The stiffness obtained in this study is one order of magnitude smaller than the recommendations, but in the range of values found from other centrifuge studies.

A new formulation of the depth factor A was proposed and used together with a hyperbolic function, and was seen to fit all of the results with a high degree of accuracy. The new formulation of A with a steep transition from 2 to a value of 0.9, could indicate a transition from one failure mechanism to another. This transition is not seen when using the methodology recommended by API 2007 which for monopiles for wind turbines always uses the shallow failure mechanism in the calculation of the ultimate capacity. This study demonstrated that the empirical related factor sough as initial stiffness and ultimate capacity is dependent on the given test condition and should be used with care when used outside the range of its calibration. Special it seems to be a need of a reformulation of the calculation of the ultimate capacity which capture the right failure mechanism and where a calibration factor as A is not needed.

References

Abdel-Rahman, K. & Achmus, M. 2005. Finite element modelling of horizontally loaded monopile foundations for offshore wind energy converters in Germany, Frontiers in offshore geotechnics; 1ST 2005, , pp. 391-396.

API 2007. API RP 2A-WSD Recommended practice for planning, designing, and constructing fixed offshore platforms - Working stress design.

Ashford, S.A. & Juirnarongrit, T. 2003. Evaluation of pile diameter effect on initial modulus of subgrade reaction, Journal of Geotechnical and Geoenvironmental Engineering, vol. 129, no. 3, pp. 234-242.

Augustesen, A.H., Brodbaek, K.T., Moller, M., Sorensen, S.P.H., Ibsen, L.B., Pedersen, T.S. & Andersen, L. 2009. Numerical modelling of large-diamter steel piles at Horns Rev, Civil Comp -CD Rom Edition.

Bienen, B., Cassidy, M.J. & Gaudin, C. 2009. Physical modelling of the push-over capacity of a jack-up structure on sand in a geotechnical centrifuge, Canadian Geotechnical Journal, vol. 46, no. 2, pp. 190-207.

Bolton, M.D. 1986. Strength and dilatancy of sands, Geotechnique, vol. 36, no. 1, pp. 65-78.

Briaud, J., Smith, T.D. & Meyer, B.J. 1983. Using the pressuremeter curve to design laterally loaded piles, Proceedings - Annual Offshore Technology Conference, vol. 1, pp. 495-502.

Broms, B. 1964. Lateral resistance of piles in cohesionless soils, ASCE - Proceedings - Journal of the Soil Mechanics and Foundations Division, vol. 90, pp. 123-156.

Cassidy, M.J., Randolph, M.F. & Byrne, B.W. 2004. A comparison of the combined load behaviour of spudcan and caisson foundations on soft normally consolidated clay, Geotechnique, vol. 54, no. 2, pp. 91-106.

De Nicola, A. & Randolph, M.F. 1999. Centrifuge modelling of pipe piles in sand under axial loads, Geotechnique, vol. 49, no. 3, pp. 295-318.

Dyson, G.J. & Randolph, M.F. 2001. Monotonic lateral loading of piles in calcareous sand, Journal of Geotechnical and Geoenvironmental Engineering, vol. 127, no. 4, pp. 346-352.

Fan, C. & Long, J.H. 2005. Assessment of existing methods for predicting soil response of laterally loaded piles in sand, Computers and Geotechnics, vol. 32, no. 4, pp. 274-289.

Fuglsang, L.D. & Nielsen, J. 1988. Danish centrifuge hardware and usage, Centrifuges in Soil Mechanics, pp. 93-95.

Fuglsang, L.D. & Ovesen, N.K. 1988. The application of the theory of modelling to centrifuge studies, Centrifuges in Soil Mechanics, pp. 119-138.

Georgiadis, M., Anagnostopoulos, C. & Saflekou, S. 1992. Centrifuge testing of laterally loaded piles in sand, Canadian Geotechnical Journal, vol. 29, no. 2, pp. 208-216.

Hald, T., Mrch, C., Jensen, L., Bakmar, C.L. & Ahle, K. 2009. Revisiting monopile design using p-y curves. Results from full scale measurements on Horns Rev, Proceedings of European Offshore Wind 2009 Conference.

Hansen, J.B. 1961. Ultimate resistance of rigid piles against transversal forces, Danish Geotechnical Institute - Bulletin, no. 12, pp. 5-9.

Kim, B.T., Kim, N., Lee, W.J. & Kim, Y.S. 2004. Experimental load-transfer curves of laterally loaded piles in Nak-Dong River sand, Journal of Geotechnical and Geoenvironmental Engineering, vol. 130, no. 4, pp. 416-425.

Klinkvort, R.T., Leth, C.T. & Hededal, O. 2010. Centrifuge modelling of a laterally cyclic loaded pile", Physical Modelling in Geotechnics, pp. 959-964.

Kondner, R.L. 1963. Hyperbolic stress-strain response; cohesive soils, ASCE - Proceedings - Journal of the Soil Mechanics and Foundations Division, vol. 89, pp. 115-143.

Lesny, K. & Wiemann, J. 2006. Finite-element-modelling of large diameter monopiles for offshore wind energy converters, GeoCongress 2006: Geotechnical Engineering in the Information Technology Age, vol. 2006.

Leth, C.T. 2011. Centrifuge modelling of large diamter pile in sand subject to lateral loading, Technical report, DTU Civil Engineering.

Li, Z., Haigh, S.K. & Bolton, M.D. 2010. Centrifuge modelling of mono-pile under cyclic lateral loads, Physical Modelling in Geotechnics, pp. 965-970.

McClelland, B. & Focht, J., J.A. 1956. Soil modulus for laterally loaded piles. American Society of Civil Engineers -Proceedings - Journal of the Soil Mechanics and Foundations Division, 82, 1956.

Murchison, J.M. & O'Neill, M.W. 1984. Evaluation of p-y relationships in cohesionless soils, Analysis and Design of Pile Foundations.Proceedings of a Symposium in conjunction with the ASCE National Convention, pp. 174-191.

Norris, G. 1986. Theoretically based BEF laterally loaded pile analysis, Numerical Methods in Offshore Piling 3rd International Conference, pp. 361-386.

Pender, M.J., Carter, D.P. & Pranjoto, S. 2007. Diameter Effects on Pile Head Lateral Stiffness and Site Investigation Requirements for Pile Foundation Design, Journal of Earthquake Engineering, vol. 11, no. 1.

Reese, L.C., Cox, W.R. & Koop, F.D. 1974. Analysis of laterally loaded piles in sand, Proceedings of sixth Annual Offshore Technology Conference, Houston.

Reese, L.C. & Matlock, H. 1956. Non-dimensional solutions for laterally-loaded piles with soil modulus assumed proportional to depth, Proceedings of eighth Texas Conference on Soil Mechanics and Foundation Engineering.

Remaud, D. 1999 Pieux sous charges latrales: tude exprimentale de l'effet de groupe, Ph.D. thesis.

Rosquot, F., Thorel, L., Garnier, J. & Khemakhem, M. 2010. P-y curves on model piles: Uncertainty identification, Physical Modelling in Geotechnics, pp. 997-1002.

Rosquoet, F., Thorel, L., Garnier, J. & Canepa, Y. 2007. Lateral cyclic loading of sand-installed piles, Soils and Foundations, vol. 47, no. 5, pp. 821-832.

Schofield, A.N. 1980. Cambridge geotechnical centrifuge operations, Geotechnique, vol. 30, no. 3, pp. 227-268.

Smith, T.D. 1987. Pile horizontal soil modulus values, Journal of Geotechnical Engineering, 1987.

Sorensen, S.P.H., Brodbaek, K.T., Moller, M., Augustesen, A.H. & Ibsen, L.B. 2009. Evaluation of the load-displacement relationships for large-diamter piles in sand, Civil Comp -CD Rom Edition.

Terzaghi, K. 1955. Evaluation of coefficients of subgrade reaction, Geotechnique, vol. 5, no. 4, pp. 297-326.

Wesselink, B.D., Murff, J.D., Randolph, M.F., Nunez, I.L. & Hyden, A.M. 1988. Analysis of centrifuge model test data from laterally loaded piles in calcareous sand, Engineering for calcareous sediments, vol. 1, pp. 261-270.

Zhang, L., Silva, F. & Grismala, R. 2005. Ultimate lateral resistance to piles in cohesionless soils, Journal of Geotechnical and Geoenvironmental Engineering, vol. 131, no. 1, pp. 78-83.

Paper IV

"Centrifuge modelling of a laterally cyclic loaded pile"

R.T. Klinkvort, C.T. Leth & O. Hededal

Published in: *Physical Modelling in Geotechnics, 2010*

Physical Modelling in Geotechnics – Springman, Laue & Seward (eds)
© 2010 Taylor & Francis Group, London, ISBN 978-0-415-59288-8

Centrifuge modelling of a laterally cyclic loaded pile

R.T. Klinkvort, C.T. Leth & O. Hededal
Technical University of Denmark, Copenhagen, Denmark

ABSTRACT: A total number of 9 monotonic and 6 cyclic centrifuge tests on laterally loaded piles in very dense, dry sand was performed. The prototype dimensions of the piles were 1 meter in diameter and penetration depths varying from 6 to 10 meters. The static tests were used to investigate the initial subgrade reaction modulus and as a reference for cyclic tests. For the cyclic tests the accumulation of deflections and the change in secant stiffness of the soil from repetitive loading were investigated. From all the tests carried out accumulations of deflections were seen. From the centrifuge tests it was seen that no reduction occurs of the overall bearing capacity and that deflections accumulate due to cyclic loading. This paper presents test results and discusses the effects from load eccentricity and effects from cyclic loading with focus on accumulations of the deflection and the change in secant stiffness.

1 INTRODUCTION

Over the last decades there has been an increasing focus on alternative sustainable energy. One of these alternative sources is energy from wind turbines. The most widely used foundation method for offshore wind turbines is single large diameter tubular steel piles commonly denoted monopiles. The monopile design has been used in Denmark at the wind turbine parks at Samsø and Horns Rev. The design of monopiles is commonly based on the theory of laterally loaded piles. This theory relies on empirical data originated from the oil and gas industry, Reese & Matlock (1956) & McClelland & Focht (1958). The design for the lateral capacity is carried out by modelling the pile as a beam and the soil as a system of uncoupled springs, known as a Winkler model. The springs are described by p-y curves which defines the load displacement relationship for the interaction between soil and pile, API (1993). The formulation of these curves was originally calibrated to slender piles, but is today even used for design of large diameter monopiles. However, the monopiles used for wind turbine foundations act as stiff piles. Therefore it is relevant to investigate the behavior of stiff piles in more detail. The current test program comprises piles with a prototype diameter of 1 m and penetration depths up to 10 m and is intended to investigate the behavior of the larger monopiles used offshore today.

2 SCOPE OF WORK

Two major loads act on an offshore wind turbine. One due to the wind at the top of the wind turbine and one due to the waves and ice at sealevel. The purpose of the research carried out is to investigate the pile behavior when changing the location of force resultant and the penetration depth. The investigation will for the static tests focus on the initial stiffness of the pile-soil response. The cyclic tests will focus on the gradual change in secant stiffness and the accumulation of deflection as a function of the number of load cycles.

3 DESIGN METHODOLOGY

The method for sand presented here is the one used in API (1993), which is based on the formulation proposed by Murchison & O'Neill (1984).

The p-y relationship for sand is typically approximated by

$$p = A \cdot p_u \tanh\left[\frac{k \cdot X}{A \cdot p_u} y\right] \tag{1}$$

The value k represents the initial modulus of subgrade reaction and X is the distance to soil surface. p_u is the ultimate soil resistance and is found using plasticity theory. A is an empirical constant which is used to fit the test results with theory. For static loading $A = \left(3.0 - \frac{0.8X}{D}\right) \geq 0.9$. For cyclic loading $A = 0.9$.

The initial stiffness of the p-y relationship can be found if p is differentiated with respect to y,

$$E_{py,ini} = \frac{\partial}{\partial y}\left[A \cdot p_u \tanh\left(\frac{k \cdot X}{A \cdot p_u} y\right)\right]_{y=0} = k \cdot X \tag{2}$$

From Equation 2 it can be seen that the design codes uses a initial stiffness of the p-y relationship which is increasing linearly with depth.

4 EXPERIMENTS

The centrifuge test program was performed on solid steel piles with a diameter d = 16 mm and penetration depths between 96–160 mm. The gravity field was increased to obtain a scaling factor of approximately $N = 62.5$. This resulted in prototype piles with a diameter of $d = 1$ m and penetration lengths between $L = 6$–10 m.

The different definitions are shown in Figure 1. The test program for the static and cyclic tests can be seen in Table 1. Here L is the penetration depth, e is the load eccentricity, while m and c indicate monotonic and cyclic test, respectively. All static and cyclic tests were performed in dry Fontainebleau sand. Leth et al. (2008) has collected classification parameters for the Fontainebleau sand which can be seen in Table 2. The average grain size of the Fontainebleau sand is 0.18 mm. The test piles have a diameter of 16 mm. This leads to a "model diameter/grain size diameter" ratio of 16/0.18 = 88. This ratio should be large enough to avoid particle size effects when applying the artificial gravity field according to the observations described in Fuglsang & Ovesen (1988).

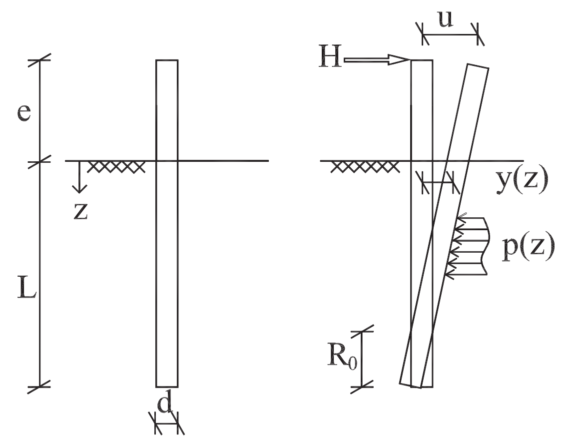

Figure 1. Sketch of pile.

Table 1. Test program for the centrifuge tests.

$e \backslash L$	$6d$	$8d$	$10d$
$2.5d$	m c	m c	m c
$4.5d$	m c	m c	m
$6.5d$	m c	m	m

Table 2. Classification parameters for the Fontainebleau sand.

Specific gravity of particles	G_s	2.646
Minimum void ratio	e_{min}	0.548
Maximum void ratio	e_{max}	0.859
Average grain size	d_{50}	0.18
Coefficient of uniformity	C_u	1.6

A spot pouring hopper (SPH) was used for the preparation of the sand sample. This equipment was developed according to a setup described in Huei-Tsyr et al. (1998). Due to the geometry of the container and pile the sand is prepared using a circular travelling loop as described in Zhao et al. (2006). CPT tests have been carried out to validate the pouring method. All these CPT tests showed the soil sample has a good homogeneity in the container, Gottlieb et al. (2005). After the sand is prepared, the pile is installed at 1 g.

A total of 15 centrifuge tests have been performed: nine monotonic and six cyclic. For all the tests the relative density was found to vary in the range 0.9–0.95 The relative densities are calculated by measuring the weight and the volume of the sand sample. The average value for both the static and cyclic tests is $I_D = 0.924$ and a void ratio of $e = 0.57$. It is assessed that the small variation of the density not will affect the results significantly.

4.1 *Monotonic tests*

The force and deflection are normalized to facilitate comparison between the different tests. The normalized force is defined as

$$P = \frac{H}{\gamma . d^3} \tag{3}$$

and normalized deflection is defined as

$$U = \frac{u}{d} \tag{4}$$

In Figure 2 the observation on the change between load with an eccentricity on $6.5d$ and $4.5d$ or $2.5d$ is clear. The tendency is that for load eccentricity of $6.5d$ and $4.5d$ the normalized lateral bearing capacity is nearly identical. This indicates that a change in failure mechanism occurs.

More tests have to be conducted in order to clarify how the load eccentricity and pile penetration depth affects the pile-soil failure mechanism.

The design codes assume a linear increase in the initial stiffness with depth as indicated by Equation 2. Several authors have, however, proposed alternative distributions e.g. Lesny & Wiemann (2006) and Haahr (1989). Therefore the increase in initial stiffness is investigated further.

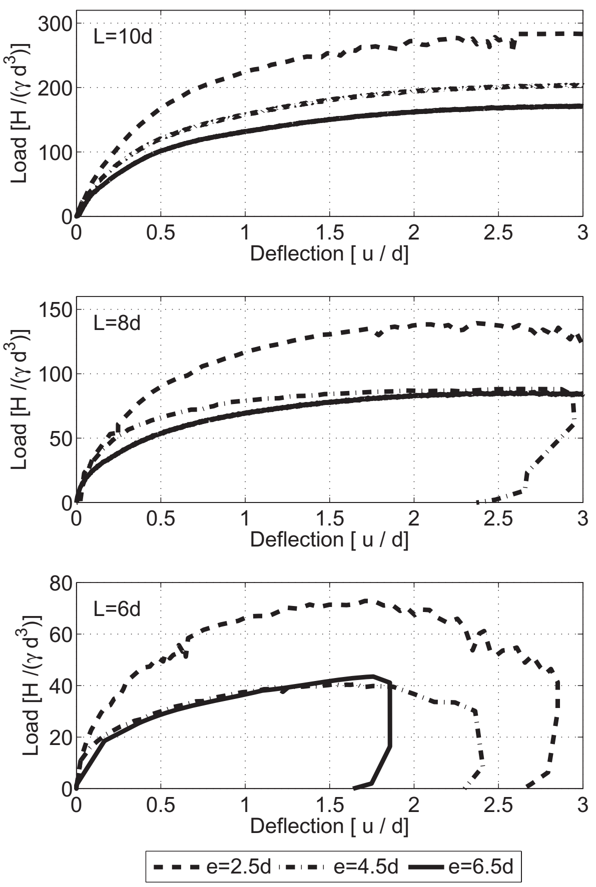

Figure 2. Normalized plot with the nine monotonic tests.

At initial loading the pile is assumed to behave as a rigid pile and only elastic deformations occur in the sand. This implies that the pile deflection can be described knowing the pile head deflection and the rotation.

$$y(z) = u - \theta(e + z) \tag{5}$$

In the present setup, the pile may be assumed to behave rigidly if, according to Equation 6 by Poulos & Hull (1989), the stiffness of the sand is less than $E_s = 100\ MPa$.

$$1.48\left(\frac{E_p I_p}{E_s}\right)^{\frac{1}{4}} < L_{inter} < 4.44\left(\frac{E_p I_p}{E_s}\right)^{\frac{1}{4}} \tag{6}$$

The soil reaction on the pile can be described as an initial stiffness times the deflection of the pile.

$$p(z) = -E_{py,\ ini}(z)\ y(z) \tag{7}$$

The initial stiffness may be assumed to have a nonlinear variation with depth as e.g. given in Equation 8. Here $n = 1$ corresponds a linear distribution and $n = 0.5$ corresponds to a parabolic distribution.

$$E_{py,ini}\left(\frac{z}{d}\right) = A_n \cdot \left(\frac{z}{d}\right)^n \tag{8}$$

Considering moment and horizontal equilibrium, the constant A_n can be found to be

$$A_n = \begin{cases} \dfrac{144 + 384\left(\dfrac{e}{L}\right) + 288\left(\dfrac{e}{L}\right)^2}{8L} \dfrac{H}{u}\dfrac{d}{L}, & n = 1 \\ \dfrac{75 + 210\left(\dfrac{e}{L}\right) + 175\left(\dfrac{e}{L}\right)^2}{8L} \dfrac{H}{u}\sqrt{\dfrac{d}{L}}, & n = 0.5 \end{cases} \tag{9}$$

For the nine static tests the constant An has been calculated using both relations for the development of the initial stiffness. The applied force has been found for the entire test series at an initial deflection of $u/d = 0.1$. The results are presented in Table 3. It must be expected that the soil has the same subgrade modulus for all the tests. Therefore, considering the smaller variation of the constant A_n for $n = 0.5$, it is assessed that the parabolic distribution gives a better description of the initial subgrade modulus. This parabolic distribution is also observed by Haahr (1989) and a distribution with $n = 0.6$ is observed by Lesny & Wiemann (2006).

The design codes prescribe a linear distribution of the initial subgrade reaction. This distribution was found using data from tests on long slender piles. For long slender piles only deformation on the upper part of the pile is seen and it is therefore only in the upper part of the pile data can be withdrawn. The tendency according to initial stiffness seen in the upper part is then extrapolated to the lower part. A linear distribution and a parabolic distribution may be nearly identical in the upper part of the pile but yield large differences in the lower part. The effects on a long slender pile from

Table 3. Calculated subgrade reaction modulus for the nine monotonic tests.

L [*d*]	*e* [*d*]	*An* = 1 [*kPa*]	*An* = 0.5 [*kPa*]
10	2.5	3962	6883
10	4.5	3994	7105
10	6.5	4845	8753
8	2.5	4851	7603
8	4.5	4908	7883
8	6.5	5211	8595
6	2.5	6532	8972
6	4.5	6015	8466
6	6.5	6268	8943

assuming a wrong distribution will therefore not be critical. This is not the case for a short rigid pile.

Sørensen et al. (2009) compared $FLAC^{3D}$ calculations with the p-y approach recommended by design codes. They adopted a distribution proposed by Lesny & Wiemann (2006) which is identical with Equation 8 with $n = 0.6$. They observed that the use of this distribution gave a better fit to the results from the three dimensional numerical model, but more tests have to be conducted in order to clarify the distribution of the initial subgrade reaction.

In Table 4 different values of initial subgrade modulus for dense dry sand is presented. For these values proportional distribution is expected. From this table it can be seen that the values proposed by API (1993) and Reese & Impe (2001) are much larger than the values found by Remaud (1999).

Some of the tests presented here were numerically modelled using the Winkler method by Klinkvort (2009). The best fit to the monotonic curves was done using an initial subgrade modulus of $k = 2.7\ MN/m^3$.

This study and the study by Remaud (1999) both used centrifuge modelling where the deflection is scaled with a factor of N and the force is scaled with a factor of N^2. The scaling factors are found using dimensional theory. More tests have to be conducted in order to clarify results from centrifuge modelling in order to determine the magnitude and distribution of the initial stiffness.

4.2 *Cyclic tests*

In the cyclic tests the pile was subjected to 100 force controlled load cycles. To investigate the influence from previous loading three of the tests were performed in three phases. The first phase with large cycles, second phase with smaller cycles and the third phase with cycles equal to cycles in the first phase. To investigate the effects from cyclic loading this paper uses methods described in LeBlanc (2009) to account for accumulation of deflections and the change in secant stiffness.

A set of load characteristic constant are used to describe the cyclic loading. The load characteristics are denoted ζ_b and ζ_c. They are determined as shown in Equation 10.

Table 4. Comparison of modula of initial subgrade reaction.

	k_{py} $[MN/m^3]$
API (1993)	83
Reese & Impe (2001)	61
Remaud (1999)	8

$$\zeta_b = \frac{H_{\max}}{H_{\text{static}}} \quad \zeta_c \frac{H_{\min}}{H_{\max}} \tag{10}$$

Here $H_{\max}$ and $H_{\min}$ are the maximum and minimum applied force in the cyclic loading. H_{static} is the maximum bearing capacity found from the static test. ζ_b describes how close the cycles are carried out to the static bearing capacity. $\zeta_b = 1$ is therefore cycles carried out to the maximum bearing capacity. ζ_c describes the direction of the loading. For one-way loading $\zeta_c = 0$ and for two-way loading $\zeta_c = -1$.

In all of the 6 cyclic tests, accumulation of the deflection was seen. The best fit in all the tests was with a power fit as proposed by Long & Vanneste (1994) and LeBlanc (2009), cf. Equation 11.

$$\Delta u(N) = u_0 \cdot N^{\delta} \tag{11}$$

Here u_0 is the accumulated deflection at the first cycle and δ is an empirical coefficient which control the shape of the curve. The accumulated deflection for a given cycle is defined as the average value for the cycle.

A small increase in secant stiffness was observed for the first 100 cycles for all the tests. The best fit to the change in secant stiffness was done with a exponential function cf. Equation 12.

$$\kappa(N) = \kappa_0 \cdot e^{\kappa N} \tag{12}$$

κ_0 describes the initial secant stiffness in the first cycle. κ describes the change in secant stiffness.

Figure 3 shows the results for cyclic testing on the pile with a load eccentricity $e = 2.5d$ and a penetration depth $L = 10d$. This way of analyzing the cyclic tests has been done for all the performed tests.

As it can be seen from Figure 3, the determination of the secant stiffness and accumulation of the deflection involves a great scatter of data. This was also reported by LeBlanc (2009). This is to a some extent attributed the fact that measurements involves differences of small displacements.

The results from the cyclic tests are shown in Table 5. No clear relationship for the coefficients can be seen concerning load eccentricity and penetration depth. Neither do the results show any clear correlation to the loading characteristic constants ζ_b and ζ_c. Table 5 shows that the loading characteristic constants ζ_b and ζ_c has a large difference from test to tests. Therefore it is not possible from the performed test to conclude on the effect of the loading eccentricity and pile penetration, and further tests need to be conducted.

It seems like the development of the secant stiffness can be expressed in a more simple form

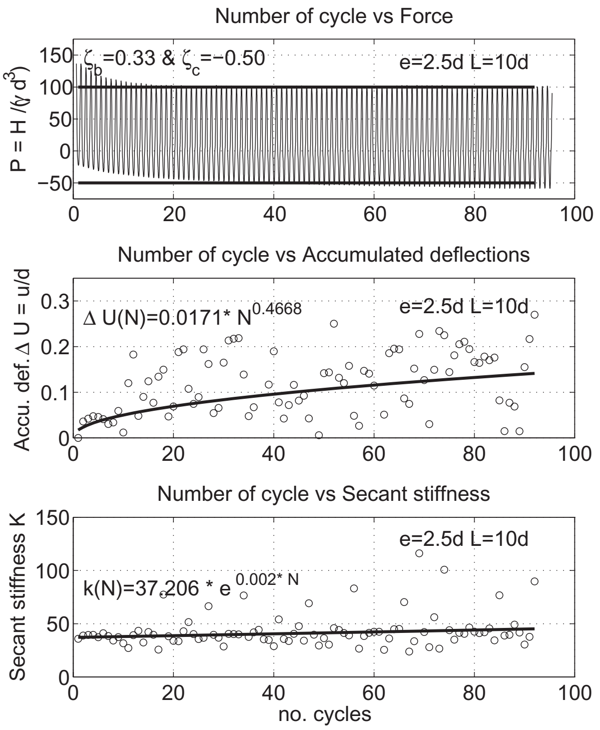

Figure 3. Displacements difference versus secant stiffness for cyclic test $e = 2.5$ & $L = 10d$.

Table 5. Dimensionless results from the cyclic testing.

L	e	ζ_b	ζ_c	Δu_0	δ	κ_0	κ
10	2.5	0.3	–0.5	0.02	0.46	37	0.002
10	4.5	0.3	–0.8	0.04	0.11	6.6	0.018
10	6.5	0.7	–0.6	0.02	0.72	11.4	0.003
8	4.5	1.0	–0.6	0.1	0.31	4.1	0.006
8	6.5	0.8	–0.9	0.1	0.01	2.2	0.000
6	6.5	0.6	–0.8	0.1	0.45	5.7	0.004

than proposed in Equation 12. In the last column in Table 5 κ is shown. For all the tests except the test $e = 4.5$ $L = 10d$, this value is very small. This indicates that the change in secant stiffness is very small and it may be sufficient to described the change in secant stiffness in a linear fashion. For three of the cyclic test ($e = 4.5d$ $L = 8d$, $e = 4.5d$ $L = 6d$ & $e = 6.5d$ $L = 6d$) new cyclic loading was done after the first 100 cycles. The new cyclic testing was done with a smaller amplitude than the first. Only in the test with a load eccentricity of $4.5d$ a decrease in the secant stiffness was seen. It must be expected that when performing a loading series with a smaller amplitude the secant stiffness will decrease as long as no equilibrium in the cyclic loading is found. When the pile has compacted the sand around the pile in a constant manner, the cyclic behavior will stabilize and the secant stiffness will increase. When performing cyclic loading again with a larger amplitude the secant stiffness in all the tests shows an increase.

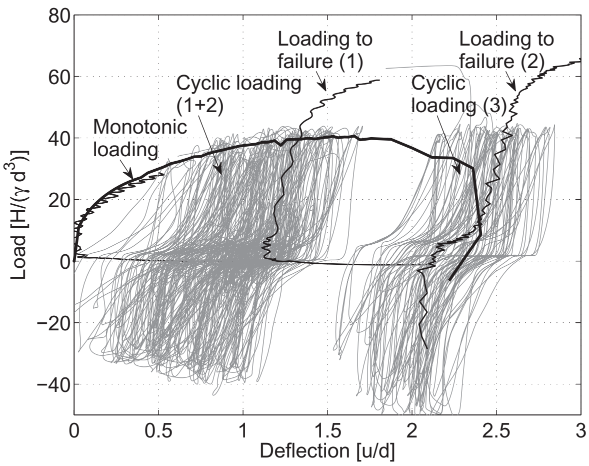

Figure 4. Normalized plot for the cyclic test $e = 4.5d$ & $L = 6d$.

An example of a cyclic tests series is shown in Figure 4. The plot contains two different tests; the monotonic test and the corresponding cyclic test series. The cyclic test series contains of first 100 cycles, followed with 100 cycles with smaller amplitude. After these cycles, the pile is loaded to failure and unloaded, then 100 cycles are applied again with a monotonic loading to failure at the end.

The pile is loaded to failure twice and it can be seen that the pile reaches a higher bearing capacity than the monotonic test. Cyclic loading is handled in the design codes by a reduction of the static soil resistance. This leads to a reduction of the bearing capacity and the pile—soil stiffness. These tests indicate that no reduction of the bearing capacity will occur.

From the cyclic load series it can also be seen that the secant stiffness increases for the cyclic loading in the investigated cases.

5 CONCLUSIONS

The monotonic tests revealed a relationship between the lateral bearing capacity of the pile and the load eccentricity. This indicates that there are different failure mechanisms for piles with large load eccentricity and piles with smaller load eccentricity. In practise this may be of importance for offshore wind turbines subjected to a combination of wind load from the rotor acting 60–100 m above seabed level and wave forces acting relatively closer to the seabed.

The centrifuge modelling indicates that using the design code recommendations to generate p-y curves led to a overestimation of the pile—soil stiffness. Due to this observation it is believed that the recommendations to generate the distribution and magnitude of the initial subgrade modulus should be changed. Further research is needed to gain knowledge about this.

From all the cyclic tests carried out, accumulations of deflections were seen. The secant stiffness of every cycle was measured revealing that the cyclic loading led to an increase in secant stiffness. From the centrifuge tests it was clearly seen that no reduction of the bearing capacity of dry sand occurs due to cyclic loading.

It seems like the influence of the location of the applied force on a laterally loaded pile was most critical for the monotonic bearing capacity. It is believed that this also affects the accumulations of deflection and the change in secant stiffness but it was not clearly seen in this research.

REFERENCES

API 1993. *Recommended Practice For Planning, Designing and Construction Fixed Offshore Platforms—Load and Resistance Factor Design.* American Petroleum Institute.

Fuglsang, L.D. & Ovesen, N.K. 1988. *The application of the theory of modelling to centrifuges studies.* Balkema, Rotterdam.

Gottlieb, S., Klinkvort, R.T., Petersen, J. & Christensen, L.K. 2005. Calibration and the use of mini-cpt. Student report, Technical University of Denmark (in Danish).

Haahr, F. 1989. *Interaction between latterally laoded model piles in sand*. Ph.D. thesis, Technical University of Denmark. (in Danish).

Huei-Tsyr, C., Chung-Jung, L. & Hung-Wen, C. 1998. The travelling pluvation apparatus for sand specimen preparation. *Centrifuge 98 1*: p. 143–148.

Klinkvort, R.T. 2009. Laterally loaded piles—centrifuge and numerically modelling. Master's thesis, Technical University of Denmark.

LeBlanc, C. 2009. *Design of Offshore Wind turbine Support Structures*. Ph.D. thesis, Aalborg University.

Lesny, K. & Wiemann, J. 2006. Finite-element-modelling of large diameter monopiles for offshore wind energy converters. In *Geo Congress*.

Leth, C.T., Krogsbøll, A., & Hededal, O. 2008. Centrifuge facilities at danish technical university. In *15th Nordic Geotechnical Meeting*.

Long, J.H. & Vanneste, G. 1994. Effects of cyclic lateral loads on piles in sand. *Journal of Geotechnical Engineering 120*: 225–244.

McClelland, B. & Focht, J.A. 1958. Soil modulus for laterally loaded piles. *Journal of the soil mechanics and foundations division—Proceedings of the American Society of Civil Engineers*: 1–22.

Murchison, J.M. & O'Neill, M.W. 1984. Evaluation of p-y relationships in cohesionless soils. In *Proc., Symposium of Analysis and Design of Pile Foundations, ASCE, San Fransisco*, 174–191.

Poulos, H. & Hull, T. 1989. The role of analytical geomechanics in foundation engineering. *Foundation Engineering: Current principles and Practices, ASCE, Reston 2*: 1578–1606.

Reese, L.C. & Impe, W.F.V. 2001. *Single Piles and Pile Groups Under Lateral Loading*. A.A. Balkema.

Reese, L.C. & Matlock, H. 1956. Non-dimensional solutions for laterally loaded piles with soil modulus assumed proportional to depth. *Proceedings of the 8th Conference on Soil Mechanics*: 1–41.

Remaud, D. 1999. *Pieux sous charges laterales: Etude Ex-perimentale de l'effect de groupe*. Ph.D. thesis, Ecole Centrale de Nantes. (in French).

Sørensen, S., Brødbæk, K.T., Møller, M., Augustesen, A.H. & Ibsen, L.B. 2009. Evaluation of the load-displacement relationships for large-diameter piles in sand. In *Proceedings of the Twelfth International Conference on Civil, Structural and Environmental Engineering Computing*.

Zhao, Y., Gafar, K., Elshafie, M., Deeks, A., Knappett, J. & Madabhushi, S. 2006. Calibration and use of a new automatic sand pourer. In *Physical modelling in Geotechnics, 6th ICPMG '06*, p. 265–270.

Paper V

"Laterally cyclic loading of monopile in dense sand"

R.T. Klinkvort, O. Hededal & M. Svensson

Published in: *Proceedings of the 15th European Conference on Soil Mechanics and Geotechnical Engineering, 2011*

Proceedings of the 15th European Conference on Soil Mechanics and Geotechnical Engineering
A. Anagnostopoulos et al. (Eds.)
IOS Press, 2011

doi:10.3233/978-1-60750-801-4-203

Laterally cyclic loading of monopile in dense sand

Chargement lateral cyclique de monopile dens le sable dense

R. T. Klinkvort[1], O. Hededal and M. Svensson
Technical University of Denmark (DTU)

ABSTRACT

In order to investigate the response from laterally cyclic loading of monopiles a large centrifuge tests series is ongoing at the Technical University of Denmark (DTU). This paper will present some of the tests carried out with a focus on the influence of accumulation of rotation when changing the loading conditions. In these tests the load conditions are controlled by two load characteristics, one controlling the level of the cyclic loading and one controlling the characteristic of the cyclic loading. The centrifuge tests were performed in dense dry sand on a pile with prototype dimensions as following: The diameter of the pile was d = 2 m, the penetration depth of the pile was L = 6 d = 12 m and a load eccentricity of e = 15 d = 30 m. The loading of the pile was performed with a load setup which applies the load on the monopile in a manner that corresponds to the load condition for a monopile used for wind turbine foundation. This is important in order to get the right failure mechanism in the sand. The load frame is controlled with a feedback system which enables force controlled load series. A total number of 8 tests have been carried. In all of the tests, the pile was loaded with 500 load controlled cycles and for the entire test series accumulation of rotation was seen.

RÉSUMÉ

Afin d'étudier la réponse de chargement latéral cyclique de monopieux, une importante série d'essais en centrifugeuse est en cours à l'Université technique du Danemark (DTU). Ce document présente quelques-uns des tests effectués avec un accent sur l'influence de l'accumulation de rotations pour des conditions de chargement variables. Dans ces essais, les conditions de charge sont contrôlées par deux caractéristiques de charge, une contrôlant le niveau de la charge cyclique et l'autre contrôlant l'orientation du chargement cyclique. Les essais en centrifugeuse ont été effectués sur un pieu situé dans du sable dense et sec ; le pieu a les dimensions suivantes : d = 2 m de diamètre, profondeur de L = 6 d = 12 m et excentricité de la charge de e = 15 d = 30 m.
Le chargement du pieu a été réalisé avec une configuration de charge qui applique la charge sur le monopieu d'une manière correspondant au chargement rencontré lors de l'utilisation d'un monopieu comme fondation d'une éolienne. Ceci est important afin d'obtenir le mécanisme de rupture correct dans le sable. Ce cadre de chargement est contrôlé à l'aide d'un système de rétroaction qui permet des séries de chargement contrôlées par la force. Un total de 8 essais a été effectué. Dans tous les tests, le pieu a été chargé avec 500 cycles contrôlés par la force et une accumulation de la rotation a pu être notée pour toute la série de tests.

Keywords: Foundations, monopiles, centrifuge testing, sand, load-amplitude effects

[1] Corresponding Author.

1 INTRODUCTION

Monopiles are today one of the most popular foundation methods for offshore wind turbines. The monopile is a single large diameter tubular steel pile driven 5 to 6 times the diameter into the seabed. The water depth for installation of wind turbines is increasing. The design methodology for monopiles therefore needs a reformulation if the monopile concept shall succeed into deeper waters. Monopiles for wind turbines are affected by lateral loads from waves and winds which subject the pile at seabed with shear forces and corresponding moments due to the load eccentricity. The design for these loads is today done by model the pile as a beam and the soil as a system of uncoupled non-linear springs. From this e.g. rotation of the monopile can be calculated. This method has successfully been used in pile design for offshore oil and gas platforms. The design methodology originates from tests on long slender piles, [1] & [2]. In the case of monopile foundation for wind turbines the relationship proposed by [3], showed in equation 1, is often used. Even though these curves were originally calibrated to slender piles, they are still used for design of large diameter monopiles with a slenderness ratio L/D as low as 5. With a slenderness ratio of 5 the monopile for wind turbine foundation acts as a stiff pile. Therefore it is relevant to investigate the behaviour of stiff piles in more detail. The tests series presented in this paper are a part of a program that intends to investigate the response of monopiles subjected to cyclic loads.

2 SCOPE OF WORK

The loading condition for a monopile for offshore wind turbines is dominated by environmental loads from waves and wind. These loads act on the monopile in a cyclic manner with a variation in amplitude as well as orientation. This study investigates the effect from load orientation and amplitude. For the design of a monopile foundation for wind turbines, three issues are important; the accumulation of rotation, the change in secant stiffness and the damping in the soil. Here we will focus on the accumulation of the rotation.

3 DESIGN METHODOLOGY

The design method for sand presented here [3] is based on the formulation proposed by [4]. As described, the pile is modelled as a beam and the soil is modelled as non-linear springs. The formulation of the spring also known as the p-y relationship is typically for sand approximated by

$$p = A \cdot p_u \cdot tanh\left[\frac{k \cdot z}{A \cdot p_u} y\right] \tag{1}$$

The value k represents the initial subgrade reaction modulus and z is the distance to soil surface. p_u is the ultimate soil resistance as determined by plasticity theory. A is an empirical constant which is used to fit the test results with theory. For static loading $A = (3.0\text{-}0.8X/ D) \geq 0.9$. For cyclic loading $A = 0.9$. The non-linear system is typically defined and solved using an FE program.

4 EXPERIMENTS

The centrifuge test program was performed with a solid steel pile. The pile was made of a 24 mm steel core with a 2 mm epoxy coating leading to a total diameter of d = 28 mm. The load eccentricity e and the penetration depth of the pile was also kept constant as e = 15d and L = 6d. The response of the pile is influenced by load eccentricity and penetration depth which was shown in [5]. Therefore a load setup which applies the load in a way similar to a wind turbine foundation is used. A more detail description of the test setup is given in [6]. A sketch of the pile with definitions is shown in figure 1.The centrifuge is used to increase the gravity so soil stresses corresponds to a pile with a diameter of 2 meters. Scaling laws for the test are quite standard, see e.g. [7].

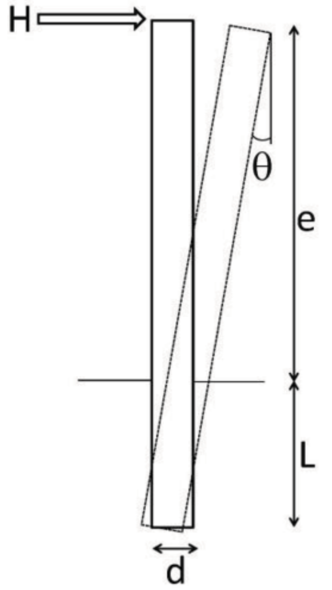

Figure 1. Sketch of pile

The static and all cyclic tests were performed in dry Fontainebleau sand. The classification parameters shown in Table 1 are taken from [7].

Table 1. Classification parameters for the Fontainebleau sand

Specific gravity of particles, G_s	2.646
Minimum void ratio, e_{min}	0.548
Maximum void ratio, e_{max}	0.859
Average grain size, d_{50}, in mm	0.18
Coefficient of uniformity, C_u	1,6

The test pile has a diameter of 22 mm. This leads to a "model diameter/grain size diameter" ratio of 22/0.18 = 122. This ratio should be large enough to avoid particle size effects when applying the artificial gravity field according to the observations described in [8].

A spot pouring hopper was used for the preparation of the sand sample. After the sand is prepared, the pile is installed at 1 g. Only one test is carried out per soil sample.

A set of non-dimensional parameters are used to describe the applied cyclic loads. This approach is similar to the one chosen by [9].

$$\zeta_b = \frac{H_{max}}{H_{mon}} \quad , \quad \zeta_c = \frac{H_{min}}{H_{max}} \qquad (2)$$

Here, H_{mon} is the maximum bearing capacity found from a monotonic test, H_{min} is the minimum force in cyclic loading and H_{max} is the maximum force in cyclic loading. The value ζ_b is thus a measure of how close the cyclic loading is to the maximum bearing capacity, and ζ_c is defining the characteristic of the cyclic loading. From these non-dimensional parameters a test program was designed. The procedure for the test program was to start with a monotonic test (T1). From this test the maximum bearing capacity was found. Then four cyclic tests were performed changing ζ_c, the load orientation (T2-T5). From these four tests the most critical load orientation was found and used for the last four cyclic tests (T3, T6-T8). In this test series the effect of load amplitude is investigated by changing ζ_b. A total number of eight centrifuge tests were carried out - one monotonic and 7 cyclic. All cyclic tests were carried out with 500 cycles except one of the test which was performed with 1000 cycles (T7).

4.1 *Installation of piles*

After the sand is prepared the piles are jacked into the soil at 1g. Figure 2 shows the jacking force measured during installation. It can be seen that the sand samples are homogeneous and that deviation can be attributed mainly to the variation in void ratio. From this it is concluded that the soil samples for all the performed tests can be assumed identical. The installation data of T6 was not recorded - the relative density for this test was found to I_D=0.84.

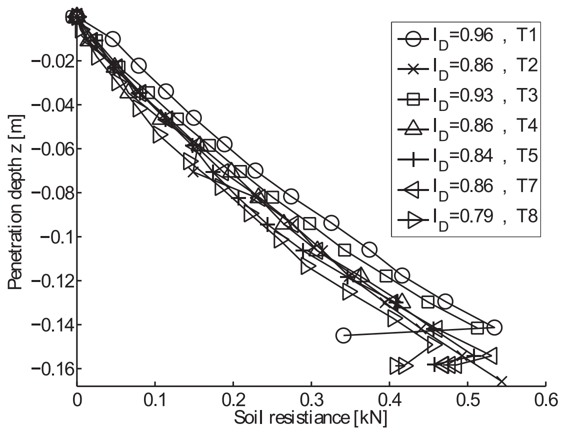

Figure 2. Monotonic test results.

4.2 *Monotonic test*

The monotonic test (T1) was performed as a deformation controlled test where the pile was moved at a constant rate until a displacement of one diameter at sand surface was reached. The displacement, the applied force and the rotation were recorded. In Figure 3 the result from the monotonic load test can be seen. Here the rotation of the pile top is plotted against the applied force. As it can be seen from the figure no maximum capacity is reached. Therefore a rotation criterion was used for define the failure.

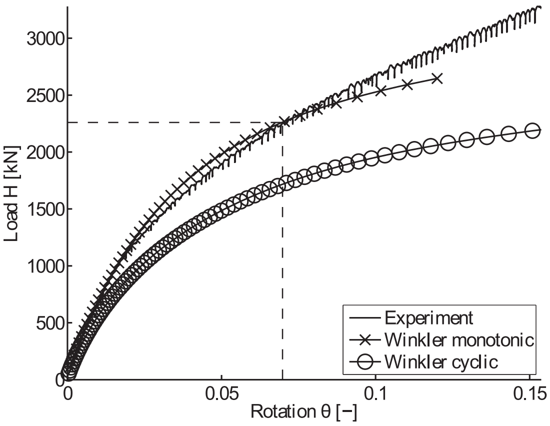

Figure 3. Monotonic test results.

The failure is defined at a rotation of 4 degrees = 0.0698 rad. The maximum prototype load is thus found to be H_{mon}=2295 kN. The Winkler model is here fitted to the monotonic test and shows therefore a good agreement with the experiments. For comparison, the load-displacement curve for cyclic loading is also shown at figure 3. Note that the design methodology leads to a general reduction in capacity of stiffness, but does not take load orientation, load level and number of cycles into account for cyclic loading.

4.3 Cyclic tests

With the maximum capacity found from the monotonic test, the values for the cyclic testing can be determined. The cyclic loading is carried out using a feedback control system. A sinusoidal signal is generated according to the non-dimensional parameters wanted. Due to the feedback control system it is not always that the pile response is exactly as wanted. This can lead to difference between the measured non-dimensional parameters and the planned.

In figure 4 an example of a cyclic test series is shown. A small difference in maximum and minimum values can be seen. This is due to difficulties in the feedback control. From a test like this maxima and minima from every cycle can be found.

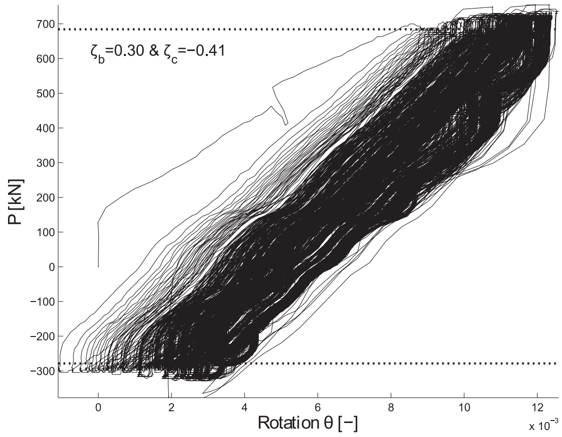

Figure 4. Load deflection result for cyclic test T3.

When the extremes are found, deflection, rotation, damping and secant stiffness from every cycle can be determined. Figure 5 shows the maximum rotation from every cycle of test T3. The accumulation of rotation may be fitted to a power function, see equation (3). This corresponds with observations done in [10].

$$\frac{\theta_{max,N}}{\theta_{max,1}} = N^{\alpha} \tag{3}$$

Some scatter in the data can be seen, but the power function seems to capture the accumulation of rotation quite well, see Figure 5. This is the case for all the cyclic tests performed in this test series.

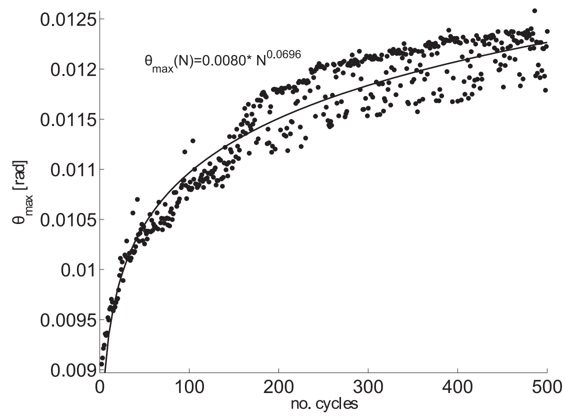

Figure 5. Maximum rotation from every cycle, test T3

From Figure 5, it can be seen that an asymptotic value of the rotation is not reached. Even for test number T7 with 1000 identical cycles it was not possible to assess that an asymptotic value was reached. Hence, tests with an even larger number of cycles should be carried out in order to get a more reliable estimate on the accumulation law.

4.3.1 Load orientation, ζ_c

To investigate the load orientation, four cyclic tests was performed. Recently, [9] reported that a ζ_c value of -0.6 was the most critical one, based on tests carried out as 1g test.

Table 3. Centrifuge test program, N = number of cycles

ζ_c	ζ_b	N	α	Test nr.
-0.84	0.28	500	0.0154	T2
-0.41	0.30	500	0.0696	T3
0.17	0.30	500	0.0307	T4
0.55	0.30	500	0.0227	T5

To investigate this, four tests were performed, with the non-dimensional cyclic parameters as listed in Table 3. ζ_b is more or less kept constant and the influence from changing ζ_c can therefore be seen.

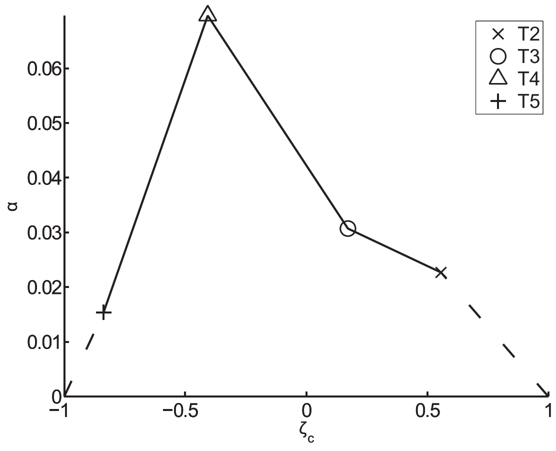

Figure 7. Load orientation effects from cyclic tests.

The results from the power fit of the first four cyclic tests can be seen in Table 3 and Figure 7. It confirms the observation made by [9]. A cyclic load situation between one-way and two loading results in larger accumulation of rotation compared with pure one-way loading. It was therefore chosen to continue the cyclic testing with a ζ_c=-0.4.

4.3.2 Load amplitude, ζ_b

Having identified the most critical load orientation, the effect from the load amplitude was investigated. The non-dimensional cyclic parameters and the results from the four tests can be seen in Table 4.

Table 4. Centrifuge test program, N = number of cycles

ζ_c	ζ_b	N	α	Test nr.
-0.36	0.08	500	0.0132	T6
-0.31	0.20	500	0.0406	T7
-0.41	0.30	500	0.0696	T3
-0.46	0.38	500	0.1148	T8

It is clear that an increase in amplitude leads to an increase in accumulation of rotation. Even though it has not been possible to keep ζ_c constant for the four tests, it is seen in Figure 8 that the deviation does not seem to affect the result. A power function seems to be a good approximation. This deviates with the 1g experiments from [9], where a linear relationship is reported. The power function furthermore ensures that no accumulations occur for a ζ_b=0 which seems more appropriate.
The power function can be written as:

$$\alpha(\zeta_b, \zeta_c) = A \cdot \zeta_b{}^{B(\zeta_c)} \tag{4}$$

A and B was found to A=0.4 and $B_{\zeta c=-0.41}$=1.37. The value A is independent of the load orientation and amplitude.

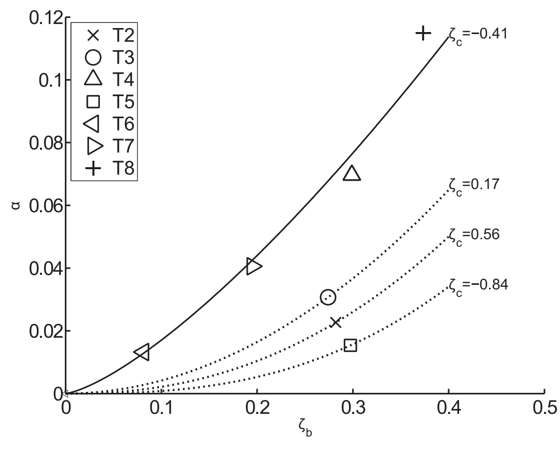

Figure 8. Rotational accumulation parameter.

The value B can be found and calculated from Figure 7 in the following way.

First the α-value for a given load orientation is found using Figure 7. This value is used in Equation 5 with the A value found from the test on load amplitude effects.

$$B(\zeta_c) = \frac{ln\left(\frac{\alpha(\zeta_c)}{0.4}\right)}{\ln(0.3)} \tag{5}$$

When B is found, Equation 4 can be used to determine the rotational accumulation parameter α, for the given load situation.

5 EXAMPLE

The maximum rotation is wanted for a 2 m in diameter monopile. The cyclic loading is pure one-way loading (ζ_c=0) and has and amplitude of 25% of the maximum bearing capacity (ζ_b=0.25). The pile is subjected to 10^7 cycles which is the fatigue limit state. The maximum bearing capacity was found to be H=2295 kN, giving H_{max} = 2295 · 0.25 = 574 kN. The maximum rotation for this load for the first cycle can then be found from Figure 3 as: $\theta_{max,1} = 0.008$. From Figure 7, the rotational accumulation parameter α for ζ_c=0 can be found to α=0.04. This is used in Equation 5, and the B value is found to:

$$B = \frac{ln\left(\frac{0.04}{0.4}\right)}{\ln(0.3)} = 2.9 \tag{5}$$

The rotational accumulation parameter α, for the given load situation (ζ_b=0.25) can then be calculated by Equation 4:

$$\alpha = 0.4 \cdot 0.25^{2.9} = 0.007 \tag{6}$$

The maximum rotation for the monopile subjected to 10^7 cycles can then be found using equation 3 to:

$$\theta_{max} = 0.008 \cdot (10^7)^{0.007} = 0.009\, rad \tag{7}$$

6 CONCLUSIONS

A series of cyclic centrifuge tests was carried out at the geotechnical centrifuge at DTU. One of the key issues for the design of a monopile for wind turbine was investigated. It was clearly seen that the accumulation of rotation is highly affected by the characteristic of the cyclic loading, and by the load amplitude. A design procedure for monopile with a diameter of 2 m has been given and can be applied for any load amplitude, orientation and number of cycles. This is not the case for the current design methodology.

All the cyclic tests do not reach a steady state and it can therefore be concluded that 500 cycles is not enough. This should therefore be increased in further cyclic centrifuge tests.

REFERENCES

[1] L. C. Reese & H. Matlock, Dimensional Solutions for Laterally Loaded Piles with Soil Pile Modulus Assumed Proportional to depth, Proceedings of the 8th Conference on Soil Mechanics (1956), 1-41

[2] B. McClelland & J. A. Focht, Soil modulus for laterally loaded piles, Journal of the soil mechanics and foundation division – Proceedings of the American Society of Civil Engineers (1958), 1-22

[3] API RP 2A-WSD, Recommended Practice for Planning, Designing and Constructing Fixed Offshore Platforms - Working Stress Design (2000)

[4] J. M. Murchison & M. W. O'Neill, Soil modulus for laterally loaded piles in sand, Journal of Geotechnical Engineering Vol.120 (1984), 174-191

[5] R. T. Klinkvort C. T Leth & O. Hededal, Centrifuge modeling of a laterally cyclic loaded pile, International Conference on Physical Modelling in Geotechnics - 7th, (2010), 959-964

[6] R. T. Klinkvort, Centrifuge modelling of monopiles, Geotechnical Engineering 20, View of Young European Geotechnical Engineers (2010)

[7] C. T Leth, A. Krogsbøll & O. Hededal, Centrifuge facilities at Danish Technical University, 15th Nordic Geotechnical Meeting (2008)

[8] J. Garnier et al., Catalogue of scaling laws and similitude questions in centrifuge modelling, International Journal of Physical Modelling in Geotechnics Vol 7 III (2007)

[9] C. Leblanc, G. T. Houlsby & B. W. Byrne, Response of stiff piles in sand to long-term cyclic lateral loading, Géotechnique 60 no 2 (2010), 79-90

[10] R. T. Klinkvort & O. Hededal, Centrifuge modelling of offshore monopile foundation, Frontiers in Offshore Geotechnics II (2010), 581-586

Paper VI

"Lateral response of monopile supporting an offshore wind turbine"

R. T. Klinkvort & O. Hededal

Submitted for publication -, *2012*

Lateral response of monopile supporting an offshore wind turbine.

Rasmus Tofte Klinkvort[1] and Ole Hededal[2]

1) Ph.D. research student, Dept. of Civil Engineering, Technical University of Denmark, Sec. of Geotechnics and Geology, Brovej Building 118, 2800 Kgs. Lyngby, Denmark. Phone: (+45) 25 38 78 13, rakli@byg.dtu.dk.

2) Associate Professor, Dept. of Civil Engineering, Technical University of Denmark, Sec. of Geotechnics and Geology, Brovej Building 118, 2800 Kgs. Lyngby, Denmark. Phone: (+45) 45 25 50 20, olh@byg.dtu.dk.

Date written: Monday, June 25, 2012

Date revised: -

Number of words: 4455

Number of pages: 21

Number of figures: 10

Number of tables: 2

Abstract

One of the geotechnical challenges for a monopile supported offshore wind turbine is to create a foundation design procedure that incorporates the effects of cyclic loading from wind and waves in a safe and easy way. Improved procedures may enable the use of monopiles on deeper waters, securing still a robust and cost beneficial foundation design. In order to develop new design procedures it is essential to understand the pile-soil interaction. With centrifuge tests as the basis, this paper discusses the effects of the soil-pile interaction with the focus on accumulation of displacements and change in secant stiffness in dense sand. Hence, a centrifuge test series simulating idealised cyclic load on a monopile supporting an offshore wind turbine was carried out. The validity of these centrifuge tests is discussed and a simple design procedure for the prediction of the accumulation of displacements and change in secant stiffness based on the results from the centrifuge tests is presented.

Keywords: Renewable energy, Offshore engineering, Geotechnical engineering

Notations

d:	Diameter of pile
l_e:	Load eccentricity
l_L:	Pile penetration depth
φ'_{max}:	Maximum angle of friction
φ'_{cr}:	Critical state angle of friction
I_D:	Relative density
p':	Mean pressure
η :	Gravity scaling factor
N_s:	Geometrical scaling factor
Y :	Pile displacement
$\tilde{Y}$:	Normalised pile displacement
H :	Applied lateral load
$\tilde{P}$:	Normalised applied load
$\tilde{K}$:	Normalised secant stiffness
ζ_b, ζ_c :	Load characteristic parameters
N :	Number of cycles
α, κ :	Evolution parameter
T_b, T_c :	Dimensionless functions
κ_b, κ_c :	Dimensionless parameters
$\tilde{K}_s, \tilde{K}_c$:	Dimensionless parameters

INTRODUCTION

Today one of the most common foundation methods for offshore wind turbines is the monopile. The monopile is a single, large diameter tubular steel pile with a diameter of 4-6 meters, driven to a depth 5-6 times the diameter into the seabed. Wind turbines are affected by lateral cyclic loads from waves and winds, which at seabed subject the pile to shear forces and bending moments. The combined loads on the wind turbine have to be supported by the foundation, (Byrne, Houlsby 2003).

The pile design for the lateral loads is today normally based on a Winkler model where the pile is modelled as a beam and the soil as a system of uncoupled non-linear springs, e.g. (API 2007). From this, one overall displacement and stiffness of the monopile can be calculated. This procedure neither takes the number of cycles nor the characteristics and the magnitude of the cyclic loading into account. The design methodology originates from tests on long slender piles with a few number of cycles, (Reese, Matlock 1956) & (McClelland, Focht 1956). Even though calibrated to slender piles, the method is – without modifications – applied in the design of large diameter monopiles. Furthermore, since the dynamic response of the integrated structure - turbine, tower and foundation – is sensitive to stiffness and displacements of the soil pile system, it is important to take such variation into account in the design.

Several studies on the cyclic response of laterally loaded piles have been reported (Briaud, Smith & Meyer 1983), (Long, Vanneste 1994) & (Lin, Liao 1999) . Still, the number of investigations is limited and the majority of studies have been carried out on long slender piles. The performance of monopiles subjected to cyclic loading was investigated by (LeBlanc, Houlsby & Byrne 2010) in a series of 1g model tests. They found that the evolution of rotation and stiffness depends on the number of cycles, as well as on the magnitude and the characteristic of the load cycles. With these findings in mind, this paper propose a model which can be used to determine displacement and stiffness depending on the number of cycles, the magnitude and the characteristic of the load cycles. The model is based on a set of centrifuge tests.

MODEL FRAMEWORK

The cyclic response of a pile can be described in terms of pile head displacement, Y, and the applied lateral load of the pile, H. Normalising these parameters enables comparison of results across scale. Here it is chosen to normalise with the diameter of the pile and the effective density γ'.

$$\tilde{Y} = \frac{Y}{d} \qquad \& \qquad \tilde{P} = \frac{H}{\gamma' \cdot d^3}$$

Equation 1

A schematic response of a pile for constant amplitude cyclic loading is shown in Figure 1. In each load cycle the maximum and minimum value of the load ($\tilde{P}_{\max,N}$, $\tilde{P}_{\min,N}$) and the displacement ($\tilde{Y}_{\max,N}$, $\tilde{Y}_{\min,N}$) can be obtained. The maximum displacement and the cyclic secant stiffness from each cycle can therefore be determined. The maximum displacement is found as the displacement when the load is at the maximum of each cycle and the cyclic secant stiffness is found as the slope of a straight line between the extremes for every cycle, see Figure 1.

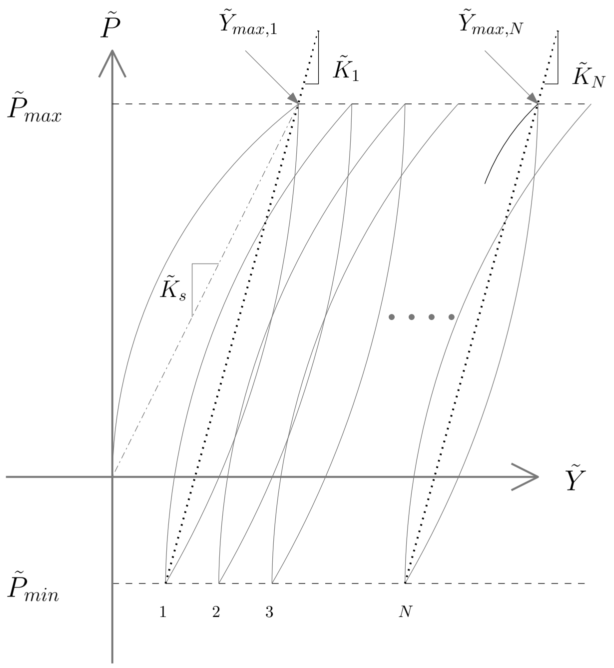

Figure 1 Schematic drawing of determination of secant stiffness and maximum accumulated displacement.

Having determined the bearing capacity of the pile from a monotonic test, ($\tilde{P}_{mon}$), the cyclic loading can be described by two non-dimensional parameters.

$$\zeta_b = \frac{\tilde{P}_{\max}}{\tilde{P}_{mon}} \qquad \zeta_c = \frac{\tilde{P}_{\min}}{\tilde{P}_{\max}}$$

Equation 2

The value ζ_b defines the load amplitude relative to the maximum bearing capacity, $\tilde{P}_{mon}$, and ζ_c defines the characteristic of the cyclic loading.

Evolution models

Having cyclic loading described by the parameters (ζ_b, ζ_c), the maximum displacement from the number of cycle (*N*) may be determined from a power function,

$$\tilde{Y}_{\max,N} = \tilde{Y}_{\max,1} \cdot N^{\alpha}$$

Equation 3

The coefficient, α, is dependent both on the load characteristic described by ζ_c and the magnitude of the loading described by ζ_b. Assuming the two effects to be independent, the value of α can be calculated as a product of two non-dimensional functions.

$$\alpha(\zeta_c, \zeta_b) = T_c(\zeta_c) \cdot T_b(\zeta_b)$$

Equation 4

The first function, T_c, depends on the load characteristic, ζ_c, and the second function, T_b, depends on the load magnitude, ζ_b.

The cyclic secant stiffness in every cycle is described by a logarithmic function;

$$\tilde{K}_N = \tilde{K}_1 \left(1 + \kappa \cdot \ln(N)\right)$$

Equation 5

In Equation 5, κ is the accumulation rate, $\tilde{K}_1$ is the cyclic secant stiffness for the first cycle and $\tilde{K}_N$ is the cyclic secant stiffness for cycle number N.

As for the accumulation of displacements, it is chosen to describe the value of κ by two independent non-dimensional functions.

$$\kappa\left(\zeta_c,\zeta_b\right)=\kappa_c(\zeta_c)\cdot\kappa_b(\zeta_b)$$

Equation 6

The non-dimensional cyclic secant at the first cycle, $\tilde{K}_1$, is found using the secant stiffness of the monotonic response.

$$\tilde{K}_s(\zeta_b) = \frac{\tilde{P}_{\max}}{\tilde{Y}_{\max}}$$

Equation 7

This value is appropriately scaled by $\tilde{K}_c(\zeta_c)$ which depends on the cyclic load characteristic, i.e.

$$\tilde{K}_1\left(\zeta_c,\zeta_b\right)=\tilde{K}_c(\zeta_c)\cdot\tilde{K}_s(\zeta_b)$$

Equation 8

The input to the two evolution models can be established from a monotonic test combined with the non-dimensional functions, $(T_c(\zeta_c),T_b(\zeta_b)$, $\kappa_c(\zeta_c),\kappa_b(\zeta_b)$ and $\tilde{K}_c(\zeta_c),\tilde{K}_s(\zeta_b))$. These functions can be empirically determined by a series of cyclic load tests.

METHOD

To determine the non-dimensional function used in the prediction model a centrifuge test series is designed. A model pile subject to idealized load cycles representing a monopile supporting an offshore wind turbine is used. In order to model the response correctly, it is important to design a load setup, which applies the load in a way similar to a wind turbine foundation, (Klinkvort, Leth & Hededal 2010). Here, the combined cyclic loads acting on a wind turbine is simplified to a single total force resultant acting between sea level and nacelle height, see Figure 2.

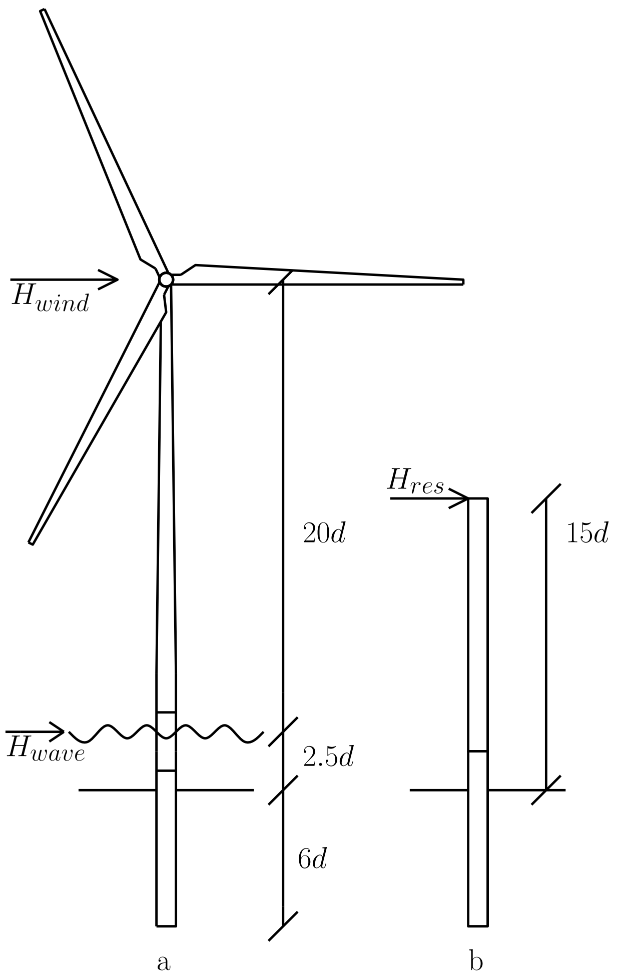

Figure 2 Non-dimensional drawing of offshore wind turbine and centrifuge model pile

A sketch of the centrifuge pile setup is shown in Figure 3. A circular barrel with an inner diameter d_b=500mm is used. The soil sample consists of a homogenous dense sand layer with a height of h_b=388mm. The cyclic tests series was performed with two different solid steel piles. The piles are made of respectively 24 and 36 mm steel core with a 2 mm epoxy coating leading to a total diameter of d = 28 mm and d = 40 mm. The load eccentricity and the penetration depth of the piles were kept constant, $l_e = 15d$ and $l_L = 6d$ for the all tests. The load is measured at pile head and lateral displacements are measured 2d above sand surface.

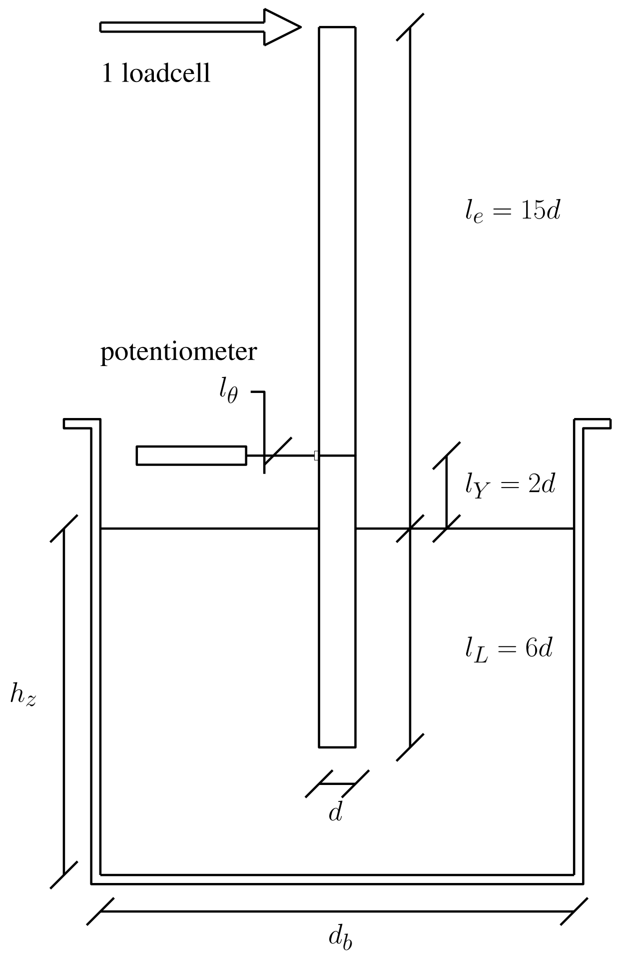

Figure 3 Sketch of the centrifuge setup

The sand was prepared in the centrifuge container by dry pluvation using a single spot hopper. An average relative density is calculated from the weight of the sand sample. The saturated tests samples were flooded from below with de-aired water after pluvation. All centrifuge tests were performed in dense Fontainebleau sand with a relative density of approximate 90 %. The triaxial results showed a maximum angle of friction corresponding with the observations done by (Bolton 1986) using a critical state angle of $\varphi'_{cr}=30^{o}$. The classification and triaxial parameters are shown in Table 1, (Leth, Krogsbøll & Hededal 2008).

The pile was installed by jacking. All d = 28 mm piles were installed at 1g while all d = 40 mm piles were installed at an elevated g-level in order to minimize installation effects. Installation at full stress level is preferable, but a 20 kN limit on the jack precluded full in-flight installation. The procedure for the test sequence was to spin the centrifuge up; install the pile and then stop the centrifuge.

Table 1 Classification and triaxial parameters for the Fontainebleau sand

Specific gravity of particles, G_s	2.646
Minimum void ratio, e_{min}	0.548
Maximum void ratio, e_{max}	0.859
Average grain size, d_{50}, mm	0.18
Coefficient of uniformity, C_u	1,6
d/d_{50}	156-222
$\varphi'_{max} \approx \varphi'_{cr} + 3\left(I_D\left(10 - ln(p')\right) - 1\right)$	

After the pile was installed the jack was removed and the lateral loading equipment was placed. Finally the centrifuge was accelerated to the prescribed g-level, and the load tests were performed.

The centrifuge is used to increase the effective density of the soil corresponding to a offshore prototype pile with a diameter of approximately 3 meters. The centrifuge technique can be seen e.g. (Schofield 1980) & (Garnier et al. 2007). The increase in g-field, η and the geometrical scaling factor, N_s does not have to be the same if no excess pore pressure is generated, (Li, Haigh & Bolton 2010). To verify the effective stress scaling approach, four monotonic tests were performed, two in saturated sand and two in dry sand, with effective stress levels corresponding to a prototype pile with a diameter of respectively 1 and 3 meters. As seen in Figure 4, there is practical no differences between the responses of a pile in saturated and dry sand. This validates the scaling approach as long as fully drained conditions are maintained during loading.

Results

Five monotonic and twelve cyclic tests have been performed, see Table 2;. The monotonic tests were used as validation of the scaling approach and as a reference for the cyclic tests. First seven cyclic tests on the d=28 mm pile in dry sand was performed. From these test, the non-dimensional functions was established. This was done by first changing the load amplitude of the cyclic loading (ζ_b), while keeping the characteristic of the cyclic loading (ζ_c) constant. Afterwards the effect of the characteristic of the cyclic loading was investigated by changing ζ_c while keeping ζ_b constant. Later, two tests on a *d*=40 mm pile were performed to see the influence of number of cycles and three tests were used to see the influence from performing cyclic test in saturated sand. Although tests were performed on different sized piles and in dry or saturated conditions, the non-dimensional functions determined from the first 7 tests proved representative for the entire test series.

Monotonic test

All monotonic tests were performed with deformation controlled loading of the pile with a constant rate of one diameter per minute. This was so slow that fully drained loading conditions were ensured, as seen in Figure 4.

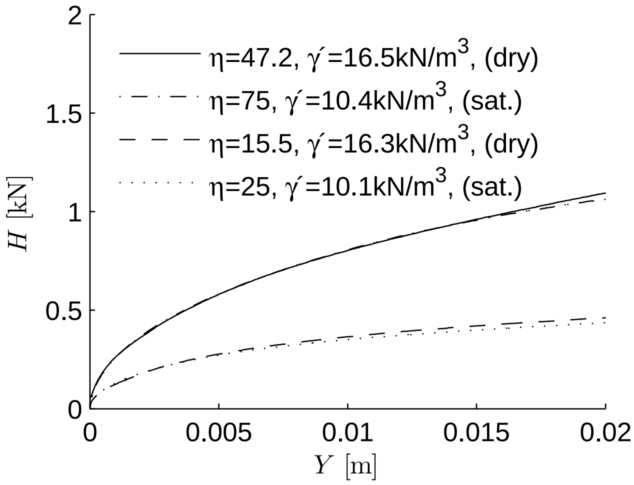

Figure 4 Validation of scaling approach, d=40mm

In Figure 5 the result from the monotonic load tests can be seen. Here the normalised displacement of the pile is plotted against the applied normalised force. The two monotonic tests performed on the model pile with a diameter of d = 40 mm show identical results. The pile with a diameter of d = 28 mm shows initially the same response as the two other piles, but the response starts to deviate from a pile head displacement above 0.05 d. A reason for the deviation could be that the d = 28 mm piles is installed at 1g, whereas the d = 40 m piles are installed at an elevated stress field. As demonstrated by (Dyson, Randolph 2001) 1g installation leads to a softer response.

It can be seen from Figure 5 that the ultimate capacity was not reached for any of the tests. Therefore a rotation criterion was used to define the reference bearing capacity, $\tilde{P}_{mon}$. Failure was defined at a rotation of 4 degrees for the piles with a diameter of d = 40 mm. The maximum normalised force was found to be

$\tilde{P}_{mon} = 19$. This is shown in Figure 5 as a dotted line. At load level less than $0.4\,\tilde{P}_{mon}$, the monotonic response from the three tests is identical. Since all cyclic tests were performed below this level. it is chosen to use the results from the different pile diameter to calibrate the model.

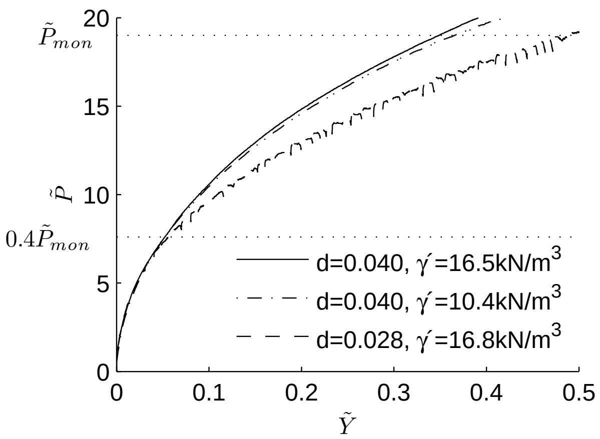

Figure 5 Normalised monotonic test results

Calibration of model

The cyclic tests series consist of 12 tests performed with a setup which subjects the piles with load controlled cycles with a period of 10 sec. The tests were designed so the cyclic loading of the pile was performed with a magnitude comparable to the serviceability load of an offshore wind turbine, according to (LeBlanc, Houlsby & Byrne 2010).

Evolution of deflection

The accumulation of displacement may be described by a power function. The maximum deflection for all cycles plotted together with the power fit is shown in Figure 6. It can be seen that the power fit captures the accumulation of displacement well. The results together with the non-dimensional cyclic load characteristics can be seen in Table 2.

Table 2 Test program

Test nr.	Type	Diameter [mm]	Saturated	I_D	ζ_c	ζ_b	*no. of cycles*	α	$\tilde{K}_0$	κ
1	Monotonic	28	No	0.88	1	1	-	-	-	-
2	Monotonic	40	No	0.94	1	1	-	-	-	-
3	Monotonic	40	Yes	0.96	1	1	-	-	-	-
4	Monotonic	40	No	0.83	1	1	-	-	-	-
5	Monotonic	40	Yes	0.80	1	1	-	-	-	-
6	Cyclic	28	No	0.86	0.54	0.27	500	0.068	1185	-0.017
7	Cyclic	28	No	0.93	0.16	0.25	500	0.097	881	-0.021
8	Cyclic	28	No	0.86	-0.41	0.29	500	0.117	486	0.10
9	Cyclic	28	No	0.84	-0.84	0.28	500	-0.115	304	0.27
10	Cyclic	28	No	0.84	-0.37	0.08	500	0.032	1618	0.09
11	Cyclic	28	No	0.86	-0.32	0.18	1000	0.077	557	0.06
12	Cyclic	28	No	0.79	-0.46	0.36	500	0.088	360	0.13
13	Cyclic	40	No	0.93	-0.50	0.33	10000	0.089	332	0.16
14	Cyclic	40	No	0.94	-0.96	0.34	3000	-0.349	193	0.29
15	Cyclic	40	Yes	0.96	-0.39	0.36	250	0.137	309	0.14
16	Cyclic	40	Yes	0.87	-0.47	0.36	250	0.126	424	0.07
17	Cyclic	40	Yes	0.95	0.05	0.15	300	0.087	968	-0.023

The value of α can be calculated using two non-dimensional cyclic functions as shown in Equation 4. By normalising $T_c = 1$ for pure one-way loading, $\zeta_c = 0$, the non-dimensional function T_b can be found from a series of test where ζ_b is changed while $\zeta_c = 0$.

$$\alpha\left(\zeta_c = 0, \zeta_b\right) = 1 \cdot T_b(\zeta_b)$$

Equation 9

When T_b is created the function T_c may be found by performing a series of test with a constant ζ_b and then dividing the results with the T_b function, i.e.

$$T_c(\zeta_c) = \frac{\alpha}{T_b(\zeta_b)}$$

Equation 10

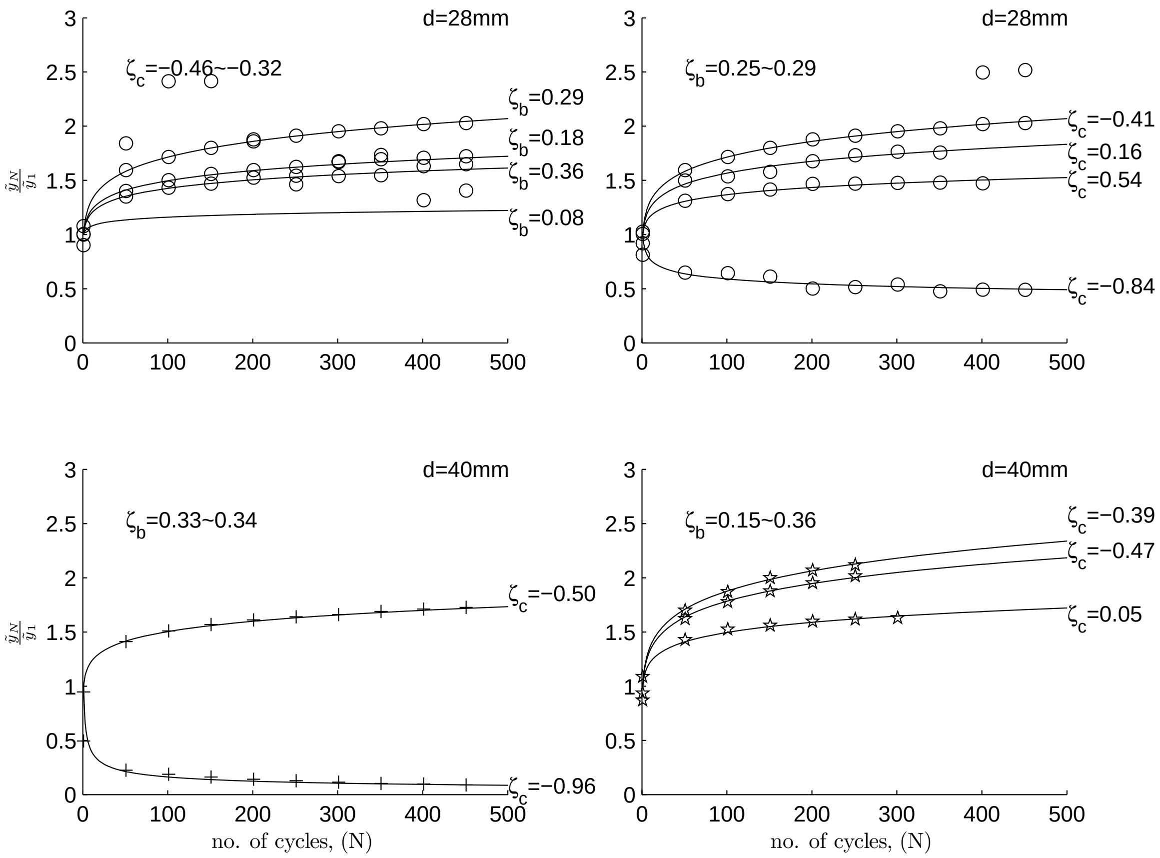

Figure 6 Accumulation of displacement from cyclic tests

The result of this analysis can be seen in Figure 7. It was chosen to force the values of T_b to be a straight line and then to plot the corresponding value of T_c. The linear dependency of the load magnitude can be seen in Equation 11.

$$T_b(\zeta_b) = 0.61\zeta_b - 0.013$$

Equation 11

The function T_b cannot be negative, hence cyclic loading with a small magnitude $\zeta_b \leq 0.02$, will lead to a value $T_b = 0$, implying that the pile-soil interaction is reversible and no accumulation of displacements will occur.

Figure 7 shows results for the cyclic load characteristic function T_c. The results seem to follow a third order polynomial, see Equation 12.

$$T_c(\zeta_c) = (\zeta_c + 0.63)(\zeta_c - 1)(\zeta_c - 1.64)$$

Equation 12

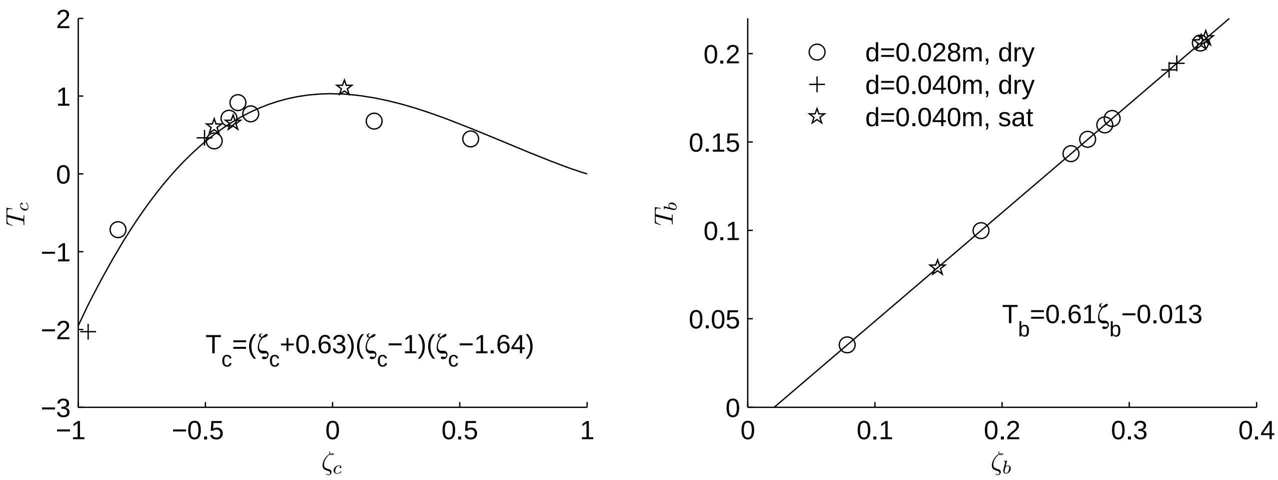

Figure 7 Cyclic dimensionenless functions for accumulation of displacements

The function secures that $\alpha = 0$ for monotonic loading, $\zeta_c = 1$. The maximum value of the function is found $\zeta_c = -0.01$, which means that the most damaging load situation is when the monopile is loaded in a more or less pure one-way loading. When $\zeta_c \leq -0.63$ the function T_c becomes negative, which means that the accumulation of displacement is reversed and the pile moves towards its initial position.

Since both dry and saturated condition have been used in the tests, this shows that all tests are fully drained and the chosen scaling approach seems valid also for quasi static cyclic loading. From the non-dimensional functions we can conclude that the accumulation coefficient, α, is increasing with increasing magnitude of the cyclic loading, and that the most damaging cyclic load orientation is in the interval of $-0.4 \leq \zeta_c \leq 0$.

The displacement for the first cycle is easily found from a monotonic test, and is only depending on the load magnitude. Having the monotonic load-displacement curve together with the non-dimensional functions shown in Equation 11 and Equation 12 thus makes it possible to estimate the displacement to a given number of cycles using Equation 3.

Evolution of secant stiffness

In Figure 8, the secant stiffness is plotted against the number of cycles. It shows that the logarithmic function seems to describe the changes in secant stiffness reasonably. The results of the logarithmic fits can be also been seen in Table 2.

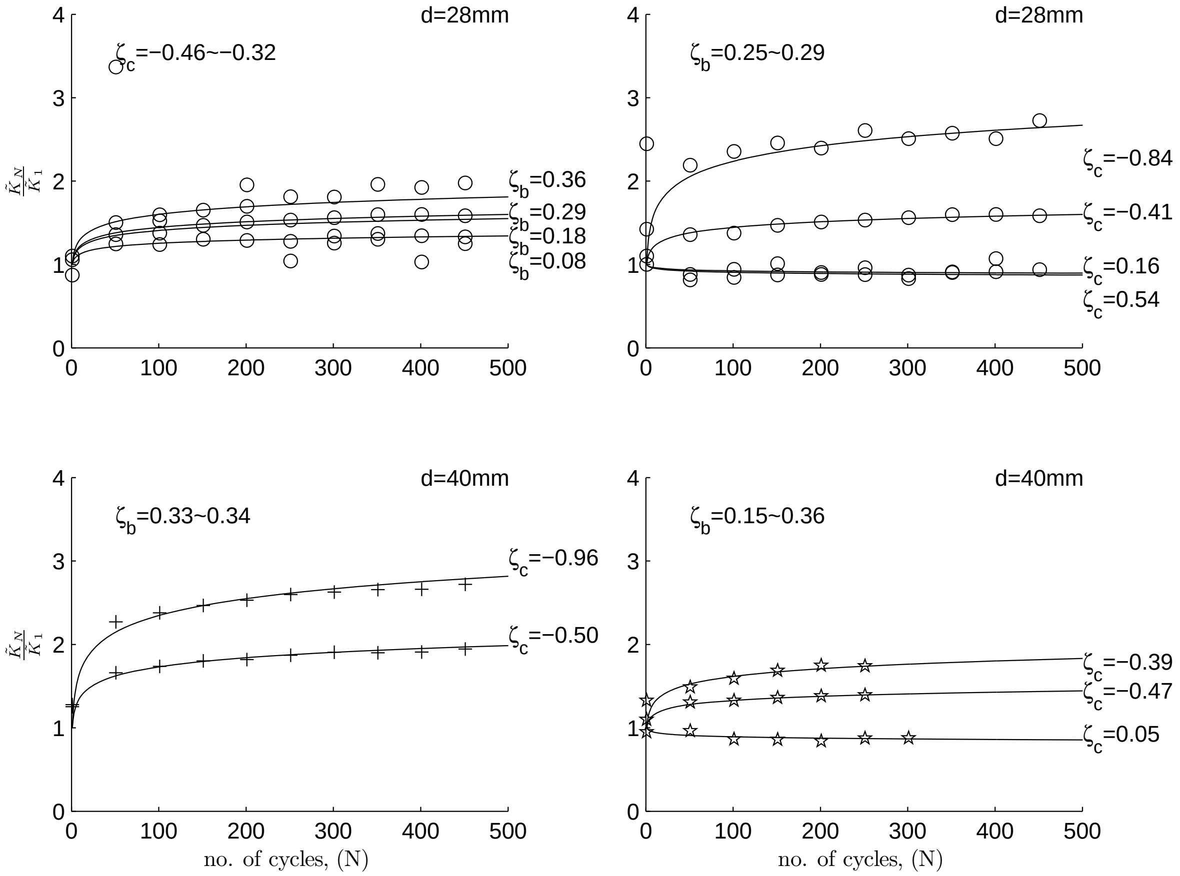

Figure 8 Change in secant stiffness from cyclic tests

The determination of the non-dimensional functions follows the same methodology as described for the displacements. The results are shown in Figure 9.

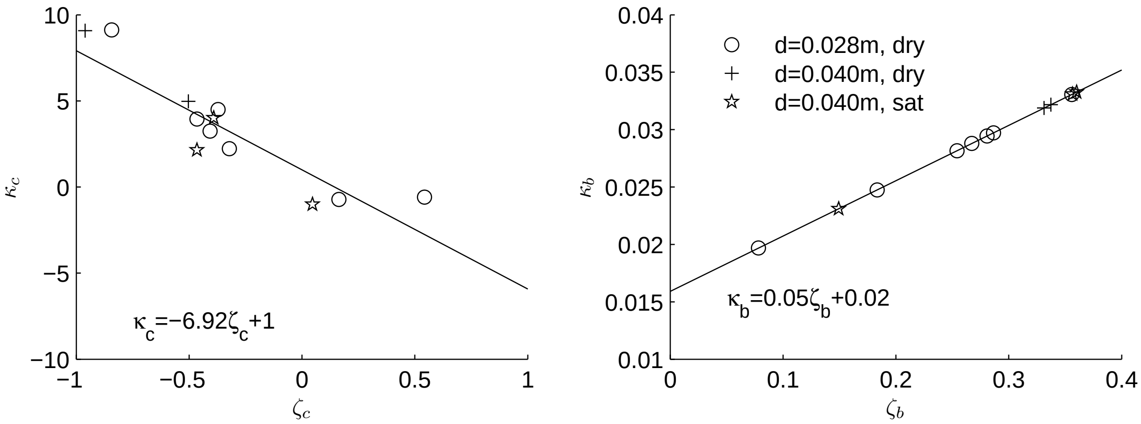

Figure 9 Cyclic dimensionenless functions for change in secant stiffness

A linear dependency of the load magnitude is found;

$$\kappa_b(\zeta_b) = 0.05\zeta_b + 0.02$$

Equation 13

Equation 13 implies that an increase in the cyclic load magnitude leads to an increase in the accumulation secant stiffness accumulation rate, κ . Having determined κ_b , the values of κ_c are plotted and it is seen that a linear fit seems to capture the trend, see Equation 14.

$$\kappa_c(\zeta_c) = -6.92\zeta_c + 1$$

Equation 14

It can be seen that going from one-way to two-way loading will lead to an increasing accumulation of stiffness.

The initial cyclic secant stiffness is found by considering the results of a monotonic test and cyclic tests with varying amplitude. The function $\tilde{K}_s(\zeta_b)$ is established directly from the monotonic load-displacement curve. The function $\tilde{K}_c(\zeta_c)$ is then evaluated from the cyclic tests. The results are shown in Figure 10, and it can be seen that a second order polynomial describe the variation of $\tilde{K}_c(\zeta_c)$,

$$\tilde{K}_c(\zeta_c) = 1.64\zeta_c^{\ 2} + 3.27\zeta_c + 3.27$$

Equation 15

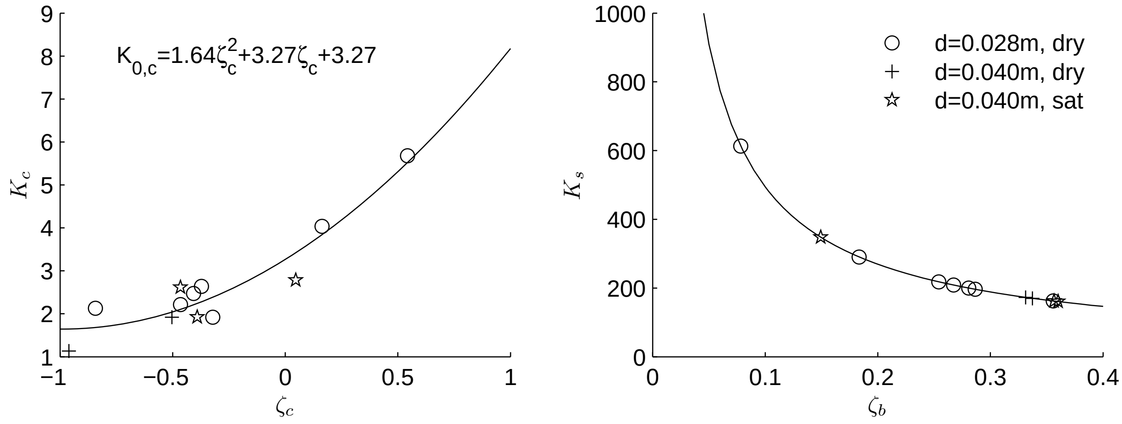

Figure 10 Cyclic dimensionenless functions for initial stiffness

From this equation, it should be recognized that the initial stiffness due to cyclic loading is stiffer than the monotonic stiffness. Depending on the characteristic of the cyclic loading, the initial cyclic secant stiffness may be 2 to 8 times the monotonic secant stiffness.

DISCUSSION

We have proposed a simple framework for the predication of displacements and stiffness from cyclic loading for monopiles supporting offshore wind turbines. This framework was calibrated by a set of centrifuge tests in order to determine a set of non-dimensional functions. The centrifuge tests represent simplifications of the complex wind-water-structure-soil interaction problem and these simplifications are discussed in connection with offshore prototype monopile conditions.

First of all, an offshore monopile is situated in saturated soil conditions. The centrifuge test series was carried out in primarily dry dense sand. Choosing an effective stress scaling approach enables us to model piles situated in saturated conditions using dry sand. This was demonstrated by four monotonic tests. A direct comparison between cyclic tests performed in dry and saturated conditions was not carried out, but looking at the non-dimensional functions derived from testing in dry and saturated condition, no difference is registered. The scaling approach therefore seems valid. It is important to recognize that the results only are valid for drained loading conditions. Testing in water saturated sand does not represent full scale drainage which means that the water flow in the centrifuge setup is occurring N_s times faster compared to the prototype and it is therefore unlikely that pore pressures can build up at the current rate of loading. The possible accumulation of pore pressure has to be studied in more details.

Secondly, monopile diameters for offshore wind turbine foundations are ranging from 4 - 6 meters and are continuously increasing. The cyclic investigation was performed at a stress level corresponding to a d = 3 meter pile. Pilot tests carried out at The Technical University of Denmark indicate that the normalized response for centrifuge monopiles is identical, when the stress field is equal or larger than the stress field for a 3 meter in diameter pile. The reason for this can be recognized using the equation from the maximum angle of friction by (Bolton 1986) shown in Table 1. From this equation it can be seen that the maximum angle of friction at pile tip reduces only from 38^{o} to 37^{o} going from a stress field for 3 meter in diameter pile to 6 meter in diameter pile. It is therefore believed that the results of this tests series also can be used for larger diameters than 3 meters.

At last, the main part of the tests in this study involved 250-500 load cycles. Three tests were performed with more than 500 cycles; one test with 1000 cycles on the d=28mm pile and two tests on the d=40mm pile with respectively 3000 and 10000 numbers of cycles. From these tests it was seen that accumulation of displacement and secant stiffness was well described with the predictions based on the first 500 cycles. It therefore seems reasonable to use the results for up to 10000 cycles. This is still below the number of cycles for the fatigue limit state ($N = 10^7$), but it is an improvement compared to the original design method, (API 2007), which is based on tests with fewer than 50 cycles (Murchison, O'Neill 1984).

We have discussed some of the limitations of our simplified model. In general, the model framework is similar to the one proposed by (LeBlanc, Houlsby & Byrne 2010), but differences between the models are seen. One of the main findings from the 1g experiments was that the most damaging load situation was for two-way loading, i.e. $\zeta_c \approx -0.6$. The present centrifuge test series does not show this trend, instead it indicates that one-way loading, $\zeta_c \approx 0$, is the most damaging one. From the tests by (LeBlanc, Houlsby & Byrne 2010) accumulation of rotation was seen regardless of the characteristic of the loading. This is also in contrast to the observation done in this study, where it was seen that the pile starts to move back against its initial position for pure two-way loading. This observation was also done by (Rosquët 2004) who performed centrifuge tests on long slender piles. One explanation of these disagreements can be the fact that the tests performed by (LeBlanc, Houlsby & Byrne 2010) was carried out in loose sand in order to model the maximum angle of friction correctly. The sand in the 1g experiments thus most likely starts to compact when loaded. Tests performed in a centrifuge model stresses and relative densities correctly, so the dilatant behaviour of sand is therefore better accounted for.

The correct modelling of stresses together with the chosen simplification indicates that the findings from our study are reliable and can be used in the predications of prototype monopiles.

CONCLUSION

The design of monopiles supporting offshore wind turbine is today one of the great geotechnical challenges for renewable energy, if this foundation concept shall succeed to deeper waters. The prediction of accumulation of displacements and change in pile-soil stiffness from cyclic loading are some of the main design drivers and models have to be improved. In order to establish a better design methodology, a series of centrifuge tests was carried out at the Technical University of Denmark. A setup simulating load conditions for an offshore monopile supporting a wind turbine was used to investigate the response.

Two key issues for the design of a monopile for wind turbine were investigated, accumulation of displacements and the change in secant stiffness. It was clearly seen that the accumulation of displacement and secant stiffness is affected by the characteristic of the cyclic loading, and by the load amplitude.

An empirically based design procedure for a monopile installed in dense saturated sand has been given, but should only be used for drained conditions. The design procedure can be applied for any load amplitude, load characteristic and number of cycles. Together with three sets of non-dimensional functions, the procedure only needs a monotonic response in order to an address the accumulation of displacement and the change in stiffness. This gives a very simple design procedure which is superior the given methodology used in the industry today.

REFERENCES

API 2007, "API RP 2A-WSD Recommended practice for planning, designing, and constructing fixed offshore platforms - Working stress design,".

Bolton, M.D. 1986, "Strength and dilatancy of sands", *Geotechnique*, vol. 36, no. 1, pp. 65-78.

Briaud, J., Smith, T.D. & Meyer, B.J. 1983, "USING THE PRESSUREMETER CURVE TO DESIGN LATERALLY LOADED PILES", *Proceedings - Annual Offshore Technology Conference,* vol. 1, pp. 495-502.

Byrne & Houlsby 2003, "Foundations for offshore wind turbines", *Philosophical Transactions of the Royal Society London, Series A (Mathematical, Physical and Engineering Sciences),* vol. 361, no. 1813, pp. 2909-2930.

Dyson, G.J. & Randolph, M.F. 2001, "Monotonic lateral loading of piles in calcareous sand", *Journal of Geotechnical and Geoenvironmental Engineering,* vol. 127, no. 4, pp. 346-352.

Garnier, J., Gaudin, C., Springman, S.M., Culligan, P.J., Goodings, D., Konig, D., Kutter, B., Phillips, R., Randolph, M.F. & Thorel, L. 2007, "Catalogue of scaling laws and similitude questions in geotechnical centrifuge modelling", *International Journal of Physical Modelling in Geotechnics,* vol. 7, no. 3, pp. 1-23.

Klinkvort, R.T., Leth, C.T. & Hededal, O. 2010, "Centrifuge modelling of a laterally cyclic loaded pile", *Physical Modelling in Geotechnics,* pp. 959-964.

LeBlanc, C., Houlsby, G.T. & Byrne, B.W. 2010, "Response of stiff piles in sand to long-term cyclic lateral loading", *Geotechnique,* vol. 60, no. 2, pp. 79-90.

Leth, C.T., Krogsbøll, A.S. & Hededal, O. 2008, "Centrifuge facilities at Technical University of Denmark", *Proceedings Nordisk Geoteknikermøte nr.15,* pp. 335-342.

Li, Z., Haigh, S.K. & Bolton, M.D. 2010, "Centrifuge modelling of mono-pile under cyclic lateral loads", *Physical Modelling in Geotechnics,* , pp. 965-970.

Lin, S. & Liao, J. 1999, "Permanent strains of piles in sand due to cyclic lateral loads", *Journal of Geotechnical and Geoenvironmental Engineering,* vol. 125, no. 9, pp. 798-802.

Long, J.H. & Vanneste, G. 1994, "Effects of Cyclic Lateral Loads on Piles in Sand", *Journal of Geotechnical and Geoenvironmental Engineering,* vol. 120, no. 1.

McClelland, B. & Focht, J., J.A. 1956, "Soil modulus for laterally loaded piles", *American Society of Civil Engineers -- Proceedings -- Journal of the Soil Mechanics and Foundations Division,* vol. 82.

Murchison, J.M. & O'Neill, M.W. 1984, "EVALUATION OF P-Y RELATIONSHIPS IN COHESIONLESS SOILS", *Analysis and Design of Pile Foundations.Proceedings of a Symposium in conjunction with the ASCE National Convention.,* , pp. 174-191.

Rosquët, F. 2004, *PIEUX SOUS CHARGE LATERALE CYCLIQUE*, L'École Centrale de Nantes et l'Université de Nantes.

Schofield, A.N. 1980, "Cambridge geotechnical centrifuge operations", *Geotechnique,* vol. 30, no. 3, pp. 227-268.

Paper VII

"An elasto-plastic spring element for cyclic loading of piles using the p-y-curve concept"

O. Hededal & R. T. Klinkvort

Published in: *Numerical Methods in Geotechnical Engineering, 2010*

Numerical Methods in Geotechnical Engineering – Benz & Nordal (eds)

A new elasto-plastic spring element for cyclic loading of piles using the p-y-curve concept

Ole Hededal & Rasmus Klinkvort
Department of Civil Engineering, Technical University of Denmark

ABSTRACT: Modeling the response of large diameter piles subjected to lateral loading is most often done by means of p-y-curves in combination with Winkler beam models. Traditionally the p-y curves are formulated as non-linear (elastic) relations between the lateral movement *y* and the soil response pressure *p* in terms of monotonic loading (until failure) as e.g. prescribed by API (2000). However, the cyclic and dynamic performance is only to a limited degree accounted for. Here the elasto-plastic framework is applied allowing definition of unloading-reloading branches, hence enabling modeling of cyclic response. The present model can account for effects like pre-consolidation and creation of gaps between pile and soil at reversed loading. Results indicate that the model is able to capture hysteresis during loading with full cycles and model the accumulated displacement observed on piles subjected to "half cycles" as e.g. seen from centrifuge tests carried out. This article presents the theoretical formulations, discusses numerical implementation and finally presents simulations.

1 INTRODUCTION

Modeling the response of large diameter piles subjected to lateral loading is most often done by means of p-y-curves in combination with Winkler beam models. Traditionally, the p-y curves are formulated in terms of non-linear (elastic) relations between the lateral movement *y* and the soil response pressure *p* in terms of monotonic loading (until failure). These curves were established by back-analysis of a series of tests carried out in the 1950*es* by Matlock and co-workers. The tests were primarily static, monotonic load tests, but also a few cyclic tests were carried out.

Matlock (1970) carried out further cyclic tests on piles in clay that revealed a general reduction of the ultimate capacity for piles subjected cyclic loading compared to monotonic loading. This led to a general reduction of the cyclic ultimate capacity compared to the monotonic ultimate capacity. This reduction or cyclic degradation as it is commonly denoted is incorporated in almost all design codes, e.g. API (2000), as a formal reduction of the ultimate capacity. Still, the models does not directly correlate the reduction to the characteristics of the cyclic loading, i.e. number of cycles, loading amplitude or frequency.

Matlock (1970) and later Mayoral et al. (2005) set up a conceptual model for pile-soil interaction from these observations, cf. Figure 1. The model consists of 3 parts. Firstly, a loading phase where the soil-pile interaction follows the virgin curve. Secondly, an unloading phase that due to irreversible deformations in the soil will imply the development of a gap between the pile and the soil. Finally, a phase where the pile moves towards the initial position and into the opposite soil face in the cavity created behind the pile during initial loading. In this phase it may be assumed that there exists a drag or friction along the side of piles. Whether or not the gap will develop may depend on the type of soil type. El-Naggar et al. (2005) assumes that the gap will develop for cohesive soils, whereas for cohesionless soils, the soil will cave in and close the gap. Still, centrifuge tests carried out on a pile in

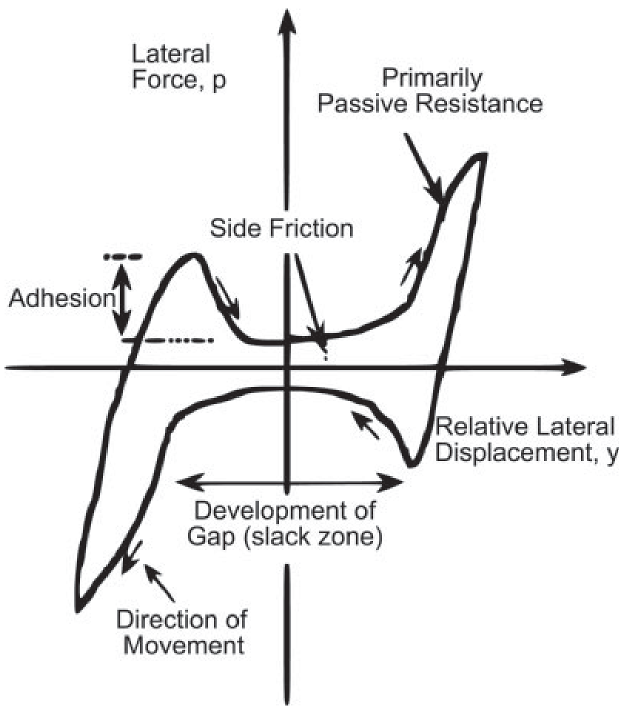

Figure 1. Typical loading cyclic for a model pile in clay, from Mayoral et al. (2005).

dry sand indicate that this cave-in effect may not be fully developed, Klinkvort (2009), thus there is probably a need to include the drag effect in a model even for cohesionless soils. Klinkvort (2009).

One of the first attempts in formulating p-y-curves that reflected the observed behavior was done by Matlock et al. (1978). Later, Boulanger et al. (1999) proposed an elasto-plastic p-y model based on a two component set-up in which the loading response is handled by a series connection of springs – one spring handling loading (passive failure mode) and another spring handling the unloading-reloading properties of a pile subjected to cyclic loading that is gradually creating a gap behind the pile. Taciroglu et al. (2006) further developed these ideas and proposed a macro-element consisting of three components; leading-face element, rear-face element and drag-element. The two face-elements are formulated in terms of elasto-plastic springs supplemented with a tension cut-off. The drag element controls the side friction, when the pile is moving inside the cavity during unloading.

In the present work, the principles of the above-mentioned models are incorporated in a single spring element that can be directly incorporated in a standard finite element code. In the following the elasto-plastic constitutive relations will be presented. Then follows a discussion about the implementation and finally some results from simulations.

2 ELASTO-PLASTIC MODEL

A simple one-dimensional elasto-plastic spring is defined. The model is expressed in terms of the earth resistant force p and the associated displacement u.

The standard procedure for development of elasto-plastic models are used. First the operator split between elastic and plastic components is assumed.

$$du = du^e + du^p \tag{1}$$

where du^e is the elastic part and du^p is the plastic part of the total displacement increment du.

The plastic displacement component is defined in terms of the gradient to the plastic potential, i.e.

$$du^p = d\lambda \frac{\partial g}{\partial p} \tag{2}$$

with $d\lambda$ as the plastic multiplier. The direction of the plastic displacement increment is fixed to the loading plane, implying that the plastic flow potential is by definition associated to the yield surface, i.e. $f = g$.

The simplest yield function may be written as

$$f = |p| - p_u(\boldsymbol{\alpha}) = 0 \tag{3}$$

in which $p_u(\boldsymbol{\alpha})$ is the current strength yield strength and $\boldsymbol{\alpha} = (\alpha_1, \alpha_2, \dots)$ are the hardening parameters (to be defined later).

As mentioned above the flow rule is associated to the yield function, hence rewriting Eqn. (2) by use of Eqn. (3), we find

$$du^p = d\lambda \frac{\partial f}{\partial p} = \frac{p}{|p|} d\lambda \tag{4}$$

In case of plastic loading $f = 0$ the consistency requirement requires the stress point to remain on the yield surface, hence

$$df = \frac{\partial f}{\partial p} dp + \frac{\partial f}{\partial \boldsymbol{\alpha}} \frac{\partial \boldsymbol{\alpha}}{\partial \lambda} d\lambda = \frac{p}{|p|} dp - H\, d\lambda = 0 \tag{5}$$

where the hardening modulus H is the scalar contraction of the partial derivatives of the yield function with respect to $\boldsymbol{\alpha}$. For isotropic hardening, only a single hardening parameter is needed, i.e. $\boldsymbol{\alpha} \equiv \alpha$, but since we need to account for the development of a gap on the front and on the rear of the pile, respectively, it is necessary to introduce two hardening parameters as is presented in the coming sections.

As always the fundamental assumption of common elastic and plastic stress is used, hence

$$dp = k\, du^e = k(du - du^p) = k\left(du - \frac{p}{|p|} d\lambda\right) \tag{6}$$

where k is the elastic stiffness. Combining Eqn. (5) and Eqn. (6) yields the definition of the plastic multiplier $d\lambda$,

$$d\lambda = \frac{p}{|p|} \frac{k}{k+H} du = \frac{k}{k+H} |du| \tag{7}$$

Here it is used that the displacement increment is associated to the loading direction, hence $p \cdot du = 1$.

This relation is then entered back into Eqn. (6) to produce the elasto-plastic tangent stiffness,

$$k^{ep} = \frac{k\, H}{k+H} \tag{8}$$

This completes the formal definition of the plasticity model. Remaining is now to define the yield strength as a function of the hardening parameters.

2.1 *Yield function*

Following the terminology of Mayoral et al. (2005) and Matlock (1970) we divide the current yield strength into two parts; one relating to the drag contribution and one relating to the earth pressure.

$$p_u(\boldsymbol{\alpha}) = p_u^{\text{drag}} + p_u^{\text{face}}(\boldsymbol{\alpha}) \tag{9}$$

The first term p_u^{drag} is the drag capacity, which in this version of the model is assumed to be constant. Below this value, the spring is assumed linear elastic with a stiffness k. The second term must account for the

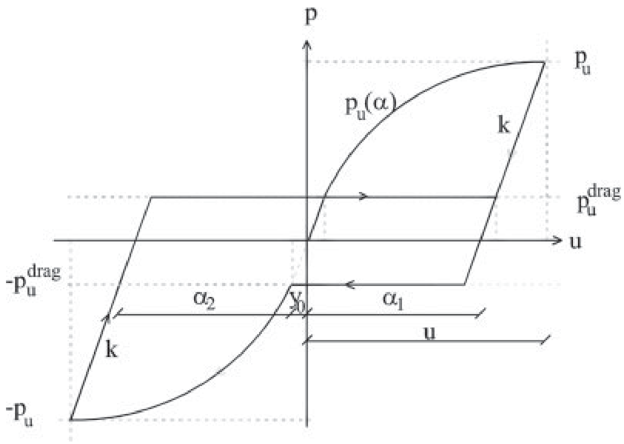

Figure 2. Schematic drawing of the spring element.

earth pressure when either of the pile faces are in contact with the soil. If there is no contact, this term must vanish. This can be achieved by introducing a multiplier to the virgin curve. The obvious candidate is a smooth step function,

$$S(x) = \frac{1}{1 + e^{-2\beta x}} \tag{10}$$

The parameter β defines the curvature and the coordinate x is

$$\begin{aligned} x_1 &= u - p_u^{\text{drag}}/k - \alpha_1 \quad \text{for} \quad u > 0 \\ x_2 &= -u + p_u^{\text{drag}}/k + \alpha_2 \quad \text{for} \quad u < 0 \end{aligned} \tag{11}$$

A typical value for β would be around 1.000.000. The coordinate x thus defines the current position of the pile relative to the soil. If the pile is in contact with the soil $x \geq 0$ and if there is a gap $x < 0$. Using Eqn. (9) we can write the yield function as

$$p_u^{\text{face}}(\boldsymbol{\alpha}) = \sum_i S(x_i)\, p_u^{\text{virgin}}(\alpha_i) \tag{12}$$

The hardening parameters $\alpha_i, i = 1, 2$ represents either loading of the front or rear face of the pile. The virgin curve $p_u^{\text{virgin}}(\alpha)$ depends on the soil conditions as e.g. given by API (2000).

2.2 *Evolution law for hardening parameters*

Referring to Figure 2 it is easily seen that the hardening parameter α_i is defined as the plastic displacement accumulated during contact between soil and pile. Physically α is representing the progressive development of the gap. Using the experience from contact mechanics, it is deemed that a formulation of unloading and reloading in terms of a displacement criterion (rather than the usual stress based criterion) allows us to keep the formulation simple, even for the discontinuous phase when the pile is moving in the developed cavity.

The evolution law for the hardening parameters should thus be defined in such a way that they only develop when the pile is in contact with the soil. As long as the pile is sliding in the cavity created by the cyclic motion, the model should behave ideally plastic. Introducing once again the step function we may find

$$d\alpha_i = S(x_i) du^p = \frac{p}{|p|} S(x_i)\, d\lambda \tag{13}$$

in which the definition of the plastic displacement, Eqn. (4), is utilized. Having established the evolution law, it is finally possible to identify the model specific hardening modulus, H, by revisiting the consistency equation, Eqn. (5). After some manipulation we find that

$$\frac{p}{|p|}\, dp + \underbrace{\frac{p}{|p|} \sum_i \left[\frac{\partial p_u^{\text{virgin}}}{\partial \alpha_i} S^2 + p_u^{\text{virgin}} \frac{\partial S}{\partial \alpha_i} S \right]}_{-H} d\lambda = 0 \tag{14}$$

Note that the arguments α_i and x_i has been omitted in the formula. Analyzing Eqn. (14), it is noted half of the contributions vanishes if the soil is in contact with either the front face or the rear face of the pile, since the for the unloaded face $S = 0$. Likewise this relation ensures that $H = 0$ in the cavity since $S = 0$ for all terms.

3 IMPLEMENTATION

The proposed spring element is implemented in an inhouse MATLAB based FE code, Hededal and Krenk (1995). The implementation consists of two parts. Firstly implementation of the spring element using a backward Euler integration scheme for integration of the constitutive relation. Secondly, a Winkler model based on the proposed model has been defined and analyzed using a Newton Raphson based non-linear solver.

For this specific application it has been chosen to use the (API 2000) definition of the p-y curves for sand,

$$p_u^{\text{virgin}}(u) = A\, p_{ult} \tanh\left(\frac{kX}{A\, p_{ult}} u\right) \tag{15}$$

Here p_{ult} is the ultimate capacity, A is a strength reduction parameter, k is the subgrade reaction modulus, X is the depth and u is the total lateral displacement.

Still, in order to implement this relation into the proposed format, it is necessary to divide the total resistance into a drag contribution and a face loading contribution, i.e.

$$p_u^{\text{virgin}}(u) = p_u^{\text{drag}} + p_u^{\text{face}}(\boldsymbol{\alpha}) \tag{16}$$

This is not a trivial task, since the hyperbolic function can not be easily inverted in order to allow

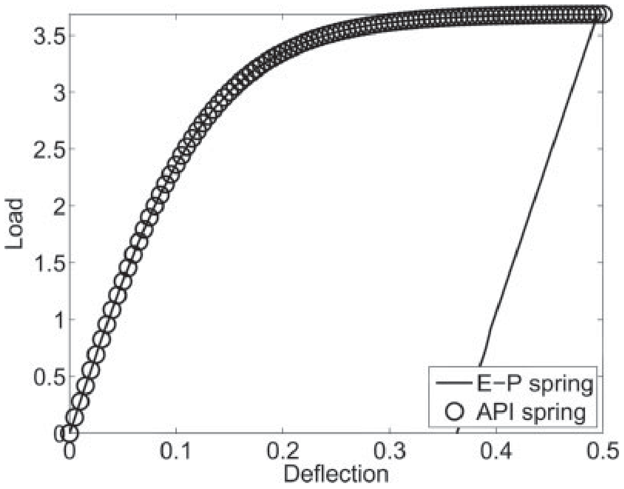

Figure 3. API curve versus the elasto-plastic curve.

Table 1. Pile soil properties.

Pile diameter	D	$1\,m$
Pile length	L	$6\,m$
Load eccentricity	e	$2.5\,m$
Frictional angle	ϕ	$42°$
Soil density	γ	$16\,kN/m^3$

for a split of elastic and plastic contribution. In the present situation, it has be chosen to use the following approximation,

$$p_u^{\text{face}}(\alpha_i) = A\,p_{ult}\tanh\left(\frac{kX}{A\,p_{ult}}u\right) - p_u^{\text{drag}} \tag{17}$$

Eqn. (17) is a implicit function in α since we have $u = \alpha + p/k$. This implies that the derivative with respect to α is not trivial. Here we use

$$\frac{\partial p_u}{\partial \alpha} \approx \frac{\partial p_u}{\partial u} \tag{18}$$

as a first order approximation. Comparing the API curve to the prediction of the model, Figure 3, this approximation appears to be acceptable.

4 RESULTS

To demonstrate the ability of the model to capture the pile-soil interaction as observed by Matlock (1970) and Mayoral et al. (2005), three test simulations have been carried out.

The material properties used in the three test examples are shown in Table 1. The three tests have been performed with a monotonic or cyclic laterally load applied in the top of the pile. A rather large stiffness has been used for the sand in order to clearly demonstrate the capability of the spring element.

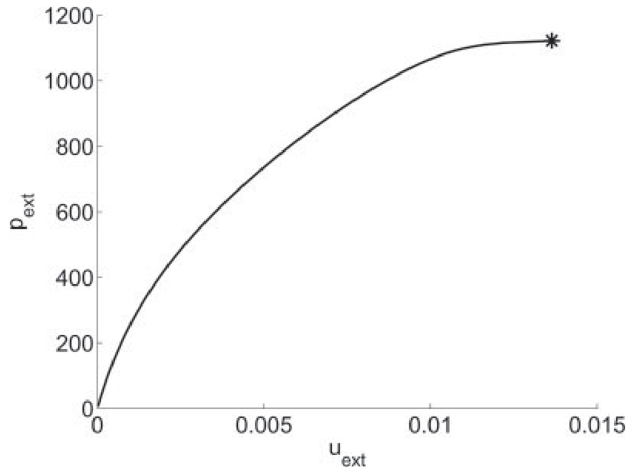

Figure 4. Overall response on a pile subjected to monotonic loading loading.

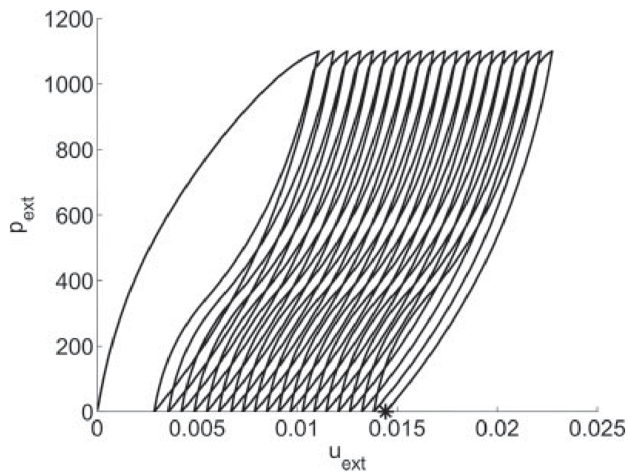

Figure 5. Overall response on a pile subjected to one-way loading.

4.1 *Example 1 – monotonic loading*

The spring element presented here is capable of performing cyclic tests. As demonstrated in Figure 3 the elasto-plastic element follows the virgin curve recommended by API (2000). Monotonic tests can therefore also easily be performed with this element. In Figure 4 the result as pile head deflection versus applied laterally load from a monotonic test can be seen. The maximum bearing capacity of the pile is calculated to $P_{max} = 1122\,kN$. Using the theory from Hansen (1961), the maximum bearing capacity can be calculated to $P_{max} = 1152\,kN$. This results fits very well with the calculation performed in the model.

4.2 *Example 2 – one way loading*

The second example illustrates a pile that is subjected to a load varying from zero and to a given value in the same direction, this is called one-way loading. The maximum load during the cycles is close to the ultimate capacity, so that the accumulation effect is clearly seen.

The overall pile response can be seen in Figure 5. This figure shows the pile top deflection versus the

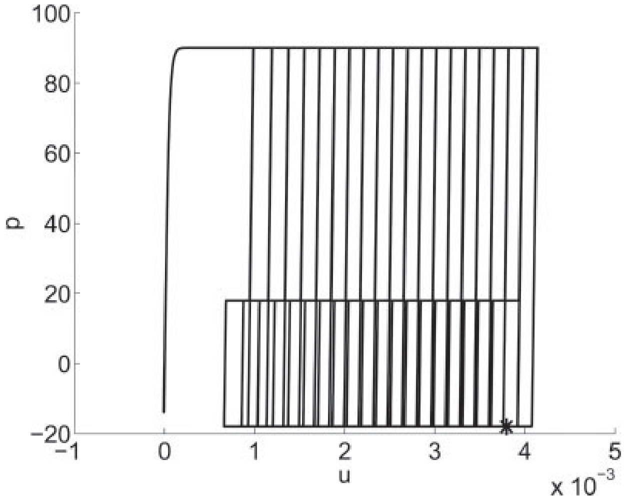

Figure 6. Spring response on a pile subjected to one-way loading.

applied force. The model simulates a load controlled test with constant load amplitude in a total of ten cycles. It can be seen from Figure 5 that the deflection increases with every cycle. Still, the rate of increase for every cycle is getting smaller and smaller. This shows that the model is able to take account for the accumulation of displacement when the model is subjected to one-way loading.

The response from one of the springs near the soil surface can be seen in Figure 6. The spring reaches fast the maximum bearing capacity. This is due to the high stiffness. It unloads elastically and then the development of a cavity can be seen. As described in section 2.2, no hardening occurs when the pile is moving in this cavity. It can also be seen that after the first cycle the the spring does not go back to its initial position, but exhibits a permanent deformation. This is due to the accumulation of deflection. The accumulation of deflections occurs due to the development of cavity in several springs and the subsequent redistribution of the force therefore occurs.

4.3 *Example 3 – two way loading*

In this example the pile is subjected to a given load varying between negative and positive values, this is called two-way loading. The overall pile response can be seen in figure Figure 7. The pile is loaded five full cycles. The same maximum force is applied for both direction. It can be seen from Figure 7 that the deflection is getting larger and larger from every load cycle. This is valid for both sides and the increase in deflection is also the same for both sides. This means that the average deflection of the load cycles is constant and equal to zero. It is though interesting that the deflection amplitude increases, hence the secant stiffness will decrease as a consequence of cyclic loading. This effect is extremely important if we are to model the cyclic response of monopile foundations for wind turbine, since the load here is frequency dependent.

It should be noted that the number of iterations increases dramatically after the first half cycle when

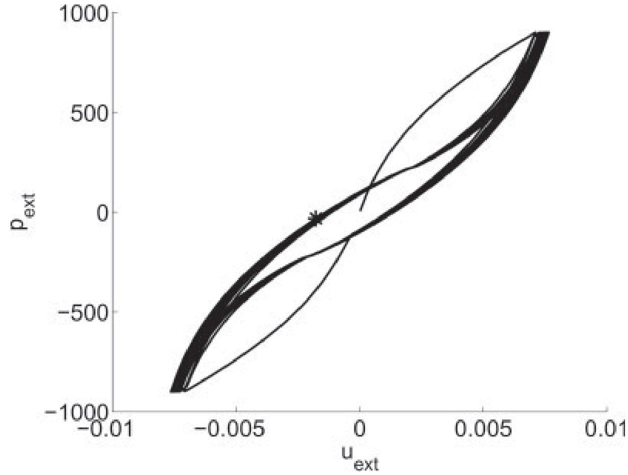

Figure 7. Overall response on a pile subjected to two-way loading.

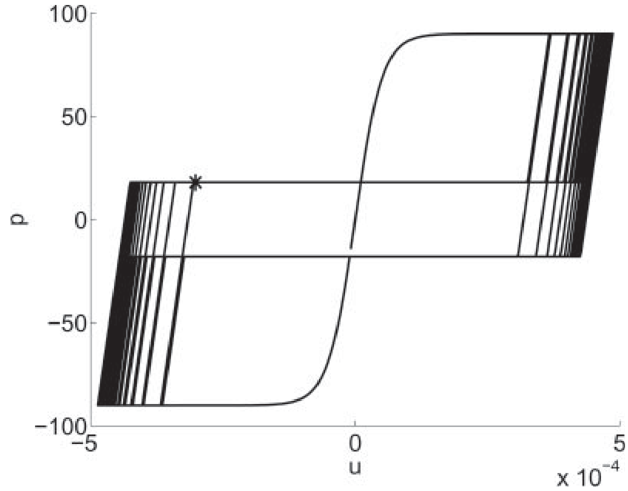

Figure 8. Spring response on a pile subjected to two-way loading.

the pile is in a position around the mean deflection. This is due to the development of a cavity in nearly all spring elements. In this position the system have very low stiffness. A simple remedy to this could be to include a small amount of kinematic hardening to the drag-term in a manner as proposed by Hededal and Strandgaard (2008).

The response from one of the springs can be seen in Figure 8. It can be seen that a cavity develops as expected. As for the overall pile response, an increase in deflection of the single spring for every load cycle is observed. Also here the average deflection for an overall load cycle is constant and equal to zero. There is no degradation of the springs which can be seen in one-way loading example.

5 DISCUSSION

The cyclic spring presented in this paper is capable of capture physical aspects as seen in tests Matlock (1970), Mayoral et al. (2005) and Klinkvort (2009). Still, improvements are needed. In this section ideas which will improve the performance of the spring element and the representation of the physical world.

The presented model operates with the same virgin stiffness as un-/reloading stiffness. This could be changed and it must also be expected that a soil not will load and unload with the same stiffness. With a change like this the model will probeable start to accumulate displacements in a smaller loading range.

When springs moving in the cavity some sort of hardening should occur. This can also be seen in the Figure 1 by Mayoral et al. (2005). As a side effect an introduction of hardening in the cavity will help the global iterations to converge faster.

Other effects which should be incorporated in the future is suction release for clay springs and the fall back of sand particle when dealing with sand springs.

6 CONCLUSION

An elasto-plastic spring element has been defined. The spring element embeds two fundamental features of cyclically loaded piles. It is able to account for preloading of the soil by tracing the virgin curve. Secondly, the creation of a gap after reloading, which is undeniably developing in cohesive soils, is accounted for by introducing a smoothed step function that keeps track of the current position of the pile-soil interfaces. The element is not only relevant for the quasi-static loading with random time series, but also has a potential in dynamic analysis, where it will provide a physically based hysteretic damping.

REFERENCES

API (2000). American petroleum institute. recommended practice for planning, designing and constructing fixed offshore platforms- working stress design, api recommended practice 2a-wsd (rp2a-wsd), 21st edition, dallas.

Boulanger, R. W., C. J. Curras, B. L. Kutter, D. W. Wilson, and A. Abghari (1999). Seismic soil-pile-structure interaction experiments and analyses. *Journal of Geotechnical and Geoenvironmental Engineering 125*(9), 750–759.

El-Naggar, M. H., M. A. Shayanfar, M. Kimiaei, and A. A. Aghakouchak (2005). Simplified bnwf model for nonlinear seismic response analysis of offshore piles with nonlinear input ground motion analysis. *Canadian Geotechnical Journal 42*, 365–380.

Hansen, J. B. (1961). The ultimate resistance of rigid piles against transversal forces. *Danish Geotechnical Institute, Copenhagen, Denmark Bulletin NO. 12*, 5–9.

Hededal, O. and S. Krenk (1995). *FEMLAB – matlab toolbox for the Finite Element Method*. Aalborg University.

Hededal, O. and T. Strandgaard (2008). A 3d elasto-plastic soil model for lateral buckling analysis. In *Proc. 18th International Offshore and Polar Engineering Conference, ISOPE 2008*.

Klinkvort, R. T. (2009). Laterally loaded piles – centrifuge and numerical modelling. Master's thesis, Technical University of Denmark.

Matlock, H. (1970). Correlations for design of laterally loaded piles in soft clay. In *Offshore Technology Conference*, pp. 577–594.

Matlock, H., H. C. Foo, and L. M. Bryant (1978). Simulation of lateral pile behavior under earthquake motion. In *Proc. American Society of Civil Engineers Specialty Conference on Earthquake Engineering and Soil Dynamics*, Volume 2, pp. 600–619.

Mayoral, J. M., J. M. Pestana, and R. B. Seed (2005). Determination of multidirectional p-y curves for soft clays. *Geotechnical Testing Journal of Computational Mechanics Vol. 28*, No.3.

Taciroglu, E., C. Rha, and J. Wallace (2006). A robust macroelement model for soil-pile interaction under cyclic loads. *Journal of Geotechnical and Geoenvironmental Engineering, ASCE 132*(10), 1304–1314.